Universidade de Lisboa

Faculdade de Ciências

Departamento de Geologia

Sedimentological signatures of extreme marine inundations

Pedro José Miranda da Costa

Doutoramento em Geologia

Especialidade em Geologia Económica e do Ambiente

2012

Universidade de Lisboa

Faculdade de Ciências

Departamento de Geologia

Sedimentological signatures of extreme marine inundations

Pedro José Miranda da Costa

Doutoramento em Geologia

Especialidade em Geologia Económica e do Ambiente

Tese orientada pelo Prof. Doutor César Augusto Canelhas Freire de Andrade e pelo Prof. Doutor Alastair George Dawson, especialmente elaborada para a obtenção do grau de doutor em Geologia, especialidade em Geologia Económica e do Ambiente

2012

Resumo

A identificação e diferenciação de depósitos de invasões marinhas extremas (*i.e.* tsunamis e tempestades), é essencial para a reconstrução da sua distribuição espacial e para a determinação de tempos de recorrência de eventos desta natureza. As características de depósitos de paleotsunamis podem variar de local para local com as características geomorfológicas e sedimentológicas do sector costeiro em análise, bem como, com a deposição e/ou erosão associadas à inundação e ao retorno das ondas. Estes factores tornam o reconhecimento de paleotsunamis, numa sequência sedimentar, uma tarefa ousada. Além de que, existem também variadíssimas similaridades entre depósitos sedimentares de tsunamis e de tempestades, o que pode restringir de sobremaneira a precisão no seu reconhecimento e, consequentemente, na determinação de períodos de retorno para invasões marinhas extremas.

Esta trabalho tem como objectivo fundamental contribur para mitigar estas dificuldades, focando-se sobre a aplicação de análise litoestratigráfica, textural, morfoscópica, microtextural e de composição mineralógica, para identificar depósitos de inundações marinhas extremas e determinar as suas prováveis fontes sedimentares. O trabalho aqui apresentado emerge do estudo de uma variedade de locais (Salgados e Boca do Rio - Portugal; Lhok Nga - Indonésia; Voe of Scatsta e Stoneybridge - Escócia) e considera eventos de diferentes cronologias e fontes distintas (tsunami: AD 1755, 26 de dezembro de 2004 e Storegga; e a Grande Tempestade, de 11 de Janeiro de 2005) que afectaram, e deixaram registo sedimentar peculiar, áreas com diferentes ambientes sedimentares e condições oceanográficas regionais.

Os métodos usados nas amostras de cada área de estudo foram: interpretação litoestratigráfica, granulometria, análise e interpretação de dados texturais; caracterização de populações sedimentares através de análise morfoscópica, caracterização microtextural de grãos de quartzo usando imagens de microscópio electrónico de varrimento e estudo das associações de minerais pesados.

A costa Sul do Algarve caracteriza-se por um regime de agitação de baixa energia e é raramente afectada por tsunamis ou tempestades muito intensas. O tsunami mais devastador que afectou a costa portuguesa em tempos históricos foi o de 1 de Novembro de 1755. Vários estudos discutiram a sedimentação associada a este evento no Algarve em contextos rochosos do Barlavento (Furnas, Barranco, Martinhal e Boca do Rio) e num único caso do Sotavento (Ria Formosa). No presente trabalho descreve-se uma nova ocorrência sedimentar detectada na depressão dos Salgados (Algarve central) cuja caracterização original, enquadramento na sequência de colmatação holocénica, datação e origem se apresentam e discutem. A depressão dos Salgados localiza-se na baía entre Armação de Pêra e a ponta da Galé. Este troço costeiro contém uma praia arenosa intermédia-reflectiva com 6 km de comprimento, marginada por um cordão dunar múltiplo, vegetado (cota apical entre 3 e 17m acima do nível médio do

mar), que reveste um afloramento alongado de *beachrock* e eolianitos holocénicos. Obtiveram-se 145 sondagens curtas (< 1.5m) e 13 "longas" (2 a 4.5m), no enchimento sedimentar da Lagoa dos Salgados. Onze amostras de lodo orgânico foram datadas por ^{14}C e um testemunho sujeito a análise de ^{210}Pb e ^{137}Cs. Foi possível caracterizar 6 unidades litoestratigráficas fundamentais, acumuladas na segunda metade do Holocénico ao abrigo de uma barreira já estabelecida e contemporâneas de um nível do mar próximo do actual. As unidades denominadas A, B e a C, depositadas pós *ca*. 5900 BP são constituídas por areias com intercalações vasosas e vasas com intercalações arenosas, com transição lateral de fácies frequente. Estas unidades correspondem ao preenchimento da depressão em ambiente subtidal a intertidal inferior, com crescente influência marinha para o topo. As unidades D e F, com cerca de 1m de espessura, são constituídas por vasas mais ou menos arenosas.

Intercalada entre as unidades D e F, e aproximadamente a 0.40m de profundidade, ocorre uma lâmina lateralmente contínua, formada essencialmente por areia média com abundantes bioclastos e intraclastos de lodo, com espessura variável entre 0.8m e alguns milímetros, diminuindo para terra. Na sua região distal o calibre da areia diminui e observou-se granulotriagem positiva nos testemunhos com maior espessura. O contacto basal é erosivo e a transição a tecto bem marcada. O depósito apresenta-se em forma de gota alongada e estende-se para terra até um máximo de aproximadamente 800m. O perfil vertical do excesso de ^{210}Pb e ^{137}Cs indica uma taxa de sedimentação de 2.6mm/ano nos 0.30m superficiais. A extrapolação deste valor localiza a base dos lodos a tecto da unidade E na primeira metade do século XIX e as idades radiocarbono do sedimento subjacente à unidade E sugerem ablação de espessura considerável de lodos aquando da deposição das areias. Estes resultados são consistentes com um evento raro de inundação marinha extrema e muito intensa de um espaço lagunar muito assoreado, com injecção de sedimento exótico a grande distância da linha de costa, excedendo a capacidade de transporte das correntes de maré e do galgamento por tempestade. Trata-se do único registo deste tipo de evento detectado nesta coluna sedimentar nos últimos séculos e compatível com o tsunami gerado pelo sismo de 1 de Novembro de 1755, do qual existem testemunhos documentais nesta região. Para a determinação de prováveis fontes sedimentares foram recolhidas ainda cerca de 30 amostras sedimentares de análogos actuais (*i.e.* praia, duna e fundos submarinos), foram ainda detectadas evidências de um possível depósito arenoso de tempestade intercalado na unidade lodosa de topo e constrangido espacialmente à zona adjacente à barra.

Outra área de estudo foi a planície aluvionar de Boca do Rio (também situada no Barlavento algarvio, próximo da Praia da Salema). Nesta localização uma unidade litoestratigráfica associada ao tsunami de AD 1755 foi reconhecida anteriormente por diversos autores. A área aluvionar é constituída por uma planície de inundação supratidal que é periodicamente sujeita a inundações fluviais. Esta encontra-se separada do mar por uma barreira de cascalho e areia e por um esporão rochoso que, juntos, impedem o galgamento durante as tempestades mais frequentes. Amostras de sedimentos depositados pelo tsunami e de análogos actuais foram recolhidas nesta área e analisadas neste trabalho. Três amostras de tsunami

(correspondente a um perfil normal à linha de costa) foram detalhadamente estudadas. Adicionalmente, 11 amostras de sedimentos (cinco de fundos submarinos, três de duna, uma praia e duas recolhidas na planície aluvial) também foram recuperadas e utilizadas neste trabalho para caracterizar ambientes sedimentares actuais (possíveis fontes sedimentares do tsunami).

Nas ilhas Shetland (Escócia) uma lâmina arenosa intercalada em turfas tem sido comummente associada ao tsunami provocado pelo deslizamento submarino de Storegga que terá ocorrido à *ca*. 8000 BP. Esta unidade litoestratigráfica composta por areia média a grosseira caracteriza-se pelo contacto erosivo basal, incorporação de clastos de camadas subjacentes e pela sua granulotriagem positiva. Quatro amostras, recolhidas nesta unidade, a partir das paredes de duas trincheiras escavadas na enseada de Voe of Scatsta (Sullom Voe), separadas por menos de 50 m, e alinhadas transversalmente, foram estudadas em pormenor. Cada par de amostras estudadas contém uma amostra correspondente à base do depósito de areia e uma segunda amostra, localizada perto do contacto superior da unidade tsunamigénica.

Por sua vez, Stoneybridge localiza-se na costa oeste da ilha de South Uist (arquipélago das Hebrides, Escócia). Sedimentos depositados por ondas de tempestade foram recuperados imediatamente após a denominada Grande Tempestade de 11 de janeiro de 2005. Este evento provocou extensa erosão nalgumas localizações costeiras e noutras (*e.g.* Stoneybridge) depositou uma contrastante e espessa camada arenosa (areia média a fina) a consideráveis distâncias da costa. Quatro amostras sedimentares deste tempestito foram analisadas neste trabalho.

Lhok Nga Bay (Samatra, Indonésia) é uma praia contínua em baía, quebrada por pequenas fozes de ribeiros sazonais, que foi fortemente afectada pelo tsunami de 26 de Dezembro de 2004. As amostras utilizadas neste trabalho foram recolhidas algumas semanas após esse evento. Estas correspondem a um perfil normal à linha de costa sendo importante notar que nalgumas localizações mais do que uma amostra do sedimento tsunamigénico foi recolhida por forma a avaliar as variações verticais do depósito. Os depósitos associados ao tsunami de 2004 consistem em areias média a grosseira, acinzentada a amarelada, que exibem variações laterais e verticais de espessura e dimensão. O contacto inferior da unidade tsunamigénico é erosivo. A espessura dos depósitos de tsunami diminui para terra.

O facto de o registo sedimentar de uma série significativa de eventos de inundações marinhas extremas, com morfologias e cronologias diversas, ter sido analisado permitiu a utilização e a generalização da aplicação de técnicas sedimentológicas, tais como a análise microtextural em grão de quartzo e a composição mineralógica de amostras de tsunami e tempestade, bem como, das suas prováveis fontes sedimentares.

Os depósitos de tempestade e tsunami estudados constituem uma peculiaridade litoestratigráfica, um carácter arenoso, apresentando também um contacto basal abrupto ou erosivo, diminuindo de dimensão verticalmente e diminuindo de espessura horizontalmente. Os depósitos de tsunami exibem uma notável variação lateral em todas as características sedimentares e geométricas, mesmo em distâncias curtas, e todos apresentam uma estrutura interna massiva, com excepção do caso mais recente (tsunami

de 26 de Dezembro de 2004 em Lhok Nga - Indonésia). Estes depósitos tsunamigénicos apresentam também uma frequente incorporação de clastos de camadas subjacentes que foram erodidos durante o processo de inundação das ondas.

Os resultados obtidos a partir do estudo morfoscópico de partículas arenosas (*e.g.* esfericidade e forma) revelaram que nos casos das amostras dos Salgados e Boca do Rio (Portugal) e Lhok Nga (Indonésia), que estes atributos são úteis na discriminação de ambientes sedimentares e/ou no estabelecimento de material fonte que alimenta os depósitos de tsunami.

Resultados da análise microtextural revelaram que esta prática é uma técnica sedimentológica complementar valiosa e que pode ser aplicada quer na discriminação de ambientes sedimentares, bem quer na identificação de depósitos de inundação marinhas extremas, especialmente se levado em consideração o contexto regional sedimentológico e geomorfológico. As superfícies dos grãos de quartzo das amostras de tsunami e tempestade analisadas revelaram uma presença mais destacada de marcas de percussão e superfícies recentes. Este resultado inovador foi detectado em todas as localizações geográficas estudadas.

Determinou-se que, genericamente, a concentração de minerais pesados na fração de sedimento total diminui para topo nas camadas tsunamigénicas e nos tempestitos analisados. Num dos locais estudados (Salgados), foi possível estabelecer que o conteúdo de minerais pesados apresenta semelhanças qualitativas e quantitativas com as amostras de dunas. Em Lhok Nga (Indonésia) e Boca do Rio (Portugal), também foi possível identificar uma assinatura mineralógica específica da deposição associada ao processo de retorno das ondas de tsunami.

O reconhecimento da assinatura sedimentar do mesmo evento tsunamigénico (AD 1755) e a sua contextualização estratigráfica forneceu motivos para sugerir uma escala milenar como período de retorno para eventos. No entanto, as limitações na identificação e diferenciação no registo sedimentar de evidências geológicas de inundações marinhas extremas (*e.g.* a preservação do depósito, a inexistência de contrastes litológicos e texturais, *etc*.) precisam ser superadas para que seja possível estabelecer períodos de retorno com maior assertividade.

A diferenciação entre depósitos de tsunami e de tempestade foi essencialmente evidenciada pela incorporação de clastos de camadas subjacentes em depósitos tsunamigénicos enquanto se observou a sua ausência nos depósitos de tempestade analisados.

Resultados globais deste trabalho sugerem que características locais geomorfológicas e sedimentares podem limitar extrapolações acríticas sobre os mecanismos de deposição (tsunami *vs* tempestade) de aplicação generalizada a todo o mundo. Em alguns casos analisados (Salgados e Boca do Rio) foi possível evidenciar quais os prováveis materiais fonte de cada um desses depósitos tsunamigénicos. Este trabalho demonstra ainda a utilidade de técnicas sedimentológicas tais como textura,

morfoscopia, análise microtextural e composicional e contribuí para aumentar os critérios sedimentológicos a ser utilizados no reconhecimento e diferenciação de depósitos de tsunami e tempestade.

Os objetivos iniciais estabelecidos para este trabalho foram alcançados:

a) Unidades litoestratigráficas depositadas por inundações marinhas extremas, durante o Holocénico, foram identificadas, descritas, caracterizadas e datadas;

b) As amostras foram analisadas usando uma abordagem multidisciplinar, que incluiu a caracterização e interpretações litoestratigráficas, geométricas, dimensionais, texturais, de características microtextural e composicionais, tendo sido abordadas as contrastantes escalas espaciais (que vão desde a escala do afloramento ou coluna sedimentar à microscopia de partículas individuais) para alcançar uma interpretação dos processos que controlam o transporte e deposição de sedimentos terrígenos de alta energia durante eventos extremos de inundação marinha;

c) A análise microtextural foi aplicada em grãos de quartzo a fim de determinar o material fonte e/ou para identificar assinaturas específicas de inundações marinhas extremas. Esta metodologia foi testada com resultados encorajadores;

d) A composição mineralógica da malha de amostragem foi utilizada, com resultados relevantes, para estabelecer os materiais fonte e/ou determinar composições específicas de amostras depositadas por inundações marinhas extremas.

e) Foi feita uma previsão, com base no registo sedimentar, sobre períodos de retorno para inundações tsunamigénicas para a costa do Algarve, em Portugal;

f) De forma genérica, esta tese contribuiu para o desenvolvimento do conhecimento actual sobre os critérios usados para caracterizar os sedimentos depositados por eventos extremos de inundação marinha, e para aumentar a nossa capacidade de distinguir e relacionar esses depósitos com cada processo forçador (*i.e.* tsunamis ou tempestades).

Palavras-chave: sedimentologia, tsunami, tempestade, minerais pesados, microtexturas em quartzo

Abstract

This thesis aims to characterize (and distinguish) tsunami and storm deposits in the sedimentary record by focusing on the application of textural, morphoscopic, microtextural and compositional analysis, and establish their likely source materials. This work presents results from a variety of locations (Portugal, Indonesia and Scotland) and considers events of different chronologies and sources (AD 1755, 26 December 2004 and Storegga Slide tsunamis; Great Storm of 11 January 2005) that affected contrasting coastal settings with different regional oceanographic conditions. Typically these statigraphically peculiar (essentially sand-sized) deposits exhibited an abrupt basal contact, thinning and finning inland, massive structure and relevant lateral variation. Differentiation between tsunami and storm deposits was evidenced by the incorporation of rip-up clasts solely in the tsunamigenic deposits. Grain surface microtextural analysis proved to be a valuable complementary technique to be applied in the identification of extreme marine inundation deposits, especially when considered within a regional context. Tsunami and storm grains presented a more frequent presence of percussion marks and fresh surfaces when compared with potential source material. Generally the concentration of heavy minerals decreased up unit and in Salgados (Portugal) the assemblage presented similarities with dune samples. In Lhok Nga (Indonesia) and Boca do Rio (Portugal) it was possible to identify a mineralogical signature of the tsunami backwash.

The assumption of a tsunami millennial return period for the Algarve (Portugal) coast was possible through the study of the lithostratigraphy of two locations affected by the AD1755. Overall results revealed that site-specific effects precluded clear-cut extrapolations on a storm *vs* tsunami emplacement mechanism of worldwide application although it demonstrated that the use of textural, morphoscopic, microtextural and heavy mineral data will enhance the criteria to recognize and differentiate these deposits if the regional context is sufficiently constrained.

Keywords: sedimentology, tsunami, storm, heavy minerals, quartz microtextures

Dedicated to:

XII

IX

Acknowledgments

This thesis is the culmination of a long journey that began in early 2008. Many adventures, misadventures, joys and sorrows were experienced during the execution of this work. The motivation to complete this doctoral thesis was fuelled by the valuable assistance of many people. In the following statement I present my deep gratitude to all those people.

I would like to express my enormous gratitude to my supervisor and friend Professor César Andrade for his dedication, commitment and ingenuity in various stages of the Ph.D. His support, reviews, ethic, rigor and enthusiasm with which he addresses any issue of Coastal Geology, was and will be an example to follow. It was a privilege to be his student, and if today I feel a better geologist I have to be thankful, in a very great part, to Professor César.

My heartfelt thanks to my co-supervisor and friend Professor Alastair Dawson with whom I learned immensely about tsunami deposits and storminess. The numerous visits to Scotland were unique opportunities to enrich me as a geologist and as a person. His commitment to the successful completion of this thesis was crucial. The way Alastair explains complex concepts with a disarming simplicity will, forever, be an example to follow.

Professor Conceição Freitas, although not officially my co-supervisor, was instrumental in the success of this work by how earnestly she helped in the completion of this thesis. Her unique work capacity, management skills, her attention to detail and her scientific accuracy are of such quality that I will seek to follow them in the coming years.

To Prof. William Mahaney my sincere and deep thanks for his support throughout this thesis. The short-visit to Toronto (Canada) was, without a doubt, one of the defining moments of this Ph.D. The contribution of Bill Mahaney did not stopped in the microtextural analysis, our frequent conversations and the privilege of working with him provided me the knowledge on a range of other geological subjects.

I am sincerely thankful to Dr João Cascalho (MNHN) for his invaluable help in the observation of heavy minerals and for the important discussions on various geological subjects. My thanks to Dr Raphael Paris (Université Clermont, France) who contributed to this work as a supervisor of a short-visit to Clermont-Ferrand, also with numerous conversations about tsunami deposits and with the very kind offer of sediment samples collected in Lhok Nga. I would like to express my gratitude to Dr Lenka Lisa (Institute of Geology, Czech Republic) for her guidance and support during a short-visit to Prague. I express my appreciation to Prof. Pedro Cunha and Prof. Jorge Dinis (University of Coimbra) for stimulating discussions on the stratigraphy and age-estimation of tsunamigenic deposits. I am thankful to Dr Sebastião Teixeira for the generous offer of nearshore samples (Armação de Pêra, Portugal) and for his availability to help during this

work. I express my gratitude to Prof. Rui Taborda and to Prof. Francisco Fatela (both FCUL) for valuable discussions regarding different themes of the thesis.

I am grateful to GeoFcul, the academic staff, employees and students for the conditions they offered me to carry out and complete this doctoral dissertation. My heartfelt thanks to ProCost (FCUL) and to fellow PhD students (GeoFcul) for the thousand and one times I have felt their support and for their contribution to the progress of this work. In particular I want to thank my very supportive office colleagues Alexandra Oliveira, Tiago Silva, Vera Lopes and to Rita Pires, Rute Ramos, Sandra Moreira, Tanya Silveira, Bárbara Proença, Ivana Bosnic, Mónica Ribeiro, Cristina Lira, Cristiano Ribeiro, Marco Alves, Paula Figueiredo and João Moedas.

My acknowledgments to projects GETS (FCT-PTDC/CTE-GEX/65948/2006) and NEAREST (EU-037110-GOCE-2006) for providing the financial conditions for the realization of part of this work. My gratitude to FCT for awarding me a doctoral grant (SFRH/BD/35900/2007) that enabled this research to be carried out.

My deep thanks to my colleagues from my 1st degree in Geology (Coimbra) and to my Briosos friends for their unquestionable and constant support. The yearly dinners during the Queima and the Briosos Domingos were always a cause of rapprochement to Coimbra and to Geology.

My sincere gratitude to Luís Ramos, Filipe Saavedra, Angelina, João Brito, João Caldas, Bruno Soares, Nelo Guedes, Ana Morais, Hugo Brito, Ana F., Zira, Ricardo Branco, Adelino and other friends that always gave me moments where true and unquestionable friendship served as an important support and motivation to pursue and conclude this thesis.

A special word to my grandfather José Miranda, my grandmother Alice, to Rui H., Paula and Carla my profound thanks for their support and for motivating me at different stages in the long path that brought me from secondary school to the present academic achievement.

A special and heartfelt thanks to my uncle Joaquim, Fátima, João, Octávio and José Mário, and to my brother Jorge, my sister-in-law Ana and my nephew José because always, and in all moments, they supported and encouraged me in a unique way.

With the completion of this thesis I give my parents a brief proud moment. Those moments are the humblest way a son can thank their parents, especially in my case because they always trusted on me and never asked for anything in return. The many good examples that they gave me, will last with me.

My deepest thanks to the centre of my life: my son and Ana. Rui, my son, has changed and enriched my life in an inimitable way, and was also a strong motivation to complete the thesis.

I am deeply grateful to Ana who accompanied me throughout this adventure and with whom I shared all the frustrations, joys, disappointments, achievements and who always gave me a peaceful and permanent support, help, understanding, friendship, companionship and love.

For all, Obrigado!

Contents

Resumo I
Palavras-chave V
Abstract VII
Keywords VII
Acknowledgments XI
Contents XIII
1. Introduction 1
1.1. Relevance of study 1
1.2. Aims and objectives 1
1.3. Structure of document 3
2. State of the art 5
2.1. Extreme marine inundations: origin and mechanisms 5
2.2. Tsunami and storm deposits in the geological record 12
2.2.1. Nearshore and offshore deposits 13
2.2.2. Onshore boulder deposits 14
2.2.3. Onshore cobble and gravel deposits 16
2.2.4. Onshore fine-grained deposits 17
2.2.5. Hydrodynamic models of transport of fines, gravel and boulders 17
2.3. Sedimentological features of onshore tsunami deposits 20
2.3.1. Sedimentary structures 23
2.3.2. Sedimentary sources 25
2.3.3. Palaeontological signature 27
2.3.4. Geochemical signature 30

2.3.5. Geomorphological signature 31
2.4. Sedimentological features of onshore storm deposits (palaeotempestology) 34
2.5. Record of tsunami and storm deposits in the study areas 42
2.5.1. Atlantic Iberia 42
2.5.2. Scotland 47
2.5.3. Indonesia 50
3. Study areas 53
3.1. Algarve 53
3.1.1. Geographical and Geological setting 53
3.1.2. Oceanography 57
3.1.3. Salgados 59
3.1.4. Boca do Rio 62
3.2. Shetland Islands 65
3.2.1. Geographical and Geological setting 65
3.2.2. Oceanography 67
3.2.3. Voe of Scatsta 68
3.3. Hebrides Islands 70
3.3.1. Geographical and Geological setting 70
3.3.2. Oceanography 72
3.3.3. Stoneybridge 73
3.4. Sumatra 75
3.4.1. Geographical and Geological setting 75
3.4.2. Oceanography 78
3.4.3. Lhok Nga 78
4. Methodology 81
4.1. Sampling and lithostratigraphic description 81
4.2. Textural analysis 81
4.2.1. Grain-size analysis 81
4.2.2. Calcium carbonate and organic matter content 82

4.2.3. Morphoscopy 82
4.3. Microtextural analysis 82
4.3.1. Laboratory procedure 83
4.3.2. Microtextural classification 83
4.3.3. Atlas of microtextural features in quartz grains 84
4.4. Mineralogy 85
4.4.1. Heavy minerals 85
4.4.2. Micromorphology analyses 85
4.5. Age-estimation methods 85
4.5.1. OSL 86
4.5.2. ^{210}Pb and ^{137}Cs 86
4.5.3. Radiocarbon 87
5 Results 89
5.1. Salgados 89
5.1.1. Lithostratigraphic features 89
5.1.2. Textural features 96
5.1.3. Morphoscopic features 100
5.1.4. Microtextural features 108
5.1.5. Heavy mineral features 114
5.2. Boca do Rio 121
5.2.1. Lithostratigraphic features 121
5.2.2. Textural features 123
5.2.3. Morphoscopy features 126
5.2.4. Microtextural features 129
5.2.5. Heavy mineral features 132
5.3. Voe of Scatsta 135
5.3.1. Lithostratigraphic features 135
5.3.2. Textural features 137
5.3.3. Morphoscopy features 138

5.3.4. Microtextural features 140
5.3.5. Heavy mineral features 141
5.4. Lhok Nga 145
5.4.1. Lithostratigraphic features 145
5.4.2. Textural features 146
5.4.3. Morphoscopy features 147
5.4.4. Microtextural features 149
5.4.5. Heavy mineral features 150
5.5. Stoneybridge 153
5.5.1. Lithostratigraphic features 153
5.5.2. Textural features 154
5.5.3. Morphoscopy features 154
5.5.4. Microtextural features 157
5.5.5. Heavy mineral features 158
6. Discussion 161
6.1. Textural signatures of extreme marine inundations 161
6.2. Morphoscopic signatures of extreme marine inundations 167
6.3. Microtextural signatures of extreme marine inundations 173
6.4. Heavy mineral signature of extreme marine inundations 185
6.5. Sedimentary environments and sedimentological differentiation 193
6.6. Single event signatures: the spatial contrast 195
6.7. Multiple event signatures 199
6.8. Storm vs tsunami deposits 203
7. Conclusions 205
7.1. Achievements and future work 205
References 209
Annex 1 – Geological legend lithostratigraphy of the windward sector of the Algarve 226
Annex 2 – Atlas of quartz grains 228

List of Figures

Figure 1.1 - Ph.D. studied areas. Figure 1A – Regional location of the Algarve. Figure 1B – Regional location of Shetland and Hebrides Islands. Figure 1C – Regional location of Sumatra. _____ *3*

Figure 2.1. - Schematic illustration of principal pathways of tsunami sediment transport and deposition (Dawson and Stewart, 2007 after Einsele et al., 1996). _____ *10*

*Figure 2.2 - Schematic summary diagram of different characteristics of tsunami and storm surge: in the ocean, at the coast, during run-up and inundation, along with a basic description of the resulting sediments. (Switzer and Jones, 2008).*_____ *40*

Figure 2.3 - Locations where some tsunami deposits have been described along the Atlantic Iberia coastline (sandy deposits numbered in red; boulder deposits numbered in black). 1: Aveiro - Corrochano et al. (2000); 2: Tagus estuary - Andrade et al. (2003); 3: Cascais - Scheffers and Kelletat (2005); 4: Tagus prodelta - Abrantes et al. (2005, 2008); 5: Huelva estuary - Morales et al. (2008); 6: Doñana - Ruiz et al. (2005); 7: Valdelagrana - Luque et al. (2001); 8: Cape Trafalgar - Whelan and Kelletat (2005); 9: Barbate and Tarifa - Reicherter et al. (2010); 10: Martinhal - Andrade et al. (1997), Kortekaas and Dawson (2007); 11: Barranco - Costa et al. (2011); 12: Boca do Rio - Dawson et al. (1995), Hindson and Andrade (1999), Hindson et al. (1996); 13: Salgados - Costa et al. (2009), Costa et al. (2012a); 14: Quateira - Schneider et al. (2009); 15: Ria Formosa - Andrade (1992). _____ *42*

Figure 2.4 - White dots show where tsunami deposits associated with theStoregga slide have been mapped. Other slides are the Trænadjupet slide dated to ca. 4000 14Cyr BP, slides on the NE Faroe margin and the small Afen slide in the Faroe–Shetland Channel (adapted from Bondevik et al., 2005). _____ *48*

Figure 2.5 – Areas studied by the International Tsunami Survey Team after the 2004 Indian Ocean tsunami (1- Krueng Sabe, 2- Leupeung, 3- Lhok Nga, 4- Lampuuk, 5- Banda Aceh, 6- Sigli). _____ *50*

Figure 3.1 - Main geomorphologic features and detailed tectonic characterization of the Gulf of Cadiz (adapted from Duarte et al., 2010). SWIM lineaments are several major WNW–ESE trending lineaments, recently interpreted as aligned arrays of also deep seated, sub-vertical dextral strike–slip faults. A) Location of the offshore SW Iberian Margin (3D digital bathymetry model from MATESPRO dataset); (B) general drainage system of the local continental shelf and slope. _____ *54*

Figure 3.2 - Geological map of the Algarve. Modified from Manuppella (1992). Legend is in Annex 1. _____ *56*

*Figure 3.3 – Geographical location of Lagoa dos Salgados.*_____ *60*

*Figure 3.4 - Oblique aerial view of Salgados lowland in March 2011 (provided by SB Teixeira - ARH-Algarve).*_____ *60*

Figure 3.5 – Drainage basin of Ribeira de Espiche/Lagoa dos Salgados. Modified from Manuppella (1992). Legend is in Annex 1. _____ *61*

Figure 3.6 – Geographical location of Boca do Rio. _____ *62*

Figure 3.7 – View to the Boca do Rio alluvial plain and beach (photo facing the east – C. Freitas). _____ *63*

*Figure 3.8 – Drainage basin of Budens, Vale de Boi and Vale de Barão streams that drain to Boca do Rio alluvial plain (east of Praia da Salema). Modified from Manuppella (1992). Legend is in Annex 1.*_____ *64*

Figure 3.9 - Geological map of the Shetland Islands (Geological Sketch map of Shetland, 2012, adapted from landforms.eu). 66
Figure 3.10 – Geographical location of Voe of Scatsta. 69
Figure 3.11 – View of Voe of Scatsta (photo P. Costa). To the north Sullom Voe terminal can be identified. 70
Figure 3.12 - Geological map of the Hebridean Terrane, NW Scotland (adapted from maps in Geology of Scotland, 2003). 72
Figure 3.13 – Geographical location of Stoneybridge. 74
Figure 3.14 - View of Stoneybridge (photo A. Dawson). 75
Figure 3.15 - Main geographical features of SE Asia (adapted from Hall, 2002). 76
Figure 3.16 - Geological and tectonic map of Sumatra (Barber and Crow, 2005). 77
Figure 3.17 - Geographical location of Lhok Nga. 79
Figure 3.18 - Figure A – Image of Lhok Nga area obtained by satellite Ikonos immediately after the tsunami of December 2004. Figure B – Orthophotography of Lhok Nga area obtained in June 2005. 79
Figure 4.1 Microtextural features. A0 to A5 – angularity (very rounded to very angular). B1 – percussion marks. B2 – detailed view of percussion mark. C1 – fresh surface (in this case, sharp edge, fractures and steps). C2 – detailed view of fresh surface. D – dissolution (especially visible on the right face of the grain). E – adhering particles (more visible in the center of the grain). 84
Figure 5.1.1 – Cores and surface samples collected in Lagoa dos Salgados. 89
Figure 5.1.2 – Photos of contact of Unit E with under and overlying units identified in Lagoa dos Salgados. 93
Figure 5.1.3 – Cross-sections based in the lithostratigraphical correlation of cores collected across the Salgados lowland. A-Profile N-S; B- Profile NE-SW; C- Profile NW-SE. See text for lithostratigraphic unit characterization. 94
Figure 5.1.4 – A - Interpolated values of Unit E median grain size. B- Interpolated values of D10. 97
Figure 5.1.5 – A - Percentage of sand of unit E sediments. B – Simple skewness measure of unit E sediments. 97
Figure 5.1.6 - Compositional characteristics of sample from unit E and sample 14_(0.20-0.28) from Lagoa dos Salgados, based in morphoscopic observation. 102
Figure 5.1.7 - Roundness classification of quartz grains from unit E and sample 14_(0.20-0.28) from Lagoa dos Salgados, based in morphoscopic analysis. 102
Figure 5.1.8 – Lagoa dos Salgados unit E and sample 14_(0.20-0.28) shape characteristics based in morphoscopic observation. 103
Figure 5.1.9 – Dune and beach samples (Lagoa dos Salgados) compositional characteristics based in morphoscopic observation. 103
Figure 5.1.10 – Dune and beach samples from Lagoa dos Salgados and their roundness classification based in morphoscopic observation. 105
Figure 5.1.11 –Dune and beach samples (Lagoa dos Salgados) shape characteristics based in morphoscopic observation. 105

Figure 5.1.12 – Nearshore samples from Lagoa dos Salgados and their compositional aspects based in morphoscopic observation. 106
Figure 5.1.13 – Nearshore (Lagoa dos Salgados) samples roundness characteristics based in morphoscopic observation. 106
Figure 5.1.14 – Nearshore (Lagoa dos Salgados) samples shape characteristics based in morphoscopic observation. 107
Figure 5.1.15 – SEM images of quartz grains from the Lagoa dos Salgados. A- Dune; B- Beach; C- Proximal nearshore; D- Distal nearshore; E- unit E, F- detail of percussion marks (approximately 12 microns in length) imprinted on the surface of a grain from unit E. 108
Figure 5.1.16 – Microtextural results and their spatial distribution in fraction 1-3 Φ of samples from unit E and 14_(0.20-0.28) from Lagoa dos Salgados. 109
Figure 5.1.17 - – Microtextural results and their spatial distribution in samples from the dune and beach from Lagoa dos Salgados. 110
Figure 5.1.18 - – Microtextural results and their spatial distribution in the nearshore samples from Lagoa dos Salgados. 111
Figure 5.1.19 - – Heavy minerals results and their spatial distribution in samples from unit E and 14_(0.20-0.28) from Lagoa dos Salgados. 116
Figure 5.1.20 - Heavy minerals results and their spatial distribution in dune and beach samples from Lagoa dos Salgados. 117
Figure 5.1.21 - Heavy minerals results and their spatial distribution in nearshore samplesfrom Lagoa dos Salgados. 117
Figure 5.2.1 – Lithostratigraphic and macroscopic log description of sample-core SAO that roughly corresponds to the schematic lithostratigraphy of the alluvial plain topmost meter. 122
Figure 5.2.2 – Photographs of sampling in one trench within the alluvial plain of Boca do Rio. The yellowish sand is the unit associated with the AD 1755 tsunami. The plastic box is 0.30 m long. 122
Figure 5.2.3 – Sampling locations within Boca do Rio area. A – Regional location. B - Samples collected within the alluvial plain. C- Samples collected in the nearshore of the Boca do Rio area. 123
Figure 5.2.4 – Inverse Distance Weighting extrapolation for percentage of sand (A) and median grain size (b) for samples retrieved from the tsunamigenic unit in Boca do Rio. 125
Figure 5.2.5 - Image of a 7.5x4.5 cm thin section from the tsunamigenic layer and underlying mud (sample BDR_T2_97_105). 126
Figure 5.2.6 - Morphoscopic compositional characteristics of samples from Boca do Rio. A – Nearshore samples. B – Beach, dune, alluvial and tsunami samples. 127
Figure 5.2.7 – Roundness classification of nearshore samples (A) and beach, dune, aluvial and tsunami samples (B) from Boca do Rio. 127
Figure 5.2.8 - Sphericity classification of nearshore samples (A) and beach, dune, aluvial and tsunami samples (B) from Boca do Rio. 129

Figure 5.2.9 – Microtextural results and their spatial distribution in Boca do Rio. A- Nearshore samples. B-Beach, dune and tsunami samples. _____ *130*
Figure 5.2.10 – Heavy mineral composition of nearshore samples (A) and beach dune and tsunami sample (B) from Boca do Rio. _____ *133*
Figure 5.3.1 – Location of cores obtained in Voe of Scatsta, Shetland Islands. _____ *135*
Figure 5.3.2 – Photo of the trench wall (left image) were sample SHT_1 was collected. Detail of the tsunamigenic unit (right image; blue rectangle is app. 0. 10 m). _____ *136*
*Figure 5.3.3 – Lithostratigraphy of core SHT_1 retrieved in Voe of Scatsta.*_____ *136*
*Figure 5.3.4 – Image of a 7.5x4.5 cm thin section from sample SHT_3 (22-30).*_____ *138*
Figure 5.3.5 – Morphoscopic compositional features of samples retrieved from Voe of Scatsta. _____ *139*
Figure 5.3.6 – Roundness classification for quartz grains from samples collected in the Voe of Scatsta. _____ *139*
Figure 5.3.7 - Shape classification for quartz grains from samples collected in the Voe of Scatsta. _____ *140*
Figure 5.3.8 - Microtextural features results and spatial distribution in samples retrieved from the Voe of Scatsta. _____ *141*
Figure 5.3.9 - Heavy mineral composition of tsunamigenic samples collected in Voe of Scatsta. _____ *143*
Figure 5.4.1 - Location maps of the Lhok Nga Bay and collected samples (Paris et al., 2007). _____ *145*
Figure 5.4.2 - Sequence stratigraphy and interpretation of the vertical trends along the Lhok Nga transect (Paris et al., 2007). _____ *146*
Figure 5.4.3 - Morphoscopic compositional features of samples retrieved from Lhok Nga. _____ *148*
Figure 5.4.4 - Roundness classification for quartz grains from samples collected in Lhok Nga. _____ *148*
Figure 5.4.5 - Shape classification for quartz grains from samples collected in Lhok Nga. _____ *149*
*Figure 5.4.6 - Spatial distribution of microtextural results in sediments retrieved from Lhok Nga.*_____ *150*
Figure 5.4.7 - Heavy mineral composition of tsunamigenic samples collected in Lhok Nga. _____ *152*
Figure 5.5.1 - – Location of samples obtained in Stoneybridge, Hebrides Islands _____ *153*
Figure 5.5.2 - Image of the sandy storm deposit retrieved from Stoneybridge. _____ *154*
Figure 5.5.3 - Morphoscopic compositional features of samples retrieved from Stoneybridge. _____ *155*
Figure 5.5.4 - Roundness classification for quartz grains from samples collected in Stoneybridge. _____ *156*
Figure 5.5.5 - Shape classification for quartz grains from samples collected in Stoneybridge. _____ *156*
*Figure 5.5.6 - Microtextural features results and their distribution across the storm layer retrieved in Stoneybridge.*_____ *157*
Figure 5.5.7 - Heavy mineral composition of tempestite samples collected in Stoneybridge. _____ *159*
Figure 6.1 - Percentage of sand and calcium carbonate within the tsunamigenic unit E on cores LV7 and LV10 (Salgados). _____ *162*
Figure 6.2 – Principal component analysis; morphoscopic compositional study of Salgados samples. Note: left image - B-beach samples; D- dune samples; N-nearshore samples; Tsu – tsunami samples. _____ *168*
Figure 6.3 – Principal component analysis; roundness of Salgados samples. Note: left image - B-beach samples; D- dune samples; N-nearshore samples; Tsu – tsunami samples. _____ *168*

Figure 6.4 – Principal component analysis; sphericity of Salgados samples. Note: left image - B-beach samples; D- dune samples; N-nearshore samples; Tsu – tsunami samples. 169
Figure 6.5 – Principal component analysis; roundness of Boca do Rio samples. Note: left image – A – alluvial sample; B - beach sample; D- dune samples; N-nearshore samples; Tsu – tsunami samples. 169
Figure 6.6 – Principal component analysis; sphericity of Boca do Rio samples. 169
Figure 6.7 – Principal component analysis; roundness of Lhok Nga samples. 171
Figure 6.8 – Principal component analysis; sphericity of Lhok Nga samples. 171
Figure 6.9 – Analysis of microtexture features in box-plot diagrams for each group of samples (extreme marine inundations and sedimentary environments). 175
Figure 6.10 – Comparison of microtextural (angularity; fresh surfaces; dissolution; adhering particles; percussion marks) results according to the location where the tsunami or storm samples were collected. 176
Figure 6.11 – Bivariate plot of percussion marks vs dissolution on all samples analysed. 178
Figure 6.12 – Ternary plots of percussion marks, fresh surface and dissolution (left image) and percussion marks, fresh surface and adhering particles (right image) on all samples analysed. (Note: StormHB- storm sample from Hebrides; StormP- storm sample from Portugal; TsuInd- tsunami sample from Indonesia; TsuPort- tsunami sample from Portugal; TsuSHT- tsunami sample from Shetland). 178
Figure 6.13 – Principal components analysis of the microtextures analysed and samples based in the two main factors identified. (Note: StormHB- storm sample from Hebrides; StormP- storm sample from Portugal; TsuInd- tsunami sample from Indonesia; TsuPort- tsunami sample from Portugal; TsuSHT- tsunami sample from Shetland). (Clr –centered log-ratio transformation; Z – random vector; T – variation matrix; Γ – covariation matrix; V – matrix used in clr transformation; U – random vector). 179
Figure 6.14 – Glass microsphere image. A – Microsphere image before experiments. B – Microsphere image after 60 minutes at 1100 rpm with a sediment concentration of 20%. Red arrow marks fresh surface. C – Microsphere image after 6 minutes at 1100 rpm with a sediment concentration of 2%. Red arrow marks fresh surface. D - Microsphere image after 60 minutes at 700 rpm with a sediment concentration of 40%. Red arrows mark percussion marks and white arrow marks long abrasion mark. 181
Figure 6.15 - Conceptual transport model for sedimentary environments and high energy events based in microtextural features of quartz grains analysed. A – Sedimentary environments and associated dominant microtextures. B – Grain transport during a tsunami wave incursion. 183
Figure 6.16 – Principal component analysis of extreme marine inundations samples and their heavy mineral assemblage. Note: left image – IND – tsunami samples Indonesia; P – tsunami samples Portugal; Str_P – storm sample Portugal; Str_HB – storm sample Hebrides; SHT – tsunami samples Shetland. 185
Figure 6.17 – Ternary plot of staurolite, andalusite and tourmaline assemblages in Salgados. 187
Figure 6.18 – Percentage of heavy mineral in total sediment fraction (left image) and percentage of staurolite (right image) observed in beach, dune, nearshore, tsunami and storm samples retrieved from Salgados. 188
Figure 6.19 – Principal component analysis of heavy mineral assemblage retrieved from Salgados. Note: left image - B-beach samples; D- dune samples; N-nearshore samples; Tsu – tsunami samples. 190

Figure 6.20 – Ternary plot of staurolite, andalusite and tourmaline assemblage from Boca do Rio samples. _ 190

Figure 6.21 – Box-plot diagrams of heavy mineral assemblages from samples retrieved in Boca do Rio. ____ 191

Figure 6.22 – Principal component analysis of heavy mineral assemblages from samples retrieved in Boca do Rio. _____ 191

List of Tables

Table 2.1 - Beaufort wind scale (US Army Corps of Engineering, 2003). 6
Table 2.2 - Table summarizing the criteria to identify and differentiate tsunami deposits. 33
Table 3.1 - Storm occurrences offshore the Algarve coast between 1955 and 1986 (LNEC, 1987). 58
Table 3.2 - Return period offshore the south facing coast of the Algarve (Pessanha and Pires, 1981). 58
Table 3.3 - Extreme water levels and local chart datum in metres above Ordnance Datum (Richard and Phipps, 2007). 73
Table 5.1.1 - Radiocarbon dates obtained for Lagoa dos Salgados Upper Holocene stratigraphic sequence. 95
Table 5.1.2 - Textural data from selected samples of Lagoa dos Salgados. 98
Table 5.1.3 - Microtextural results obtained with the Lagoa dos Salgados samples. 112
Table 5.1.4 - Percentage of heavy minerals in total sediment in samples from Lagoa dos Salgados. 115
Table 5.1.5 - Heavy mineral composition in samples from Lagoa dos Salgados. 119
Table 5.2.1 - Summary of textural attributes of samples collected in Boca do Rio. 124
Table 5.2.2 - Microtextural results of samples from Boca do Rio. 131
Table 5.2.3 - Percentage of heavy mineral composition in total sediment of samples from Boca do Rio. 132
Table 5.2.4 - Results from heavy mineral assemblages in the Boca do Rio samples. 134
Table 5.3.1 - Summary from the textural results obtained for samples collected in Voe of Scatsta. 137
Table 5.3.2 - Summary of microtextural results obtained in samples from Voe of Scatsta. 141
Table 5.3.3 - Percentage of heavy mineral content in total sediment of samples from Voe of Scatsta. 142
Table 5.3.4 - Heavy mineral assemblages in sand samples of Voe of Scatsta. 142
Table 5.4.1 - Mean grain size of samples retrieved from Lhok Nga (data provided by R. Paris). 147
Table 5.4.2 - Summary of microtextural results obtained in samples from Lhok Nga. 150
Table 5.4.3 - Percentage of heavy mineral content in total sediment of samples from Lhok Nga. 151
Table 5.4.4 - Results from heavy mineral assemblages in Lhok Nga samples. 151
Table 5.5.1 - Summary of textural characteristics of samples retrieved from Stoneybridge. 154
Table 5.5.2 - Summary of microtextural results obtained in samples from Stoneybridge. 158
Table 5.5.3 - Percentage of heavy mineral content in total sediment of samples from Stoneybridge. 158
Table 5.5.4 - Results from heavy mineral assemblages in the Stoneybridge samples. 159
Table 6.1 - Mean values for textural data from present day analogues from Salgados. 165
Table 6.2 - Summary of sedimentological data by studied site. 165
Table 6.3 – Specific gravity for main minerals studied. 186
Table 6.4 – Comparison of sedimentological features of the tsunamiites studied in this work. 201
Table 6.5 – Sedimentological characteristics of storm deposits from Salgados and Stoneybridge and their differentiation from tsunami deposits. 204

Every great advance in science has issued from a new audacity of imagination.

John Dewey (1859-1952)

1. Introduction

1.1. Relevance of study

The study and understanding of coastal hazards is a fundamental aspect for most modern societies. The consequences of extreme events such as tsunamis and storms are being regarded as major threats for coastal regions. Furthermore, the rising costs of natural hazards (in human lives and economically) as a direct effect of the increasing occupation of the coast has raised the public awareness on the importance of the study of these events. Although many studies have been conducted in this subject there is still a wide range of aspects that need further investigation in order to fundament effective mitigation or adaptation procedures. Because of the non-deterministic nature of processes underlying coastal inundation the quantitative approach to their occurrence is in essence empirical and requires long series of observations to fundament estimations of vulnerability and risk. Some scientists have extended the empirical database beyond the historical record through the use of palaeoevent sedimentary deposits and have derived frequency and intensity estimates from the stratigraphic record. Because palaeoevent analyses are used to predict event recurrence and to conduct vulnerability and risk assessments, it is essential to be able to distinguish between tsunami and storm deposits in the sedimentary record. In that sense, the enhancement of the recognition and differentiation of tsunami and storm sedimentological signatures through the application of diverse techniques is a pertinent and innovative contribution of this work, which applies microtextural analysis and heavy mineral characterization to discuss marine inundation deposits and their possible source materials together with other attributes more widely used. Furthermore, this thesis presents results from a variety of geographical locations (Portugal, Indonesia and Scotland), of different chronologies (AD 1755, 26th December 2004, the 2nd Storegga Slide tsunamis and the Great Storm of 11th January 2005) and different coastline configurations and contrasting oceanographic conditions (Figure 1.1). The use of such a multiplicity of contexts provides a unique sustenance for conclusions to be drawn regarding the characterization and differentiation of extreme marine inundations sedimentary signatures.

1.2. Aims and objectives

This work offers a novel opportunity to address a relevant aspect for many coastal areas worldwide: to extend the time dimension of the database analysed for the establishment of extreme marine inundation risks. With that purpose a location in the Algarve coast of Portugal (Salgados), where a new tsunamigenic deposit associated with the AD 1755 was observed and characterized, is presented. This location offers a number of features providing further evidences of the path followed by the tsunami overwash and hopefully will contribute to the clarification of the on-going debate about the AD 1755 epicentre and tsunami

generation area. Furthermore, the re-analyses of several locations (Boca do Rio, Sullom Voe and Lhok Nga), where tsunami deposits have been previously detected, allows an adequate background to test the application of different sedimentological proxies in areas that suffered from the impact of extreme marine inundations of which independent descriptions exist and where the sediment record conserved evidences of those events.

A specific storm deposit (Stoneybridge, Scottish Outer Hebrides) was also analysed and compared with tsunamigenic signatures from the above mentioned locations. The fact that a significant range of locations, age and events were analysed permits the successful application and generalization of techniques such as grain microtextural imprints and mineralogical signature observed in samples from all locations. Although local details can be relevant factors, an important achievement of this work is to test and increase the number of proxies that can be used in the sedimentological analysis of tsunami and storm deposits.

In agreement with the line of thought mentioned above, a number of work purposes were identified and subsequent field and office work and laboratory analyses were conducted in order to achieve the following objectives:

a) To recognize coastal sediments deposited by Holocene extreme marine inundations;

b) To analyse sediment samples using a multidisciplinary approach;

c) To apply microtextural analysis in order to establish the source material or/and to identify specific signatures of extreme marine inundations in coastal sediments;

d) To apply heavy minerals to establish source material or/and to identify specific signatures of extreme marine inundations in those materials;

e) To forward, whenever possible, return periods for extreme marine inundations;

f) To contribute to developing criteria able to recognize and differentiate tsunami and storm deposits.

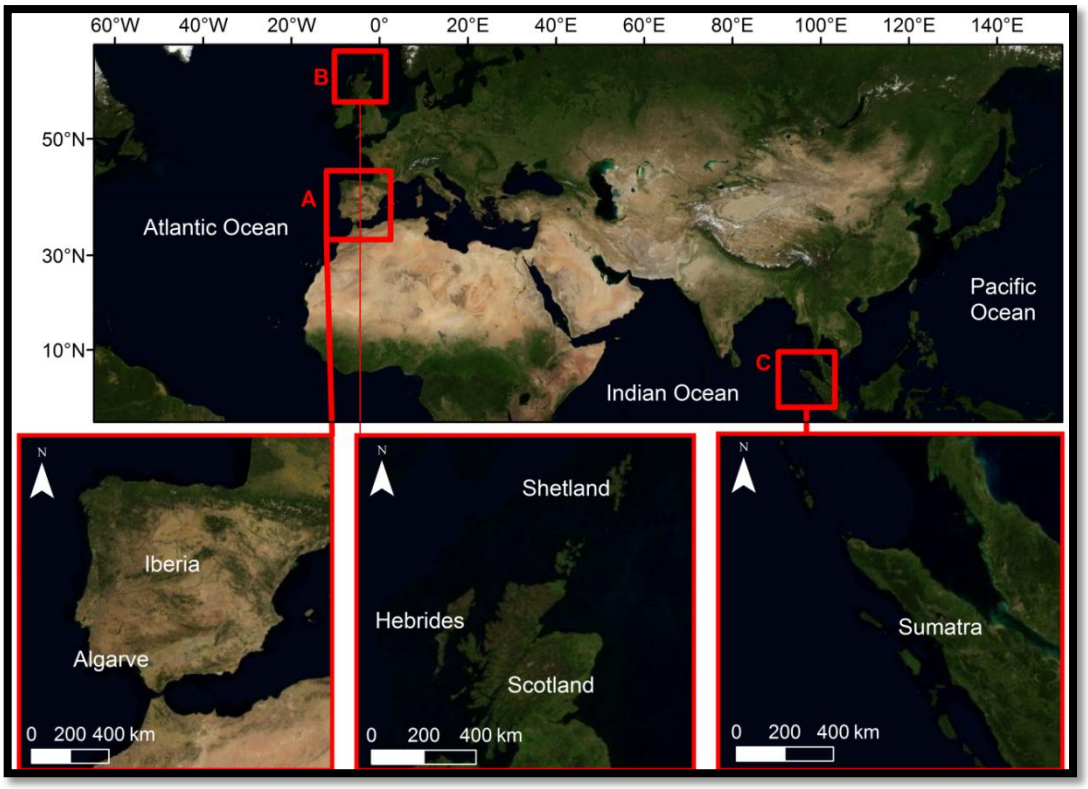

Figure 1.1 - Ph.D. studied areas. Figure 1A – Regional location of the Algarve. Figure 1B – Regional location of Shetland and Hebrides Islands. Figure 1C – Regional location of Sumatra.

1.3. Structure of document

This document is organized in order to present the data in association with each study area mainly due to the fact that this structure would provide the reader the opportunity to analyse each case on its own and generalize interpretations and conclusions at a later stage. The adopted structure also permits a better understanding of each methodological result regardless of the number of samples (that varied due to constrains in sampling).

The thesis is divided in an introductory part (Chapters 1, 2, 3 and 4), a data presentation part (Chapter 5) and a discussion and conclusion part (Chapters 6 and 7). Chapter 1 presents a brief description of the aims and structure of the thesis. This chapter stresses the relevance of this research for the wider problem of coastal hazard and the contribution to tsunami and storm sedimentary recognition and their differentiation. Chapter 2 is organized in five sub-chapters. Sub-chapter 2.1 presents a concise summary of the physical aspects associated with storms and tsunamis (*i.e.* generation, propagation, run-up and backwash). The following sub-chapter (2.2) considers the geological signature of extreme marine inundations by presenting a summary of the work conducted and by describing the different types of characteristics associated with these extreme marine events. Sub-chapter 2.3 presents a revision of the criteria associated with the recognition of tsunami deposits in coastal stratigraphy. Sub-chapter (2.4) debates the controversy associated with the differentiation of tsunami and storm deposits and the respective coastal

hazards. A summary of previous research conducted in the study areas is the focus of sub-chapter 2.5. This sub-chapter is sub-divided in three parts, one for each regional study area (Algarve, Scotland and Indonesia). The detailed geographical, geological and oceanographic characterization of the study areas is the focus of Chapter 3. Chapter 4 presents the methodology used in this research. A description of the sampling, lithostratigraphic, textural, morphoscopic, micromorphological, microtextural, mineralogical and age-estimation techniques used in this work are presented in this chapter. Chapter 5 presents results from Salgados (Algarve, Portugal), Boca do Rio (Algarve, Portugal), Voe of Scasta (Shetland Islands, Scotland), Lhok Nga (Sumatra, Indonesia) and Stoneybridge (Hebrides Islands, Scotland). This chapter is divided into five sub-chapters (*i.e.* one for each specific study area). The results in each sub-chapter are presented in the following order: lithostratigraphic, textural, morphoscopic, microtextural and mineralogical results. In the lithostratigraphy section the sampling strategy, the lithostratigraphic data, the spatial architecture of the deposit and the chronology are presented. In the textural results, the data presented include an analysis of grain-size characteritics. The morphoscopy data presents the percentage of quartz, lithic material and bioclasts within the studied samples, as well as the roundness and sphericity character of quartz grains from the analysed samples. The microtextural results include the exoscopic analysis of quartz grains. Finally, the mineralogical results provide an analysis of the heavy mineral content for each study area.

The final part of the thesis is dedicated to the Discussion (Chapter 6) and Conclusions (Chapter 7). Chapter 6 interprets and discusses the results presented in the previous chapter and it is divided into eight sub-chapters. Sub-chapter 6.1 considers the textural and lithostratigraphical features of extreme marine inundations. Sub-chapter 6.2 debates the morphoscopic signatures of the analysed tsunami and storm samples. The following sub-chapter (6.3) discusses the microtextural features associated with extreme marine events. Sub-chapter 6.4 comprises an investigation of heavy mineral assemblages as an aid in the differentiation of tsunami and storm deposits. Sub-chapter 6.5 briefly discusses the differentiation of sedimentary environments. Sub-chapter 6.6 compares several sedimentological characteristics of deposits lay down by a single event. Sub-chapter 6.7 widens the discussion by addressing the sedimentological characterization of multi-tsunamigenic events. The succeeding sub-chapter (6.8) presents an analysis of the sedimentary characteristics of tsunami and storm deposits while comparing different events.

The conclusions in chapter 7 summarize the major achievements and inferences resulting from this work and these are completed by the proposal of future research lines and work to be conducted in this field of Science. In addition to the main document, this Ph.D. thesis includes supplementary information organized in 2 Annexes. Annex 1 consists of the geological legend of the Geological map of the Algarve. Annex 2 presents an Atlas of microtextural features observed in quartz grains; this annex provides a comprehensive view of the full variety of microtextures found, studied and interpereted by the author and is a contribution to the few existing publications on microtexture characterization and interpretation of quartz grains.

2. State of the art

2.1. Extreme marine inundations: origin and mechanisms

Extreme marine inundations triggered by tsunami and storms have an undoubtedly important significance for studies on coastal evolution and coastal management. The investigation of these events is a major concern for many scientists, trying to understand the underlying processes and contributing to mitigate impacts of the inundations. The understanding of the associated physics is of unquestionable interest for obvious reasons, but also from a (less immediate) geological perspective: allowing a better comprehension of the consequences of such events, namely of those that will certainly occur in the future with magnitude exceeding the largest observed or documented event in history.

Storms are produced by meteorological disturbances and generate high energy waves and surf, whereas the most frequent causes of tsunamis are related with offshore rupture and significant vertical displacement of the seafloor, thus implying large magnitude ruptures. These are induced either by tectonic stress and associated to earthquakes, or by both sub-areal and submarine large-scale landslides. Furthermore, meteorite impacts and the collapse of volcanic buildings and other large-scale volcanic processes may also generate tsunamis.

Storms are one of the most alarming natural hazards due to their frequency at annual time scales and concentration of resources and population in coastal areas. The erosional capacity of storms is one of its main features; however, in some circumstances, storms can also leave a sedimentological signature in the stratigraphy of a given coastal area normally resting above sea level, if overwash allows for extensive inundation of the landward section of the coastal area by sediment-loaded marine water. Storms are produced by effects of wind and atmospheric-pressure differences in the surface of the ocean. Storms can be classified in agreement with the Beaufort wind scale (Table 2.1).

Extreme storms such as hurricanes (also called Typhoons in the Indian Ocean) are produced when high-speed winds tend to spiral inland towards a core of very low pressure. When any storm occurs the rise in wave heights (and thus in the energy they carry and dissipate at the coast when breaking) is noticeable. In addition to wave energy, low pressure may increase the sea level well above the astronomical tide level, raising the ocean surface by considerable amounts and facilitating the inundation of the coastal land.

Storms are major agents of coastal forcing given their potential to transport sediments alongshore and cross-shore. According to Andrade *et al.* (2004) clastic shores in mesoscale equilibrium with the wave regime, as well as starved coasts, are particularly sensitive to storms because the instantaneous disturbances generated by storms may exceed the resilience of the coastal system, which is unable to resume the previous equilibrium conditions in the absence of a relevant external source of sediment.

Table 2.1 - Beaufort wind scale (US Army Corps of Engineering, 2003).

Beaufort number	Wind speed (knots)	World Meteorological Organization description
0	<1	Calm
1	1-3	Light air
2	4-6	Light Breeze
3	7-10	Gentle Breeze
4	11-16	Moderate Breeze
5	17-21	Fresh Breeze
6	22-27	Strong Breeze
7	28-33	Near Gale
8	34-40	Gale
9	41-47	Storm Gale
10	48-55	Storm
11	56-63	Violent Storm
12	>64	Hurricane

It is necessary to examine the past decadal- to millennial-scale variability of storm activity in order to determine the frequency of the most extreme events in relation to the climate evolution. Regional studies on the long-term variability of storm frequency, magnitude and tracks and of storm-related hazards (*e.g.* Orford *et al.*, 1996; Langenberg *et al.*, 1999; Kaas *et al.*, 2000) suggest that they have been changing throughout the last 150 years, although there is no evidence of a trend in this time interval The extension of the observation period further back in time, therefore including the geological record, allows the reconstruction of storminess patterns that may be used to re-evaluate the return period of most extreme events, which are generally extrapolated from short-term instrumental series of observations (Andrade *et al.*, 2004). Furthermore, it has been established that negative North Atlantic Oscillation (NAO) index winters are associated with a southward shift in the Atlantic storm activity and a noticeable increase in storm activity in Iberia (Hurrell, 2003). They are also reflected in Portugal by increased precipitation and fluvial floods (Trigo *et al.*, 2004), as well as higher sea-level caused by barometric lows and reinforced westerly winds (Guerra *et al.*, 2000). An inverse correlation between NAO values and the solar activity was also established (Kirov and Georgieva, 2002) and consequently low solar irradiance corresponds to lower storminess. One can state that research on causes and variations in storm intensity, and especially in investigation of storminess trends, is a key issue in projecting the impact of storminess in the future evolution of coasts. In this context, finding sedimentological records of past catastrophic storm events are essential to evaluate the long term climatic evolution in a given coastal area allowing to separate variations corresponding to trends from long term oscillations.

In terms of risk to coastal assets and probability of generating a conspicuous record in the coastal sedimentary archive surges generated by storms is their most relevant facet. Storm surges are changes in sea level caused by extreme weather events. In both tropical and extra-tropical regions they are generated by intense cyclones and especially hurricanes, the latter being characteristic of the former regions. The impact of the surge is dependent of the size, duration, strength, velocity and track of the meteorological disturbance but it also depends of the morphology and extension of the shelf margining of the target coast.

Storm surges are common in many coastlines all over the world and literature on storm impacts is to a large extent biased to the settings where they play the major role in coastal forcing and responsibility for damages. However, this is not the case of mainland Portugal, where the dimensions and morphology of the shelf, location within the extratropical zone and exposurue to high wave energy, indicate that direct wave action exceeds in relevance the effects of storm surge (*e.g.* SIAM I and II project - Santos *et al.*, 2002 and Santos and Miranda, 2006). In this respect, storm waves, even exceptional in energy, differ from tsunamis because they break and release most of the associated energy within the seaward section of the coastal zone. An increase in height of a wind wave will inevitably induce breaking at increased depth, thus extending the dimension of the surf zone. This is in clear contrast with tsunami waves which, regardless their height, are always very large in length, exceeding by far the longest wind-gerated wave. This makes a substantial difference in the type and amount of work and impact that a wind or a tsunami generated wave can produce when impinging on a coastal area.

The word tsunami is a phonetic transcription from the Japanese word meaning “harbour wave”, not in the sense used in hydraulics and coastal enegineering (seiche) but reflecting the belief that they formed very close to the harbours or fishing settlements. According to Lapidus (1990), “Tsunami is the gravity-wave system that follows any short-duration, large-scale disturbance of the free sea surface.” A tsunami generally consists of a small number of long-period solitary waves that can be generated by any disturbance that displaces a large water mass from its equilibrium position. Tsunami waves are usually small in height and barely noticed in the deep ocean, but they grow in height (sometimes to dramatic dimensions) and increase the potential to cause damage when travelling in shallow water, namely just before impacting the coast (Sugawara *et al.*, 2008). Tsunami waves can travel virtually unnoticed through the open ocean because of extreme low values of steepness (essentially modulated by very large wavelength), an attribute that normally prevents breaking throughout the whole travel distance. Thus destruction caused by tsunamis is the direct result of abrupt inundation of extensive costal ribbons, accompanied by impact on structures and erosion. Besides hitting coastal targets unbroken, one other important difference to wind waves is that the time intervals spent by the inundation and seaward back flow associated to each tsunami wave exceeds by at least two orders of magnitude the ones of a wind wave.

The life span of a tsunami may be divided into three stages: the generation (discussed above), the stage of propagation to the coast and finally the inundation of the coastal fringe with intensity that may be quantified in terms of run-up and run-in.

The equation describing tsunami wave celerity while propagating anywhere in the sea is given by linear theory as the "shallow water equation":

$$c = \sqrt{gh} \qquad \textbf{Equation 2.1}$$

where c is wave celerity (ms^{-1}); g is gravitic acceleration (ms^{-2}) and h is local depth (m).

The non-linear character of this relation, showing that celerity (and thus wavelength) solely depends on depth and nearly complete conservation of total energy by water waves during propagation, explains the dramatic consequences of shoaling effects on tsunami waves when propagating in very shallow coastal waters. Conservation of total energy can only be achieved if the very significant reduction in the kinetic component accompanying propagation in progressively shallower water is compensated by an increase in potential energy, measurable by the difference in elevation between crest and trough – the wave height.

If the triggering mechanism of a tsunami corresponds to a point-source (*e.g.* vocanic explosion, slope mass movement) the waves will radiate from the source with a strong angular dispersion and affect a progressively wider fan-shaped domain. The length of the leading wave crest will increase exponentially with time and thus the associated energy density will necessarily decrease. This explains the strong attenuation characterizing most events triggered by avalanches, slides or volcanic activity, their impacts being felt essentially in targets located at short distances from the source. The exceptions are associated with infrequent mechanisms capable of displacing extremely large volumes along the sea floor (such as the 2nd Storegga slide) and affecting the shores of a wide oceanic basin. In contrast, an extensive rupture of the sea floor, such as promoted by a major thrust fault system, can better be described as a linear source, thus disturbing the simple circular-shaped radiation model. In this case, most of the wave energy is focused in the direction perpendicular to the strike of the main source and only the energy propagating parallel to the regional tectonic trend leaks laterally and is strongly diminished in density. If the rupture area is located close to or within a continental margin, within several minutes after generation the initial disturbance is split into a wave set that travels out to the deep ocean (a distant or tele-tsunami regarding the impacted areas on the opposite margin) and another that travels towards the nearby coast (local tsunami). Several events happen as the local tsunami travels over the continental slope and shelf. The most obvious one is that the wave amplitude increases. The tsunami energy flux, which is dependent on both the wave speed and wave height, remains nearly constant. Consequently, as the tsunami speed diminishes as it travels into shallower water, its height grows. Because of this shoaling effect, a tsunami, imperceptible at deep sea, may grow to be several meters in height near the coast. Moreover, the propagation path is sensitive to the ocean bottom morphology, an effect shared also by wind waves and described by the laws of wave refraction. Bottom morphology, analogously to an optical lens, may focus or defocus (*sic*, Tinti, 1990) the water wave rays, thereby increasing or decreasing the wave amplitude by modulating their energy and power density. The effects of refraction are more evident in the case of tsunamis given their larger wave length and explain why in most cases the wave angles at the shore are reduced.

As the tsunami wave travels from the deep-water through the continental slope and shelf to the nearshore and finally the coastal region, the height attained by the wave crest may exceed the shore elevation, thus allowing for inundation of terrestrial land (Figure 2.1). The excess water brought in by the incoming wave crest (which extends hundreds of meters into the ocean) is pushed further inland at very high speeds until the counter effects of attrition and gravity stop inundation from progressing further inland. The intensity of the inundation is usually described in terms of run-up and run-in. Run-up is usually defined as the maximum height attained by the flood water onshore, measured above a reference sea level, though some authors have used the term to describe the maximum height (on land) reached by a tsunami as it encounters the coast. Both definitions yield different values characterizing the same event and the former is adopted in this study. Run-in or depth of inundation is the maximum horizontal distance landward of the coastline that the tsunami inundation was able to reach. Run-up is primarily controlled by the length and amplitude of the tsunami waves, coastal shape and by the bathymetric profile of the sub-littoral shelf and slope regions across which the tsunami is approaching the coast (Bourgeois *et al.* 1999; Tappin *et al.* 2001; Weiss *et al.* 2006). In addition, roughness and slopes of the dryland met by the inrushing flood also control both the run-up and run-in. Consequently, run-up heights, distances and flow depths of inundation can vary significantly along a given shoreline.

After the inundation, part of the tsunami energy is returned back to the ocean as a huge, long-lasting and typically channelled backwash. In addition, a tsunami can excite a particular type of standing waves (edge waves) that oscillate parallel to shore and are entrapped in the coastal zone. The interference between incoming and edge waves may further complicate the longshore distribution pattern of wave height at the shore with implications in run-up and run-in. Because of this complicated behaviour near the coast and of the changes in attrition of the coastal surface following the first inundation, the first run-up and run-in of a tsunami are often not the largest. The arrival of a tsunami surge is sometimes preceded by extensive retreat of the sea, exposing the sea-bottom, and there are several terms that are used to describe this phenomenon. The one to use depends on circumstances (*e.g.*, whether the tsunami is in a bay or estuary) and on personal preference. The terms “negative wave”, “drawdown” and “withdrawal” are most often used to describe this type of initial onset. Less formal are the terms 'waterline receding' and “bay emptying”. The underlying reason for this effect is that both offshore landslides and earthquakes may create a negative pattern of disturbance of the sea surface (trough) on the shoreward side of the bottom deformation, in relation with sudden and localized decrease of the water depth, if this trough propagates to the shore and arrives there before the following crest, it produces the drawdown (GITEC-2, 1995). In coastal areas the devastation produced by a high magnitude tsunami can be enormous. The destruction of infrastructures caused by tsunamis is due to “drag and flotation forces associated with the waves (...), strong induced currents (...) and floating debris” (Tinti, 1990).

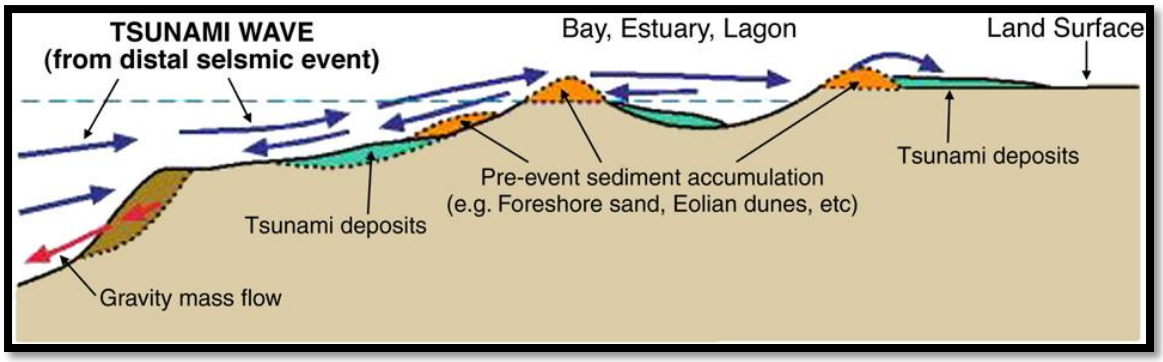

Figure 2.1. - Schematic illustration of principal pathways of tsunami sediment transport and deposition (Dawson and Stewart, 2007 after Einsele *et al.*, 1996).

The two most important aspects that characterise tsunamis are the magnitude and the intensity. The traditional magnitude scale is the so-called Imamura-Iida (Iida, 1963). The magnitude value (m) is approximately equal to:

$$m = \log_2 h \qquad \textbf{Equation 2.2}$$

where h is the maximum run-up height in meters.

Hataori (1979) extended the Imamura-Iida m scale to include far-field tsunami data, and considering the effect of distance. Another magnitude scale, Mt, called tsunami magnitude, was defined and assigned for many earthquakes by Abe (1979). The definition of Mt for a Trans-Pacific tsunami (Abe, 1979) is:

$$M_{t=\log H+C+9.1} \qquad \textbf{Equation 2.3}$$

and for a regional tsunami (100km< Δ< 3500km) tsunami (Abe, 1981) is:

$$M_{t=\log H+\log \Delta+5.8} \qquad \textbf{Equation 2.4}$$

where H is the maximum amplitude recorded on tide gauges in meters, C is a distance factor depending on the location of the source and the observation points and Δ is the actual travel distance in km. The empirical formulas above where calibrated for earthquakes with moment magnitude Mw 3.

The above mentioned magnitude scales have focused in the more frequent earthquake generated tsunamis. However, although most tsunamis are triggered by earthquakes, it is unquestionably important to devote the necessary attention to tsunamis triggered by landslides or volcanic eruptions. In fact the largest ever recorded tsunami wave was observed in 1958 on a tsunami caused by a major submarine landslide (Aleutya Bay, Alaska, United States). Submarine landslides frequently occur in the aftermath of an earthquake (causing tsunamis much more localized than those from the earthquake itself, but at the same time potentially very destructive) (Bardet *et al.* 2003; Okal and Synolakis 2003). The fact that submarine

landslide tsunamis often have large run-up heights close to the source area but appear to propagate much less efficiently than earthquake tsunamis was exemplified by the 1998 Papua New Guinea tsunami, where run-up heights up to 15 m affected a 20 km segment of the coast (Dengler and Preuss 2003; McSaveney *et al.* 2000), while farther afield the tsunami was not a significant event (Okal and Synolakis 2004; Satake and Tanioka 2003).

Volcanic triggered tsunamis present similar features. There are at least nine different mechanisms by which volcanoes produce tsunamis, including volcanic earthquakes, eruptions of undersea volcanoes, flow of pyroclastic masses into the sea, caldera collapse, debris avalanches and landslides, large lahars entering the sea, phreatomagmatic explosions, coupling between water and turbulent air waves travelling from an explosive eruption, and collapse of lava benches during effusive lava eruptions (Beget, 2000). In particular, volcanic tsunamis are typically generated within a very small geographic area on the flank of a volcano, and may even be modelled as a point source (Kienle *et al.*, 1987). All evaluations of volcanic tsunami hazard should integrate both investigations of ancient volcanic tsunami deposits and studies of volcanic eruption history of island volcanoes and volcanoes located near coastal areas, to connect records of volcanic activity with the much more fragmentary geologic record of past tsunamis. Paris *et al.* (2011a) acknowledged that tsunamis generated by volcano flank failures represent a very low frequency but very high magnitude hazard. These volcano-gravitational events involving tens to hundreds of km³ are evidenced by voluminous submarine debris, such as in the Hawaiian Islands (Moore *et al.*, 1989; Normark *et al.*, 1993; McMurtry *et al.*, 2004), Reunion Island (Oehler *et al.*, 2004), Canary Islands (Krastel *et al.*, 2001; Masson *et al.*, 2002; Paris *et al.*, 2005) or the Cape Verde Islands (Masson *et al.*, 2008; Madeira *et al.*, 2011).

Independently of the source mechanism, tsunami intensity scales can be established based on the effects in coastal areas. For tsunami intensity three different scales have been proposed. Soloviev (1970) pointed out that Imamura-Iida's scale is more like an earthquake intensity scale rather than a magnitude. He also distinguished the maximum tsunami height (h) and the mean tsunami height along a stretch of coast (hr). He then defined tsunami intensity (i) as:

$$i = \log_2(hr) \qquad \textbf{Equation 2.5}$$

The Sieberg intensity scale – a descriptive intensity scale based on the physical destruction caused by tunami waves (Ambraseys, 1962) - ranks tsunamis from light tsunamis (Level 1) to disastrous tsunamis (Level 6) by their impacts. Furthermore, Papadopoulos and Imamura (2001) proposed a new intensity scale based in the effect on humans and on objects (of different sizes and nature) and the damage caused to buildings. This new scale varies from level I (Not felt) to level XII (completely devastating).

2.2. Tsunami and storm deposits in the geological record

The Holocene stratigraphy of a specific region reflects the group and succession of sedimentological processes that affected the area during time. These processes include intra-basinal, regional or global-scale mechanisms operating at different scales. In addition to the processes operating in permanence in a region, which prevail in the facies architecture and succession of the sedimentary record, catastrophic events such as tsunamis and storms can contribute significantly to the stratigraphy of any given area. In contrast to modern tsunami, for which eyewitness accounts and field measurements of both erosional and depositional effects are utilized in modelling studies, (palaeo)tsunami recognition depends on the identification of ancient tsunami deposits (*e.g.* Bourgeois *et al.*, 1988; Long *et al.*, 1989; Smit *et al.*, 1992; Bondevik *et al.*, 1997, Dawson and Stewart, 2007, Mahaney *et al.* 2010; Chagué-Goff *et al.*, 2011). More recently, the term "tsunamiite" has also been used to describe onshore sedimentary deposits lay down by tsunami events (Shiki *et al.*, 2008). Tsunami deposition is commonly characterized by the re-deposition of coarse shallow marine or coastal sediments in terrestrial and/or transitional (*e.g.* lagoonal, estuarine) environments. Recognition of these deposits is the primary method for reconstructing tsunami minimum inundation distance and run-up, although patterns of erosion and deposition by both landward- and seaward-directed flows are complex, these patterns being further complicated by the existence of more than one wave associated with the same tsunami (Moore and Moore, 1984; Synolakis *et al.*, 1995; Bondevik *et al.*, 1997; Dawson and Shi, 2000; Le Roux and Vargas, 2005; Paris *et al.*, 2007), thus introducing uncertainties in those reconstructions. In particular, because the maximum altitude at which tsunami sediments are deposited in the coastal zone is nearly always lower than the height reached by the tsunami. In fact, the upper sediment limit is generally regarded as a minimum level reached by the tsunami waves (this assumption is of crucial importance for hazard and physical and numerical modelling because sediment evidence might underestimate the flooding penetration).

The nature of tsunami deposits varies greatly with coastal and nearshore morphology, the height of tsunami waves at the coast and run-up, and with the nature and amount of existing sediment in any coastal setting when affected by such an event. Consequently, the possible variations in sedimentary processes and products during these complex events remains poorly understood but in general a tsunami deposit will only be produced if there is a suitable supply of sediment and accommodation space in the coastal zone. More recently, the subsequent backwash, or return flow, has been regarded as a process of significant geomorphic and sedimentologic consequences (*e.g.* Dawson, 1994; Dawson, 1999; Hindson and Andrade, 1999; Dawson and Shi, 2000; Le Roux and Vargas, 2005; Paris *et al.*, 2010b), though the spatial extension of the correspondent signature is usually more restricted due to channelling effects. The geomorphological consequences of tsunamis and storms in coastal dunes or barrier islands have also been addressed (*e.g.* Andrade, 1990; Andrade *et al.*, 2004; Regnauld *et al.*, 2008; Oliveira *et al.*, 2009; Dinis *et al.*, 2010; Goff *et al.*, 2010b).

Due to their specific physics and sediment transport processes tsunami and storms tend to leave their sediment imprint in a wide range of environments (*e.g.* alluvial plains, estuaries, coastal lagoons, embayments, nearshore and offshore areas) although storms usually present a smaller amount of inland penetration. However, many of these environments display a low preservation potential for event deposits (Einsele *et al.*, 1996) and the recognition of tsunami and storm deposits is many times constrained by the poor preservation of those deposits (or absence) in the stratigraphic record. In many cases, the anthropogenic activity, the erosion characteristics of the event, the relative changes in sea level in a millennium timescale and the absence of lithological differentiation makes palaetsunami deposits difficult to identify and therefore also makes it difficult to make inferences regarding the return intervals of such events (Szczucinski, 2011; Yawsangratt *et al.*, 2011).

2.2.1. Nearshore and offshore deposits

Nearshore and offshore deposits have been described essentially in association with several specific tsunami events worldwide (Smit *et al.*, 1992; Cita *et al.*, 1996; Fujiwara *et al.*, 2000; van der Bergh *et al.*, 2003; Terrinha *et al.*, 2003; Abrantes *et al.*, 2005; Noda *et al.*, 2007; Abrantes *et al.*, 2008; Gracia *et al.*, 2010) and were considered by Dawson and Stewart (2008) a "very much neglected research area" within tsunami sedimentary recognition. Weiss and Bahlburg (2006) considered that offshore tsunami depositon in deep marine environments well below the wave base of severe storms are theoretically much more likely to preserve tsunami deposits than shallow settings. Despite of that fact, these authors noted that there are only a few descriptions in the literature of marine, and particularly subtidal, tsunami deposits (Pratt, 2001, 2002; Bussert and Aberhan 2004; Cantalamessa and Di Celma 2005; Schnyder *et al.* 2005).

In the offshore area, the term "deep-sea homogenite" has been used to define a massive, poorly sorted, grain-supported unit that contains large reworked shallow-marine fossils and occasional large intraclasts that have been described in association with the Bronze Age Santorini tsunami event (Cita *et al.*, 1996). Other tsunamigenic deposits were discussed in an offshore sedimentary context and related with events such as the K/T meteoric tsunami (*e.g.* Smit *et al.*, 1992; Albertão and Martins, 1996), the AD 1755 tsunami (Terrinha *et al.*, 2003; Abrantes *et al.*, 2005 and 2008; Gracia *et al.*, 2010), the 2003 Tokashioki earthquake (Noda *et al.*, 2007) or to try and match earthquake-triggered turbidites with tsunamigenic events from the Saguenay (Eastern Canada) and Reloncavi (Chilean margin) (St Onge *et al.*, 2012). In fact, another peculiar note in terms of offshore tsunami deposits is that some have been specifically attributed to processes of tsunami backwash and the generation of gravity-driven flows of turbid water from nearshore to deep water (*e.g.* Abrantes *et al.*, 2008; Paris *et al.*, 2007).

2.2.2. Onshore boulder deposits

There are two main types of onshore sedimentary evidences associated with tsunami and storms: one consisting in deposits of large boulders and the other in the deposition of finer (typically sand-sized) sediments in coastal areas. The universally accepted scale of grain sizes of siliciclastic sediment is the Uden-Wentworth (Wentworth, 1922) scale that is composed of four basic groups: clay (< 4μm), silt (4μm - 63μm), sand (63μm - 2mm) and gravel (> 2mm). The larger particles (*i.e.* pebbles, cobbles and boulders) were all included in the gravel group. To facilitate the classification of larger particles Blair and McPherson (1999) revised the Udden-Wentworth scale to describe in greater detail the size of boulders and other larger particles. The grain size of fine, medium, coarse, and very coarse boulders range from 25.6 to 51.2cm, 51.2 to 102.4cm, 102.4 to 204.8cm, and 204.8 to 409.6cm, respectively. Larger rocks or megaclasts, include fine (4.1 to 8.2m) and medium (8.2 to 16.4m) blocks.

The identification and differentiation of tsunami and storm deposits and their association with specific events is of crucial importance for hazard or risk studies. Boulder and finer deposits can provide clues to the identification of both types of events. In the case of larger particles, the differentiation is firstly based on the identification of boulders that have been transported inland or upward from or within the coastal zone, and against gravity. In some cases, these boulders appear simply overturned a few m inland from their original source area. The recognition of boulder deposits associated with both tsunami and storms has been intensely debated in the literature (*e.g.* Bryant *et al.*, 1992; Young *et al.*, 1996; Nott, 1997; Bryant and Nott, 2001; Noormets *et al.*, 2002; Goff *et al.*, 2004; Williams and Hall., 2004, Scheffers and Kelletat, 2005; Goff *et al.*, 2006; Hall *et al.*, 2006; Bourrouilh-Le Jan *et al.*, 2007; Goto *et al.*, 2007; Scheffers and Scheffers, 2007; Kelletat, 2008; Paris *et al.*, 2010b; Scheffers, 2008; Scheffers *et al.*,2008, Etienne and Paris, 2010; Fichaut and Suanez, 2010; Goto *et al.*, 2010a; Goto *et al.*, 2010b; Nandasena *et al.*, 2011a). From the many examples in the literature a few deserve special notice because of their specific lithological, geological, geomorphological or oceanographic significance.

In terms of boulder deposits there are many examples worldwide attributed to deposition by storms and tsunami (compiled by *e.g.* Sheffers and Kelletat, 2003; Scheffers, 2008). They range from over 10 cubic metres up to 1000m^3 and, depending on the bulk rock density their mass can exceed 2000t (Scheffers and Kelletat, 2003). They have been found at various elevations from the intertidal zone to a few tens of meters above the present sea level. Shi *et al.* (1995) reported that hundreds of boulders were deposited as far as 200m inland by the December 12, 1992 tsunami in Flores (Indonesia), especially in the area of Riangkroko where the run-up reached 26m. The deposition of boulders in association with tsunamigenic events were discussed essentially after the 1990's (*e.g.* Paskoff 1991; Dawson 1994; Hindson and Andrade, 1999). For instance, Hindson and Andrade (1999) noted that at several locations on the Algarve coastline the AD 1755 tsunami was associated with the deposition of both continuous and discontinuous sand sheets, some of which containing boulders. The individual boulders were frequently pitted and sculptured by bioerosion and

in hollows marine endolithic mollusca were found and used to indicate the marine provenance of the boulders.

The imbrication of boulders (at certain altitudes and distances from the coastal edge), coupled with the presence of shell and debris inclusions, were used as a diagnostic criteria of tsunami deposits (Bryant and Nott, 2001). Hall *et al.* (2006) focused exclusively in storm wave impacts on boulders sitting at the top of cliffs in Aran and Shetland Islands (North Sea), and identified inverted boulders exclusively transported by storms. Saltation of these boulders during transport was implied by the presence of shatter marks on the upper limestone ramps on Aran (Williams and Hall, 2004) and by trails of impact marks and chipped edges visible on otherwise weathered and lichen-covered surfaces. Hansom *et al.* (2008) provide modelled solutions for the forces of wave impact and subsequent lift at those sites. According to Hall *et al.* (2006), the characteristics and distribution of cliff top storm deposits allows the definition of wave properties that could generate those boulder accumulations. According to these authors, cliff top storm deposits require full exposure to storm waves and limited nearshore attenuation.

In the Portuguese coast, namely in the Cascais-Cabo Raso area, Scheffers and Kelletat (2005) described isolated boulders and boulder fields they argue to have been deposited by the AD 1755 tsunami. The authors also indicate to have observed observed signatures of run-up *ca.* 50m above mean sea level (msl) in vegetation scars. They associated those marks and boulder transport to older tsunamis (proposed as *ca.* 2400 BP and 6000 BP). Furthermore, Whelan and Kelletat (2005) also observed boulders in Cape Trafalgar (Spain) that they associated with the AD 1755 tsunami but could not identify any field evidence for older tsunamis. Oliveira *et al.* (2011) combined field, aerial photography and wave data to characterize quarrying and transportation of two megaclasts weighting 14 and 8t, sitting at present above +1.70m above msl in the upper shore platform of Praia das Maçãs (Portugal). Both megaclasts were sourced from the same limestone bed seaward from their present location, and were transported landward and upward (against gravity) for a short distance, and in one case the block was overturned. Through the use of aerial photographs the date of transport was constrained between 1965 and 1975. The wave regime affecting this coast between 1953 and 2011 indicated high-energy modal conditions and extreme storm waves reached maximum Hs of ~13 m in only one occasion, precisely 17th January 1973.

Switzer and Burston (2010) stated that the imbrication, mixed lithology and sedimentary characteristics of boulder deposits at Little Beecroft Head and Greenfields Beach (Australia) provided compelling evidence for large-scale movement attributed to washover by single or multiple events. If the deposits were late-Holocene in age then a hypothesisc of higher Holocene sea level must be discarded and it is likely that storms and tsunami may have both played a role in the development of the high elevation boulder deposits. However, as in many other sites where boulder deposits transported against gravity have been found, it remains unclear which (*i.e.* tsunami or storms) was the exact mechanism of emplacement.

2.2.3. Onshore cobble and gravel deposits

Different size-ranged clasts associated with tsunamis and storms are also described in the literature. In terms of cobble and peeble deposits (2-256mm diameter - Krumbein and Sloss, 1963) a few studies have been conducted over recent years. For example, Morton *et al.* (2008) analysed coastal gravel-ridge complexes deposited either by tsunamis or hurricanes on islands in the Caribbean Sea. The ridge complexes of Bonaire, Jamaica, Puerto Rico (Isla de Mona) and Guadeloupe consisted of clasts ranging in size from sand to coarse boulders derived from the adjacent coral reefs or subjacent rock platforms. The authors observed that the ridge complexes were internally organized, displayed textural sorting and a broad range of ages indicative of several historical events. Some of the cobble deposits displayed seaward-dipping beds and ridge-and-swale topography, whereas other terminated in fans or steep avalanche slopes. Together, the morphologic, sedimentologic, lithostratigraphic, and chronostratigraphic evidence indicated that ridge complexes were not entirely the result of one or a few tsunamis as previously reported (*e.g.* Scheffers and Kelletat, 2003) but resulted from several events including not only tsunamigenic but also storm/hurricane events. Furthermore, in a nearby region (French West Indies) Caron (2011) used samples from beachrock and non-cemented coarse-grained coastal deposits and applied quantitative textural and taphonomic analysis to discriminate different depositional processes associated with storm and tsunami waves.

Richmond *et al.* (2011) in the island of Hawaii identified three distinct coarse-clastic depositional assemblages that could be recognized based on clast size, composition, angularity, orientation, packing, elevation and inland distance of each accumulation. These deposits were characterized as:

1) Gravel fields of isolated clasts, primarily boulder-sized, and scattered pockets of sand and gravel in topographic lows.

2) Shore-parallel and cuspate ridges composed mostly of rounded basalt gravel and sand with small amounts of shell or other biogenic carbonate. The ridges ranged in height from about 1 to 3m.

3) Cliff-top deposits of scattered angular and sub-angular (cobble and gravel) clasts along sea cliffs that were generally greater than 5m elevation.

The authors concluded that the gravel fields were primarily of tsunami origin from either the 1975 Kalapana event, or a combination of tsunamis during 1868 and 1975. The ridge deposits were presently active and sediment continues to be added during high wave events. The cliff-top deposits contained evidences of deposition by both tsunami and storm processes.

Costa *et al.* (2011) observed spreads of cobbles and boulders (typically with an A-axis of *ca.* 0.30m but some with smaller dimensions) that extended several hundred meters inland and well beyond the present landward limit of storm activity in a low-lying area of the Algarve (Portugal). The marine origin of the boulders was demonstrated by well-developed macro-bioerosion sculpturing and *in situ* skeletal remains of

endolithic shallow marine bivalves. The authors associated (using radiocarbon age-estimation of *Petricola lithophaga* whole shells) the transport of these boulders with the desctructive Lisbon tsunami of AD 1755.

2.2.4. Onshore fine-grained deposits

Most studied tsunami imprints in coastal stratigraphy are coarser sand-sized layers within low energy finer materials accumulated in depositional basins and exhibiting a distinctive sedimentological signature within the stratigraphic column (*e.g.* Atwater, 1987; Dawson *et al.*, 1988; Atwater and Moore, 1992; Clague *et al.*, 1994; Dawson *et al.*, 1995; Shi *et al.*, 1995; Hindson *et al.*, 1996; Bondevik *et al.*, 1997; Minoura *et al.*, 1997; Goff *et al.*, 2000; Nanayama *et al.*, 2000; Chagué-Goff *et al.*, 2002; Nanayama *et al.*, 2007; Moore *et al.*, 2007; Peters *et al.*, 2007; Paris *et al.*, 2009). This type of depositional arrangement is indicative of extreme marine inundations because they provide a stratigraphic context and facilitate accurate spotting and dating of individual events. Fine tsunami or storm deposits are typically sand-sized with a clearly-defined clay/silt fraction (*e.g.* Ota *et al.*, 1985; Srinivasalu *et al.*, 2007). The differentiation of tsunami events in a clayish stratigraphy was succefully attempted by Andrade *et al.* (2003) in the Tagus estuary. The combine used of sedimentological, magnetic susceptibility, micropaleontological and chronological data allowed the identification of historical tsunamis that affected the studied areas.

The identification and differentiation of finer units deposited by tsunami or storms in coastal stratigraphy requires a multi-proxy approach that mainly focuses on the allochthonous sediment and/or palaeontological content in order to establish a marine or coastal provenance. Tsunami or storm-transported sediment is typically deposited during run-up, even though deposition also occurs during backwash and in the period of time between run-up and backwash, usually correspondent to a slack where currents fall to minimum intensity and the directional pattern is ill-defined. Furthermore, in some situations the erosional capacity of run-up or the backwash constrains the sedimentary recognition of events by removing sediments deposited by earlier tsunami waves. (See sections 2.3 and 2.4).

2.2.5. Hydrodynamic models of transport of fines, gravel and boulders

Field measurements are extremely useful but are somewhat constrained to local experimental specificities, thus limiting interpretations. To overcome this restriction various numerical and physical modelling exercises have been done in order to shed further light on the properties of tsunami and storm waves, as well as, elucidate on the type/size of material that different events are capable of transporting and also in the establishment of patterns of fine-grained sedimentation, aiming at developing criteria allowing differentiation between extreme marine inundations.

In order to distinguish the transport mechanisms associated with tsunami and storms several hydrodynamic and numerical models have been proposed (*e.g.* Nott, 1997; Lorang, 2000; Felton, 2002; Nott, 2003; Noormets *et al.*, 2004; Jaffe and Gelfenbaum, 2007; Morton *et al.*, 2007; Paris *et al.*, 2007; Scicchitano *et*

al., 2007; Tappin, 2007; Hansom *et al.*, 2008; Imamura *et al.*, 2008; Weiss, 2008; Lavigne *et al.*, 2009; Paris *et al.*, 2009; Paris *et al.*, 2010b; Spiske *et al.*, 2010; Switzer and Burston, 2010; Apotsos *et al.*, 2011; Jaffe *et al.*, 2011; Nandasena *et al.*, 2011a,b). The most cited numerical approach to the differentiation of tsunami and storm transport mechanisms was proposed by Nott (1997, 2003) and is based in the estimation of threshold conditions for initiation of boulders movement under wave action. Nott (1997, 2003) presented a set of equations relating the forces involved in the transport of submerged, sub-aerial and joint-bounded boulders in coastal areas.

Noormets *et al.* (2004) determined the hydrodynamic forces acting on a low submerged shoreline cliff (in Hawaii) computing wave characteristics based on linear wave theory and experimental results taking into account he local wave climate and near-shore bottom topography. Their analyses showed that tsunami, as well as large swell waves, are capable of quarrying megaclasts, provided that sufficient initial fracturing is present. Dislodgement and emplacement most likely occurs in a sequence during impact of a single wave on a coastal cliff. Swell waves however seem to be capable of emplacing large blocks onto the platform due to their rapid disintegration after breaking. They determined that sliding was the most common mechanism of transport for larger and irregular megaclasts, whereas somewhat smaller and platy megaclasts where occasionally found in overturned positions. Inverse models of flow from tsunami deposits (Tappin, 2007) and forward models of deposits from flow (Gelfenbaum *et al.*, 2007) are relatively new and still under development. These models make use of the dependence of sediment transport on the relationship between grain size (grain settling velocity) and flow shear stress. Deposition occurs where sediment transport converges or when deceleration permits sediment to fall out of suspension.

Jaffe and Gelfenbaum (2007) proposed a tsunami sedimentation model based on the analysis of sand-sized sediment. These authors used the thickness of of tsunami deposits and mean grain particle size to reconstruct surface flow velocities. Scicchitano *et al.* (2007) reanalysed the equations proposed by Nott (2003) using a hydrodynamic approach to determine whether tsunami- or storm-generated waves were responsible for coastal boulder deposition in places of the southern coast of Italy. Their results suggested that tsunamis were responsible for the detachment and transport of the largest blocks. However, they could not exclude that storm waves could also have been responsible for the movement and/or re-orientation of smaller-sized blocks, possibly carved out and transported during previous tsunami events. Their analysis also confirmed the importance of the pre-transport setting of boulders in determining the height and velocity of the wave required for boulders to be transported.

Pritchard and Dickinson (2008) described a mathematical model of suspended and bedload sediment transport under long, non-breaking waves running over a plane beach, and used this model to investigate the relationship between the hydrodynamics of swash nd backwash and the resulting erosive and depositional processes. They found that sediment transport, both as bedload and suspended is strongly controlled by asymmetries in the direction of maximum velocity; in the latter case (suspension) transport is also affected by settling lag, especially around the point of maximum run-up. The authors concluded that

combination of these effects appears to preclude simple methods of reconstructing tsunami hydrodynamics. Using a similar approach, Weiss (2008) computed the water depth where a passing tsunami wave is able to move grains, and estimated the grain size that can be moved at a certain water depth on a sloping beach by a shoaling tsunami wave. According to Weiss (2008), tsunami waves generated by submarine slides or meteoritic impacts, unlike those generated by offshore earthquakes, could produce waves with the required larger amplitudes. Tsunamis generated by submarine landslides often have very large run-up heights close to the landslide area, but have more limited far-field effects than earthquake tsunamis (Okal and Synolakis, 2004).

Imamura *et al.* (2008) conducted hydraulic experiments in an open channel with cubic and rectangular shaped solid blocks to investigate boulder transport by tsunamis and developed a model (introducing an empirical variable coefficient of friction) that takes into account the various transport modes (*i.e.* rolling, saltation, sliding). The authors noted that the blocks were mainly transported by a bore, predominantly by rolling or saltation rather than by sliding. Imamura *et al.* (2008), also stated that previous models of boulder transport by tsunamis probably underestimated the distance the boulder travelled by influence of tsunami waves when they were transported by rolling or saltation. The model was tested using boulders from Inoda (Japan) which were transported by the 1771 Meiwa tsunami. The calculated distance of transport of the boulder was approximately 650m, which was consistent with the description in the historical documents.

On the other hand, Paris *et al.* (2009) analysing the effects of the Indian Ocean Tsunami (24th December 2004) in Lhok Nga (Indonesia) observed that large tsunami waves (25–30m high) were able to detach and transport coral boulders in excess of 10t over 500–700m and megaclasts of the rocky platform in excess of 85t over a few metres. However, the authors did not observe any landward fining trend in the boulder size distribution. The spatial and size distributions of tsunami boulder deposits are mostly depended on the location and characteristics of their source (coral reef, beach rock, platform, dams), together with clast and surface interference during transport. Density also plays an important role in boulder transport, for example, a less dense coral boulder buoyed up on water can be more easily transported inland than a more dense granitic boulder. Furthermore, Spiske *et al.* (2008) investigated the role of porosity on boulder transport and elucidated the distinction between tsunami and hurricane impacts, by performing Archimedean and optical 3D-profilometry measurements for the determination of accurate physical parameters for porous reef and coral limestone boulders from the islands of Aruba, Bonaire and Curaçao (Netherlands Antilles). The authors concluded that the calculated wave heights, the high frequency of tropical storms and hurricanes in the southern Caribbean and the occurrence of boulders exclusively on the windward sides of the islands, implicate that the boulders on those islands are more likely to be hurricane originated. More recent work on reefs indicate however that boulder size can also be used to estimate the wave current velocities generated in storms and tsunamis (Paris *et al.*, 2009; Goto, 2010b).

The transport mode of boulders from Jervis Bay (Australia) was discussed by Goff *et al.* (2010b). The authors conclude that a better understanding of the critical thresholds for the bed load transport of boulders is necessary. This issue was addressed for instance by Benner *et al.* (2010) that discussed physical modelling of tsunami and storms boulder transport debating shortfalls in calculations from previous published work. Lorang (2010) provided a simple wave-competence approach to determining the likelihood of one causal mechanism over the other by solving a system of equations to determine wave period in order to differentiate between tsunamis from wind-generated waves. Lorang (2010) revisited Nott's equations and also used the Hudson formula (United States Army Corps of Engineers, 1984) to estimate wave height for the potential wave based on size of the boulder or megaclast. Combining that information with the elevation above the initial position and the total horizontal distance of transport, density of the megaclast and assumed values of several coefficients it was possible to estimate the wave period. Furthermore, Apotsos *et al.* (2011) proposed a numerical model based on non-linear shallow water equations developed for periodic long waves inundating over planar slopes. Simulations were conducted to examine the effects on maximum tsunami run-up and water velocity of variations in wave characteristics, bed slopes and bottom roughness.

Nandasena *et al.* (2011a) revised Nott's equations in the sub-aerial and joint-bounded boulder scenarios and corrected their approach for lift and inertia and incorporated an additional description of the pre-transport location and effects of bottom slope. Calculations were performed in boulders described in published accounts and a boulder transport histogram introduced to represent the range of flow velocityies that satisfy the requirements for initial transport of a boulder in different modes: sliding, rolling, and saltation. The theoretical results were successfully compared to field data. Moreover, Nandasena *et al.* (2011b) discussed the relevance of clast-to-clast interactions and its impact in transport distance and dissipating the energy. The authors concluded that numerical results revealed that drag and friction are the dominant forces applied to boulders during transport, and therefore, accurate estimation of drag and friction coefficients is also important for validation of any transport model. The difference between the simulated results and field observations was partly attributed to limitations of the numerical model such as inability to account for boulder shape, pre-transport environment, microtopographical variation, transport mode, and inaccurate definition of coefficients.

Li and Huang (2011) used three laboratory-based measurements and results from one field survey following the 2004 Indian ocean tsunami to evaluate the performance of six widely-used sediment transport formulae (Bagnold; Van Rijn; A-W; Bijker; E-H and Yang) in modelling shoreline change due to tsunamis. The performance of these formulae proved to be inconsistent at low and high velocities with none giving reliable predictions matching both the low and high sediment transport rates observed.

2.3. Sedimentological features of onshore tsunami deposits

In this sub-chapter, the criteria used to recognize and differentiate tsunami deposits consisting of the finer fraction (*i.e.* typically sand) is presented. These features/criteria reflect the characteristics of

tsunami waves, transport peculiarities, preservation potential and sedimentary sources. The first studies to use geological record to detect prehistoric tsunamis were conducted by Atwater (1987) and Dawson *et al.* (1988). Since then many papers have been published discussing several aspects concerning features associated with tsunami deposits. The study of modern deposits carried out during immediate post tsunami surveys provided the opportunity to refine palaeotsunami diagnostic criteria, without the uncertainty of the generating event and preservation issues due to natural and anthropogenic disturbance. Understandably, the number of studies on tsunami sedimentation increased exponentially since the 2004 Indian Ocean event, but care should be taken in adopting as of unquestionable universal applicability inferences derived from research on this particular event. Typically, tsunamis can leave sedimentary imprints on shores far from the event source, and usually less than a kilometre from the coastline (Dawson and Shi, 2000; Dominey-Howes *et al.*, 2006). Tsunami deposits are usually thicker in topographic lows (areas of spatial deceleration of flows) and thin over topographic highs (areas of spatial acceleration of flows) (Gelfenbaum *et al.*, 2007). In fact tsunami sediments can also be eroded during phases of backwash and have also been linked to new phases of sedimentation during backwash. The preservation of tsunami deposit is a fundamental factor in any sedimentological study focusing in recurrence intervals of such events.

Tappin (2007) discussed sedimentary features associated with tsunami, stressing that the development of realistic scenarios of risk requires reliable data on tsunami frequency, which is obviously constrained by the sporadic absence of deposit, to which we could add the eventual unability to recognize a particular tsunami-deposited layer as such in a given sedimentary sequence. In fact, Szczucinski (2011) conducted 5 yearly surveys after the 2004 Indian Ocean tsunami and concluded that the post-tsunami recovery of coastal zones was generally in the order of a few months to a few years. The study by Nichol and Kench (2008) in the Maldives found that within 2 years, significant reworking and bioturbation of the tsunami deposit occurred. The major macroscopic change observed was the fast removal of the thin layer of very fine sediments usually representing the top of the tsunami deposits, though such a thin layer consisting of very fine-grained material has not been reported as ubiquitous in other places worldwide and surveyed shortly after tsunami inundations. Szczucinski (2011) observed that almost all the near-surface structures of the tsunami deposits were removed with time (*i.e.* after at least 1 rainy season). Tsunami deposits thinner than 10cm usually acquired a massive appearance after 1 or 2 years; the only remnants of the primary structures, for instance fining upward, having vanished out. This was attributed to bioturbation by growing roots and burrowing animals like crabs and rodents. A few years earlier Szczucinski *et al.* (2007) detected that tsunami deposits thinner than 1cm were occasionally washed away, the depositional relief was flattened and deposits at the slopes were partially eroded; and yet, in other locations, the sedimentary bodies, including thin sand *laminae*, and sedimentary structures, such as lamination and size grading, persisted at century-long timescales (*e.g.* Washington State, Boca do Rio, Martinhal) following deposition. According to Yawsangratt *et al.* (2011) micropalaeontological evidences (*i.e.* carbonate foraminifera) may be subjected to significant dissolution 4.5 years after tsunami emplacement; again, this post depositional disturbance is not

exclusive of tsunami deposits and rapid intrasediment dissolution or downwearing of carbonate foraminifera tests, ostracoda valves or diatom frustules is a common drawback micropaleontologists working in Holocene sediments of various facies are used to and aware of, and not exclusive of high-energy events of abrupt marine inundation. In this context, it is somewhat surprising that Lowe and de Lange (2000) suggested, based on a study from New Zealand, that a tsunami needs to raise a height of at least 5m in order to leave any long-term, recognisable sedimentary signature (cf. Goff *et al.*, 2010a). This statement disregards the effect of sediment concentration in tsunami waves in determining the size and preservation potential of the depositional signature, just as a number of other relevant variables, such as the presence of a compatible source, accommodation space, rapid capping of the inundation deposit, among other, which are completely independent of the tsunami amplitude.

During the last two decades, several authors (*e.g.* Shi and Dawson, 1995; Goff *et al.*, 1998; Gelfenbaum and Jaffe, 2003; Dawson and Stewart, 2007; Huntington *et al.*, 2007; Shiki *et al.*, 2008; Switzer and Jones, 2008; Chagué-Goff *et al.*, 2011) have postulated criteria to distinguish (palaeo)tsunami deposits. These are described below and summarized in Table 2.2. Dawson and Stewart (2007) discussed the processes of tsunami deposition, identifying the three main aspects that make the depositional process unique, tsunami source, propagation and inundation. The establishment of source material has been widely used (*e.g.* Moore and Moore, 1986; Atwater and Moore, 1992; Dawson *et al.*, 1996; Minoura *et al.*, 1997; Bourgeois *et al.*, 1999; Hindson and Andrade, 1999; Gelfenbaum and Jaffe, 2003; Switzer *et al.*, 2005; Szczucinski *et al.*, 2006; Babu *et al.*, 2007; Morton *et al.*, 2007; Narayana *et al.*, 2007; Dahanayake and Kulasena, 2008; Higman and Bourgeois, 2008; Morton *et al.*, 2008; Switzer and Jones, 2008 Jagodzinski *et al.*, 2009; Costa *et al.*, 2009; Paris *et al.*, 2009; Mahaney and Dohm, 2011) because it allows one to reconstruct the origin and pathway of former tsunami waves. However, it has been commonly reported that tsunami waves transport essentially sediment that is available in the coastal fringe landward of the boundary defined by the seasonal depth of closure of the beach (and coastal) profile (*e.g.* Atwater and Moore, 1992; Clague and Bobrowsky, 1994; Dawson 1994; Moore *et al.* 1994; Hindson *et al.*, 1996; Dawson, 2004; Kortekaas and Dawson, 2007; Oliveira *et al.*, 2009; Paris *et al.*, 2010b; Goff *et al.*, 2010a; Costa *et al.*, 2012a,b). In contrast with this, micropalaeontological evidences have indicated either relevant changes in the population of Nannoplankton, Foraminifera, Diatoms and Ostracods or that marine species from offshore/nearshore have been transported inland and deposited by tsunami (*e.g.* Hemphill-Haley, 1996; Hindson *et al.*, 1996; Patterson and Fowler, 1996; Shennan *et al.* 1996; Clague *et al.*, 1999; Dominey-Howes *et al.*, 2000; Chagué-Goff *et al.*, 2002; Dawson and Smith, 2002; Abrantes *et al.*, 2005; Dawson, 2007; Horton *et al* 2007; Kortekaas and Dawson, 2007; Mamo *et al.*, 2009; Sawai *et al.*, 2009; Paris *et al.*, 2010a; Ruiz *et al.*, 2010). Although a site-specific component might be a central feature of any tsunami deposits some generalizations are possible interrelated with sedimentary structures, sediment source, palaeontological, geochemical and geomorphological signatures (Table 2.2).

2.3.1. Sedimentary structures

In terms of sedimentological structures, an erosive/sharp/abrupt basal contact is a common feature and is symptomatic of the energy involved in the emplacement of tsunami deposits. However, this criterion was also recognized in storm deposits (Switzer, 2008). The sharp/abrupt/erosive contact of tsunamigenic layers were firstly described by Dawson *et al.* (1988), Moore and Moore (1988) and Minoura and Nakaya (1991). Bondevik *et al.* (1997), analysing evidences lay down by the Storegga tsunami in Norway, detected that the tsunami deposit rest on an erosional unconformity which in cases has removed more than 1 m of underlying sediment. Moreover, Nanayama *et al.* (2000) observed deposits that resulted from the 1993 Hokkaido-nansei-oki (Japan) tsunami and identified distinctive sharp erosional bases in the tsunamigenic unit. Gelfenbaum and Jaffe (2003) analysed the erosion and sedimentation associated with the 1998 Papua New Guinea tsunami and observed that the beach face and berm showed no evidence of deposition from the tsunami. However, on the berm, exposed roots and scour at the base of some palm trees indicated erosion of approx. 20-30cm of backbeach sand and they observed that only erosional signatures had been left by this tsunami to the landward side of the berm, up to about 50m from the shoreline. Chandrasekar (2005) described erosion of up to 2m over large tracts of beach associated with the return flow of the 2004 Indian Ocean tsunami. In Thailand, Szczucinski *et al.* (2005) and (2006), Hori *et al.* (2007) and Fujino *et al.* (2009) observed an erosive sharp basal contact between the tsunamigenic and the underlying layers. Choowong *et al.* (2009) also noted that during the same event, erosion and deposition occurred mainly during two periods of inflow and that the return flow was mainly erosive. Paris *et al.* (2009) described erosion associated with the 2004 Indian Ocean Tsunami in Banda Aceh (Indonesia) that extended up to 500m inland. These authors quantified the overall coastal retreat from Lampuuk to Leupung as of the order of 60m (*ca.* 550,000 m^2) and locally in excess of 150m. The erosional impact of tsunamis is still controversial, not only the recognition of associated patterns in the sedimentary record, other than the erosive base and quantification of the amount of sediment removed but also the mechanisms and processes associated and responsible for the erosional/depositional balance during a tsunami. In fact, Bahlburg and Spiske (2011) analysing the sedimentary record of the February 2010 tsunami at Isla Mocha (Chile) observed that the tsunamigenic unit was produced essentially (*i.e.* >90%) by the backflow. These authors suggest that due to the lack of sedimentary structures, many previous studies of modern tsunami sediments assumed that most of the detritus were deposited during inflow and an uncritical use of this assumption may lead to erroneous interpretations of palaeotsunami magnitudes and sedimentary processes if unknowingly applied to backflow deposits. Typically tsunami deposits present sediment size that can vary from mud to boulders and, in many cases, grain-size variation in tsunami deposits is controlled by the size of sediment available for transport, rather than by flow capacity (Bourgeois, 2009) or direction.

The detection of sedimentary structures is limited by sampling methods because coring (which is frequently used), in contrast to trench excavation, is in general destructive. Sedimentary structures are also difficult to identify in tsunami deposits due to the common deposition as massive deposit (*e.g.* Dawson *et al.*,

1995; Dahanayake and Kulasena, 2008). However, there has been several tsunami deposits where sedimentary structures including *laminae* (*e.g.* Reinhart, 1991; Bondevik, 2003), rip-up clasts (*e.g.* Dawson, 1994; Shi *et al.*, 1995; Hindson and Andrade, 1999; Bondevik *et al.*, 2003; Gelfenbaum and Jaffe, 2003; Goff *et al.*, 2004; Morton *et al.*, 2007; Paris *et al.*, 2009), cross-stratification (*e.g.* Choowong *et al.*, 2008) and soft-sediment deformation (Matsumoto *et al.*, 2008) have been observed. Muddy *laminae* or organic layers can represent evidence for multiple waves of the tsunami wave train (*e.g.* Reinhart, 1991; Bondevik 2003). Furthermore, loading structures at the base of the deposit have been reported in literature (*e.g.* Dawson *et al.*, 1991; Minoura and Nakaya, 1991; Costa, 2006; Dominey-Howes, 2007; Martin and Bourgeois, 2012).

Another peculiar feature observed in many tsunamigenic deposits worldwide is the enrichment in bioclasts or shells (many of them broken) when compared with the under and overlying layers (*e.g.* Moore and Moore, 1988; Bryant *et al,.* 1992; Albertão and Martins, 1996; Imamura *et al.,* 1997; Clague *et al.*,1999; Donato *et al.*, 2008) and in cases platy or prolate shell fragments occur aligned suggesting a ghosty lamination (*e.g.* Dawson *et al.*, 1995, Hindson et al, 1996, Hindson and Andrade, 1999). For example, Clague and Bobrowsky (1994) observed that tsunami sand deposits commonly include fragments of bark, twigs, branches, logs and other plant material. Moreover, Donato *et al.* (2008) showed that shell features could be used as useful indicators of tsunamigenic deposit due to their vertical and lateral extent, to the allochthonous mixing of articulated bivalve species (*e.g.* lagoonal and nearshore) out of life position, and to the high amount of fragmented valves, with angular breaks and stress fractures. The authors suggested that the taphonomic uniqueness of tsunami deposits should be considered as a valid tool for tsunamigenic recognition in the geological record.

The sedimentological fingerprint of currents associated with tsunami events have also been observed in the form of parallel lamination, cross-lamination, convolutions and ripple-marks (*e.g.* Shiki *et al.*, 2008). Moreover, Morton *et al.* (2007) detected palaeocurrent indicators in tsunami deposits indicating seaward return flow. In deposits laid down by the 2004 Indian Ocean tsunami, in Thailand, Choowong *et al.* (2008) observed capping bedforms and parallel *laminae*, cross-lamination, rip-up mud and sand clasts. The authors also observed normal grading but some reverse grading was locally recognized. According to Choowong *et al.* (2008) reverse grading in tsunami deposits indicates a very high grain concentration within the tsunami flow, and was possibly formed at the initial stages of inundation in shallow water. Cross-bedding was seen as restricted to return-flow sediments (Nanayama *et al.,* 2000). Individual deposits are generally well sorted (many are massive) and characterised by sets of fining-upwards sediment sequences that were interpreted by Shi (1995) as indicative of deposition by individual tsunami waves. Dawson and Smith (2000) characterised a tsunami sequence in Scotland by several fining upward sequences indicative of a series of tsunami waves and episodes of backwash. Furthermore, run-up and return flow deposits were also differentiated by Dawson *et al.,* (1996), Nanayama *et al.,* (2000) and Goff *et al.,(*2001). In the case of the Indian Ocean tsunami, Paris *et al.* (2007) observed a landward sequence thinning, fining and sorting. Normally-graded couplets or triplets of layers were used to identify the run-up of each wave. The topmost

layers, interpreted as the backwash deposition, describe a seaward sequence of decreasing mean grain-size.

The time lag separating tsunami wave-trains is occasionally marked between different sub-units by the presence of mud drapes. Moreover, Fujiwara and Kamataki (2007) observed the presence of a vertical stack of many coarse-grained sub-layers separated by mud drapes interpreted as due to incremental deposition from multiple sediment flows separated by flow velocity stagnation stages and concluded that it is unlikely that the mud drapes were deposited by short-period storm waves.

More recently, different techniques have been explored to identify the sedimentary structures in tsunami deposits. An example of this is ground penetrating radar, used by Switzer *et al.* (2006) to survey the erosional contact between an event layer and the under and overlying units. Koster *et al.,* (2011) also used ground penetrating radar in combination with electrical resistivity tomography measurements and sedimentology for tsunamiite recognition in Greece and Spain. According to these authors, ground penetrating radar data indicated unconformable thicknesses of tsunamigenic beddings, channel-like structures (backwash deposits) and to some extent basal erosion, as well as abrasion-scours in various places, and boulder accumulation inside the deposits (see Table 2.2.)

2.3.2. Sedimentary sources

Several authors have argued that tsunamis are frequently associated with the deposition of continuous and discontinuous sediment sheets across large areas of the coastal zone, provided that there is an adequate sediment supply (*e.g.*, Dawson *et al.*, 1996; Hindson *et al.*, 1996; Dawson and Shi, 2000). The decrease of energy associated with the run-in of tsunami inundations is evidenced in stratigraphic and sedimentary architecture by the fining inland and thinning inland and ramping upwards of tsunamigenic deposits. This is probably the most common feature/criteria to recognize tsunami events in the stratigraphy of any given coastal area mainly due to the settlement of the particles through the water column, related to a decrease of the turbulence of the flow, generally forming fining-upward depositional sequences. Grain size characteristics of the tsunami deposits reflect both the origin of the displaced sediment and hydrodynamic conditions of sedimentation (Sugawara *et al.*, 2008), with normally graded sand layers related to the decrease of the hydrodynamic energy during sedimentation (*e.g.* Dawson *et al.*, 1988, 1991; Shi *et al.*, 1995; Minoura *et al.*, 2000). Although not a frequent situation, each fining-upward sequence can be attributed to individual tsunami waves as referred to by Ota *et al.* (1985), Moore and Moore (1988), Clague and Bobrowsky (1994). In contrast, coarsening upwards sequences have also been recognized and were ascribed to the long duration time of the tsunami (Higman and Jaffe, 2005) or high-density flow, as cited above. The same authors stated that tsunamis with narrower source regions are more likely to deposit sediment that is normally graded than those with wider sources who produce more complex deposits. Although local topography plays a decisive role (*e.g.* Hori *et al.*, 2007) the thickness and mean grain size of tsunami deposits generally decrease landwards (*e.g.* Shi *et al.*, 1995; Hindson *et al.*, 1996; Minoura *et al.*,

1997; Dawson and Shi, 2000; Gelfenbaum and Jaffe, 2003; Goff *et al.*, 2004; Paris *et al.*, 2009). Landward coarsening deposits have also been exceptionally observed (*e.g.* Higman and Bourgeois, 2008). In fact, the sediment texture of tsunami deposits is mostly related to material available for transport in the coastal zone tsunami deposits can therefore vary immensely from location to location. Differences in the tsunami records preserved tend to reflect the unique character of each tsunami, and may be attributed to source differences, coastal configuration, tide level, and sediment supply. For example, tsunami sediment source has been attributed to beaches and berms (*e.g.* Sato *et al.*, 1995; Gelfenbaum and Jaffe, 2003), aeolian grains (*e.g.* Switzer *et al.*, 2006) or to the inner shelf (*e.g.* Switzer and Jones, 2008).

The use of heavy minerals to establish provenance of tsunamigenic deposits has also been investigated by several authors (*e.g.* Switzer *et al.*, 2005; Bahlburg and Weiss, 2007; Szczucinski *et al.*, 2006; Babu *et al.*, 2007; Morton *et al.*, 2007; Narayana *et al.*, 2007; Higman and Bourgeois, 2008; Morton *et al.*, 2008; Switzer and Jones, 2008). For example, Bahlburg and Weiss (2007) observed the presence of thin heavy-mineral concentrations at the base of individual sand layers inferred to have been laid down by different waves from the same event. Furthermore, Switzer and Jones (2008) identified a mixed heavy mineral assemblage characteristic of barrier sediments with a component of inner shelf material characterised by immature platy minerals in a tsunami deposit. Morton *et al.* (2008) observed that vertical textural trends showed an overall but non-systematic upward fining and upward thinning of depositional units with an upward increase in heavy mineral laminations at some locations. However, most of these studies were limited to one study area and also by local differences in source material. Jagodzinski *et al.* (2009) tried to compare tsunami deposits, beach sediments and pre-tsunami soils in Thailand. The difference between tsunami deposits and beach sediments and soils was reflected in differences in the respective proportions of mica and tourmaline. These differences were attributed to the mode of sediment transport and deposition with mica, due to its low density, being more abundant in the topmost part of the tsunami deposit.

Scanning Electron Microscopy (SEM) of mainly quartz grains has also been used to establish the source material of tsunami deposits (*e.g.* Bruzzi and Prone, 2000; Dahanayake and Kulasena, 2008; Costa *et al.*, 2009; Mahaney and Dohm, 2011). Bruzzi and Prone (2000) compared SEM microtextural signatures of quartz grains deposited by the AD 1755 tsunami (Boca do Rio, Portugal) and other quartz grains deposited by a storm in the Rhone delta (France) in November 1997. According to the authors, several features were associated with a specific event (*e.g.* tsunami) such as upturned plates, fractures and marks of considerable size. Dahanayake and Kulasena (2008) identified diagnostic criteria to distinguish tsunami sediments from storm-surge sediments in southern Sri Lanka noting that in tsunami sediments, reworked marine microfauna are abundant, quartz sand is not well rounded, and heavy minerals were rare, when compared with storm-surge sediments, although they do not explain the reasons underlying these differences.

Anisotropy of magnetic susceptibility has also been used to provenance studies of tsunamigenic deposits (*e.g.* Sugawara *et al.*, 2008; Font *et al.*, 2010; Wassmer *et al.*, 2010) but the application of this

technique is still in its early days and always require that the data produced is normalised in respect of the grain size distribution. One example of these studies was conducted by Font *et al.* (2010) in Boca do Rio (Portugal) where the magnetic data showed a dominance of paramagnetic minerals (quartz) mixed with lesser amount of ferromagnetic minerals, namely titanomagnetite and titanohematite both of a detrital origin and reworked from the underlying sedimentary units. Statistical analyses pointed to a scenario where the energy released by the tsunami wave was strong enough to overtop and erode sand from the littoral dune and mixed it with reworked materials from underlying layers from at least 1m in depth (see Table 2.2).

2.3.3. Palaeontological signature

Macrofossils and microfossils have been used to identify and interpret sedimentary units as tsunamigenic. To date, the use of palaeontological characteristics to recognise tsunami deposits has focused on diatoms, foraminifera, ostracods, nannoplankton, pollen, molluscs and plant fragments. Typically the palaeontological signature is characterized by marked changes in the population indicating the increase in abundance of marine to brackish fossils and/or the high-energy of the event (*e.g.* presence of broken shells, *etc.*).

Diatoms have been widely used as a proxy to detect extreme marine inundations (*e.g.* Dawson *et al.*, 1996 a,b; Hemphill-Haley, 1996; Chagué-Goff *et al.*, 2002; Abrantes *et al.*, 2005; Dawson, 2007; Nichol *et al.*, 2008; Sawai *et al.*, 2009). Generally, diatom assemblages in tsunami deposits are chaotic (mixture of freshwater and brackish–marine species), because tsunami crosses coastal and inland areas eroding, transporting and re-depositing freshwater taxa (Dawson *et al.*, 1996b; Smith *et al.*, 2004).

Dawson *et al.* (1996b) analysed the diatom assemblages contained within tsunami deposits in Scotland, related to the Second Storegga Slide and also associated with Grand Bank tsunami of 1929, and detected the presence of exceptionally large numbers of the species *Paralia sulcata* with most individuals exhibiting evidence of breakage. Normally, tsunami deposits are characterized by a high percentage of broken valves (*e.g.* more than 65%: Dawson *et al.*, 1996b; more than 75%: Dawson, 2007, 90% of pinnate: Dawson and Smith, 2000; more than 60%: Sawai, 2002). This is in contrast with Sawai *et al.* (2009) who analysed diatoms in tsunami deposits from the Indian Ocean tsunami of 2004 and concluded that the breakage of diatom valves was relatively low. Moreover, low breakage of diatoms in tsunami deposits has also been reported in the Pacific coast of Washington State and Puget Sound, USA (Hemphill-Haley, 1996), and considered to have resulted from rapid sedimentation. At first sight it may appear that large percentages of broken diatoms may be indicative of former tsunamis. However, this issue is made problematic since owing to the varying robustness of lenticular and circular diatoms, tests of some species are more able than others to withstand fracturing.

In a study of tsunami sediments deposited by the Papua New Guinea tsunami of 1998, Dawson (2007) observed a contrast between the sedimentological/textural data suggesting that the beach shore-face, the

berm as well as the sand spit were the source of the tsunami deposit. However, the examination of the diatom content of the sand suggested that the majority of diatoms were originated from the area immediately offshore. Benthic marine-brackish species (*e.g. Surirella sp.*, *Cocconeis scutellum* and *Diploneis smithii*) were dominant within the tsunami sands along the length of transect including the sample furthest inland. Moreover, in one sample located 200m inland, the presence of the fully marine *Triceriatum favus* attests to the allochthonous (transported) nature of the species within the deposit.

Sawai *et al.* (2009) analysed the diatom assemblages of Phra Thong's (Thailand) 2004 tsunami deposit and concluded that it contained surprisingly few freshwater specimens considered to have been a result of strong currents of the tsunami. Turbulent tsunami currents can cause rapid entrainment of a mixture of freshwater species, eroded soil and benthic marine species within a mass of coastal sand. However, if the currents are very strong, only benthic marine diatoms attached to heavier sandy substrate are able to settle out of the water column. When current velocity slows, the suspended freshwater specimens and soil fractions are able to settle out of the water column and deposit on top of the sandy, marine diatom-dominated portion of the deposit.

Foraminiferal content is also a common micropalaeontological proxy that has been used in tsunami sediment provenance studies (*e.g.* Hindson *et al.*, 1996; Patterson and Fowler, 1996; Shennan *et al.,* 1996; Andrade *et al.*, 1997; Dominey-Howes *et al.*, 1998; Hindson and Andrade, 1999; Clague *et al.*, 1999; Hawkes *et al.*, 2007; Kortekaas and Dawson, 2007; Mamo *et al.*, 2009). Bahlburg and Weiss (2007) observed in Kenya that the samples contained abundant tests of benthic foraminifera (*Quinqueloculina* and *Spiroloculina)* typically derived from shallow and protected shelf regions in water depth of less than 30m). Also present were several species of *Amphistegina sp.* including *Amphistegina lessonii d'Orbigny* which may occur down to water depths of 80 m. The foraminifera content indicated that the tsunami very likely entrained most of the sediment in shallow depths of less than 30m. Hawkes *et al.* (2007) analysed tsunami deposits in Malaysia and Thailand, and observed that the pre-tsunami assemblages were mainly composed of intertidal and inner shelf species (*i.e. Ammonia* spp., *Elphidium hispudula*) while the tsunami sediment also contained a minor but important addition of mangrove species, such as *Haplophragmoides. wilberti* and *Haplophragmoides manilaensis* and some radiolarian species. According to the authors, the mangrove and radiolarian species reflected the chaotic nature of deposition where swash up and backwash combine to create turbulence, mixing the assemblages together. Foraminiferal assemblages within tsunami sediments were also able to provide information about sediment provenance and wave characteristics. In one location (Sungai Burong), species assemblages in the tsunami sediment revealed at least two separate episodes of deposition that contained inrushed species from the inner-shelf, as well as backwash species from the mangrove environment. In the study by Dahanayake and Kulasena (2008), also on the 2004 Indian Ocean tsunami, more abundant planktonic species such as *Globigerinita glutinata*, *Hantkenina sp.* and also benthic *Quinqueloculina sp.* as well as *Amphistegina lessonii D'Orbigny* were detected. Kortekaas and Dawson (2007) analysing a tsunami deposit in Martinhal (Portugal) noted a clear abrupt change from the brackish

foraminifera assemblage of the underlying layer to a fully marine assemblage consisting of *Elphidium macellum*, *Elphidium crispum*, *Quinqueloculina seminulum*, *Cibicides refulgens*, *Eponides repandus* and *Ammonia beccarii var. batavus*.

More recently, Mamo *et al.* (2009) summarized the many procedures, characteristics and limitations associated with foraminiferal assemblages and their use in the recognition of tsunami deposits. Characteristics such as changes in assemblage composition (Hindson *et al.*, 1996; Hindson and Andrade, 1999; Hawkes *et al.*, 2007), for example, marine shelf species within a lagoon or brackish environment; changes in test size or in juvenile to adult ratios (Guilbault *et al.*, 1996); a shift in population numbers (Cundy *et al.*, 2000; Hawkes *et al.*, 2007; Kortekaas and Dawson, 2007); or a change in the taphonomic character of the tests (Hindson *et al.*, 1999; Hawkes *et al.*, 2007) can be used to recognise tsunami deposits. Given that the exact composition of an assemblage varies from location to location, it is impossible to expect to see a specific diagnostic specie(s) or assemblage in association with tsunami-deposited sediments. Some authors (Dominey-Howes *et al.*, 1998; Nanayama and Shigeno, 2006; Uchida *et al.*, 2007) suggested that given ideal conditions a tsunami deposit might contain deeper water species that would not otherwise be expected from the shallow water.

Ostracods have also been used as tsunami indicators (*e.g.* Ruiz *et al*, 2010; Mischke *et al.*, 2010). For example, Mischke *et al.* (2010) analysed a tsunami deposit in Lake Hersek (Turkey) and suggested that the simultaneous occurrence of ostracods of different origin (lagoonal: *Cyprideis. torosa* and *Loxoconcha elliptica*; shallow marine: *Loxoconcha rhomboidea*, *Xestoleberis* sp., *Pontocythere* sp. and *Aurila cf. arborescens*; and inland waters: *Heterocypris salina* and *Eucyprinotus cf. rostratus*) within beds of brackish-marine mollusc shells and fragments indicates that the shell layers were deposited under high-energy environmental conditions (Ruiz *et al.*, 2010). In the case of Lake Manyas (140 km west of Lake Hersek), ostracods of different origins were also interpreted as reflecting an event of large amplitude (seiche) (Leroy *et al.*, 2002). In Hersek, the use of ostracods as tsunami indicators was argued on the basis of: (1) the large number of ostracod shells accumulated during the high-energy events, (2) the higher number of *taxa* which is not typical for an undisturbed lagoon setting, and (3) the mixture of ostracod valves with clear marine, lagoonal and non-marine origin.

Changes in Nannoplankton have also been discussed in association with tsunami deposits (*e.g.* Andrade *et al.*, 2003; Paris *et al.*, 2010a). Andrade *et al.* (2003) observed within the clay/sitl fraction changes in samples from the Tagus estuary (Portugal) subtle variations (*i.e.* increases) in calcareous nannoplankton that were correlated with magnetic susceptibility, foraminifera and geochemical changes. Paris *et al.* (2010a) observed that a characteristic of the Lhok Nga (Indonesia) tsunamigenic sediments is their nannolith coastal assemblages despite their relative impoverishment in clay content, which under normal marine hydrodynamic conditions would prevent nannoliths to settle. The abundance of nannoliths in the 2004 tsunami deposits tends to decrease landward and upward, despite variations due to successive phases of erosion/sedimentation by waves (see Table 2.2).

2.3.4. Geochemical signature

Several studies were conducted in tsunami deposits with the aim of identifying a distinctive geochemical signature (*e.g.* Minoura and Nakaya, 1991; Minoura *et al.*, 1994; Andrade *et al.*, 1998; Goff and Chague-Goff, 1999; Chagué-Goff *et al.*, 2002, Andrade *et al.*, 2003; Goff *et al.*, 2004; Srinivasalu *et al.*, 2007; Chagué-Goff, 2011). Usually geochemical features of tsunami deposits simply indicate the presence of saltwater inundation and thus do not provide information on the specific type of inundation. In fact, increases in the concentration of chemical elements of marine origin or elements indicative of coarser-sized sediments have been recognised in the past as a proxy in the study of extreme marine inundations. Newson (1979) detected increases in the concentration of some elements which was interpreted as evidence of marine originated sediment (Ca) and water (Na, Mg, Cl, SO_4, K) influx. A similar trend was observed by Minoura and Nakaya (1991) that also detected increases in Na, Ca, K, Mg and Cl. This was further supported by increases in Cl, Na, Ca, SO_4 and Mg observed by Minoura *et al.* (1994). Andrade and Hindson (1999) were able to detect increases in SiO_2 (indicating increase in sand material) CaO (indicating a larger presence of bioclasts), Cr, MgO, I and Cl (all indicating a marine water influx). On the other hand, increase in Fe and S and dilution of anthropogenic elements were observed by Goff and Chagué-Goff (1999) which suggested a sudden marine inundation. Van der Bergh *et al.* (2003) observed the presence of exotic sediments derived from outer coastal or continental shelf environments that were richer in heavy metals (Pb, Cu, Ni, Fe and Cr) when compared with *in-situ* sediments. A similar pattern was observed by Szczucinski *et al.* (2005) who studied sediments, deposited by the 2004 tsunami in Thailand, and noticed that they contained significantly elevated contents of salts (Na^+, K^+, Ca^{+2}, Mg^{+2}, Cl and SO_4) in water-soluble fraction, and of Cd, Cu, Zn, Pb and As.

Andrade *et al.* (2003) observed in the Tagus estuary (Portugal) in association with major compositional breaks increases in the ratios of SiO_2/Al_2O_3 and CaO/Al_2O_3 both accompanying increasing carbonate content in comparison with the under and overlying layers. The authors indicated that these elemental pairs have similar crystallochemical properties and changes of the ratios should primarily reflect variations in sediment source. The geochemical data coupled with palaeontological and magnetic susceptibility results allowed association with tsunami events that had affected that region.

Srinivasalu *et al.* (2007) reported, in India, a high content of dissolved salts in sediments (Na^+, K^+, Ca^{+2}, Mg^{+2}, Cl^-) indicating that Cu, Pb, Zn were more enriched in the tsunami deposit than the other neighbouring coastal regions. The geochemical signature is a valuable tool in the tsunami recognition but cannot be used *per si* as a diagnostic signature of tsunami deposits. In fact, the changes in geochemistry observable in a geochemical profile are mainly due to saltwater inundation, carbonate enrichment (caused by increase in shells) and changes in sediment source, all these features being also observed in storm deposits provided (Table 2.2).

2.3.5. Geomorphological signature

Dawson (1994) discussed the importance of changes caused by tsunami in coastal landscapes not only by direct tsunami-driven flow orthogonal to the shoreline, but also by episodes of vigorous backwash and by water flow sub-parallel to the coastline. He suggested that the combined effect of these processes could produce coastal landforms dominated by the effects of high-magnitude erosion and deposition. Even prior to this statement, Andrade (1990, 1992) studied the Ria Formosa (Algarve) barrier chain and noticed severe damage of the barrier chain in field observations, supported by cartographic and written documents. Such damages included the drowning of the western barrier, truncation of the oriental extremity of the barrier chain and extensive overwash of two of the eastern barrier islands (Armona and Tavira) accompanied by fast progradation of the easternmost ribbon of the Algarve sandy coast in the middle 18th century, and attributed these changes to the AD 1755 earthquake. Andrade (1992) showed that most of the the backbarrier surface of Tavira and Armona islands revealed a unique geomorphological pattern, compatible with the exceptional overwash event and with the drainage network reorganization process that must have followed the AD 1755 tsunami.

Shi and Smith (2003) described evidence for coastal erosion and retreat that occurred along the northern coastal line of Flores Island (Indonesia) as a result of the 1992 tsunami. The authors correlated the scale of geomorphological changes with the observed tsunami run-up heights over a wide area. Similarly, Regnauld *et al.* (2004) and Oliveira *et al.* (2009) described dune erosion caused by multiple tsunami events in New Zealand and to the AD 1755 tsunami in Portugal. Meilianda *et al.* (2007) presented a quantitative budget of shoreline sediment fluxes before and immediately after a tsunami in Banda Aceh, Indonesia. Through the study of remote sensing images they determined a chaotic shoreline retreat just after the tsunami. In the following six months 60% of the sediment loss had been compensated by shoreline accretion on the west coast of Banda Aceh city whereas further erosion (15% of the sediment loss during the tsunami) occurred on the northwest coast. The fact that not all locations showed a beach recovery after the tsunami stresses the importance of inner shelf processes and longshore currents in redistributing the sediment eroded at the coastline. In the same location, Fagherazzi and Du (2008) revealed that most of the morphological change occurred in the shore-normal direction, with large volumes of sand removed by the tsunami at the coastline later returned to the beach in a short time interval. A series of parallel, tapered incisions widening toward the coastline are characteristics of large flooding events such as tsunamis. In fact, flood scour features are indicator of tsunami events, given their unique morphology with width and depth of the same order of magnitude and their sharp boundaries. Goff *et al.* (2008) recognised region-wide dune remobilisation caused by tsunami inundation in New Zealand.

In general terms, and based upon field evidence from 2004 Indian Ocean tsunami, inundation by large, region-wide events is likely to cause multiple breaching of dune systems (Higman and Jaffe, 2005). In other words, multiple tsunami-scour fan assemblages can be formed during a single inundation. The assemblages could include remnant dune ridges, or pedestals, between each breach, and individual

overwash fans that could coalesce to form landward sand sheets that may or may not be mobile depending upon aeolian and dune swale conditions (Goff *et al.*, 2008). If landward sand sheets infill or overlay a wetland they can stabilise and weather *in situ* to form a low-profile hummocky topography. If they remain dry and are exposed to aeolian onshore processes they can form extensive, region-wide parabolic dune systems (Goff *et al.*, 2008). Kench *et al.* (2009) observed that reef islands in the Maldives were geomorphically resilient to the impact of the 2004 Indian Ocean tsunami with the most immediate impacts being relatively minor with reductions in island area ranging from <1% to 9%. Overwash deposits, in the form of sand sheets and sand lobes, as well as strandlines and individual clasts of coral rubble, were the most common accretionary forms. These deposits represented a net addition to island surfaces, although their preservation potential as tsunami signatures may be low.

See summary of tsunamigenic geomorphological signatures in Table 2.2.

Summary:

In summary, it is important to note that the criteria to recognize tsunami deposits (see Table 2.2) are still, at the present state of knowledge, ambiguous. Although the conjunction of the identification of sedimentary structures, the establishment of source material, the micropalaeontological analysis, geochemical characteristics and the study of geomorphological imprints in coastal landscape facilitates the identification of tsunami deposits; even if erosion and preservation is constrained by several facts. In fact, the contrast/peculiarity of the tsunami layers, especially when compared with under and overlying layers, provides in many cases the conclusive evidence for the recognition of such deposits. Data is commonly obtained through the use of sedimentologoical techniques - some have been widely used (*e.g.* textural and geomorphological) while others have been scarsely applied (*e.g.* microtextural analysis and heavy mineral assemblages); both have been used in modern tsunami sediments as well as in palaeotsunamis. Based in the references summarized in this sub-chapter and in Table 2.2 it is possible, through the use of diverse sedimentological proxies, to obtain information about the presence or absence of tsunami indicators, to establish their likely source or to collect valuable information about tsunami run-up, backwash or wave penetration inland. Recent events in Sumatra and Japan have been used to further develop the application and definition of sedimentary criteria to be used in the identification of tsunami deposits. However, in the study of palaeotsunamis a group of other questions (*e.g.* understanding mechanisms of inundation and deposition for each specific location, preservation of sedimentary structures and palaeontological evidences) still needs to be addressed in future studies in order to contribute to the development of more detailed and rigourous criteria that can further contribute to the accuracy of hazard maps.

Table 2.2 - Table summarizing the criteria to identify and differentiate tsunami deposits.

Criteria	Features (from selected references)
Physics	Very long wave length Very high velocity and speed current Few waves but with backwash Swift inundation with high shear stress and erosion
Sedimentary structures (requires stratigraphic context/analysis)	Erosional/abrupt/sharp/unconformity basal contact Massive/chaotic unit Normal grading (in places repeated) Unit with several laminae Cross-stratification Soft-sediment deformation Loading structures Parallel lamination or cross-lamination Convolutions Ripple-marks Mud drapes Rip-up clasts Broken shells
Sediment source (requires multiple source analysis)	Typically reflects the material available in the coastal fringe (i.e. beaches and berms, aeolian, inner shelf landward of closure depth) Grain size range from mud to boulders Multi-modal grain-size distribution indicating multiple sources Increase of heavy mineral concentration in the base of the deposit Increase of platy minerals (i.e. micas) in the top of the deposit SEM microtextural imprints suggest increased presence of percussion/mechanic marks
Palaeontological features (requires stratigraphical, palaeoecological and source analysis)	Marked changes in Diatoms, Foraminifera, Ostracods, Nannoplankton, Pollen (usually presenting either a chaotic assemblage or a wider range of species and, in cases, offshore/nearshore species)
Geochemical signatures (requires source analysis)	Increase inf Cl, Na, Mg, Ca, K, SiO_2, CaO, Cr, MgO, I, Fe, S Increases in the ratios of SiO_2/Al_2O_3, CaO/Al_2O_3 Increase in carbonate content (shell) Subtle variations in source-sensitive elements: K/Rb, La/Sm and Hf/Ta Enrichment in Cu, Pb, Zn or, in contrast, dilution of anthropogenic elements
Geomorphological aspects (requires regional context)	Multiple breaching of dune systems or individual overwash fans Dune ridges and sand dune pedestals Landward sand sheets Hummocky topography Parabolic dunes

2.4. Sedimentological features of onshore storm deposits (palaeotempestology)

The understanding of storm processes, their depositional and preservation potential in coastal sedimentary sequences is until the present moment still poorly documented. There are several references to storm deposits (*tempestites*) in the sedimentary record some associated with older events (*e.g.* Rossetti, 1997; Weidong *et al.*, 1997) other with more recent (*i.e.* Holocene and present day) events (*e.g.* Liu and Fearn, 1993; Jelgersma *et al.*, 1995; Otvos and Carter, 2008; Etienne and Paris, 2010; Dezileau *et al.*, 2011). Moreover, in the literature it can be found, similarly to tsunami deposits, references to boulder and to finer (typically sand-sized) deposits again in the dependence of event characteristics and sedimentary source.

The study of storm deposits appears many times as a complementary tool to the establishment of storminess patterns associated with climatic changes (*e.g.* Donnelly *et al.*, 2001; Andrade *et al.*, 2008; Almeida *et al.*, 2011). In fact, the study of tempestites provided grounds for the development of a new field of science: Palaeotempestology. This new area of research was greatly developed by the work of Liu and Fearn (1993), Liu and Fearn (2000), Donnelly *et al.* (2001), Donnelly *et al.* (2004), Liu *et al.* (2008), Switzer and Jones (2008), Etienne and Paris (2010) and Paris *et al.* (2011b) and it has been defined as "the reconstruction of past extreme events from sedimentary or erosional evidence left in the landscape as a result of storm surge and wave action" (Nott, 2003). Palaeotempestology is based in the analysis of the sedimentary record of storms/hurricanes/typhoons and is used to extend the historical record through the use of geological data and provide further knowledge to recurrence analysis. Palaeotempestological research has mainly focused in low latitude (*i.e.* hurricane prone) areas, for instance in back-barrier environments on siliclastic coasts (Switzer and Burston, 2010) including areas of tropical cyclones in northern Australia (*e.g.* Chappell *et al.*, 1983; Chivas *et al.*, 1986; Hayne and Chappell, 2001), southern and eastern United States (*e.g.* Collins *et al.*, 1999; Donnelly *et al.*, 2001; Liu and Fearn, 1993, 2000), and to a lesser extent throughout the south Pacific islands (*e.g.* Mckee, 1959). Furthermore, records of storms have also been identified in the internal stratigraphy of coastal dune systems (Jelgersma *et al.*, 1995). Zong and Tooley (1999) suggested that reliable storm-surge signatures can only be developed by using appropriate analytical techniques, such as determining the particle-size distribution of the storm layers and comparing them to associated/under and overlying non-storm sequences (Delaney and Devoy, 1995). This later sentence confirms that textural contrast is one of the criteria that have been used to identify storm deposits. Over the past two decades, a growing list of palaeotempestology studies, including some that are supported by the comparison with modern analogue events, have confirmed that overwash sand layers within the stratigraphy of coastal lakes and marshes can be a reliable proxy for major storm events.

A number of sediment-based proxies have been developed such as cyclone surge-constructed beach ridges (Nott and Hayne, 2001; Nott *et al.*, 2009) and overwash deposits preserved in back barrier lagoons (Donnelly, 2005; Donnelly and Woodruff, 2007; Wallace and Anderson, 2010), coastal lakes (Liu

and Fearn, 1993, 2000; Lambert *et al.*, 2003, 2008), and marshes (Donnelly *et al.*, 2001, 2004; Boldt *et al.*, 2010). Liu and Fearn (1993) have shown from coastal Alabama, U.S.A., that a series of hurricanes during historical time deposited multiple sand layers across low-lying coastal wetlands. Similarly, Davis *et al.* (1989) argued that hurricanes produced graded or homogeneous deposits of sand, shell, gravel and mud within the prominently clastic sediments in the coastal lagoons of Florida. Storm deposits can leave a sheet like deposit extending a few hundred of m inland. For instance the Hurricane Ivan (2004) deposit extended 200–300m while Katrina expanded up to a maximum 450m width (Otvos and Carter, 2008). It has been observed that storms can cause localized erosional surfaces in lagoonal and lake deposits. Such surfaces also occurred near the lakeward ends of storm breaches, inlets and elsewhere in coastal basins (Donnelly and Woodruff, 2007; Woodruff *et al.*, 2009). Rip-up clasts and scours in tidal marsh deposits also reflect storm erosion. Furthermore, Donnelly *et al.* (2001) demonstrated that recent and historic major hurricanes on the United States Atlantic coast left a stratigraphically distinct and regionally consistent record of overwash sand layers in the sediments of the coastal marshes. In terms of sediment source Lu and Liu (2005) studying hurricane events in Alabama (United States) concluded that the tempestite sand layers are similar to those from the dune environments, thus suggesting that they were transported from the dunes by overwash processes. More recently Lambert *et al.* (2008) proposed the use of organic geochemical proxies as a new tool in palaeotempestology, utilizing isotope $\delta^{13}C$ and $\delta 1^{5}N$ concentrations and ratios in organic-enriched muds. The changes observed in these isotopes were attributed to specific storm events.

The use of palaeotempestology data to establish frequency of events and minimum wave heights of extreme marine inundations has been applied with success, for instance, in the eastern coast of the United States. Boldt *et al.* (2010) presented a 2000 year record of overwash deposition preserved in a backbarrier salt marsh from south eastern New England (United States) and were able to establish that during the last *ca.* 375 years only historical hurricanes with surges of at least 2m were preserved in the Mattapoisett Marsh sediments. A similar study was conducted by Lane *et al.* (2011) in Mullet Pond, Florida (United States). In this study, a 4500 year record of Holocene hurricane storm surges was obtained. The record with sub-decadal resolution allowed the establishment of an average event frequency of 3.9 storms per century, greater than that of any published palaeohurricane record. The authors acknowledge that although the largest historic hurricane events were represented in the record, some smaller events went undetected resulting in an underestimate of the number of storms impacting the site through time. The authors also observed that shallow, benthic foraminifera (living in depths of 1 to 5m below msl, *i.e.* up to 3 to 5 km seaward of the shoreline) were present in deposits associated with the AD 1941 hurricane and possibly Dennis (AD 2005). McCloskey and Keller (2009) studied six major hurricanes that were detected in the sedimentary record of the past 500 years along the central coast of Belize representing 1 to 1.2 catastrophic storms every 100 years in the study area.

The majority of palaeotempestites have been observed in the United States eastern coast due to more intensive research, favourable sedimentary basins that can retain the sedimentary deposits and to the

more hurricane-prone climatic conditions. In addition, the large width and extreme low-gradient of the shelf and morphological continuum in features characterizing the shelf and the extensive adjacent low-lying coastal areas favour the development of intensive surges in association with tropical storms. In Europe similar deposits have been described, such as reported by Jelgersma *et al.* (1995), which observed shell deposits found in dune fields at five different sites along the central Netherland coast and associated these deposits with several Holocene storm surge events. Andrade *et al.* (2004) tested the geological record of storminess through the analysis of a group of five marsh detached beaches and one active marginal beach in the Ria Formosa barrier islands (Portugal) area using sedimentological, paleoecological (Foraminifera and Diatoms), geometrical and stratigraphical information derived from sediment cores which were interpreted by comparison with present-day analogues. They concluded that the lithostratigraphical framework indicated that multiple sand bodies were present in some cores, with limited lateral extension and separated by muddy lagoonal sediments indicating that distinct episodes of entrainment of marine sand into the lagoonal space alternated with low-energy sedimentation. In the same region, Matias *et al.* (2008) studied 28 storm events during a 3 year study period (2001-2004). Depending on the volume state of the barrier island, storm waves caused either erosion of the beach (net negative supratidal sedimentary balance) or promoted intense overwash that contributed to barrier enlargement by extensive sedimentary deposition (overwash). Ruiz *et al.* (2007) studied the Holocene infilling of the Odiel estuary (Gulf of Cadiz) using lithological, stratigraphical, geochemical, and palaeontological data which allowed the recognition of the oldest known Holocene storm in this area (*ca.* 5705 ^{14}C years BP). In this area, the geological record of storm events is constituted by: (a) sandy layers with basal erosional surfaces interlayered in muddy sediments; (b) new beach ridges added periodically to sandy spits; or (c) lumachellic layers of mollusc shells interbedded within massive, bioturbated levels. Dezileau *et al.* (2011) studied the Languedoc–Roussillon region (French Mediterranean coast) and identified four distinct, overwash deposits at more than 500m from the sandy barrier. The authors demonstrated that the geomorphic setting of the studied area has not changed drastically during the last 1500 years, and attributed these four overwash deposits to catastrophic storms of category 3 intensity or more.

Storms surveys conducted immediately after the events have been carried out throughout the world. Two examples of those campaigns and the recognition of sedimentary imprints left by storms are described by Dawson *et al.* (2007) and Horton *et al.* (2009). Horton *et al.* (2009) collected data from Hurricanes Katrina and Rita storm surges along the Alabama and Mississippi (United States) coastline. Ground surveys of local topography, storm surge high water marks and flow direction were conducted. In Mississippi, Hurricane Katrina storm surge extended inland more than 750m. The differences between the pre-storm surge and storm surge sediment were defined by the following characteristics: erosional boundary between sedimentary units accompanied by a change in colour and a change in lithology; and the storm surge sediment was coarser than the pre-storm surge unit and with lower organic content. The thickness of

the Hurricanes Katrina and Rita storm surge sediments ranged from 7 to 13cm. Foraminiferal analyses in all three sites revealed a virtual absence of tests within the storm surges sediments.

Dawson *et al.* (2007) analysed the coastal changes observed in the Hebrides Islands (Scotland) associated with the Great Storm of January 2005. The hurricane-force winds together with a storm surge resulted in significant change in coastal landscape along the entire western seabord and, in particular, on headlands (Angus and Rennie, 2007). In general, severe erosion was focused along coastal areas located west of the causeways that link North Uist and Benbecula, Benbecula and South Uist and South Uist and Eriskay. According to Dawson *et al.* (2007) the coastal response to the storm was complex. In some areas, coastal dunes were subject to significant retreat. In other areas deposition of shingle and even boulders was observed. In both cases described above erosion and deposition (of material available in the coastal fringe) was observed in association with overwash caused by major storm events.

From all of the above it can be stated that storm overwash is undoubtedly a powerful agent in beach and dune erosion and backbarrier sand accumulation. Typical washovers generally consist of fan- or sheet-like subaerial to subaqueous accumulations of sand supplied by storm overwash from the nearshore areas and supratidal sediment resident on barrier island and mainland surfaces. Of highly variable thickness, these sequentially developed landforms are mutually superimposed during consecutive storm events by sediment gravity flow influenced by fluid effects (Middleton and Hampton, 1973). Washovers or overwash fans are elongated lobate, parabola- and flame-shaped landforms. Factors that influence the dimensions and outlines of fans and related overwash bedforms include wind-induced surge elevation, astronomical tide, wave setup and run-up, the intensity and duration of channelled flow, the presence of topographic obstructions, and the volumes of sand in the shoreface and beach with dunes that are available for erosion and subsequent deposition by overwash (Donnelly *et al.*, 2001; Boldt *et al.*, 2010). Sedgwick and Davis (2003), Morton *et al.* (2007) and Horton *et al.* (2009) recognized multiple sedimentary structures related to deposition of individual overwash units. Sand and mud layers of contrasting clast dimensions and microfossil (Foraminifera and Diatoms) content formed these beds.

Most of Holocene fine grain-sized storm deposits have been discussed in comparison with tsunami events. Storm deposits are difficult to distinguish from tsunami deposits because, similar to the latter, they also may contain marine or brackish water macro and microfossils, retain saltwater geochemical imprints, and thin and fine landward (Nelson *et al.*, 1996). Some studies use distance inland to indicate a tsunami source, arguing that it is not likely that storm waves or surge could deposit sand inland to the extent indicated by a number of deposit atributed to be of tsunami origin (Clague *et al.*, 2000). When layers of both events are present in the same location their number and thickness have sometimes been used to differentiate between a tsunami and a storm genesis (Williams and Hutchinson, 2000). Tsunami deposits tend to have several relatively thick normally graded beds, suggesting deposition from graded suspension by successive waves in the tsunami wave train, whereas storm deposits may be expected to have thinner and more numerous laminations, from higher frequency but lower energy storm waves (Nelson *et al.*, 1996). Moreover, Abramson (1998) uses the

presence of rip-up clasts in the deposit to indicate the higher energy deposition of a tsunami although this is in contrast with other findings (*e.g.* Switzer, 2008).

Recently, a number of papers revisited the issue of distinguishing tsunami and storm deposits (Nanayama *et al.*, 2000; Goff *et al.*, 2004; Tuttle *et al.*, 2004; Morton *et al.*, 2007; Kortekaas and Dawson, 2007; Switzer and Jones, 2008). Nanayama *et al.* (2000) described deposits associated with the 1993 Japan Sea tsunami and the 1959 Miyakojima typhoon in the same location in the Hokkaido coast, Japan. The main differences detected were that the tsunami deposit consisted of four beds, showing evidence of bidirectional currents associated with land- and seaward flow of the two main waves and contained marine sand, gravel, seashells and eroded soil. In opposition, the storm deposit showed a unidirectional current, contains foreset bedding and was better sorted than the tsunami deposit. Bryant and Nott (2001) compared geomorphological implications of tsunami and storms. They make the point that storms tend to only surge through gaps in dunes, sporadically depositing lobate fans that rarely penetrate far inland. This can be considered as a key difference between storm and tsunami geomorphology but this is more controversial in areas of low accumulation space (*e.g.* in a small pocket beach, there may be insufficient longshore and landward accumulation space for more than one lobate fan and two pedestals) (Goff *et al.*, 2008).

Gelfenbaum *et al.*, (2002) suggested that "In the absence of a historically-documented context, and/or the preservation of both types of deposit at the same location, researchers must make comparisons between the studies of the sedimentary records of individual storm and tsunami deposits from widely separated sites around the world". Indeed, one should have in consideration the countless site-specific variables such as sediment supply, nearshore bathymetry and coastal topography. Tuttle *et al.* (2004) compared the deposits of the AD 1929 Grand Banks tsunami with the AD 1991 Halloween storm in Massachusetts, in the eastern coast of the United States. The tsunami deposit had one to three sub-units of massive or normal graded sand, whereas the storm deposit showed lamination, delta foreset stratification and sub-horizontal, planar stratification with channels. The tsunami deposit can be traced further inland and to a higher elevation than the storm deposit. However, because both deposits were not found at the same location, differences due to site-specific variations have to be considered.

Goff *et al.* (2004) compared a 15th century tsunami deposits and sediments emplaced by an Easter 2002 storm. Both deposits are peculiar in local extent, thickness, and grain size. According to Goff *et al.* (2004) the main differences can be summarized as follows:

(a) The tsunami deposit thins abruptly at the margins and fines inland as opposed to exhibiting the highly variable characteristics of the storm deposit with a marked coarsening at its landward extent.

(b) The storm deposit is slightly better sorted and coarser than the tsunami deposit. A coarser grain size is probably the result of differences in sampling regime as opposed to wave energy, while a better sorting reflects the wider range of grain sizes entrained by the tsunami both on land and onshore.

(c) Differences in the landward characteristics of these inundation events are reflected in the contrast between the erosional contact and entrainment of rip-up clasts of the tsunami and the sharp contact of the storm deposit. Both are associated with buried soils and/or vegetation, but only the tsunami penetrated far enough inland to affect archaeological material.

(d) Variations in the preservation of evidence are a reflection of the age of deposition.

Morton *et al.* (2007) suggested some differences between tsunami and storms based on only two tsunami deposits (from Peru and Papua New Guinea) and two storm surge deposits (from Texas and North Carolina). The clear suggestion from their work is that tsunamis and storm deposits have much more similarities than differences. Kortekaas and Dawson (2007) analysed a group of samples from Martinhal (SW Algarve, Portugal). The authors recognised tsunami deposits (associated with the AD 1755 event) and several, more recent, storm deposits in this location. The authors concluded that Foraminifera assemblages and grain size characteristics are almost identical in both type of events although tsunami deposits present higher concentration of Foraminifera and some boulders with borings of molluscs. The main difference detected was the inland extent of the tsunami deposit when compared with the storm events. Switzer and Jones (2008) tried to establish the source of a marine deposit detected in a closed freshwater back-barrier lagoon on the southeast Australian coast. Their studies were based on comparisons with modern storm deposits from the same coast and sedimentological diagnostic criteria derived from studies of modern storm- and tsunami-deposited sandsheets (Figure 2.2).

Dahanayake and Kulasena (2008) compared tsunami, storm-surge and nearshore sediments. The authors detected that storm surge sediments were better sorted than all the tsunami samples studied. The relatively high heavy mineral content and the scarce presence of open marine microfossils also helped to diagnose the storm-surge sediments. Morton *et al.* (2008) studied coastal gravel-ridge complexes deposited on islands in the Caribbean Sea as recorders of past extreme-wave events that could be associated with either tsunamis or hurricanes. The ridge complexes of Bonaire, Jamaica, Puerto Rico (Isla de Mona) and Guadeloupe consist of polymodal clasts ranging in size from sand to coarse boulders that are derived from the adjacent coral reefs or subjacent rock platforms. Ridge-complex morphologies and crest elevations are largely controlled by availability of sediments, clast sizes, and heights of wave run-up. Together, the morphologic, sedimentologic, lithostratigraphic and chronostratigraphic evidences indicated that shore-parallel ridge complexes composed of gravel and sand that are tens of m wide and several meters thick are primarily storm-constructed features that have accumulated for a few centuries or millennia as a result of multiple high-frequency intense-wave events.

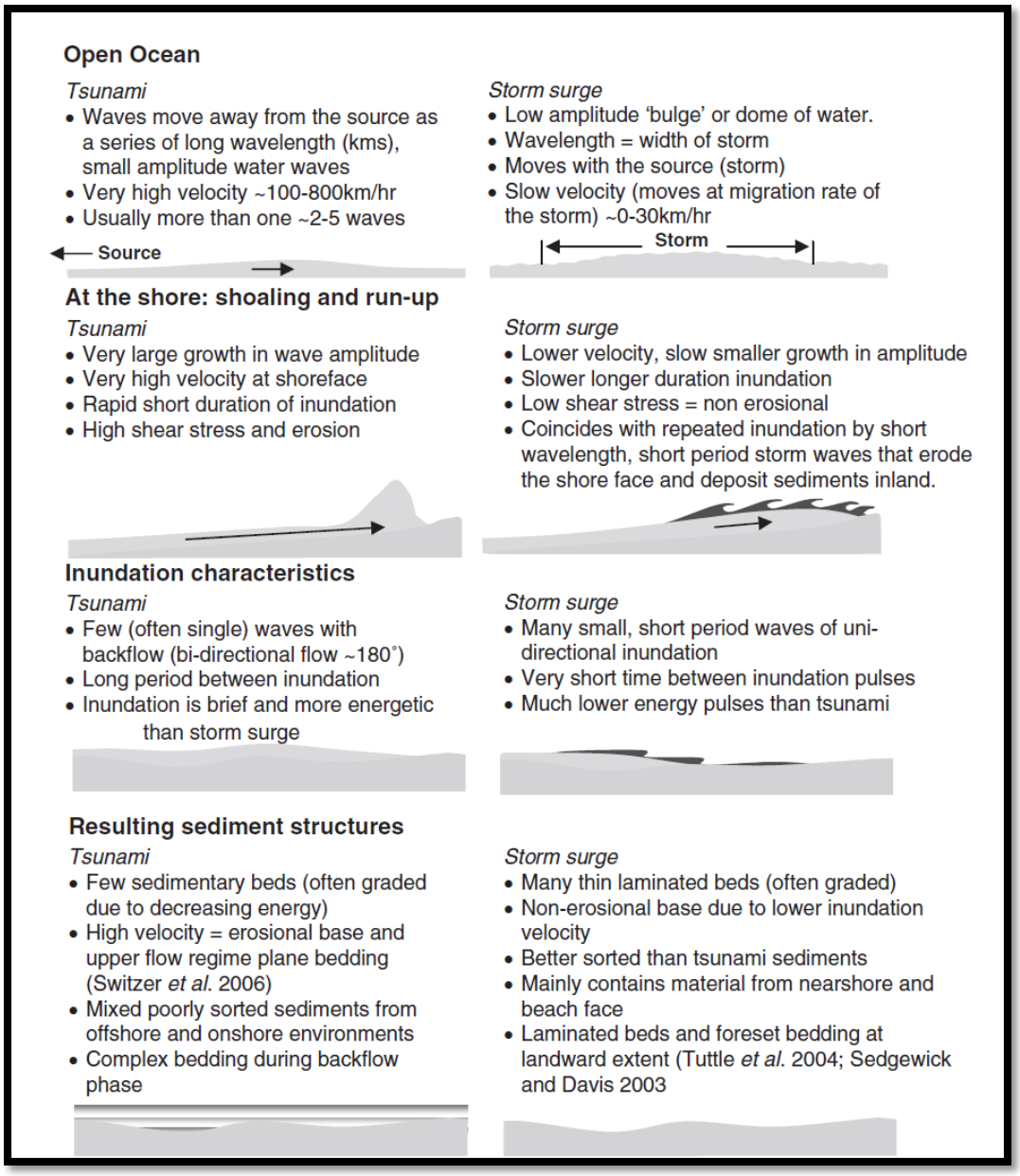

Figure 2.2 - Schematic summary diagram of different characteristics of tsunami and storm surge: in the ocean, at the coast, during run-up and inundation, along with a basic description of the resulting sediments. (Switzer and Jones, 2008).

The recognition of tsunami boulder deposits has been previously discussed in this thesis. The complex processes associated with the transport inland and upwards of boulders and their association with a specific type of marine inundations requires, almost on every occasion, the use of hydrodynamic equations to establish wave height or velocities (*e.g.* Nott, 2003) and associate them with specific events.

More recently, Goto *et al.* (2011) stressed once again the importance of the development of precise numerical modelling of boulder transport as a key method to assist in discriminating between tsunami and storm wave boulders. While these models are still being developed by the scientific community is fairly relevant that the definition of sedimentological criteria to differentiate tsunami and storm deposits is enhanced and developed. Hall *et al.* (2006) characterized cliff-top storm deposits of the Atlantic coasts of the

British Isles and were able to recognize that these deposits form a distinctive end member to the much larger group of coarse clastic storm features. The authors concluded that the detailed configuration of the coast, particularly the size, height, orientation and form of the cliff edge and top, exerts a major control on the distribution, altitude, clast orientation and clast size of the storm cliff-top deposits. Etienne and Paris (2010) provided a new insight for the interpretation of boulder deposits by highlighting the geomorphic effects of powerful storms. The authors observed that during the winter of 2008 in Iceland boulders up to 16t were transported inland. However, the authors concluded that notwithstanding the drastic seasonal individual changes, at a larger scale, boulder deposits (beaches or ridges) are landforms with a strong permanence in the landscape over years. Also recently, Paris *et al.* (2011b) edited a review on boulders and megaclasts deposited by storm waves on rocky coasts. The authors discussed the possibility of storm events as likely mechanisms for boulder transport in high and temperate latitudes.

Recent studies (Goto *et al.*, 2010a, 2010b; Etienne and Paris, 2010; Richmond *et al.*, 2011) have proposed that tsunami and storm boulder deposits can be differentiated by considering the position relative to source, size, distance travelled and breakage of boulders. They suggested that the approach of coupling sedimentology and geomorphology can be applied to other boulder fields, but requires further testing in other locations. Goto *et al.* (2011) studied the emplacement and movement of boulders by known storm waves based in field evidences from Okinawa Island, Japan. They concluded that no single method to discriminate boulders deposited by the tsunami or storm waves appears to be universally applicable to all cases in the world. Nevertheless, the authors discuss the possibility that boulders can be discriminated in each case when local complexities of waves, topography, and characteristics of boulders are considered.

The few studies specifically designed to compare characteristics of historical tsunami and storm finer grained deposits (*e.g.* Nanayama *et al.*, 2000; Kortekaas and Dawson, 2007; Goff *et al.*, 2004; Tuttle *et al.*, 2004; Switzer and Jones, 2008) were conducted at the same or nearby sites. This eliminated or reduced inter-site sediment and landscape variability but prevented the comparison of impacts of events of similar intensities, elsewhere. In conclusion, storm deposits share many textural, palaeontological, geochemical and geomorphological characteristics with tsunami deposits making their differentiation a complex task. This is also further complicated by studies addressing storm activity but not clearly separating storm surge from storm wave impacts and sedimentation. The diversity of topographic, hydrodynamic, and sedimentological settings as well as post-depositional settings account for major difficulties in correlating individual sand layers with specific prehistoric storm events. This complicates or prevents identification of specific events, their velocity categories, calculations of recurrence interval probabilities and accurate risk assessment. The differentiation of tsunami and storm deposits is of crucial importance for studies of hazard risk and the development and improvement of sedimentary criteria is a scientific requisite.

2.5. Record of tsunami and storm deposits in the study areas

2.5.1. Atlantic Iberia

Several onshore and some offshore tsunami deposits have been detected in this region. Most of the deposits have been described in association with the AD 1755 tsunami although deposits associated with older events have also been described (Figure 2.3).

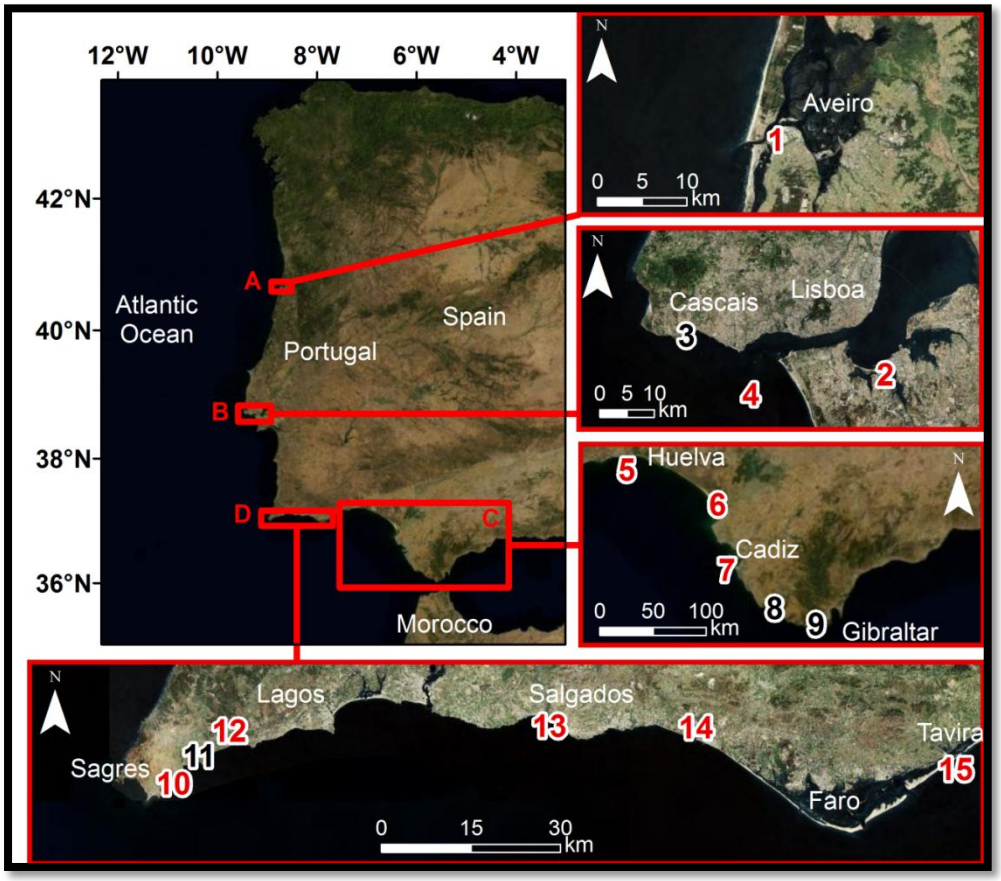

Figure 2.3 - Locations where some tsunami deposits have been described along the Atlantic Iberia coastline (sandy deposits numbered in red; boulder deposits numbered in black). 1: *Aveiro* - Corrochano *et al.* (2000); 2: *Tagus estuary* - Andrade *et al.* (2003); 3: *Cascais* - Scheffers and Kelletat (2005); 4: *Tagus prodelta* - Abrantes *et al.* (2005, 2008); 5: *Huelva estuary* - Morales *et al.* (2008); 6: *Doñana* - Ruiz *et al.* (2005); 7: *Valdelagrana* - Luque *et al.* (2001); 8: *Cape Trafalgar* - Whelan and Kelletat (2005); 9: *Barbate and Tarifa* - Reicherter *et al.* (2010); 10: *Martinhal* - Andrade *et al.* (1997), Kortekaas and Dawson (2007); 11: *Barranco* - Costa *et al.* (2011); 12: *Boca do Rio* - Dawson *et al.* (1995), Hindson and Andrade (1999), Hindson *et al.* (1996); 13: *Salgados* - Costa *et al.* (2009), Costa *et al.* (2012a); 14: *Quateira* - Schneider *et al.* (2009); 15: *Ria Formosa* - Andrade (1992).

In the western coast of Portugal, there are references to the AD 1755 tsunami washover deposits in the Aveiro lagoon (Corrochano *et al.*, 2000), to silt-clay sedimentation in the Tagus estuary (Andrade *et al.*, 2003) and erosion and deposition of coarser material in the Tagus prodelta (Abrantes *et al.*, 2005; 2008). Furthermore, in the Guincho area (W of Lisbon), Scheffers and Kelletat (2005) detected a number of megaclasts and attributed their displacement to tsunamigenic mechanisms of different ages including the AD 1755 tsunami, although the absolute age-estimation they have used is controversial. In addition to megaclasts they described boulder fields and ridges standing at heights of more than 10m above msl

bearing evidences of having been moved inland from the source region and thus associated to one or more tsunami events that affected this region. The authors also argue to have found a vegetation scar and beach sand with perfectly rounded pebbles in the same area of tsunami origin. Approximately 40 km to the north of Cascais (*i.e.* Praia dos Coxos-Ericeira) a peculiar limestone boulder accumulation was identified in a rocky platform and the possibility of its transport and deposition by one or multiple tsunami events has been discussed (Oliveira, 2011). Andrade *et al.* (2003) found evidences in sediment cored from the Tagus marshes that were correlated with the AD 1755, AD 1531 and with one older event tentatively dated of the 14th century AD. The techniques used include vertical variation of the bulk magnetic susceptibility, geochemistry, nannoplankton (abundance and diversity) and a range of sedimentological proxies. The evidences were provided by the changes detected in those units laid down by high energy marine events. These changes included slight increases in SiO_2 and $CaCO_3$ and abrupt changes in magnetic susceptibility values (suggesting temporary disturbance of sediment sources) together with increases in calcareous nannoplankton. On the other hand, in the Tagus prodelta, Abrantes *et al.* (2005, 2008) sampled the shelf area just offshore Lisbon. They were able to identify an "instantaneous deposit" of coarser material (including broken carbonate shells) on the SSW coring site; and a 1.5m "instantaneous deposit" of fine material on the W site in sediment collected in their box-cores. Magnetic susceptibility, grain-size and XRF-Fe data as well as ^{210}Pb and AMS ^{14}C age-estimation were used to characterize the material and time-constrain the deposition. By considering the ages of the underlying undisturbed unit, a hiatus was recognised at both sites studied, roughly corresponding to 355 years of sedimentation. Both the hiatus and instantaneous deposits were considered to be of tsunamigenic origin, the former corresponding to an erosive episode and the latter to sedimentation, both in association with the backwash of the same tsunami event. Also in the south western coast of Portugal, Pereira *et al.* (2007) identified, in the Malhão beach and dune field (approximately 150 km south of Lisbon), which develop in close association with aeolianite outcrops, a group of 43 boulders located from 20 up to 135m inland of the present day coastline. The highest boulder is located at 19m above msl and the heaviest boulder weights 19t. By means of a straightforward application of Nott's equations and identification of some geomorphological features, the authors concluded that the only event capable of transporting and deposited boulders of such dimensions was the AD 1755 tsunami.

The tsunami deposits of AD 1755 that were deposited along the Algarve coastline mostly consist of a laterally extensive layer of shell-rich sand, which ramps and thins landwards, displaying an erosive base and an irregular, sometime undulating, upper boundary; this boundary may be sharp or made of a subtle textural and compositional transition to the overlying sediment. In some locations, the tsunami deposit is entirely composed of sand. In other areas, the tsunami deposits are characterized by sand sheets containing isolated cobbles, which preferably concentrate at the base of the tsunami deposit. Andrade (1990, 1992) detected tsunami deposits in sections of the barrier-island chain of Ria Formosa, central Algarve. He concluded that the AD 1755 earthquake was responsible for severe damage of the barrier chain at Ria

Formosa, leading to the drawning and amputation of its oriental extremity and to the extensive overwash of two of the eastern barrier islands (Armona and Tavira). Moreover, Andrade (1992) also refers that the morphological analysis of the backbarrier surface of these two islands reveals a unique pattern, compatible with the exceptional overwash event and with the drainage network reorganization process that must have followed the AD 1755 tsunami. Dawson *et al.* (1995), Hindson *et al.* (1996) and Hindson and Andrade (1999) identified a tsunami deposit attributed to the AD 1755 tsunami, at Boca do Rio lowland, western Algarve coast of Portugal. Detailed historical record of the AD 1755 tsunami flooding described the destruction of a contemporaneous coastal dune by the incoming tsunami waves (Silva Lopes, 1841). The tsunamigenic unit, referred to by Dawson *et al.* (1995) as a "chaotic layer", "consists of a massive structureless matrix of detrital sediment ranging from a muddy/sandy conglomerate to coarse muddy sand. According to Hindson and Andrade (1999) this unit marks a distinct sedimentological and micropalaeontological break from the deposits enclosing it. Those authors noted the lowermost section of the deposit appears to have been deposited from a highly turbulent water mass, which was able to transport gravel-sized limestone clasts as well as gravel sized mud balls eroded from the underlying estuarine soft material (rip-up clasts). The water mass rapidly lost energy as it progressed inland, leading to the deposition of predominantly shell-rich sand, silt and clay particles. Andrade *et al.* (1997) and Kortekaas and Dawson (2007) also described a tsunami deposit in Martinhal, east of Sagres. This massive deposit, which extends across most of the lowland area, was suggested to have being laid down by the AD 1755 tsunami (Kortekaas and Dawson, 2007). Besides the tsunami deposit, the stratigraphy of Martinhal also displays evidence for the activity of storm waves that have breached and overtopped the barrier, flooding the lowland and leaving thin sandy overwash layers, but of smaller inland extension. Both types of marine-derived flood deposits showed similar grain size characteristics and distinctive contents in benthic Foraminifera, evidenced by the predominantly marine assemblage of the tsunamigenic unit with the presence of *Elphidium macellum*, *E. crispum*, *Quinqueloculina seminulum*, *Cibicides refulgens*, *C. lobatulus*, *Eponides repandus* and *Ammonia. beccarii* var. *Batavus,* but also brackish species such as *H. germanica* and *A. beccarii*. The most important differences between storm and tsunami deposits were the rip-up clasts and boulders that were exclusively found in the tsunami deposit and the landward extent of the tsunami deposit that everywhere exceeded that of the storm deposits. Schneider *et al.* (2009) analysed cores from the Carcavai valley, near Quarteira (east of Salgados, in the central Algarve), and detected that one prominent sand layer interrupts the fine-grained sedimentation. After radiocarbon age-estimation, the authors suggested that this peculiar unit might have been deposited by the AD 1755 tsunami, although the sum of evidences forwarded to support this origin is small and questionable. Still in the vicinity of Quarteira, in Salgados, Costa *et al.* (2009, 2012a) detected and characterized a tsunami deposit within Late Holocene lagoonal sediments of Lagoa dos Salgados, based in the recognition of many of the stratigraphical, textural and compositional diagnostic criteria used to recognize this type of deposition elsewhere. Furthermore, results of age constraining using ^{210}Pb, ^{137}Cs and ^{14}C methods yielded results that were mutually consistent and coherent with the AD 1755 tsunami. Immediately to the west of Salgados, Alcantarilha lowland is located. Within this lowland Dinis *et al.* (2010) observed geomorphological features

that provided support for a major overwash deposit that not only eroded the top part of a sector of the confining dune ridge but was also responsible for the deposition of a fan-shaped sandy layer, which attaches to the toe of the leeward slope of the dune and thins and wedges out further inland into the adjacent alluvial plain sediments. The authors interpreted that the most probable mechanism for these sedimentary evidences should be a tsunami event and ^{210}Pb and^{137}Cs data once more suggests it may date of AD 1755. Cunha *et al.* (2010) revisited Boca do Rio and Martinhal AD 1755 tsunami deposits to improve the age model by using OSL age-estimation with a higher number of aliquots. Contrary to previous works, the authors obtained a good set of dates for the deposit, although an age overestimation of the tsunami-laid sands was attributed to the rapid erosion and deposition of older sediments, with insufficient light exposure for complete bleaching during the tsunami event itself. Costa *et al.* (2011) observed in the Barranco and Furnas alluvial plains a relatively unique size-range of the particles [0.3 - 1m (a-axis diameter)] that were transported inland a few hundred meters into the alluvial plain. The radiocarbon dates obtained through the use of *in situ* endolithic shells suggested that transport was contemporary with the AD 1755 tsunami.

Further east in the Gulf of Cadiz, several tsunamigenic deposits have been recognized both onshore (*e.g.* Lario *et al.*, 2011) and offshore (*e.g.* Gracia *et al.*, 2010). Luque *et al.* (2001) conducted studies of sedimentary deposits of the Valdelagrana spit and barrier complex (Cadiz, Spain). A depositional event was detected within the barrier complex and it was suggested that it recorded an event similar to the AD 1755 Lisbon earthquake, which might have occurred at 216-218 BC. More recent single-event deposits of the Valdelagrana spit were correlated with the AD 1755 tsunami. The older deposits could be contemporaneous and correlated with deposits observed in estuarine lowlands of the Donana National Park, SW Spain (Ruiz *et al.*, 2005). Ruiz *et al.* (2005) conducted studies focused in the Mid-Holocene evolution of sedimentary environments of the Doñana National Park. They concluded that in the last 5300–3700 cal. years BP interval a progressive estuarine infilling conditioned by the growth of channel levees and the progradation of the Donana spit towards the east has occurred. This infilling pattern was being periodically interrupted by high-energy events causing the breakthrough of the Donana spit and inducing biological crisis of the estuarine faunas. These crisis induced temporary but strong reduction of the characteristic estuarine assemblages (detected in ostracods and bivalves), with introduction of reworked marine faunas towards the inner estuary. Several sedimentary units associated with these barrier breaching episodes and faunal crisis were associated with different tsunamigenic events, including the AD 1755 tsunami. Morales *et al.* (2008) investigated tsunami deposits in the Tinto-Odiel estuary (Huelva). They characterized the outer part of the estuary by extensive sand-rich sedimentary bodies of marine origin, whereas the central and inner parts were filled by muddy, tidally deposited sediment bodies. Recorded within these inner estuarine sediment bodies five laterally continuous shelly units were detected. According to Morales *et al.* (2008), each of these units displayed many of the typical characteristics of tsunami deposits, comprising an erosional base followed by a fining-upward sand-sized sequence that begins with shell accumulation and ends with bioturbated muddy sand. The results of ^{14}C ages and indirect age-estimation using accumulation rates

derived from the study of recent radionuclides suggest that these five tsunami deposits correspond with known events that occurred in AD 1755, 1531, 949 (1033?), 881, and 395 (381?), all of which are documented in historical sources (Morales *et al.*,2008).

Still in the eastern part of the Gulf of Cadiz, the work on boulder deposits of Whelan and Kelletat (2005) deserves a special note. In Cape Trafalgar, they detected approximately 280 imbricated megaclasts weighing between 1 and 10t that were observed resting between high tide level and 5m above in a coastal stretch of 100m long directly south of that headland. They argued that the larger boulders preserved at Cape Trafalgar are the only possible proofs for a tsunami event along an approximately 100 km stretch of coastline between the mouth of the Guadalquivir and Punta Camarinal, halfway between Barbate and Tarifa. However, Reicherter *et al.* (2010) identified outcrop evidences for paleo-tsunamis along a 50 km long segment of the Atlantic coast of southern Spain. According to these authors several depositional environments in the coast between Barbate and Tarifa yielded preserve tsunamigenic sediment layers among other evidences of tsunami impacts, both on top of rocky cliffs as well as in lagoons and in marshlands. The authors associated deposits identified with the AD 1755 but also attributed multiple intercalations to older tsunamis.

Storms have been defined for this area as events where the significant height (Hs) of waves is greater than 3m (Pessanha and Pires, 1981). In terms of storm deposits only over recent years the sedimentary effects have been described and/or monitored in greater detail (*e.g.* Andrade *et al.*, 2004; Kortekaas and Dawson, 2007; Matias *et al.*, 2008; Almeida *et al.*, 2011). Andrade *et al.* (2004) studied marsh detached beaches in Ria Formosa lagoon and were able to detect storm deposits within the lithostratigraphical framework observed in cores. These (multiple) sand bodies had limited lateral extension and were separated by muddy lagoonal sediments indicating that distinct episodes of entrainment of marine sand into the lagoonal space alternated with low-energy sedimentation. In the same region, Matias *et al.* (2008) using aerial photographs observed a total of 369 different washovers along the lagoonal boundary of Ria Formosa barriers during the period 1947-2001. The number of washovers remained relatively stable from 1947 to 1972 and increased dramatically between 1972 and 1976 probably as a result of the development of immature inlet margins and downdrift starvation. From 1976 to 2001, washover occurrences declined and their spatial dimensions diminished, leading to a decrease in overwash activity over this time. According to these authors, exceptional to infrequent oceanographic conditions are the only formation mechanism able to generate an overwash in well-developed and stable foredunes. Although inundation of established foredunes was not observed for the studied period, this phenomenon has been described for the eastern section of Ancão barrier (Andrade, 1990) as a result of exceptional storm conditions during the 1941 cyclone. Kortekaas and Dawson (2007) in Martinhal used a combination of grain size and foraminiferal analyses to assess differences between tsunami and storm deposits. Only the tsunami deposit contained large boulders, sometimes with borings of molluscs at their surface and intraclasts eroded from the underlying surface. Oliveira *et al.* (2011) used field observations, aerial photography and wave data to

characterize the transport of two megaclasts weighting 14 and 8t and sitting at present above 1.70m above msl in the upper shore platform of Praia das Maçãs (west Portuguese coast – approximately 20 km north of Cascais) and associate them with a specific event (storm in 1973).

2.5.2. Scotland

By far the biggest tsunami that has struck the coastline of Scotland was the tsunami associated with the giant Storegga submarine landslide located on the continental slope west of Norway that took place *ca.* 8000 yr BP (Figure 2.4). However, recent studies have shown that the Holocene Storegga Slide is just one of a series of mega-slides (>2000 km^2) that have occurred offshore mid-Norway since the end of the Pliocene, with a frequency of roughly 100,000 years over the last 0.5 Ma (Bryn *et al.*, 2002).

Deposits from the Storegga tsunami have been found in NE England (*e.g.* Horton *et al.*, 1999; Shennan *et al.*, 2000; Smith *et al.*, 2004), N Sotland (Dawson *et al.*, 1996; Dawson and Smith, 2000), NE Scotland (*e.g.* Dawson *et al.*, 1988; Long *et al.*, 1989; Tooley and Smith, 2005), Shetland Islands (*e.g.* Bondevik *et al.*, 2003; Bondevik *et al.*, 2005; Dawson *et al.*, 2006), Faroe Islands (*e.g.* Grauert *et al.*, 2001) and to north of the Arctic Circle along the coast of Norway (*e.g.* Bondevik *et al.*, 1997) and Greenland (Wagner *et al.*, 2007) (Figure 2.4). The tsunami sediments associated with the Storegga slide can be generally described as consisting mainly of fine or fine to medium sand, sometimes with some silt and clay and very occasionally containing gravel or stones in the basal layers. It often contains fragments or intraclasts of organic material and sometimes intraclasts of silt while rip-up clasts of peat have also been identified. Typically the tsunami units present at least one fining upwards sequence, commonly with bi-modal size distribution, and present a maximum thickness of 1.56m but the deposit is normally *ca.* 10–30 cm thick (Smith *et al.*, 2004). The microfossil content (Diatoms and Foraminifera) of the tsunamigenic layer provides grounds to support a high-energy event of marine origin involving sediments of probably local provenance (Smith *et al.*, 2004). In NE England, near Berwick-upon-Tweed, Horton *et al.* (1999) and Shennan *et al.* (2000) described a sand horizon of marine provenance within a coastal peat moss and attributed it to a high-energy flood. The singularity of the layer in the sediment sequence, its stratigraphically unconformable lower contact in the transect, implying erosion of underlying sediments; its rapid rise up-valley in the transect to exceed the height of later marine deposits and its age range, allowed the identification of the sand layer as a probable Holocene Storegga Slide tsunami deposit.

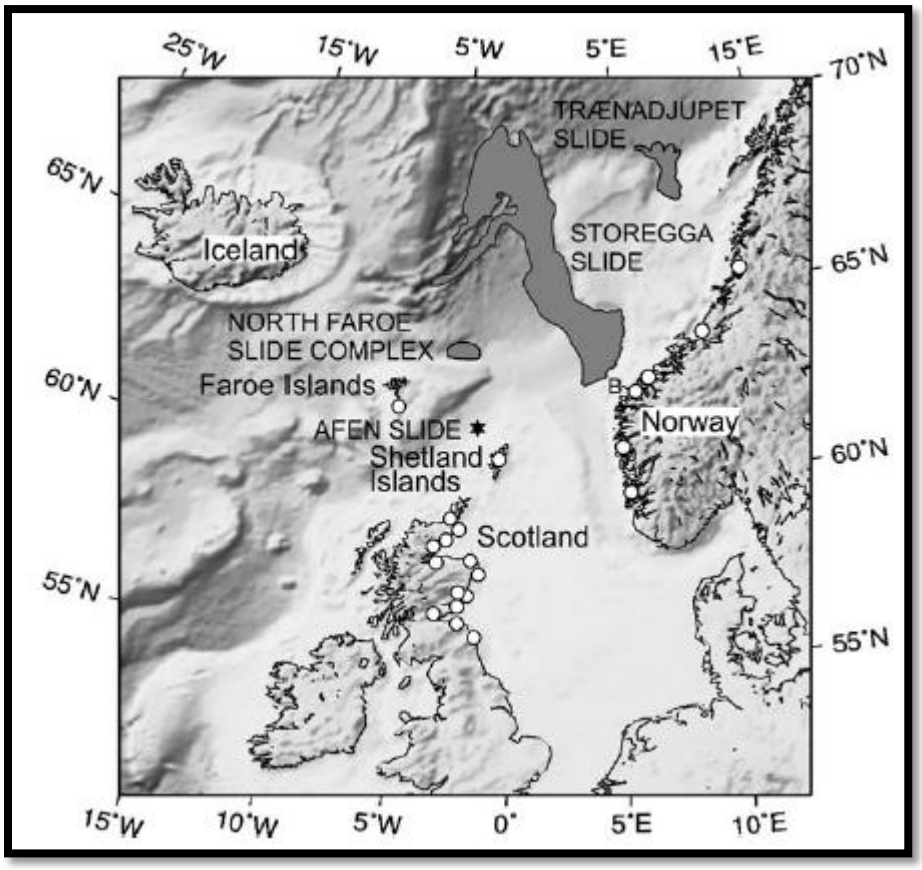

Figure 2.4 - White dots show where tsunami deposits associated with theStoregga slide have been mapped. Other slides are the Trænadjupet slide dated to *ca.* 4000 14Cyr BP, slides on the NE Faroe margin and the small Afen slide in the Faroe–Shetland Channel (adapted from Bondevik *et al.*, 2005).

In NE Scotland, in Montrose, the first traces of tsunamigenic units were discussed by Dawson *et al.* (1988) describing within uplifted coastal sediment sequences an unusual mainly fine or medium sand layer, occasionally coarser, but with some silt and sometimes containing intraclasts of peat. Other similar deposits in different locations in NE Scotland have since then been associated with the Storegga slide (*e.g.* Tooley and Smith, 2005). In Inverness, excavations revealed a Mesolithic horizon covered by a layer of marine sand that was ascribed to the Storegga tsunami (Dawson *et al.*, 1990). In northern Sutherland (North Scotland), Dawson *et al.* (1996) and Dawson and Smith (2000) described a coarser layer in marked contrast to the under and overlying sediments. A pronounced erosional unconformity with the underlying sediments was observed. The presence of a mixed diatom assemblage, although fragmentary, indicated a chaotic accumulation of the deposit with all habitats represented. Variations in particle size within the sequence disclosed strong similarities with other tsunami deposits elsewhere in the North Sea basin and previously associated with the Storegga slide.

In Norway, a group of coastal lakes recorded the marine input of water and sediment that the Storegga tsunami caused in the coastal fringe (Bondevik *et al.*, 1997). The deposits indicate patterns of chaotic sedimentation with marine sediments resting adjacent to layers of terrestrial peat and twigs. In

several basins tsunami deposition was accompanied by erosion of underlying lake sediments followed by redeposition within the suite of tsunami sediments. However, the deposits varied greatly in short distances. Bondevik *et al.* (1997) observed that lake sediment cores of tsunami deposits sampled only 1m apart are markedly different, and attributed this variability to the complicated hydrodynamic behaviour of the tsunami due to local variations in lake bathymetry.

In the Shetland Islands the Storegga tsunamigenic deposit is simply characterized as a sandy layer in peat (Bondevik *et al.*, 2003). However, more recent work by Bondevik *et al.* (2005) and Dawson *et al.* (2006) also detected two other tsunamigenic units that were attributed to more recent submarine slides. One of these events, detected in Basta Voe and dated of 1500 years BP was characterized as a fine-medium sandy unit sandwiched in peat, with frequent bimodal distribution and with clear marine micropalaeontological assemblage. In two other lakes deposits from another tsunami dated to *ca.* 5500 cal yr BP were also detected. The sediment facies were similar to those of the Storegga tsunami.

In the Faroe Islands the tsunamigenic unit associated with the Storegga slide was recognized in a coastal lake situated 4m above msl on the island of Suouroy (Grauert *et al.*, 2001). The authors identified within the lagoonal stratigraphy a major erosional and redepositional event. The (re)deposited sediment ranges from sand and sandy gyttja with marine shell fragments and foraminifera, to gyttja with rip-up clasts, wood fragments and thin sand layers. Diatom analysis indicated that the deposit contained 5–8% full marine species, decreasing to 1–2% in the undisturbed lacustrine gyttja above. The tsunami waves deposited two generations of sand overlain by organic conglomerates, after which followed a unit of suspension material and normal lacustrine gyttja (Grauert *et al.*, 2001). A 2.73m long sediment sequence from Loon Lake (East Greenland), located at 18m above msl, was recovered by Wagner *et al.* (2007). The sequence mainly consisted of fine grained homogeneous sediments, which were interrupted by a 0.72m thick sandy horizon with erosive basis and distinct fluctuations in the grain-size distribution. According to radiocarbon dates, this sandy horizon was deposited after 8500–8300 cal. yr BP and was interpreted as originated from the Storegga tsunami.

Due to its geographical location the coast of Scotland is occasionally subjected to extreme storm events that can cause major erosion and, in some cases, transport and deposition of coarser material. One example of this was the Great Storm of 11th January of 2005 that caused extensive damage across the Scottish Outer Hebrides with severe impacts having occurred across South Uist and Benbecula (Dawson *et al.*, 2007). The hurricane-force winds together with an intense storm surge resulted in significant change in coastal landscape along the entire western seabord and, in particular, on headlands (Angus and Rennie, 2007). In general, severe erosion was focused along coastal areas located west of the roads that link North Uist and Benbecula, Benbecula and South Uist and South Uist and Eriskay. According to Dawson *et al.* (2007) the coastal response to the storm was complex. In some areas, coastal dunes were subject to significant retreat. In other areas deposition of shingle and even boulders was observed. Sand drift and its association with storms (storminess) have also been identified in the Outer Hebrides. (Dawson *et al.*, 2004)

demonstrated a concentration of aeolian activity between AD 1500 and 1700. Inland-tapering sand units were detected within marshland areas. The inland extent of each sand unit was radiocarbon dated and the units were collectively interpreted as a proxy for past coastal storminess. The data appeared to indicate that for the study sites investigated, the majority of the sand units were produced during episodes of climate deterioration, both prior to and after the well-known period of Medieval warmth (Dawson *et al.*, 2004). In the Shetland Islands and in Scotland boulders transported by major storms have been described and this matter has been intensely debated (*e.g.* Williams and Hall, 2004; Hall *et al.*, 2006; Hansom *et al.*, 2008).

2.5.3. Indonesia

Although tsunami sedimentation has been studied abundantly in the Indonesian archipelago, including the events of 1883 - Krakatoa (van der Bergh *et al.*, 2003), 1992 - Flores (Minoura *et al.*, 1997; Shi *et al.*, 1995; Dawon *et al.*, 1996), 1994 - Java (Dawson *et al.*, 1996) and 1998 - Papua New Guinea (Gelfenbaum and Jaffe, 2003), after the 2004 Indian Ocean tsunami an astonishing number of papers focusing in the sedimentary evidences and consequences of this event in Indonesia were published. The island of Sumatra was strongly affected by this event and several sedimentological studies were conducted (*e.g.* Moore *et al.*, 2006; Paris *et al.*, 2007; Meilianda *et al.*, 2007; Monecke *et al.*, 2008; Paris *et al.*, 2009; Paris *et al.*, 2010a; Paris *et al.*, 2010b; Wassmer *et al.*, 2010, Spiske *et al.*, 2010). Immediately after the Indian Ocean tsunami of 2004 an International Tsunami Survey team was assembled and conducted sedimentary research in several locations in Sumatra (Figure 2.5).

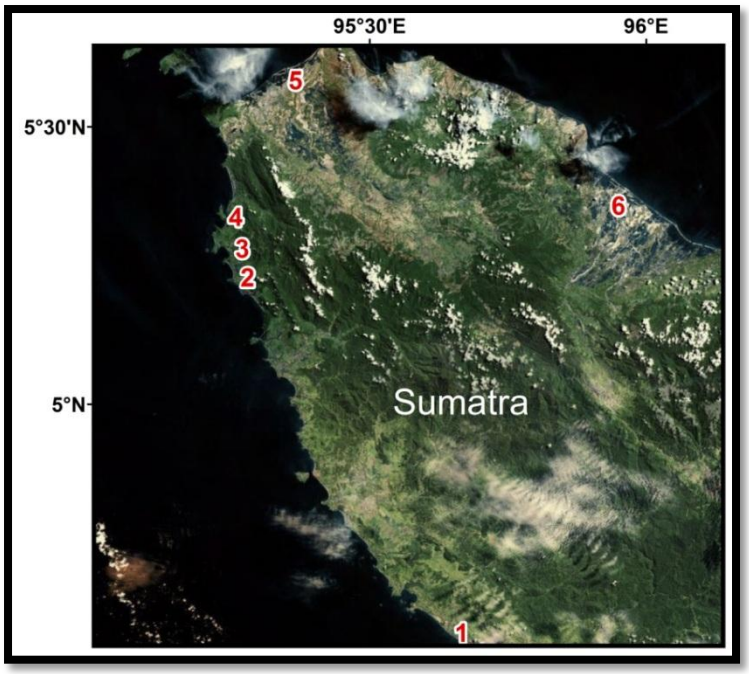

Figure 2.5 – Areas studied by the International Tsunami Survey Team after the 2004 Indian Ocean tsunami (1- Krueng Sabe, 2- Leupeung, 3- Lhok Nga, 4- Lampuuk, 5- Banda Aceh, 6- Sigli).

A progression from intense near coast erosion, deposition of sediment inland, to deposition of sediment and debris near the landward edge of inundation was observed in the area located south of Lhok Nga and north of Leupung (Moore *et al.*, 2006). Along the coastline the tsunami removed the *ca.* 10m wide beach and also removed all soil present within at least 20m of the shoreline, exposing the roots of trees that withstood the flow and scouring into underlying beach rock (Moore *et al.*, 2006). About 50 to 200m from the beach, sand was deposited in a continuous layer about 10cm thick. From about 200m from shore inland to the edge of inundation (up to about 450m from shore), debris such as tree trunks and the contents of houses were observed as an increasingly large part of the deposit (Moore *et al.*, 2006). The tsunami deposit in this area was characterized as a pinkish grey, poorly sorted coarse to very coarse sand, becoming medium sand landward (Moore *et al.*, 2006). The tsunami unit showed evidence of having multiple sources, including a source near the present shoreface, a subtidal source, and possibly an inland source (Moore *et al.*, 2006).

In nearby Lhok Nga the geomorphologic impact of the tsunami was evidenced by severe coastal erosion (Paris *et al.*, 2009). The upper limit of destruction appeared as a continuous trimline at 20-30m above mean sea level and run-up exceeded 50m at the southern point of the bay (Labuhan Point: Paris *et al.*, 2007). The erosional imprints of the tsunami extend to 500m inland and exceeded 2 km landward along the river beds (Paris *et al.*, 2007, 2010b). Paris *et al.* (2007) described the tsunami deposits in Lhok Nga as coarse to medium greyish to yellowish sands, showing important variations in thickness, grain-size and vertical trends. The deposits overlaid brown sandy soils, dune sands or beach-rock near the coast, reddish sands in the rivers, and a dark brown silty soil in the rice paddies.

According to Paris *et al.* (2007) the contact between the tsunami deposits and the buried soil was abrupt or erosional when developed over soft material such as sand. The thickness of the tsunami deposits varied and reached maxima in the topographic lows: 44cm in a small bay near Labuhan, 52cm in a lagoon between Lampuuk and Lhok Nga, 70cm between the razed dunes of Lampuuk, and 82cm flanked on a sand cliff near the cement factory. Paris *et al.* (2007) concluded that 75% of the 26 cross-sections displayed stratification into distinct layers, the number of which ranged between 7 and 15. The lower part of the sequence was usually coarse and massive whereas the upper part was usually finer and sometimes laminated by multiple pulses of deposition. Discontinuous thin mud lines were often observed in cross section intercalated between the main layers (Paris *et al.*, 2007). The same authors observed that the quartz grains were mostly sub-angular to sub-rounded, like those sampled from the present-day beach. The microfaunas identified were typical of a shallow marine environment (Paris *et al.*, 2007). The grain-size distribution observed along Lampuuk was characterised by two successive sequences of landward fining layers. In Lhok Nga, it was also observed that the abundance of nannoliths in the 2004 tsunami deposits decreased landward and upward, despite variations due to successive erosion/sedimentation phases by successive waves and to topographical effects (Paris *et al.*, 2010a).

In the same location, boulder transport and deposition was also observed during the 2004 Indian Ocean tsunami. The tsunamigenic waves were able to detach and transport coral boulders in excess of 10t

over 500–700m and megaclasts of the platform in excess of 85t over a few metres although no landward decrease in size was observed (Paris *et al.*, 2009). The authors concluded that the spatial and size distributions of tsunami boulder deposits mostly depend on the location and characteristics of their source (coral reef, beach rock, platform, dams), together with clast-clast and clast-surface interference during transport (Paris *et al.*, 2009). An estimation of the volume of sediments deposited in Lhok Nga by the 2004 Indian Ocean tsunami suggested that more than 75% of the tsunami deposits came from nearshore (Paris *et al.*, 2009), which is in contrast with the established predominant source of the sandy deposits at the same location (Paris *et al.*, 2007). The coincidence of different size modes, from boulders to fine sands suggests that the whole of the material was not transported in suspension, but rather through a combination of rolling, saltation and suspension. In Banda Aceh coastal marshes, the record of tsunamigenic deposits was extended backward in time due to the recognition of two sand layers deposited after AD 1290-1400 and AD 780-990 (Monecke *et al.*, 2008).

3. Study areas

3.1. Algarve

3.1.1. Geographical and Geological setting

Tsunami events in the Atlantic coast of the Iberian Peninsula are a consequence of the compressive tectonic environment of the Ibero-Maghrebian area (*e.g.* Baptista *et al.*, 1998; Zitellini *et al.*, 2001; Gutscher *et al.*, 2006), the transcurrent motion along the Gloria Fault and surrounding area (Kaabouben *et al.*, 2008) or the effect of other distant seismic sources (*i.e.* Azores or Grand Banks) (Baptista and Miranda, 2009) (Figure 3.1). The oldest tsunami event often considered in Portuguese earthquake catalogues is dated from 60 BC (Baptista and Miranda, 2009). In fact, the Iberian Peninsula has low frequency of tsunamis although the largest tsunami that affected the Atlantic coasts of Europe in historical times was the well-known AD 1755 tsunami, which followed the Lisbon earthquake. In many coastal regions of Portugal and SW Spain, the destructive effects of the AD 1755 tsunami were more disastrous than the direct effects of the earthquake. The first three waves of the tsunami were particularly destructive along the west and south coasts of Portugal (Oliveira, 2005). After the earthquake the tsunami quickly affected the coasts of Iberia and Morrocco, reaching Cape Saint Vincent in 15 minutes, Lisbon in 30 minutes, Cadiz in 78 minutes, Huelva in 50 minutes, Oporto in one hour, Madeira in 90 minutes and Safi in 30 minutes, (Baptista *et al.*, 1998). The effects of the tsunami were felt over the Atlantic. Detailed historical records of the AD 1755 events have been previously summarized by several authors (*e.g.* Silva Lopes, 1841; Pereira de Sousa, 1919; Oliveira, 2005; Oliveira, 2008). The driving mechanisms, sources (and thus return period) of large magnitude earthquakes and tsunami generated in the Iberian region have been extensive challenged in recent years, following the conclusion that the events of AD 1755 and AD 1969 have been sourced in different areas of the SW Iberian margin. However, the major tsunamigenic threat for the Atlantic coast of Iberia is the earthquake activity associated with the Azores-Gibraltar plate boundary and neotectonic and gravity-induced sea-floor activity offshore the Gulf of Cadiz.

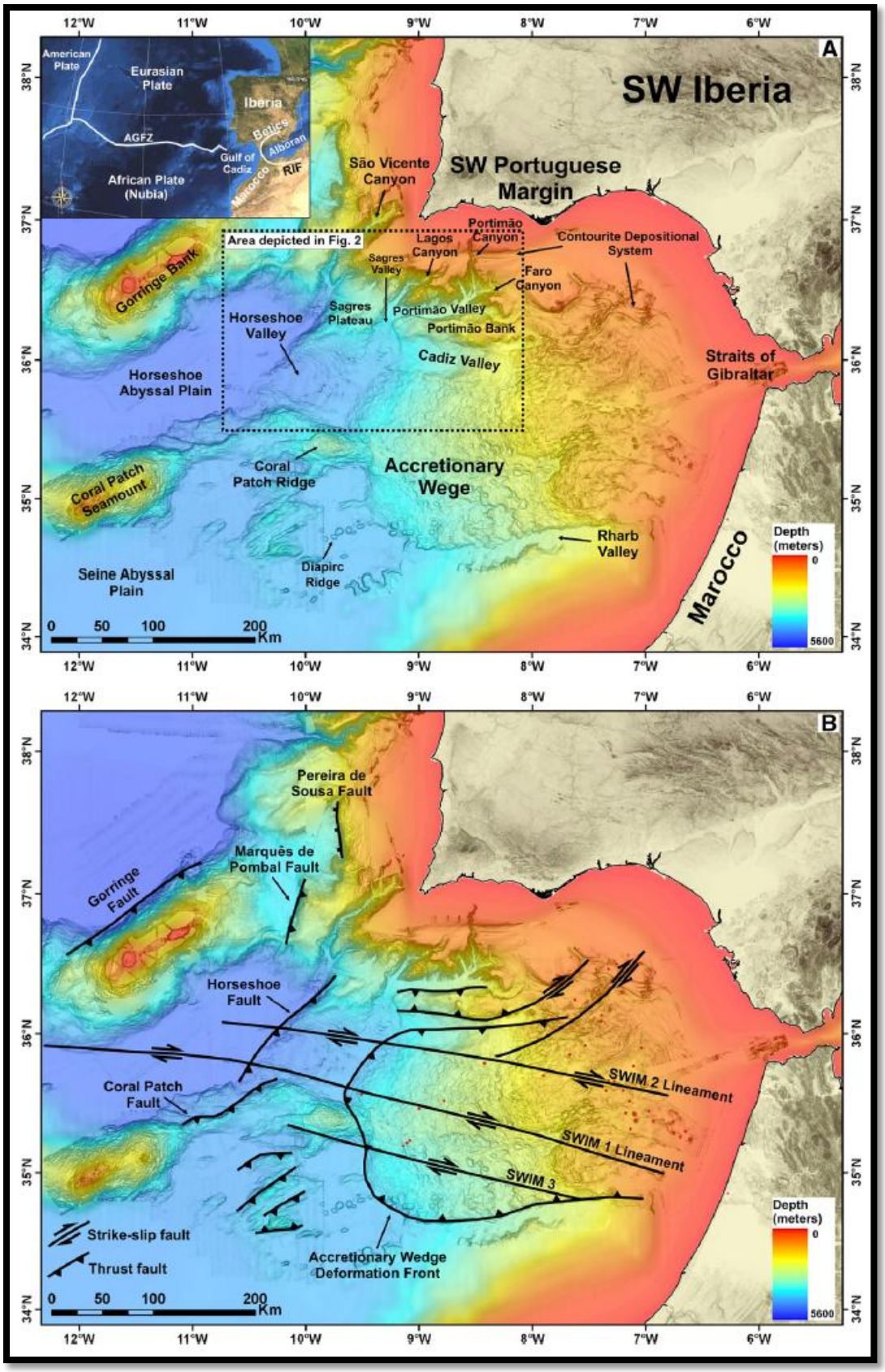

Figure 3.1 - Main geomorphologic features and detailed tectonic characterization of the Gulf of Cadiz (adapted from Duarte *et al.*, 2010). SWIM lineaments are several major WNW–ESE trending lineaments, recently interpreted as aligned arrays of also deep seated, sub-vertical dextral strike–slip faults. A) Location of the offshore SW Iberian Margin (3D digital bathymetry model from MATESPRO dataset); (B) general drainage system of the local continental shelf and slope.

The Algarve coast presents a geological and morphological asymmetry, mainly due to the occurrence of different wave regimes and to the nature and structural features of the outcropping lithologies. The coastline can be divided into two different areas (*i.e.* west coast and the south facing coast), due to the geomorphological contrast, the south coast can be further subdivided into windward and leeward coastal sectors. In this study only the windward sector will be addressed.

The windward coast has developed in resistant Mesozoic limestone, dolomite and marl and softer Miocenic limestone, detrital limestone and siltstone. Both resistant and softer lithologies form cliffs with steep slopes (Figure 3.2). Cliffs with Jurassic substrate sometimes plunge directly to the ocean whereas Tertiary rocks usually present cliffs with its toe exhibiting narrow beaches or platforms, both intertidal and subtidal. The windward coast of Algarve is limited to the west by the Cape S. Vicente and to the east by the Ancão beach (Figure 3.2). The existent morphology in the western part of the windward sector is a consequence of the tectonics, represented by numerous faults with a NNE-SSW main direction, and by alongshore succession of different lithologies, with different resistances to erosion, forming an irregular coastline with numerous headlands and narrow embayments. In this sector, the coastline is characterized by rocky cliffs, with heights varying between 40m and 110m above msl, interrupted by small beaches. The eastern sector of this windward coast presents a coastline with well-developed estuaries and bays separated by cliffs with heights varying between 20m and 50m above msl. The rivers and streams that flow in Palaeozoic and Mesozoic rocks display poorly developed catchment areas inland and alluvial plains, which are essentially composed of mud that resulted from the weathering and erosion of limestones and Flysch outcropping in the watershed. In the eastern sector of the windward coast the prevailing lithologies (i.e marls and clastic carbonate Miocene rocks) contribute to the cliffy appearance of the coastline. According to Andrade (1990), the cliffs fringe forms a marine-cut costal platform essentially affecting Miocene carbonated rock. This surface is at an average height of 45m though gently sloping to SE, and is heavily karstified. The sector located to the east of Olhos de Água and west of the Ancão beach is characterized by a narrow beach backed by a linear cliff cut in Pliocene-Pleistocene soft sand and gravel. The cliffs frequently collapse, and show the highest erosion and retreat rates found in the Algarve (Andrade, 1990). The drainage system existing in this section of the coastline, presents mainly small streams that extend to a maximum of 4 km inland, draining the Pliocene-Pleistocene bedrock, with the exception of Quarteira and Carcavai streams (Figure 3.2), which extend further inland, presenting well developed catchment areas and draining the entire Mesozoic and Cenozoic sequence.

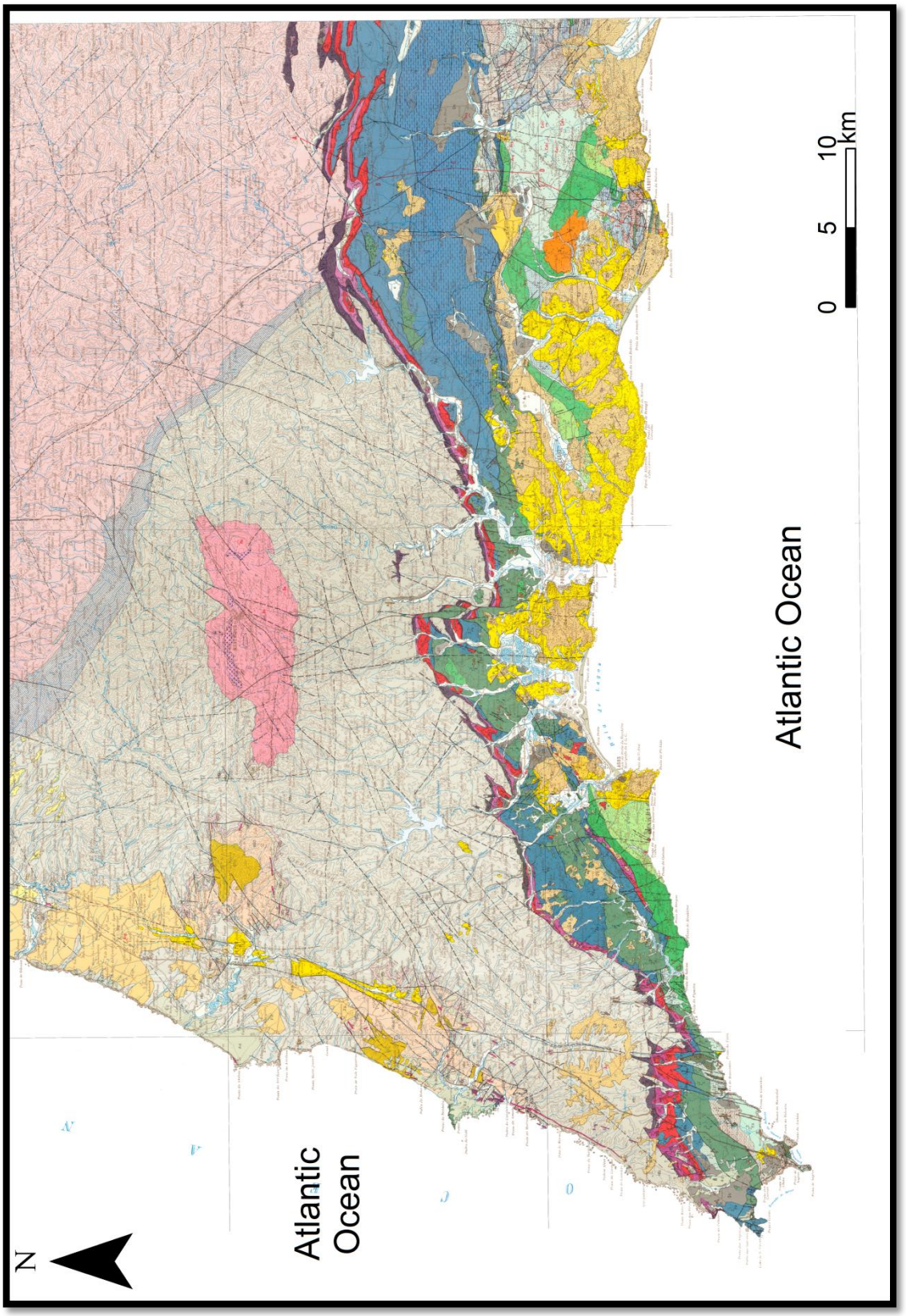

Figure 3.2 - Geological map of the Algarve. Modified from Manuppella (1992). Legend is in Annex 1.

3.1.2. Oceanography

In order to recognize extreme marine inundations it is important to assess the wave regime, oceanographic conditions, tide levels and other predominant oceanographic factors.

In 1979, the Instituto Hidrográfico was able to characterize the wave regime in the Portuguese coasts based in non-directional data gathered in several measuring stations. At a later stage the deployment of offshore buoys in Faro, Sines, Figueira da Foz and Leixões allowed the collection of wave data with a 10 minute frequency. Costa *et al.* (2001) based in the data collected by the above mentioned buoys was able to characterize the mean wave conditions for Figueira da Foz, Sines and Faro. They were able to conclude that the annual average period was 5-7s (Figueira da Foz – 6.6s; Sines - 7.2s; Faro -4.7s). The most common peak values were observed between 9-13s (Figueira da Foz - 11.4s; Sines – 10.8s; Faro – 8.2s). In the south coast of Portugal 52% of the observations correspond to a W direction, with a slight increase in the winter (Costa *et al.*, 2001). During the summer the wave direction tend to rotate to the north while the SW and WSW directions occur more typical during the winter.

The wave regime is of low energy, with mean annual significant wave height (Hs) < 1m and storms are essentially related with westerlies and west-northwest deep water waves approaching from the Atlantic. The storm wave regime is discussed in a report by LNEC (1987), using a combination of buoy and hindcasted data (Table 3.1).

The maximum astronomical high tide levels, in the Algarve, are about 1.80m above mean sea level and during extreme spring tides the high tide level may slightly exceed 2m above msl (Hindson and Andrade, 1999). The tidal range is approximately 2.1m and *ca.* 3m during spring tides, and the maximum reported elevations reached by sea-level in spring high tide during intense storms reflect just a small contribution of storm surge to the observed extreme levels: about 2.15m above msl (cf. Esaguy, 1984) Furthermore, Taborda and Dias (1992), based in the study of 2 major storms (14th of February to 3rd March of 1978; 25th to 31st of December 1981) indicated that the storm surge caused a maximum elevation of the sea of 0.42m in Lagos.

Table 3.1 - Storm occurrences offshore the Algarve coast between 1955 and 1986 (LNEC, 1987).

Date	Hs (m)	Direction
10 to 15 Feb 1955	5.6	W
15 to 20 Dec 1958	7.9	WNW
1 to 9 Dec 1959	5.6	WNW
16 to 22 Feb 1966	9.2	W
10 to 15 Jan 1969	4.8	WNW
19 to 27 Jan 1971	3.8	NW
13 to 18 Jan 1972	5.5	NW
31 Jan to 5 Feb 1972	4.5	WSW
23 to 28 Dec 1972	4.9	WNW
13 to 18 Jan 1973	9.5	W
26 to 30 Oct 1976	4.3	WNW
30 Nov to 4 Dec 1976	3.6	WNW
14 Dec 1976	3.0	---
31 Dec 1976 to 1 Jan 1977	2.5-3.0	---
22 Feb to 1 Mar 1977	5.6	W
6 to 14 Dec 1978	6.1	W
27 to 28 Dec 1978	3.5-4.5	---
27 to 28 Jan 1979	3.0-4.0	---
8 to 15 Feb 1979	7.0	NW
25 to 31 Dec 1981	7.9	SW

Pessanha and Pires (1981) calculated the probability and return period of waves offshore the Algarve (Table 3.2) and established a centennial storm with Hs of 6.5m and a decennial storm with Hs of 5.2m.

Table 3.2 - Return period offshore the south facing coast of the Algarve (Pessanha and Pires, 1981).

Hs (m)	Return period (years)
4.8	5
5.2	10
5.7	25
6.1	50
6.5	100

Costa *et al.* (1994) studied storm events based in the data series yield by the buoy of Faro and analyzing the period between 1986 and 2001. Storm events were considered when the significant wave height was higher than 3m. According with this study the average of storm events per year is 9.3 in the winter and 0.6 in the summer. According with the Instituto Hidrográfico data, during the last decade (2000-2009) the maximum wave height (Hmax) measured by the deepwater buoy of Faro was approximately 12.5m while the maximum significant wave height (HMO) measured was 7.5m (December of 2000). Moreover, only in another occasion during the last decade (February 2003) the Hmax was above 10m.

3.1.3. Salgados

The Salgados lowland is located in the bay between Armação de Pêra and Galé (Figure 3.2 and 3.3). This coast features a 6 km-long intermediate-reflective sand beach backed by a continuous, 3 to 17m-high vegetated foredune (Figure 3.4), the latter covering resistant Pleistocene-Holocene aeolianite and beachrock (Moura *et al.*, 2007). The continuity of the beach-dune system is interrupted by the ephemeral inlets of two infilled lagoons, which developed in relation with the outlet of intermitent streams: the Alcantarilha lagoon and stream, and the Salgados lagoon and Espiche stream, which drain, respectively, 204 and 41km^2 watersheds, mostly developed in Early Miocene limestone and Late Miocene siltstone and sandstone (Pinto and Teixeira, 2002) (Figure 3.2 and 3.5). The Salgados Lagoon extended across some 1.5km^2 but about half of this surface has been reclaimed and landfilled for a golf course. The remnant surface is a flat-floored depression 1.1 to 1.7m above mean sea level, collecting water and muddy sediment from the adjacent catchment and is usually flooded by about 1m of water.

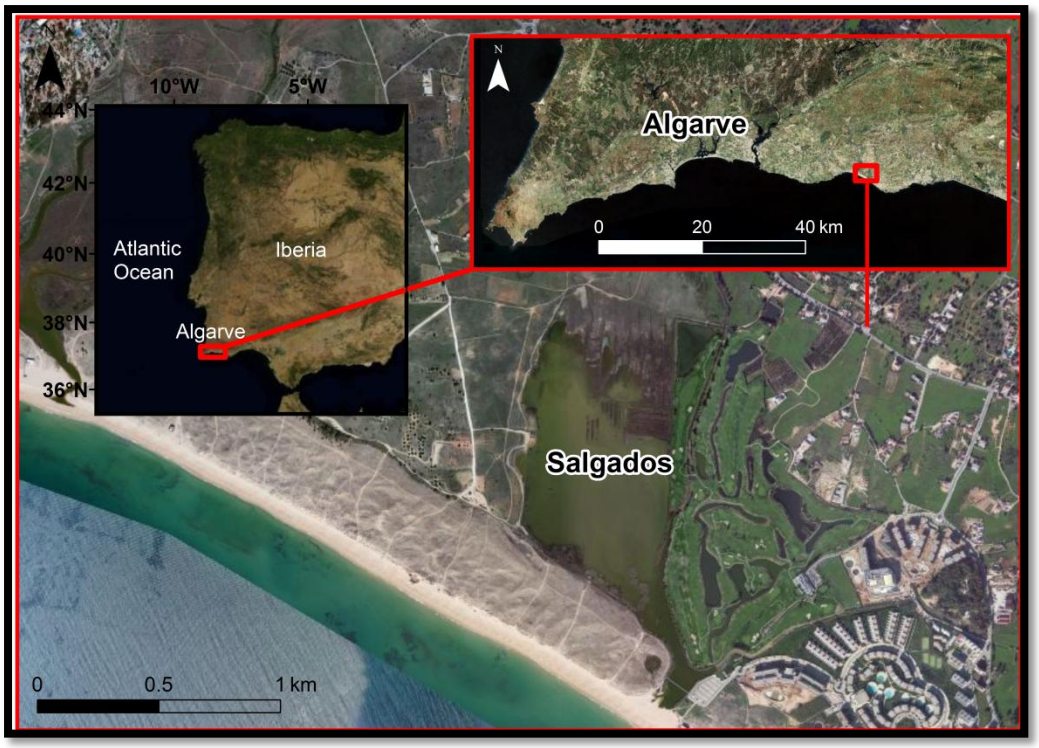

Figure 3.3 – Geographical location of Lagoa dos Salgados.

Figure 3.4 - Oblique aerial view of Salgados lowland in March 2011 (provided by SB Teixeira - ARH-Algarve).

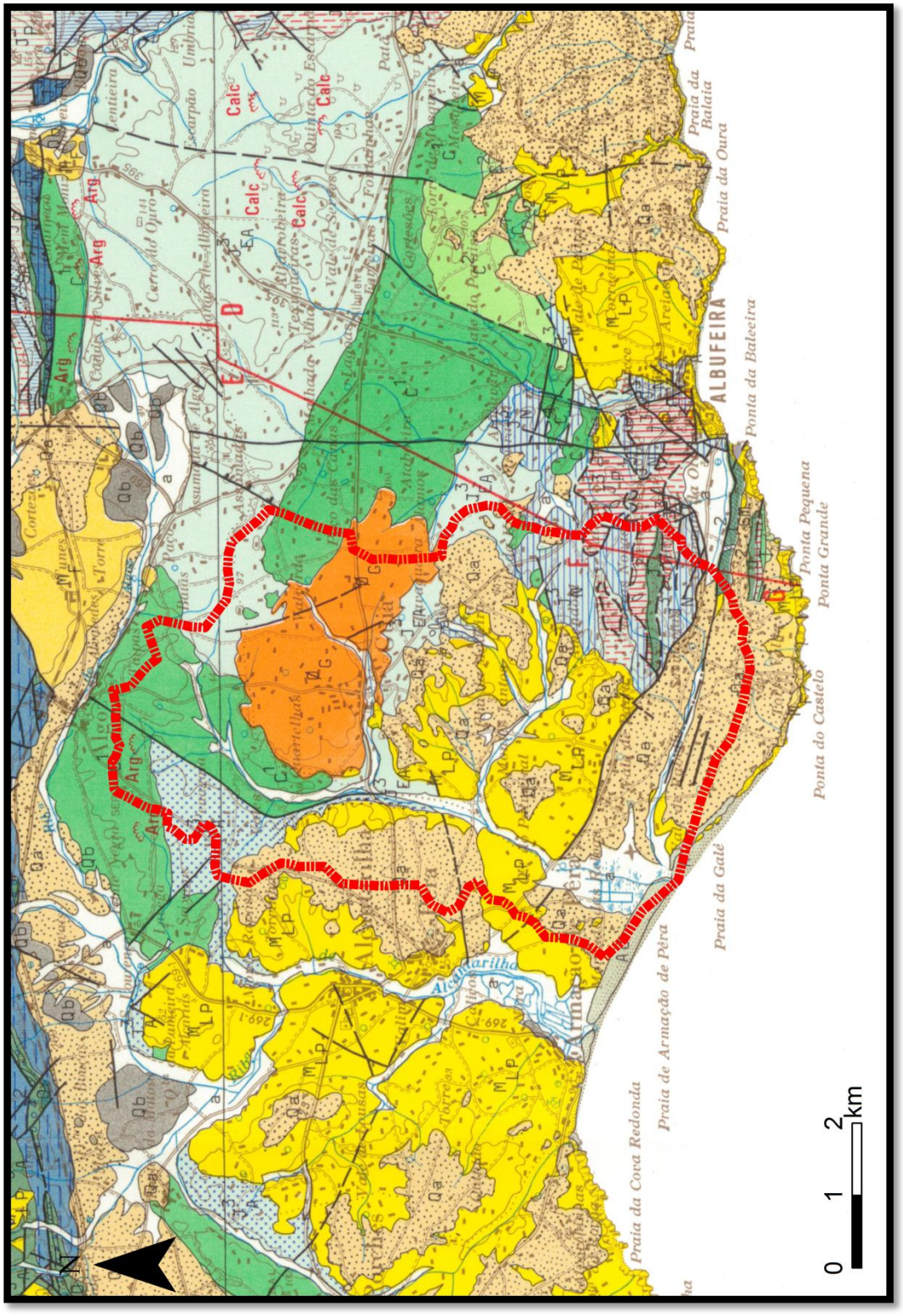

Figure 3.5 – Drainage basin of Ribeira de Espiche/Lagoa dos Salgados. Modified from Manuppella (1992). Legend is in Annex 1.

3.1.4. Boca do Rio

Boca do Rio is located between S. Vicente Cape and Lagos (Figure 3.2 and 3.6). It is a small flat-floored and sediment filled lowland located within the otherwise high-cliff coastline of the western Algarve (Figure 3.7). The lowland area consists of a supratidal floodplain that is periodically subject to extensive river flooding by the Budens, Vale de Boi and Vale de Barão streams. These rivulets present a seasonal regime with strong variations in the flow rate between rainy winters and dryer summers. The Cretaceous limestone and marly limestone E-W orientated cliffs that limit the Boca do Rio beach to the east and to the west reach heights of *ca.* 70m above msl. The flat N-S orientated alluvial plain presents an average height of 1.7m above msl and reaching 3m above msl to the north of the plain. The area is separated from the sea by a storm gravel and sand ridge and by a rock spur that together forms a barrier to wave overtopping during storms (Hindson *et al.*, 1996). A high dune at *ca.* 8-10m above msl existed in Boca do Rio at the time of the AD 1755 tsunami (Pereira de Sousa, 1919) but the natural system failed to rebuild a robust dune or beach since then (Oliveira *et al.*, 2009). The beach is 200m long and 115m wide and the beach berm rests at 2.1m above msl. The drainage basin develops along *ca.* 80 km^2 in Palaeozoic schist and greywacke, claystone, Triassic siltstone and sandstone, Jurassic and Lower Cretaceous limestone and marls and Plio-Pleistocene sand and sandstone (Figure 3.8).

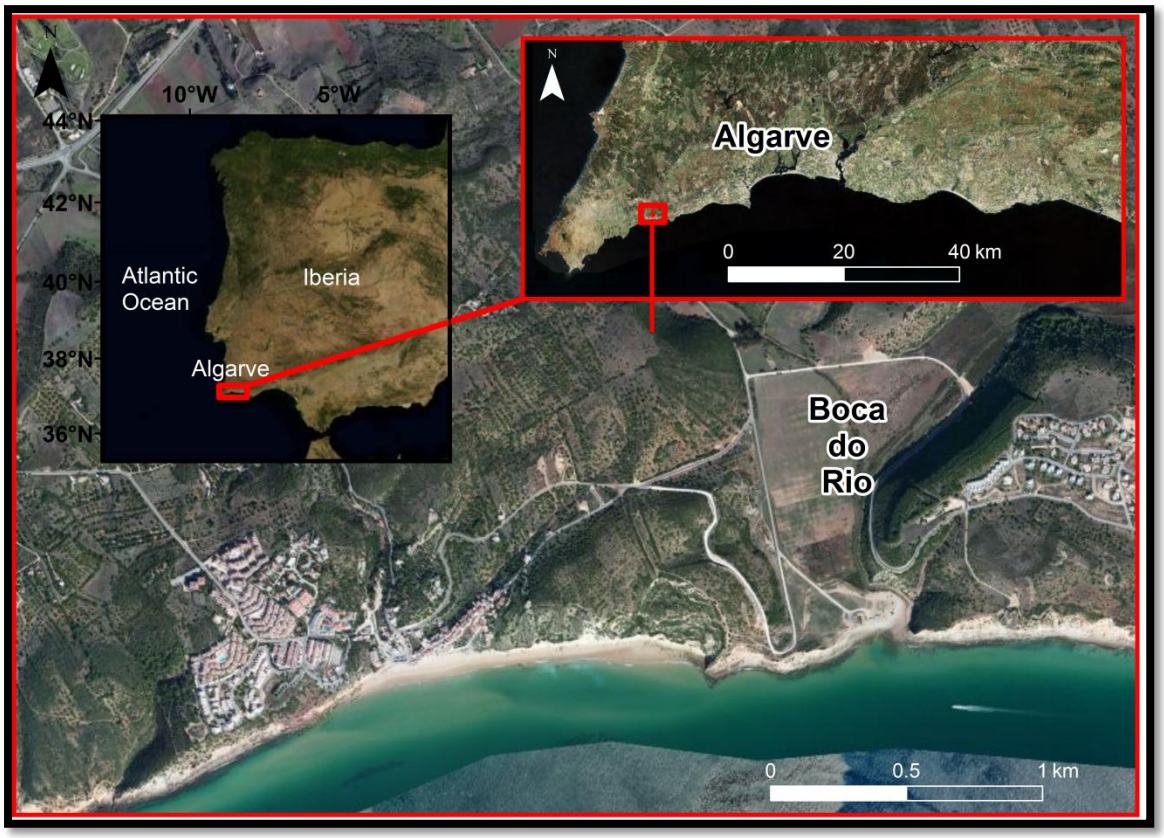

Figure 3.6 – Geographical location of Boca do Rio.

Figure 3.7 – View to the Boca do Rio alluvial plain and beach (photo facing the east – C. Freitas).

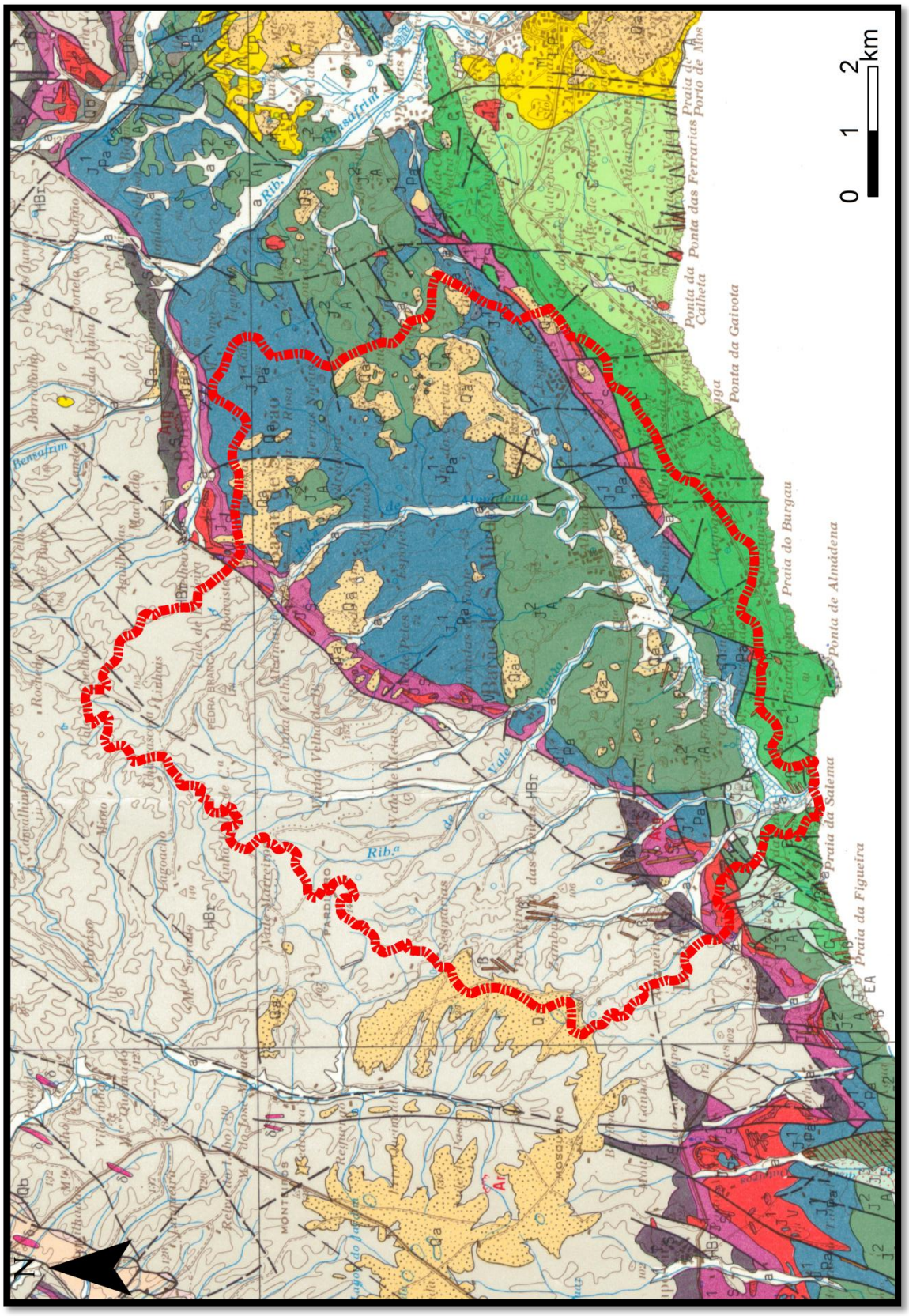

Figure 3.8 – Drainage basin of Budens, Vale de Boi and Vale de Barão streams that drain to Boca do Rio alluvial plain (east of Praia da Salema). Modified from Manuppella (1992). Legend is in Annex 1.

3.2. Shetland Islands

3.2.1. Geographical and Geological setting

Together Shetland and Orkney form the Scottish Northern Isles and are located in the North Atlantic, NE of Scotland Mainland. The main tsunamigenic risk in the northeast Atlantic is from submarine slides, which are more difficult to detect than earthquakes. There is no historical evidence for earthquakes larger than 5.4 ML (local magnitude) onshore. However, offshore seismicity, especially in the North Sea, is prone to larger events.

The geology of Shetland is varied and rather complex, principally as a result of a large number of major north-south running faults, including the northward continuation of the Great Glen Fault (Figure 3.9). Shetland now forms an important link between the East Greenland, Scottish and Norwegian parts of the Caledonian Orogenic belt (Johnson *et al.*, 1993). Like much of Scotland, the cover rocks of Shetland are supported by platform of Late Archean (2500-3000 Ma) Lewisian basement gneiss which is the northward extension of the Hebridean Craton. Historically, the Shetland metamorphic cover is called the East Mainland Succession with the Yell Sound Division (Moine) at its base, overlain by the Scatsta, Whiteness and Clift Hills Divisions (Dalradian) (Johnson *et al.*, 1993). The Devonian sandstones of Orkney and Shetland were deposited in the Orcadian Basin, a low-lying area into which rivers from the Highlands to the west and south drained. During the last Ice Age an ice-cap covered Shetland but it was much thinner than that of the Scottish mainland. Evidence for the ice does exist in the form of glacial erratics and moraines. The last ice sheet left Shetland around 14,000 years ago, though a cold snap a few thousand years later brought about a return of glaciers, the last finally disappearing *ca.* 10,000 years ago. The outline of Shetland at the end of the Ice Age was very different from today, sea levels being around 100m lower due to the amount of water locked up in the ice (Johnson *et al.*, 1993). However, since then, melting ice has caused sea levels to rise and the Shetland landmass has also been depressed as the massive weight of the ice over the continental landmass to the east was removed. Sea levels have therefore risen gradually over the past 14,000 years and by the time the first Mesolithic gatherers arrived 6,000 or 7,000 years ago it was around 9 metres below current levels – peat has been found at this level at this period on the Unst coast (Johnson *et al.*, 1993). The recent submergence of Shetland is apparent in the fine detail of its coastline. Peat formerly developed on boggy surfaces above sea level is now often found at or below sea level and sometimes buried beneath boulder and gravel beaches. The coastal edges of Shetland few sandy coastlines frequently take the form of a small, sandy cliff, suggesting progressive erosion.

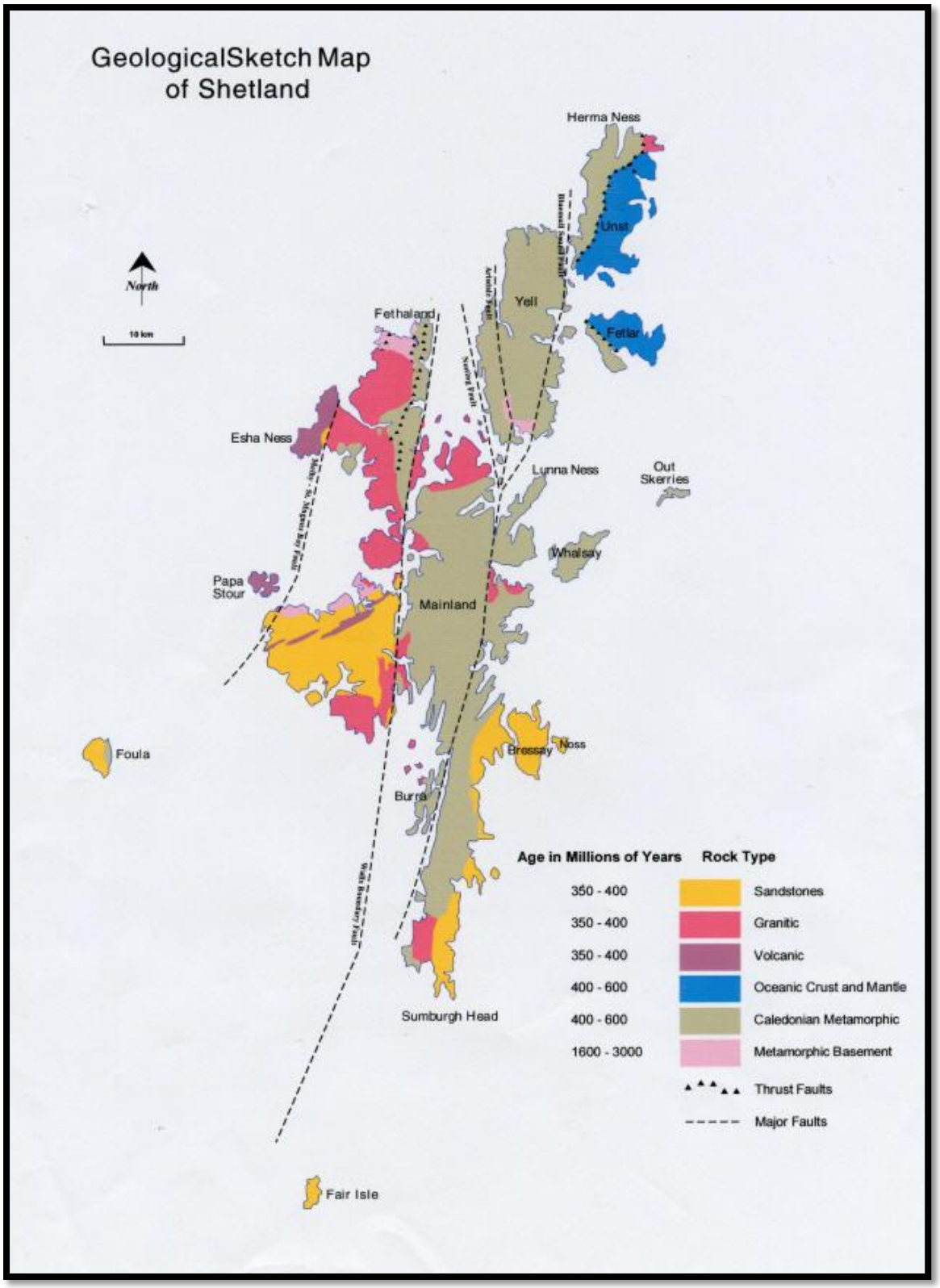

Figure 3.9 - Geological map of the Shetland Islands (Geological Sketch map of Shetland, 2012, adapted from landforms.eu).

In the words of Flinn (1977), "Shetland is a partly drowned range of hills rising rather sharply from a depth of about 82m below present sea level". The submergence of the archipelago has had a profound

effect on coastal processes, allowing deep water waves to approach parts of the outer coastline directly and without breaking and the progressive reworking of depositional features on the middle and inner coasts. The outer coast displays spectacular cliff scenery, reflecting rapid erosion along one of the highest energy coastlines in the world. The middle coast is much more sheltered and includes the anchorages of Sullom Voe and Bressay Sound, where deep water fills drowned glacial valleys. The sands and gravels along the inner coast are highly mobile, with beaches, spits and bars adapting to sea level rise and being reworked during major storms.

3.2.2. Oceanography

Shetland is one of the stormiest places in Europe. Due to its geographical location the Shetland islands are very exposed to westerly gales from the North Atlantic.The atmospheric turbulence associated with the development of mid-latitude cyclones arises principally from the interaction of cold polar air with warmer air from lower latitudes. The collision of air masses of contrasting temperature and density results in the development of frontal weather with the air mass boundaries represented respectively by warm, cold and occluded fronts. These atmospheric processes place Shetland within the North Atlantic storm track (Dawson *et al.*, 2011). During winter, this results in the passage of numerous frontal cyclones, the occurrence of high winds and associated spells of high rainfall. During other periods, the Atlantic storm track is displaced either to the north, or more commonly to the south, of the northeast North Atlantic (Dawson *et al.*, 2011). Such changes are normally associated with a change in the position of the jet stream in the upper atmosphere. When this type of circulation occurs (*e.g.* winter of 2009−10), the prevailing SW airstream can be replaced by a northerly and NE airflow (Dawson *et al.*, 2011). When the type of synoptic climate occurs, Shetland tends to experience long periods of extremely cold weather. During the summer months, the vigour of atmospheric circulation is reduced. Storms are less frequent and are commonly replaced by anticyclonic circulation that is associated with spells of fine weather. Cyclones also develop during summer but, when they occur, are typically less intense and associated with much lower wind velocities than during winter (Dawson *et al.*, 2011).

Information on wave data is limited for Shetland waters. Data is available for the wave buoys operated by the UK Met Office (Station 64045-K5 Buoy and station 64046- K7 wave buoy) and from a tide gauge in the Shetland capital (Lerwick). The tidal range in Shetland is moderate. There is a tide gauge in Lerwick Harbour, operated by Proudman Oceanographic Laboratory. Maxima data from Jan 1959 to Oct 2000 shows that the highest recorded level in this series is 1.774m (above local ordnance datum from Lerwick) in January 1993 (Crichton, 2003). Average wave heights are around 3m. By 2080, the average could be around 4m, and maximum offshore wave heights could be as high as ten metres (Dawson *et al.*, 2001). Storm surges around mainland Scotland have been predicted to become around 3 to 4m by 2080, and similar levels can perhaps be assumed in Shetland (Crichton, 2003). In the period of 1997-2009 the measured Hs varied between 2.4 to 2.6m the maximum values obtained where *ca.* 10m (Dawson *et al.*,

2011). The wave period for the same time interval varied between 8 and 12s (in Lerwick). For Lerwick the strongest winds are associated with southerly, south-westerly and westerly directions bringing wet air in from the Atlantic. The monthly averaged wind speed data for Lerwick shows temporal seasonal variability in wind speed, with a five year running mean suggesting a slight increase in wind speeds from 1972 – 2009. The annual average wind speeds (in Lerwick 15 knots/s) showed this trend more clearly Dawson *et al.* (2011). This is particularly evident in Lerwick for the years of 1957 – 1980. The lowest pressure recorded in Lerwick was 944.4 mb on the 25th December 1999 and the highest 1094 mb on the 7th of December 1997 (Dawson *et al.*, 2011). Lerwick gale day frequencies increased during the period of 1957-2009 (less than 20 days in 1987 to almost 80 days in 2007) (Dawson *et al.*, 2011).

Massive winter storms crash onto Shetland rocky coastline. The sea is an enormously powerful agent of change, especially when whipped up by the North Atlantic gales that can sweep Shetland, with gusts of over 277 km/h being recorded at Muckle Flugga lighthouse on 1st January 1992. In 1967 a wind of 283 km/h was recorded at the radar dome on top of Saxa Vord. Enormous waves crash into the shores, eroding coastal outcrops of rock and creating the massive cliffs, with their caves, rock arches and inlets that are so much a feature of the Shetland coast. Fast-moving and rapidly-developing depressions in the northeast Atlantic generate exceptional wind speeds and a high-energy wave regime. Modelling of extreme waves in deep water at Schiehallion, 160 km west of Shetland and data from a wave buoy nearby suggest that wave heights of 20m occur about 100 times per year (BP Exploration, 1995). Mathematical and physical modelling in a wave tank indicated that 20m high deepwater waves will generate breaking waves of a height roughly equivalent to the deepwater wave height on the cliff faces at The Grind (Hansom *et al.*, 2008), implying that the entire cliff top at 15–22m may be inundated during storms.

3.2.3. Voe of Scatsta

A small inlet within Sullom Voe on the north coast of the Shetland Mainland, the Voe of Scatsta lies between Scatsta Ness and Sella Ness (Figure 3.10 and 3.11). Sullom Voe lies on the southern shore of Yell Sound in Mainland Shetland. The site encompasses Gluss Voe, Sullom Voe, Orka Voe and several small subsidiary arms and embayments including Voxter, Scatsta and Garths Voes and the Bight of Haggrister (Figure 3.10). A semi-enclosed body of water at the head of the Voe of Scatsta, within Sullom Voe on the N coast of the Shetland Mainland, the Houb of Scatsta lies immediately to the northeast of Scatsta Airport (Figure 3.11).

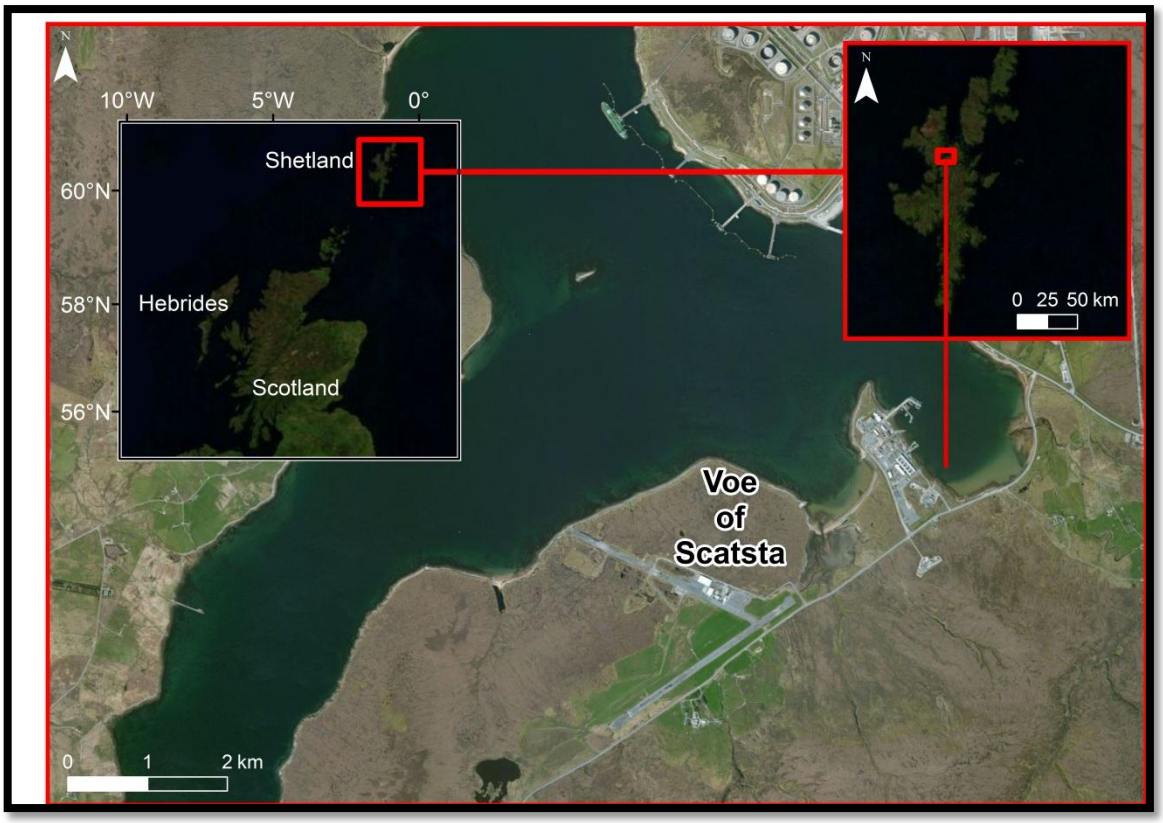

Figure 3.10 – Geographical location of Voe of Scatsta.

The shores at the entrances to Sullom Voe are moderately exposed to wave action whereas extremely sheltered conditions prevail towards the head of Sullom Voe and within the houbs. The shores of Sullom Voe, especially in the more exposed outer regions, are predominantly of bedrock and with varying slope. Inner, more sheltered, rocky shores generally vary from gently sloping bedrock to boulder and mixed cobble/sediment but there are also regions of steep cliff and boulder covered shores especially at the head of Sullom Voe. Significant areas of intertidal sediments only occur at the heads of Gluss, Garths, Scatsta and Voxter Voes, and around the spit and inside the Houbs of Fugla Ness and Scatsta (Figure 3.10). Smaller patches of intertidal sediments (coarse sands/gravel) occur sporadically around the region. The middle region of Sullom Voe is more sheltered and is a more varied coastline, indented in places by small voes and houbs/lagoons. Intertidal sediments are confined to the houbs and the heads of Gluss, Garths, Scatsta and Voxter Voes. These sediments are variable and poorly sorted, consisting mainly of coarse sand, gravel, shell debris and peat fragments.

Figure 3.11 – View of Voe of Scatsta (photo P. Costa). To the north Sullom Voe terminal can be identified.

3.3. Hebrides Islands

3.3.1. Geographical and Geological setting

The Outer Hebrides is a chain of islands, 210 km long, in the northwest of mainland Scotland. Sixty five islands compose the archipelago, with a combined coastline of 2500 km. The topography of the islands is characterized by low lying lands on the west coast and the Highlands with mountains, cliffs, fjords and skerries (rising to heights locally in excess of 200m). Here, the coast is fringed by a largely stabilised dune system consisting of a single low ridge seaward and a gently sloping surface andward, where the system ends amidst peat areas, rocky outcrops and many small lochs (Dawson *et al.*, 2004). The sand areas are known locally as machair, derived from the Gaelic word for extensive beach or plain and which describes a low-lying, grass-dominated coastal plain composed of calcareous sand with calcium carbonate content up to *ca.* 80% (Ritchie and Whittington, 1994). Machair is present in the Hebrides extending much of the whole length of the islands of Berneray, North Uist, Benbecula, South Uist and Barra and up to 2 km inland. Many of the machair systems in the Outer Hebrides are protected by a dune ridge, although there are sections of coastline where, due to erosion, this has been lost (Dawson *et al.*, 2004). It is generally considered to have formed as a result of aeolian processes and has distinctive dune morphology (*e.g.* Ritchie, 1979).

Notwithstanding the apparent uniformity of the machair surface, exposures in the dune face to seaward disclose soil and peat horizons which reflect episodes of stability and imply a complex evolution.

Most of the Outer Hebrides is comprised of Lewisian gneiss (Figure 3.12), that forms an upstanding basement high that has a discrete faulted eastern margin against Mesozoic and earlier Torridonian sedimentary basins in the Minches (Fettes *et al.*, 1992). On their western side lies an extensive shallow shelf, termed the Outer Hebrides Platform with Lewisian gneiss at or near the bedrock surface. It extends west of the Uists for some 60 to 70 km. The geology of the Outer Hebrides is dominated by Archaean and Proterozoic Lewisian gneisses, analogous in age with rocks forming the Caledonian foreland of mainland Scotland, but separated from them by sediment filled Mesozoic half-graben beneath the Minch (Fettes *et al.*, 1992). Part of this is exposed as the Stornoway beds (near the town of Stornoway in Lewis), the only non-Lewisian rocks in the Hebrides (Fettes *et al.*, 1992). Classically two major periods of tectonic and metamorphic activity has been recognized - Scourian and Laxfordian. The main elements of the gneiss complex were formed during the Scourian. Originally granodioritic, tonalitic and basaltic intrusions emplaced at mid or lower crustal levels were subjected to deformation and metamorphism (gneiss formation) between 3100 Ma and 2500 Ma. Granite bodies and microdiorite sheets were intruded near the end of the Archaean in what is termed the late Scourian at around 2600 Ma (Fettes *et al.*, 1992). There followed the widespread intrusion of the 'Younger Basic' suite of dolerite and basalt dykes and lenticular sheets in the Palaeoproterozoic at around 2400 Ma. Significant later accretion of possibly arc-related metasedimentary and metavolcanic rocks and intrusion of the South Harris Igneous Complex occurred at around 1880 Ma. The gneisses and earlier igneous bodies were reworked significantly between 1850 Ma and 1600 Ma, during the Laxfordian event, and it is the resultant Laxfordian folds, fabrics and metamorphic mineralogy that dominate the Lewisian rocks of the Outer Hebrides (Fettes *et al.*, 1992).

The most obvious major structure of the Outer Isles is the Outer Hebrides Fault Zone, a gently ESE-dipping, structure with evidence of polyphase compressional, strike slip and extensional displacement, a major eastward dipping thrust zone, marked by pseudotachylite, cataclasite and brecciated 'mashed gneiss' (Fettes *et al.*, 1992). The extensive machair, sand dunes, sandy beaches and inter-tidal sand flats, are a particularly outstanding feature of the coastal geomorphology of the area. At the end of the last glaciation (Late Devensian) the pre-machair surface was covered by glacially scoured substrate with marshes and lochs occupying the depressions. With the subsequent rise in sea level during Holocene glacially derived sands from offshore were mobilised and mixed with shell debris. This material was reworked into coastal ridges and moved onshore overriding pre-existing lacustrine and organic deposits (Ritchie, 1985).

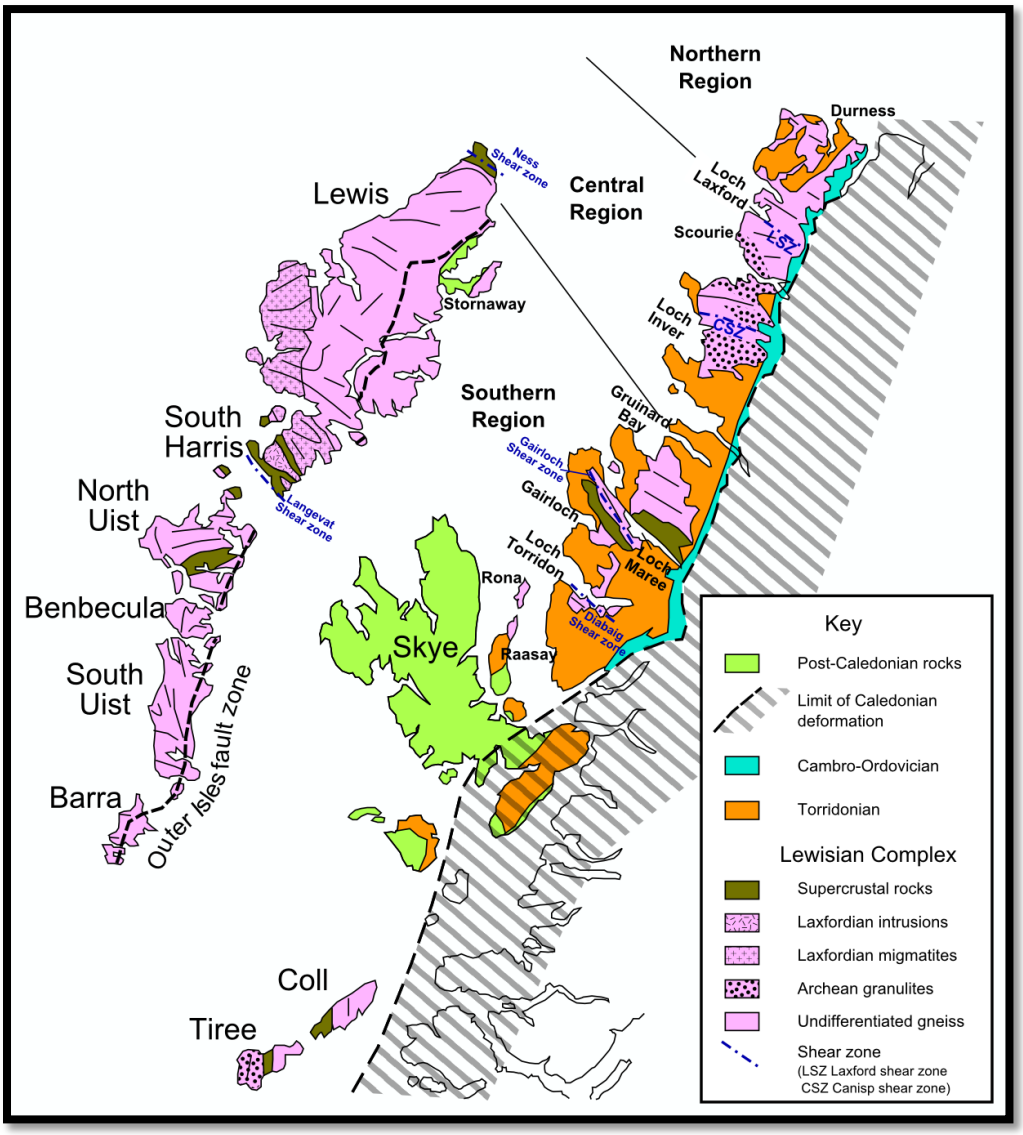

Figure 3.12 - Geological map of the Hebridean Terrane, NW Scotland (adapted from maps in Geology of Scotland, 2003).

3.3.2. Oceanography

The wave climate of the Outer Hebrides is severely depth limited. The offshore platform to the west of the Outer Hebrides is a relic of the old coastal plains which have been flooded since Neolithic times (4000-2000 BC). This eroded land provides a gently sloping platform far out to sea which forces incoming waves to shoal and lose energy before breaking on the coastline. During a storm or particularly high tide event wave heights may increase to be greater than normally anticipated owing to the increased depth of nearshore water (and consequently the decreased shoaling effect) (Richard and Phipps, 2007).

Fortnum (1981) compiled wave data from March 1976 to February 1978 at 57º18' N, 7º38' W at approximately 15 km west of the island of South Uist, where the water depth is about 42m. Predominant measured wind directions were westerly, north and south-westerly winds, while Hs varied from 1.5 to 2m (corresponding to 17.7% of the total). Wave periods lay between 2.5 and 12.5s, while the most frequently

occurring values were 6.0-6.5s (corresponding to 14.1% of the total). The wave power measured during the two year period of observation was of approximately 585 kWh/m.

There are few tidal gauges or wave rider buoys in the Western Isles and thus tides and extreme water level heights were extrapolated by Richard and Phipps (2007) from nearby ports such as Stornoway, Ullapool, Tobermory and Kinlochbervie (Table 3.3). The tidal regime in the Hebrides is semi-diurnal with a range of up to five metres.

Table 3.3 - Extreme water levels and local chart datum in metres above Ordnance Datum (Richard and Phipps, 2007).

Return Period (years)	10	25	50	100	240
Kinlochbervie	3.63	3.74	3.80	3.89	3.97
Stornoway	3.22	3.33	3.39	3.47	3.55
Ullapool	3.39	3.49	3.55	3.66	3.76
Tobermory	3.31	3.45	3.52	3.63	3.71
57.48°N 5.87°E	3.36	3.45	3.50	3.60	3.70

The coastline of the Western Isles is more prone to gales and similar storms than most of the coast of Europe. Mean monthly wind speeds range from about 12 knots in July/August to about 16 knots in December/January, though daily mean wind speed over 30 knots with gusts in excess of 50 knots are not uncommon, even occasionally during the summer months. The highest gust recorded at Stornoway in recent years was 98 knots in February 1962 (Contaminated Land: Implementation of Part IIA of the Environmental Protection Act, 2006). Atlantic storms are frequent, with severe events occurring at intervals. An extraordinary storm occurred in 2005 with deadly consequences and significant material losses. On 11th January 2005, the islands and much of the west coast of Scotland were hit by the most severe storm in living memory. Hurricane force winds ripped roofs from houses; roads, causeways and harbours connecting the low-lying islands were destroyed; fishing boats were wrecked; and livestock drowned. The wave power to the west of the Outer Hebrides is at the present moment being exploited as an important renewable energy resource.

3.3.3. Stoneybridge

South Uist is the second largest of the islands in the Western Isles, measuring some 22 miles north to south and 7 miles from east to west. The geography is divided into a series of north-south strips, each running the length of the island (Figure 3.12). The west coast faces onto the Atlantic and comprises around 20 miles of beach, broken only by a headland at the half-way point. The South Uist coastline between Ardivachar Point and Stoneybridge (Figure 3.13) is an exposed Atlantic coastline subject to on-going

submergence. The Stoneybridge to Ardivachar (*ca.* 8 miles north of Stoneybridge) beach and machair system likely responded to Holocene sea level and sediment supply constraints in the same way as other machair systems in the Western Isles and were first developed sometime in the early to mid-Holocene before about 6500 years BP (Hansom and Angus, 2001). Stoneybridge is located on the west coast of South Uist (Figure 3.13). The beach is sandy, with a shingle ridge that has been formed into an artificial knife edge shape (Figure 3.14). The area behind the ridge is machair, which slopes gently downwards (Richard and Phipps, 2007). The beach that extends between two outcrops of highly resistant Lewisian gneiss at Ardivachar and at Stoneybridge is effectively a single system broken only by the rocky outcrops of and by the exit of the Howmore River. The river exit is characterized by several sand-bars and by localized backshore accretion with embryo dune formation. Seepage of ground water from the landward surfaces seasonally affects the beach so that the higher water-tables of winter intersect the gravels of the backshore storm ridge. Such impounding of the winter water table has profound geomorphological and ecological consequences, since the low-lying parts of the machair and dunes landward remain flooded to depths of up to 0.5m for up to five months of the year (Ritchie, 1971). The backshore ridge is affected by storm wave activity and wave-transported gravels are found up to 50m inland flooring the erosion and deflation hollows in the dunes behind. To the south, near Stoneybridge, the backing dune and machair zone disappears and is replaced by a broad-crested coarse gravel ridge that reaches up to 10m above mean sea level and up to 50m wide (Ritchie, 1971). Under storm conditions the ridge is subject to roll-over of the constituent gravels that encroach into the area of marsh and lochs on the landward side.

Figure 3.13 – Geographical location of Stoneybridge.

Figure 3.14 - View of Stoneybridge (photo A. Dawson).

3.4. Sumatra

3.4.1. Geographical and Geological setting

Indonesia is an immense archipelago of more than 18,000 islands extending over 5000 km from east to west between 95° and 141° E, and crossing the equator from 6° N to 11° S. It is situated at the boundaries of three major plates: Eurasia, India-Australia, and Pacific-Philippine Sea. In western Indonesia, the boundary between the Eurasian and Indian plates is the Sunda Trench (Figure 3.15). Parallel to this in Sumatra is the right-lateral strike-slip Sumatran Fault, which results from the partitioning of oblique plate convergence into normal convergence at the trench and trench-parallel movement further north. Most active deformation in Sumatra occurs between the trench and the Sumatran fault. The subduction zones are mainly well defined by seismicity extending to depths of about 600 km and by volcanoes (95 volcanoes have erupted since AD 1500). The Indonesian archipelago is located in one of the most tsunami-prone regions in the world and has been affected by several important and destructive tsunami events caused by different geological phenomena (*i.e.* volcanism- AD 1883 Krakatoa eruption; earthquake- 2004 Indian Ocean; submarine landslide: 1998 Papua New Guinea).

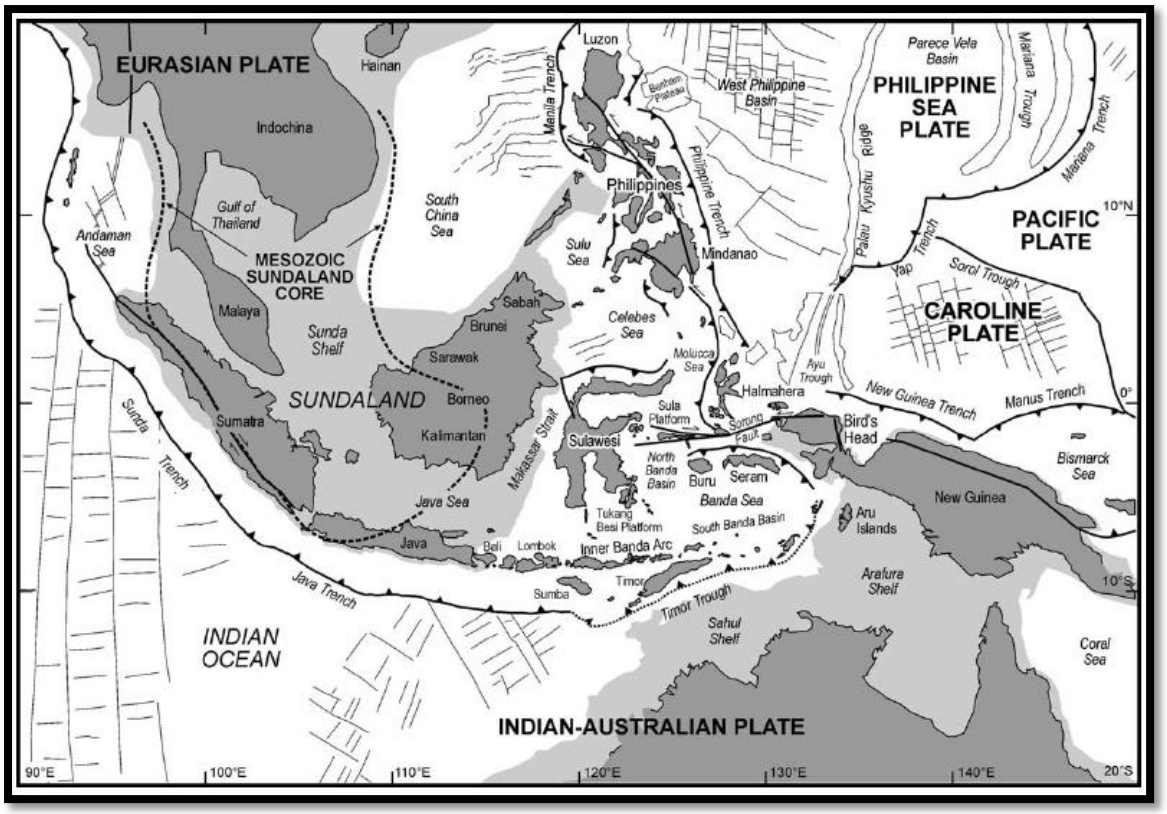

Figure 3.15 - Main geographical features of SE Asia (adapted from Hall, 2002).

Sumatra represents the geological continuation of the Malay Peninsula and contains extensive outcrops of Paleozoic and Mesozoic rocks (Figure 3.16). In western Sumatra there are Paleozoic sediments that range in age from Carboniferous to Triassic and Permian volcanic rocks (Hall, 2009). In contrast, in eastern Sumatra, Carboniferous sediments include pebbly mudstones interpreted as diamictites that formed in a glacio-marine setting. The Mesozoic sedimentary record is very limited but suggests that much of Sundaland (*i.e.* geographical area that encompasses the Sunda trench, Java, Sumatra, Borneo), including most of its Indonesian margin, was emergent. Isotopic age-estimation in Sumatra indicates that there were several episodes of granite magmatism, interpreted to have occurred at an Andean-type margin, during the Jurassic and Cretaceous. Marine sedimentary rocks were deposited in an intra-oceanic arc that collided with the Sumatran margin in the Middle Cretaceous (Hall, 2009). The collision added arc and ophiolitic rocks to the southern margin of Sumatra. Cenozoic rocks were deposited in sedimentary basins in and around Sundaland. There are products of volcanic activity at subduction margins, and there are ophiolites, arc rocks and Australian continental crust added during collision. Little is known of the Late Cretaceous and Paleocene because of the paucity of rocks of this age (Hall, 2009). From Sumatra to Sulawesi, the southern part of Sundaland was probably mostly emergent during the Late Cretaceous and Early Cenozoic, and there was widespread erosion; the oldest Cenozoic rocks typically rest unconformably on Cretaceous or older rocks. In the Java–Sulawesi sector of the Sunda arc, volcanism greatly diminished during the Early and Middle Miocene, although northward subduction continued (Hall, 2009). The decline in magmatism resulted

from Australian collision in eastern Indonesia, causing rotation of Borneo and Java. Northward movement of the subduction zone prevented replenishment of the upper mantle source until rotation ceased in the late Middle Miocene. Then, about 10 million years ago, volcanic activity resumed in abundance along the Sunda arc from Java eastward. Since the Late Miocene, there has been thrusting and contractional deformation in Sumatra and Java related to arrival of buoyant features at the trench, or increased coupling between the overriding and downgoing plates (Hall, 2009). Both islands have been elevated above sea level in the last few million years. The Pliocene (Late Miocene?) wrench tectonics resulted in uplift along the Barisan Mountains in Sumatra midlands and separated the North Sumatra Basin from the forearc region including the Simeulue Basin. This was followed by formation of the Mentawai Fault in the Pliocene – Pleistocene that offsets the western flank of the basin and overprints the accretionary prism. Clastic sedimentation with shelf progradation and deposition of pelagic turbidites in the deep basins has continued since the Late Miocene to present day (Hall, 2009).

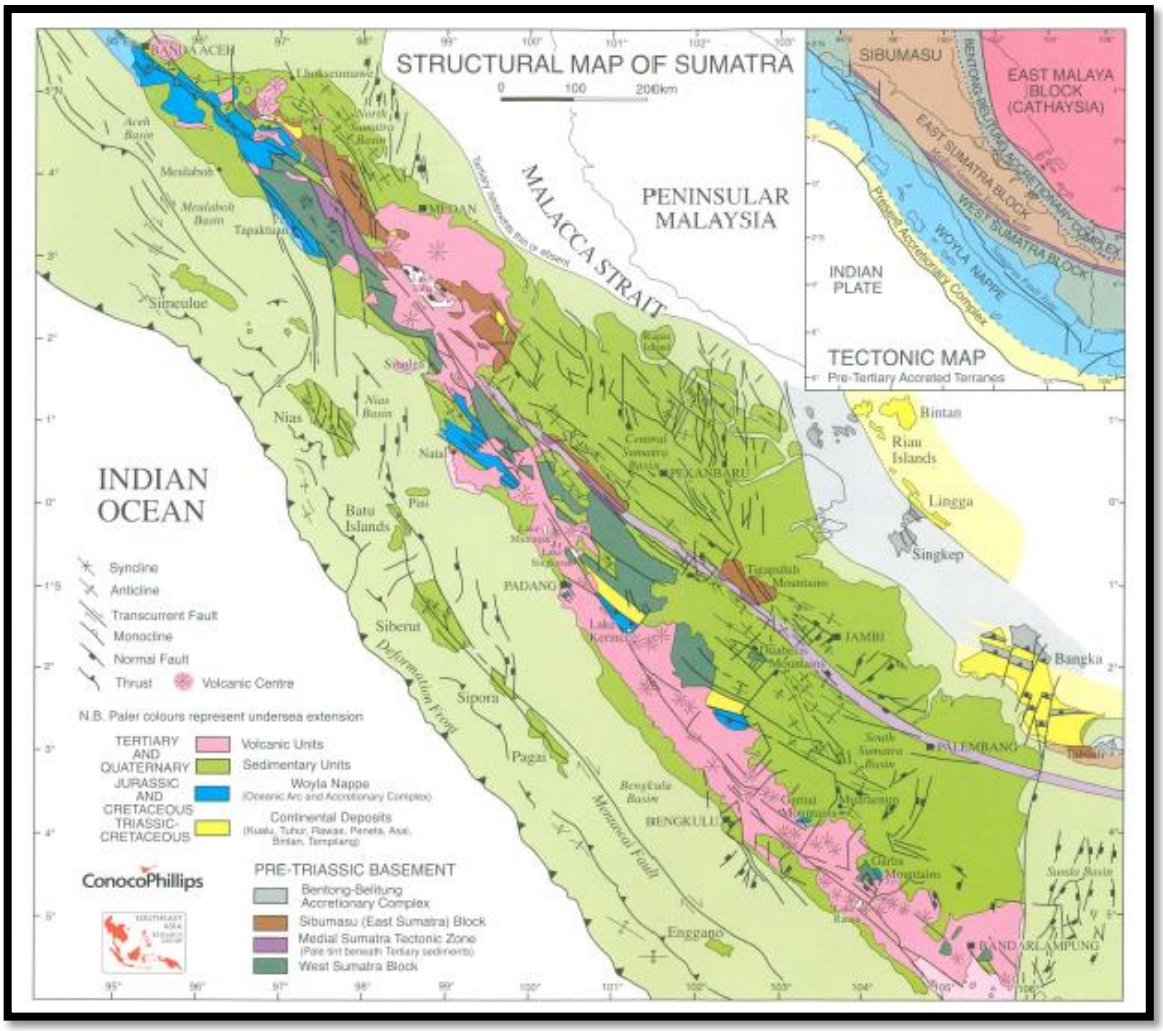

Figure 3.16 - Geological and tectonic map of Sumatra (Barber and Crow, 2005).

3.4.2. Oceanography

With the second largest coastline in the world, Indonesia has remarkably little hard information about the coastal waves that influence the shoreline and the coastal activities offshore and onshore. Reliable wave measurements over long periods of time are missing. Such data are of much importance to determine morphological changes (by natural or human causes) and to determine hazards from extreme wave situations caused by storms. The Indonesian Seas lie at the western edge of the Pacific trade wind belt where the persistent westerly directed wind stresses pile water up against the boundary. As a result, the annual mean sea-surface elevations are as much as 0.20m higher at the Pacific entrances to the archipelago south of the Philippines than in the Indian Ocean south of Java. The south-east Asian monsoon brings strong east winds across the archipelago from May to early September and west wind- from November to March.

The only available wave regime data for Sumatra was presented by Meilianda *et al.* (2010). The authors derived the wave climate of the Banda Aceh (Sumatra) coast from eleven-year daily wind data records from 1995 to 2005. The wind data were recorded by the Department of Meteorology and Geophysics in Banda Aceh, and subsequently translated into statistical wave heights and periods as functions of wind velocity, duration and fetch (CERC, 1992). About 53% of the waves approach the coast with a significant wave height of 1.0m with a period of 3s, which was influenced by the southwest monsoon between April and September. During the northeast monsoon between October and March, 30% of the waves were approaching from the northeast also with a significant wave height of 1.0m and a period of 4.5s. These numbers show that the northwest coast of Banda Aceh is typically a low energy coast.

3.4.3. Lhok Nga

The Lhok Nga Bay is a flat 5 km large coastal embayment (25 km²) opened to the west and delimited by calcareous steep slopes (Figure 3.17). The coast prior to the 2004 tsunami appeared as a continuous beach, breached by small estuaries during the wet season. Bathymetry off Lhok Nga displays a 20 km large continental shelf that is capable of providing great volumes of sediments (Paris *et al.*, 2010b). The main fringing reefs are located between Lampuuk and the Lhok Nga River (Paris *et al.*, 2007). The lowest areas correspond to lagoons, swamps and rice crops. Small hills and hummocky terrains refer to dunes, beach ridges and palaeo-dunes reaching 15m above msl (*e.g.*, Lampuuk, Lam Lho). In the southern part of the bay, the coastal morphology becomes more contrasted, especially south of the Lampuuk harbour, where the coast shows alternating cliffs and flat crescent-shaped bays and creeks.

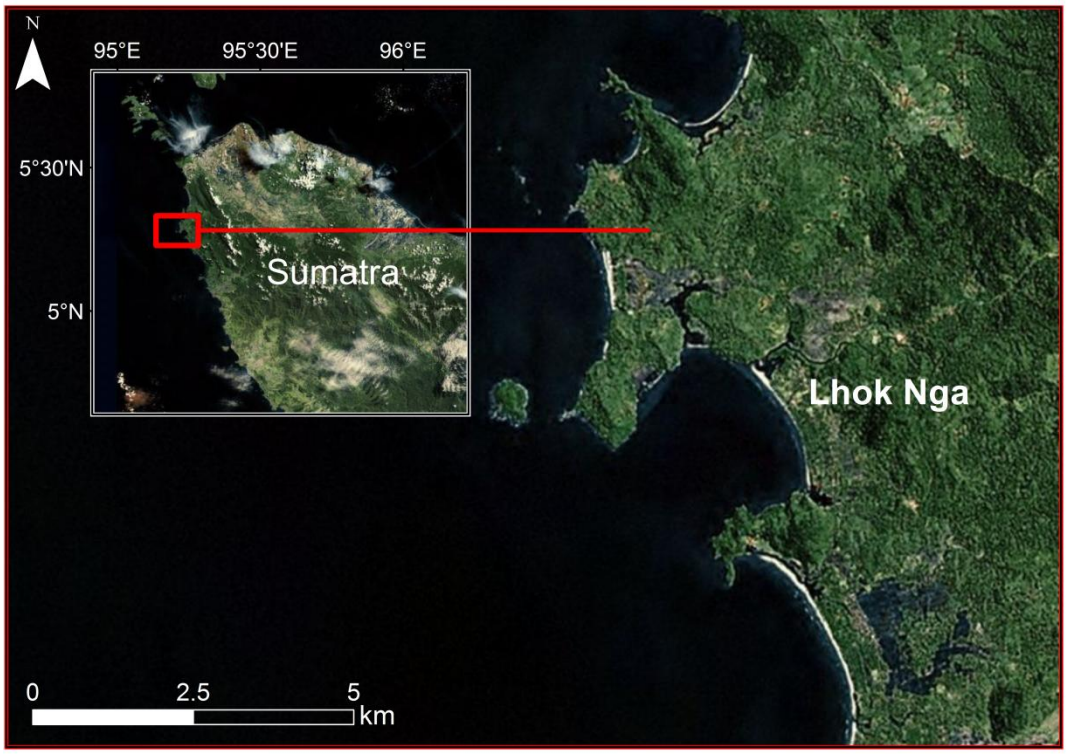

Figure 3.17 - Geographical location of Lhok Nga.

Figure 3.18 - Figure A – Image of Lhok Nga area obtained by satellite Ikonos immediately after the tsunami of December 2004. Figure B – Orthophotography of Lhok Nga area obtained in June 2005.

In Lhok Nga, the 2004 Indian Ocean tsunami waves were almost 30m high and run-ups reached 50m above msl (Lavigne *et al.*, 2009). Eyewitnesses reported 10 to 12 waves, the second and third ones being the highest. Both inflow and outflow produced extensive erosion, sediment transport and deposition until 5 km inland (Paris *et al.*, 2009). The erosional imprints of the tsunami extend to 500m from the shoreline and exceed 2 km along the river beds. The most eroded coasts were tangent to the tsunami wave train, which came from the southwest (Figure 3.18).

4. Methodology

In order to retrieve and analyse the sediment samples necessary to fulfil the objectives of this thesis a wide range of techniques was used. The proxies used are regularly applied to extreme marine inundations sedimentological studies. The textural analysis (grain-size, percentage of carbonates and organic matter; and morphoscopy), microtextural characterization and mineralogical studies of the deposits and source material are commonly used in the establishment of sedimentary provenance and in the characterization of the deposit. In order to constrain the age of deposition of the units studied several age-estimation techniques were used (OSL, radiocarbon, ^{210}Pb and ^{137}Cs). These techniques are also frequently applied to the study of Holocene extreme marine inundations and are universally used to directly date the tsunamigenic units or to obtain an age for them by dating the under and/or overlying units.

A summary description of those techniques follows.

4.1. Sampling and lithostratigraphic description

Sediment samples were obtained excavating trenches and using box-corers on trench walls, or using a Livingstone corer, hand-operated Edelman or gauge augers and\or a Van der Staay suction corer. Visual description of sediment was conducted focusing on colour, lithology, texture, contact between units, erosional features and macrofossil content. Sampling locations were geroreferenced and their elevation above msl determined using a Zeiss Elta R 50 total station and one Leica DGPS RTK. Logs were plotted and correlations were established, when possible. Samples from present day sedimentary environments (*e.g.* nearshore, beach face, beach berm, dune, dune crest and alluvial plain) were collected by hand, using a dredge or directly retrieved by scuba diving (nearshore samples).

4.2. Textural analysis

4.2.1. Grain-size analysis

Grain size analysis was conducted using a set of sieves at 0.5Φ interval. Initially, the bulk samples were washed with tap water and two fractions were separated (>63μm and <63 μm) using a 4Φ mesh. The finer fraction (<63μm) was analysed using the laser granulometer Malvern Mastersizer Hydro 2000 MU after deflocculating with 30% Sodium hexametaphosphate. The coarser fraction (>63μm) was analysed exclusively through sieving, with exception of samples that had a coarser fraction weighting less than 10g. Results derived from both methods were assumed to be comparable. Statistical parameters of the grain size distribution (*e.g.* mean grain size, Φ_{10}, Φ_{90}, median, mode, standard deviation, kurtosis and skewness) of the

samples were calculated using the graphic method (Folk and Ward, 1957) in the GranGraf software (Carvalho, 1998). A group of textural features were map-plotted to study their spatial distribution. This was done using the Inverse Distance Weighting (IDW) method of interpolation between sampling points in the ArcGis 9.3 environment. IDW is a method of interpolation that estimates cell values by weight-averaging the values of sample data points in the neighbourhood of each processing cell according to a non-linear function of distance (Davis, 1986).

4.2.2. Calcium carbonate and organic matter content

Calcium carbonate content – $CaCO_3$ - (associated with bioclasts) was determined by measuring the volume of carbon dioxide evolved during reaction with hydrochloric acid using an Eijkelkamp calcimeter (Eijkelkamp, 2008). Organic matter content (OM) was determined by *loss-on-ignition* at 550º C during 2h following Bengtsson and Enell (1986).

4.2.3. Morphoscopy

Quartz-grain morphoscopy is the study leading to statistical determination of the different types of quartz grains in sandy deposits (Cailleux, 1942). The detailed observation of the surface of the grains (in terms of angularity, sphericity, shape, luster, corrosion, coatings), permits, in many cases, the establishment of the sedimentological agents that affected them prior or during transport or following immobilization. In order to establish tipology of quartz grains, samples from all study areas were observed and counted under the binocular microscope (Leica EZ4; 30x). The fractions (1 to 3Φ) were selected for observation since the smaller fractions require more magnification and the very coarse and very fine fractions tends to yield biased results on roundness. The observation and counting of, at least, 100 grains per sample was conducted. Grains from each sample were counted and 3 major groups (*i.e.* bioclasts, lithic and quartz) were identified. Bioclast fragments (eesencially Ca-carbonate, whole or fragmented shells and plant remains more or less fermented) and lithic grains were identified whenever possible. Quartz grains were further classified in terms of roundness and sphericity. The results of each sample were compiled and charts were produced. In some cases, other statistical analyses were conducted (*e.g.* principal component and cluster analysis) using Statistica 10 software.

4.3. Microtextural analysis

Grain surface microtexture (also named exoscopy - *i.e.* the micromorphological analysis of the surface of grains) is an analysis usually reserved for quartz particles of the dimension of sand and coarser particles. Many quartz sand grains develop microtextural features that can often be referred to specific transport processes or specific sedimentary environments. In order to recognize surface microtextures, a

Scanning Electron Microscope (SEM) was used to obtain high resolution images [JEOL JSM 5200 LV (Lisbon) and a JEOL JSM-5910 LV (Clermont-Ferrand)].

4.3.1. Laboratory procedure

A minimum of 12 quartz grains per sample (maximum of 30 grains; mean of 16 grains) from the 1 to 3ϕ (125-500μm) size fraction were randomly selected under the binocular microscope and prepared for SEM analyses. This involved either mineralization with gold (Lisbon, FCUL) or metallization with carbon (Clermont-Ferrand University) of the particles. The grains were then taken to the SEM lab and photographs obtained. After this process, a visual analyse of each grain would follow focusing in a group of microtextural characteristics.

4.3.2. Microtextural classification

The microtextural classification was established based on selected references (*e.g.* Mahaney, 2002) and in the author visual criteria. Each grain was characterized using a number of descriptive microtextural features revealed in SEM microphotographs (*e.g.* fresh surfaces, percussion marks, dissolution features, angularity and adhering particles). The microtextures (Figure 4.1) can be characterized as follows:

1) Angularity - classified using Powers scale (Powers, 1953).
2) Fresh surfaces – microtexture characterized by the presence of mechanical marks (*i.e.* fractures, abrasion marks, sharp edges) that are responsible for the recent exposure of part, or the totality, of the grain surface. These are also habitually characterised by the absence of chemical dissolution or precipitation in those new surfaces.
3) Percussion marks - microtextures characterised by the presence of, usually, V-shaped depressions, typically the result of grain collision.
4) Adhering particles – characterized by the presence of microparticles on the surface of quartz grains. Usually, these microparticles are within grooves and many are attached to the surfaces of individual grains.
5) Dissolution - microtexture of chemical nature indicating the degree of dissolution on the surface of individual grains. The effects of dissolution are noticed by the destruction of fresh surfaces and sharp edges on the surface of the grains and by the formation of grooves.

A semi-quantitative approach to the microtextural classification of each grain was used, based upon the proportion of grain surface occupied by each feature [0 (absent) to 5 (> 75% of the grain surface)]. The angularity of the grains was classified from 0 to 5 (very rounded to very angular). Median values for each variable were calculated for each sample and used in the subsequent statistical analysis. Results were

interpreted based on the knowledge of present day coastal environments and supported by standard statistical methods (using Statistica 10 software) including principal components and classificatory analyses. Kruskal-Wallis tests (Kruskal and Wallis, 1952) were conducted and p-values were calculated to test the statistical significance of the results ($p<0.05$; indicating that at least the mean value of one population is different from the others).

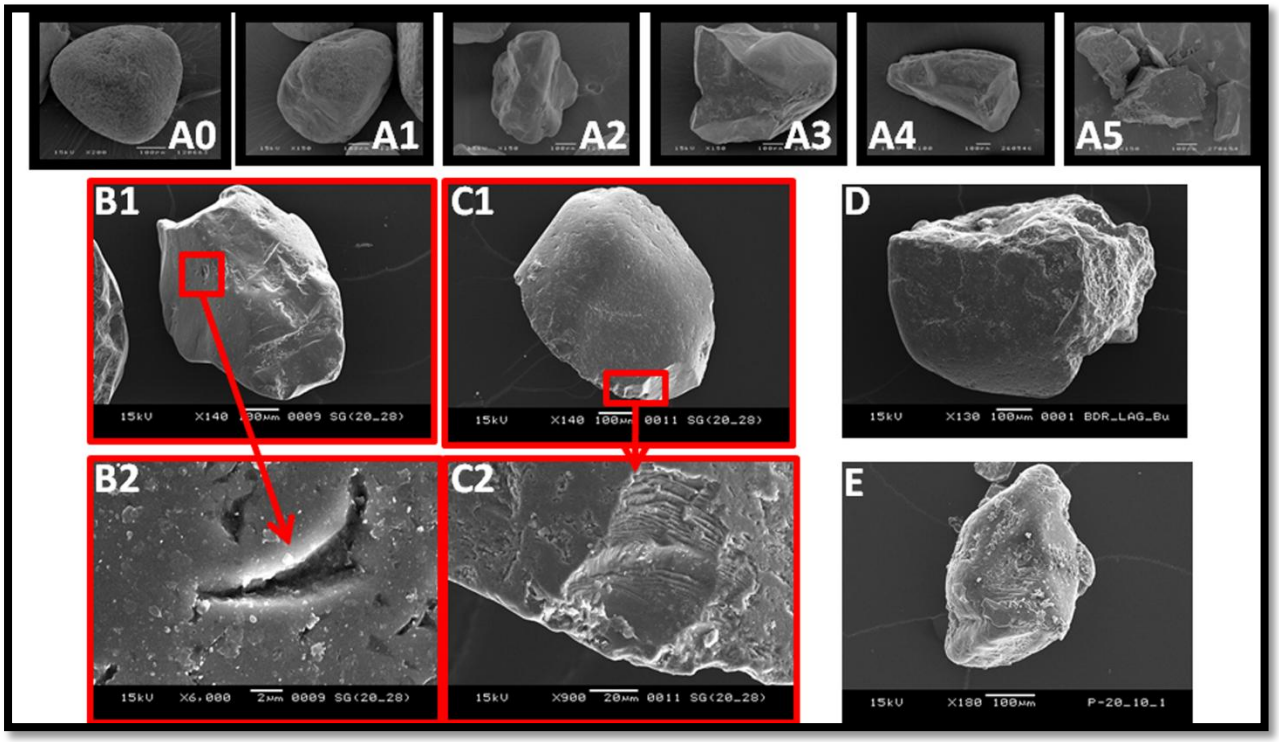

Figure 4.1 Microtextural features. A0 to A5 – angularity (very rounded to very angular). B1 – percussion marks. B2 – detailed view of percussion mark. C1 – fresh surface (in this case, sharp edge, fractures and steps). C2 – detailed view of fresh surface. D – dissolution (especially visible on the right face of the grain). E – adhering particles (more visible in the center of the grain).

In the literature, the number of grains reported as necessary for sedimentological interpretation varies within a wide range (cf. Mahaney, 2002; Costa *et al.*, 2012b for a summary and examples). In this study, an empirical assessment was conducted to evaluate the minimum size of the sample with statistical meaning, focusing on the number of grains required to hold the median value characterizing each microtextural attribute reasonably constant within the sample. Our results suggest that the median value is about 20 grains.

4.3.3. Atlas of microtextural features in quartz grains

With the collected samples, and after laboratory treatment, a large number of SEM photos of the quartz grains were gathered. A group of twenty microtextures visible in the surface of quartz grains was

identified and described and an atlas was compiled using selected photos to facilitate the identification of those microtextures. The microtextural atlas of quartz grains is presented in Annex 2.

4.4. Mineralogy

4.4.1. Heavy minerals

Heavy mineral assemblages often reflect the provenance of Quaternary deposits. Heavy minerals are those with a specific gravity greater than 2.85 and are usually separated from the lighter mineral fraction in a sample by settling in a heavy liquid such as bromoform (Specific Gravity of 2.89) (Whalley, 1990). Samples (1 to 3Φ fraction) from a wide range of sedimentary environments (*e.g.* nearshore, dune and beach) and from tsunami and storm deposits were prepared in order to observe heavy minerals under the microscope in slides and to contribute to on-going provenance studies on heavy mineral characterization of tsunami and storm deposits. The slides were prepared as followed: samples were first washed using tap water. They were then wet sieved using a set of sieves at 0.5Φ interval. The sand fraction was assembled in the 1-3Φ fractions (125-500μm). Heavy minerals present were separated using bromoform and then mounted using Entelan resin on glass slides. The required amount of grains for each slide was obtained using a micro-splitter. About 300 transparent heavy minerals per slide samples were identified and counted under an Olympus BX40 petrographic microscope in each sample.

4.4.2. Micromorphology analyses

Sediment samples from Boca do Rio and Voe of Scatsta were collected for micromorphology analyses using the methodology described by Murphy (1986). The thin sections used in this study were prepared by Julie Boreham (Earthslides). It is standard to take samples by using rigid metal tins (box corers), and wrapping the sediment or soil with cling film, tissue and tape, in order to keep it intact and undisturbed in transit to the laboratory. The raw samples are then air dried, or in some instances lyophilized dried to remove all water before impregnation with a crystic polyester resin. It usually takes 6 weeks for the impregnated samples to cold cure to a 'rock hard' stage. After this, an additional 4 weeks of sectioning production time is usually required, making the total turn-around time about 10 weeks. The final glass thin-sections are 25-30μm thick by 0.08m long, which enables the researcher to identify and understand the minerals, organic materials, and the sediment or soil structure and composition using the microscope (Olympus BX40).

4.5. Age-estimation methods

The techniques used in this work were selected because they were considered to be better suited for the time interval and sediments studied in this research. However, age-estimation of extreme marine

inundations is, in most cases, problematic. Results tend to be difficult to interpret and in many situations the dates obtained are not accurate. The samples from Stoneybridge and Lhok Nga (Indonesia) are from contemporary events and have been collected immediately after the extreme marine inundations (*i.e.* the Great Storm of January 2005 and the 2004 Tsunami, respectively).

4.5.1. OSL

Optically Stimulated Luminescence dating (a development of Thermoluminescence) is used for dating terrigenous sediments, where exposure to light prior to burial has been extensive and non-existent after burial. The information given by OSL is therefore the time elapsed since the last episode of exposure to light or light-bleaching episode of the grains (Aitken, 1992). This technique measures the luminescence emitted from the most light-sensitive electron traps in minerals - essentially quartz and feldspars - (Wintle *et al.*, 1994), though more recently illite and muscovite have been used with promising results, this energy being stored in the crystalline network and increasing with burial time. Luminescence age-estimation methods have previously been applied to tsunami deposits using thermoluminescence (*e.g.* Bryant *et al.*, 1996; Dawson *et al.*, 1995), infra-red stimulated luminescence (*e.g.* Huntley and Clague, 1996; Ollerhead *et al.*, 2001) and optically stimulated luminescence (*e.g.* Banerjee *et al.*, 2001; Cunha *et al.*, 2010).

In brief, the laboratory treatment consists of a series of conventioned sample preparation techniques (*e.g.* sieving, acid leaching and oxidation with 10% HCl, 10% H_2O_2, 40% HF) after extrusion of the sediment under controlled laboratory lighting condition. The grains are mounted on stainless steel discs and then counted. Equivalent Dose (D_e) values are obtained through calibrating the "natural" optical signal, acquired during burial, against "regenerated" optical signals obtained by administering known amounts of laboratory dose. The luminescence age is obtained by dividing D_e value by the mean total dose rate value.

The OSL results presented in this study have been obtained by collaborative work involving the Department of Earth Sciences, Marine and Environmental Research Centre, University of Coimbra (Portugal), Centro de Geofísica, Department of Earth Sciences, University of Évora, Portugal and the Nordic Laboratory for Luminescence Dating, Department of Earth Sciences, Aarhus University, Risø, Denmark.

4.5.2. ^{210}Pb and ^{137}Cs

^{210}Pb is an unstable isotope present in the atmosphere and is produced by the decay of ^{222}Rn, which is part of the U series - decay chain. This isotope is absorbed by the sediments where it decays to stable ^{206}Pb over an interval of *circa* 150 years. By measuring the ratio between ^{210}Pb and ^{206}Pb in a column of sediment in relation to depth, and assuming that the atmospheric flux of ^{210}Pb has remained constant, the time that has elapsed since the radioactive lead was deposited can be determined (Olsson, 1986). The sedimentation rate can then be established by using the vertical concentration profile of ^{210}Pb excess to infer

a uniform sedimentation rate using the constant rate supply method (Appleby and Oldfield, 1983). The laboratory procedure was followed according with description by Eakins and Morrison (1978).

^{137}Cs is an artificially generated radioactive nuclide (half-life of 30 years) that has only been produced in significant quantities as a result of thermonuclear weapons testing, which began in 1945. The temporal patterns of ^{137}Cs input can be characterised by:

1) detectable ^{137}Cs in the northern hemisphere began in 1954, though some authors use a threshold of 1950;
2) the second a remarkable peak in ^{137}Cs corresponds to 1962-1964, congruent with a maximum in thermonuclear testing.

Some areas had additional input in 1986 after the Chernobyl incident but to the present state of knowledge this is not the case of Portugal. This annual variation has been successfully used to determine sediment accumulation rates in a wide variety of depositional environments including reservoirs, lakes, wetlands, coastal areas, and flood plains. Identification of ^{137}Cs loss and gain for each sampled location in the study site is made by comparison of the measurement done using gamma spectrometry from the reference sites with those from the study field, allowing the establishment of a sedimentation rate. Sediment samples used for ^{210}Pb and ^{137}Cs were measured at the University of Bordeaux (France) and ISMAR (Italy).

4.5.3. Radiocarbon

^{14}C which is continually being produced in the upper atmosphere becomes stored in various global reservoirs (atmosphere, biosphere and hydrosphere) and is absorved by living organisms. All living organisms absorb carbon dioxide during tissue building in a ratio that is broadly in equilibrium with atmospheric carbon dioxide. After the death of the organisms the ^{14}C decays to ^{14}N. The activity of ^{14}C in the atmosphere is known (15 disintegrations per minute per gram of total carbon, on average). The half-life of ^{14}C was originally calculated at 5568±30 years (Libby, 1955), but subsequently this has been more accurately determined as 5730±40 years (Godwin, 1962). However, the value that is used by convention is the former due to the large number of dates that had been produced prior to the new measurement. The logarithmic decay curve for radiocarbon is well established (*e.g.* Stuiver *et al.*, 1998) and calculations can be made using this curve (up to app. 50000 years, which is approximately 8 times the half-life of ^{14}C).

There are four fundamental assumptions of radiocarbon age-estimation: the production of ^{14}C is constant over time; the ^{14}C:^{12}C ratio in the biosphere and hydrosphere is in equilibrium with the atmospheric ratio; the decay rate of ^{14}C can be established; a closed system has existed since the death of the organism. Over the years, these assumptions have been questioned but they can still be accepted in general terms. Two approaches are used to measure the residual ^{14}C activity in a sample: the conventional radiocarbon dating or the Accelerator mass spectrometry (AMS).

The first involves the detection and counting of β emissions from ^{14}C atoms over a period of time in order to determine the rate of emissions and hence the activity of the sample. In the calculation of radiocarbon dates obtained by conventional methods, laboratories compare sample activities to a modern reference standard. The second uses particle accelerators as mass spectrometers to count the actual number of ^{14}C atoms as opposed to their decay products (Aitken, 1990; Bowman, 1990). Comparing the two methodologies, one can conclude that AMS allows the measurements of much smaller samples and is quicker.

The time in years since the death of an organism can be calculated from the following equation (*e.g.* Stuiver *et al.*, 1998):

$$r = \frac{1}{\lambda} log_e(\frac{A_0}{A}) \qquad \textbf{Equation 4.1}$$

Where λ is the decay constant of ^{14}C, A_0 is the ^{14}C activity of the modern reference standard, and A is the measured ^{14}C activity of the sample of unknown age.

The sources of error in ^{14}C dating are the temporal variations in ^{14}C production, the isotopic fractionation, the circulation of marine carbon, the contamination of the samples (especially in shells - often used in palaeotsunami research) and the biogeochemistry of lake sediments. The radiocarbon dates used in this work were obtained at Beta Analytic Inc. (AMS) and their standard laboratory protocol was followed. Calibration was done using the CALIB 6.0 Radiocarbon program coupled with the IntCal09 curve (Stuiver and Reimer, 1993).

5 Results

5.1. Salgados

5.1.1. Lithostratigraphic features

In total, 158 sediment cores (up to 5 m) were obtained from the Salgados lowland (Figure 5.1.1) using a hand-operated gouge, Edelman augers, van der Horst, van der Staay and Livingstone corers (as described in Chapter 4). Moreover, approximately 30 surface samples from present-day sedimentary environments, including the nearshore between 6 and 19m below msl, beach face, beach berm, dune and dune crest were collected by hand or directly collected from the sea bottom by scuba diving (Figure 5.1.1).

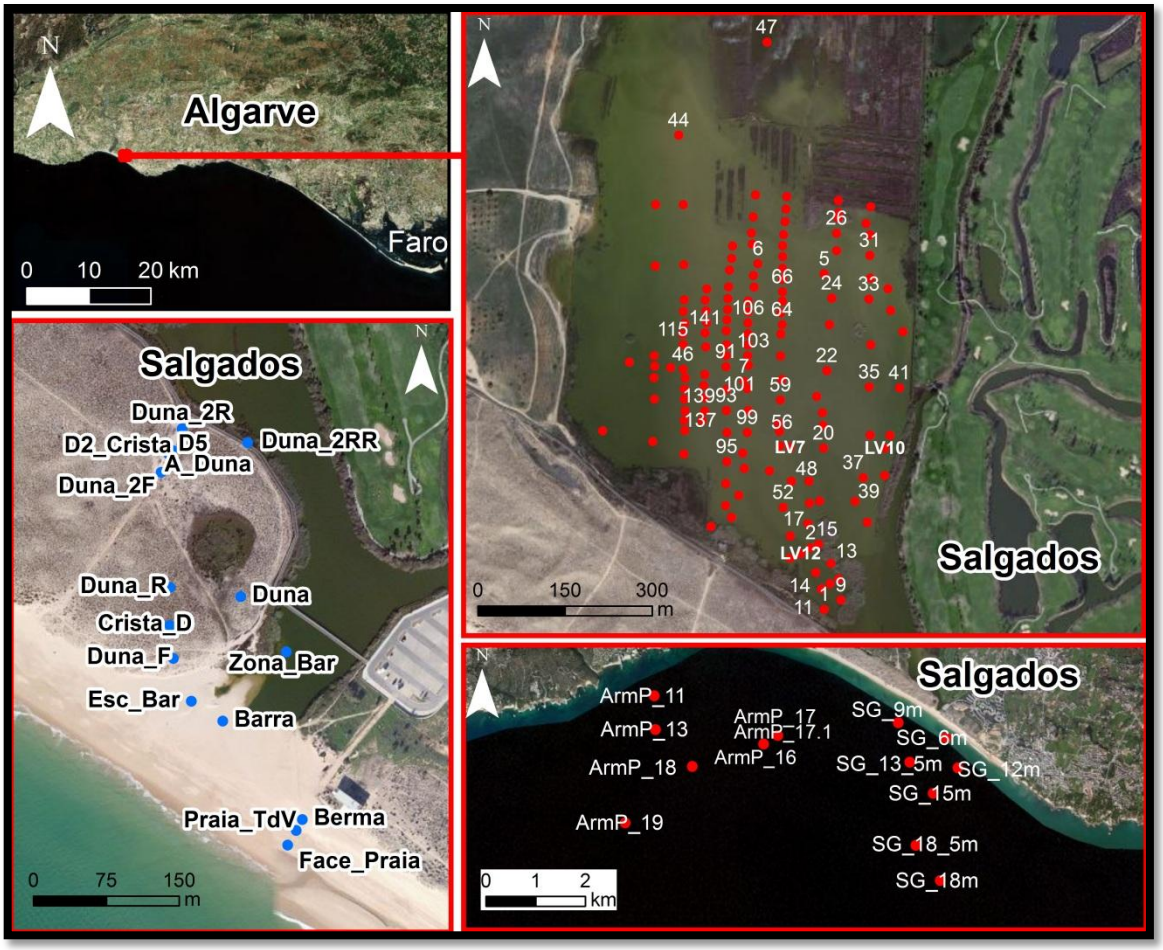

Figure 5.1.1 – Cores and surface samples collected in Lagoa dos Salgados.

The lithostratigraphy of the lagoonal area is summarized in a schematic synthetic log based on cores collected in Lagoa dos Salgados showing six lithostratigraphic units deposited on top of the Plio-Pleistocene (Areias de Faro-Quarteira) basal sand (Figure 5.1.2). Eleven sediment samples were collected from organic-rich layers or *laminae* in different cores where the major lithostratigraphical units were clearly identified and allowing for lateral correlations (see below; Table 5.1).

Unit A – The lowermost unit, with a maximum thickness of 2.48m (core SG1), rests unconformably on the reddish fluviatile Plio-Pleistocene materials and is characterized in the seaward region of the basin by alternations of yellowish to grey sand with marine shell fragments and less abundant and thinner clay *laminae*. One radiocarbon date (see below) obtained from an organic mud lamina of the upper section of this unit, at 4.32m below surface (*i.e. ca.* 3m below msl) in SG1, yielded a radiocarbon age of *ca.* 4790 ± 50 years Cal BC (Figure 5.1.2 and Table 5.1). This indicates that most of the coarser sediment of the basal unit accumulated in an essentially high-energy and shallow environment open to marine influence (*e.g.* $\delta^{13}C$ value), preceding the pronounced drop in sea-level rise rate at 6000 to 7000 cal BP that characterizes the Holocene transgression in the Algarve and elsewhere along the western Portuguese coast (Freitas *et al.*, 2003; Teixeira *et al.*, 2005; Vis, 2009). Two samples (obtained from cores SG1 and SG46) were used for sedimentological characterization of this unit. The values obtained for each core were conditioned by their position in terms of proximity to the coast confirming field observations: core SG1 presented 77.2% of coarse material (>63 μm), 8.9% for $CaCO_3$ content and 1.6% of organic matter (OM). On the other hand core SG46 (farther inland) presented 18.5% of coarse material, 1.1% for $CaCO_3$ content and 3.8% in terms of OM.

Unit B – This unit, with a maximum thickness of 1.32m (core SG44), is mainly composed of grey to brown mud with occasional intercalated layers of coarser sediment which wedge out laterally, indicating a significant decrease in the energy level of the environment with increased input of fine-grained terrigenous materials. The radiocarbon dates (obtained in different cores at *ca.* 2.4m to 3.1m below surface, *i.e. ca.* 1.0m to 1.6m below msl) constrain the deposition of this unit within the 3700 to 980 years Cal BC time span (Figure 5.1.2 and Table 5.1), a period of *quasi*-stability of mean sea level that should have favoured the build-up of the barrier and beach-dune system at the exposed facade of the Armação de Pêra embayment and increased the frequency of sediment choking of the inlet, thus favouring the retention of terrigenous sediment (*e.g.* $\delta^{13}C$ value) within the lowland. Twelve samples from 8 different cores allowed characterization of this unit in terms of average and standard deviation percentages of coarse material, $CaCO_3$ and OM, the values were 22.9±14%, 10.7±9.3% and 5.4±1.6% respectively, indicating marine signature but reduction of the energy level across the whole basin.

Unit C – This unit rests conformably with the under and overlying units (Figure 5.1.2). It essentially consists of yellowish to greyish medium to fine sand containing marine shell (essentially bivalves) fragments, and exhibits normal (fining upward) grading. Sand is intercalated with numerous muddy *laminae*. It presents a maximum thickness of *ca.* 3.25m (core SG2). An age range (approximately 3000 to 1500 Cal BP) for this

unit was estimated in context with the radiocarbon ages obtained for units B and D. Thirty three samples from thirteen different cores allowed characterization of this unit in terms of percentage of coarse material, $CaCO_3$ and OM; the average and standard deviation values were: for the mud dominated intercalations - 25.3±15.1%, 11.6±9.4% and 5.87±3.0% respectively; and for the sand dominated material: 90.1±9.9% and 20.8±9.9%, respectively, the OM being virtually nil.

Unit D – This unit is composed of brownish silt and clay material that becomes darker to the top. It presents a maximum thickness of approximately 0.75m (core SG46) and exhibits an abrupt contact with the overlying unit E. Five radiocarbon dates were obtained from organic sediment (at *ca.* 0.45 to 0.75m below surface, *i.e. ca.* 0.65 to 0.85m above msl) of this unit (Table 5.1) constraining its age of deposition between years Cal AD 420 and 1030. Thirty five samples from thirty two different cores allowed characterization of this unit in terms of percentage of coarse material, $CaCO_3$ and OM content; the average and standard deviation values were 12.2±16.7%, 9.2±7.0% and 4.1±1.3% respectively.

Unit E – this unit is essentially composed of medium to fine sand, which contrasts markedly with the underlying sediment of unit D and is separated from it by an unconformity (Figure 5.1.3). Unit E is widely distributed in the lowland and present in several cores although its thickness decreases (from 0. 79 m – core SG LV 10 - to a few mm further inland – *e.g.* core SG 26) up to its landward limit *ca.* 800m from the present day coastline. The altitude of the basal contact of unit E rises gradually inland from *ca.* -0.05 m up to 1.28m above msl. This unit is laterally variable in terms of its thickness and sedimentary characteristics. It is observed in its seaward section as a massive sandy deposit with no identifiable laminations and without sedimentary structures. Several centimetre-sized mud rip-up clasts from the underlying unit were identified throughout this unit although more noticeable at its base. However, further inland this unit is characterized by finer sediments; this spatial contrast is expressed by higher Φ10, Φ 50 and Φ 90 (implying shift towards finer size interval of the whole >63µm grain size spectrum) with increasing distance to the inlet, and simultaneous enrichment in mud-sized particles. Forty five samples from forty two different cores allowed characterization of this unit in terms of percentage of coarse material, $CaCO_3$ and MO. The average and standard deviation values for the massive sand were 87.6±4.9%, 28.7±9.0% respectively, with no OM. Further inland the corresponding values were 54.24±15.5%, 23.0±7.7% and 2.32±0.54%.

Unit F – The topmost unit is characterized as a dark brown silty/clayish layer presenting a maximum thickness of 2.20m (core SG47) and corresponds to the present-day sedimentary environment. In the field, units F and D are indistinguishable in places were unit E is absent. The upper (0.20m to 0.10m) centimetres of this unit are, in places, black. Field observations revealed some coarser intercalations (*e.g.* SG14_0.20-0.28 – storm deposit? – also present in other cores in the coastal edge of the lagoon) within the mud restricted to an area closer to the inlet and extending northwest along the back barrier. ^{210}Pb and ^{137}Cs sedimentation rates were established for the top 0.30m of the stratigraphic column (Figure 5.1.2) and the results suggest that the low-energy deposits resting on top of the coarser unit E in core SG48 are younger than AD 1865. Forty four samples from thirty five different cores allowed characterization of unit F in terms of

the percentage of coarse material, $CaCO_3$ and OM. The bulk of unit F yielded average and standard deviation values of 18.8±14.2%, 9.2±4.2% and 4.5±1.32%, respectively. In contrast, the coarser intercalations presented values of 66.6±9.6%, 20.3±8.2% respectively, the OM being virtually absent.

Results indicate a time-integrated accumulation rate derived from the vertical profile of ^{210}Pb excess of *ca.* 2.6mm/yr. Moreover, taking AD 1963 as the maximum nuclear testing in the northern hemisphere (Ritchie and McHenry, 1990) the accumulation rate obtained from the ^{137}Cs peak at 0.10m below surface is 2.3mm/yr, which is in rough agreement with the value inferred from ^{210}Pb (Figure 5.1.2).

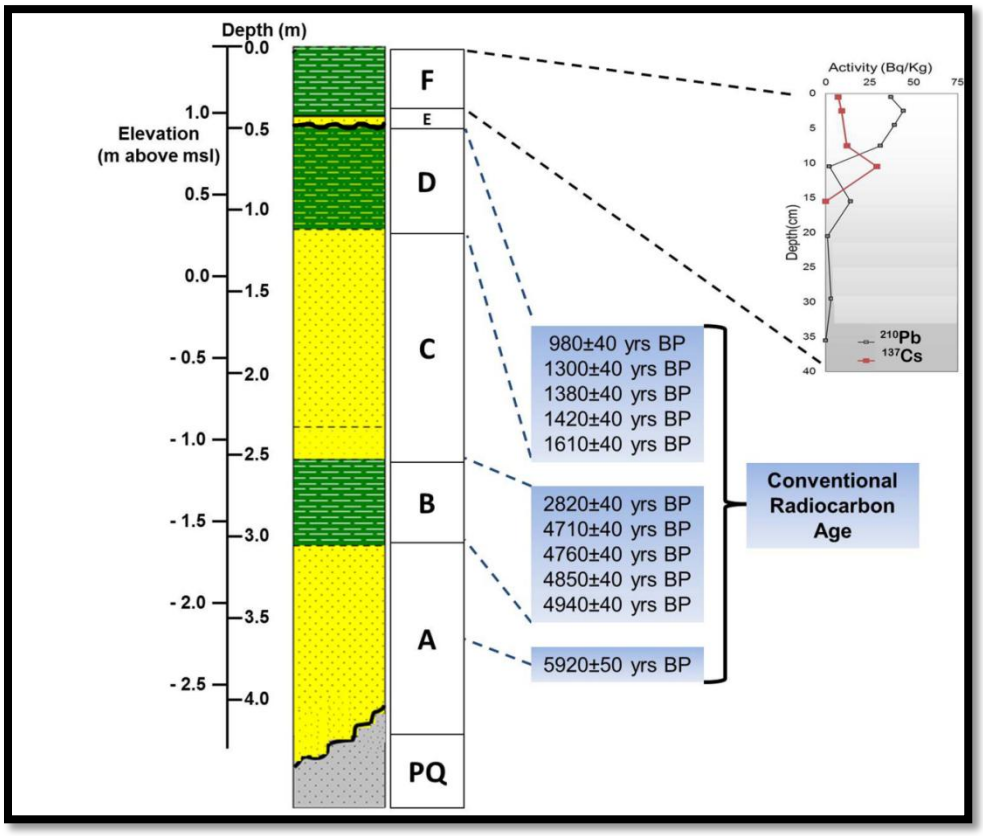

Figure 5.1.2 - Schematic log of Lagoa dos Salgados showing main Holocene lithostratigraphic units resting upon Plio-Pleistocene dissected basement (see text for details); the relative location of cores from which 11 radiocarbon dates and one ^{210}Pb and ^{137}Cs concentration profile were obtained are also shown in Figure 5.1.1.

Figure 5.1.3 – Photos of contact of Unit E with under and overlying units identified in Lagoa dos Salgados.

A repeating lithostratigraphic sequence occurs in the flat-floored depression of Lagoa dos Salgados (Figure 5.1.4). Within this stratigraphical sequence a peculiar feature was observed in the geometrical distribution of unit E. This unit is thicker in the coastal edge of the lowland space and it decreases to millimetric thickness in the northern part of the Lagoa dos Salgados, just before wedging out. In Figure 5.1.4 in profile A-A', it is observed that unit E decreases its thickness with increasing distance inland, presenting *ca.* 0.50m in the core section nearest to the coast and decreasing to millimetric thickness at about 400m inland. In addition, the elevation of the basal contact increases inland. On the other hand, profiles B-B' and C-C' exhibit unit E consisting of a very thin (centimetric) sand lamina quickly disappearing inland. Thus, one can conclude that unit E is a distinct wedge-shaped and ramping up lens of coarse sediment extending across the lowland for several hundred meters inland, being thickest at the coast, closest to the present-day inlet.

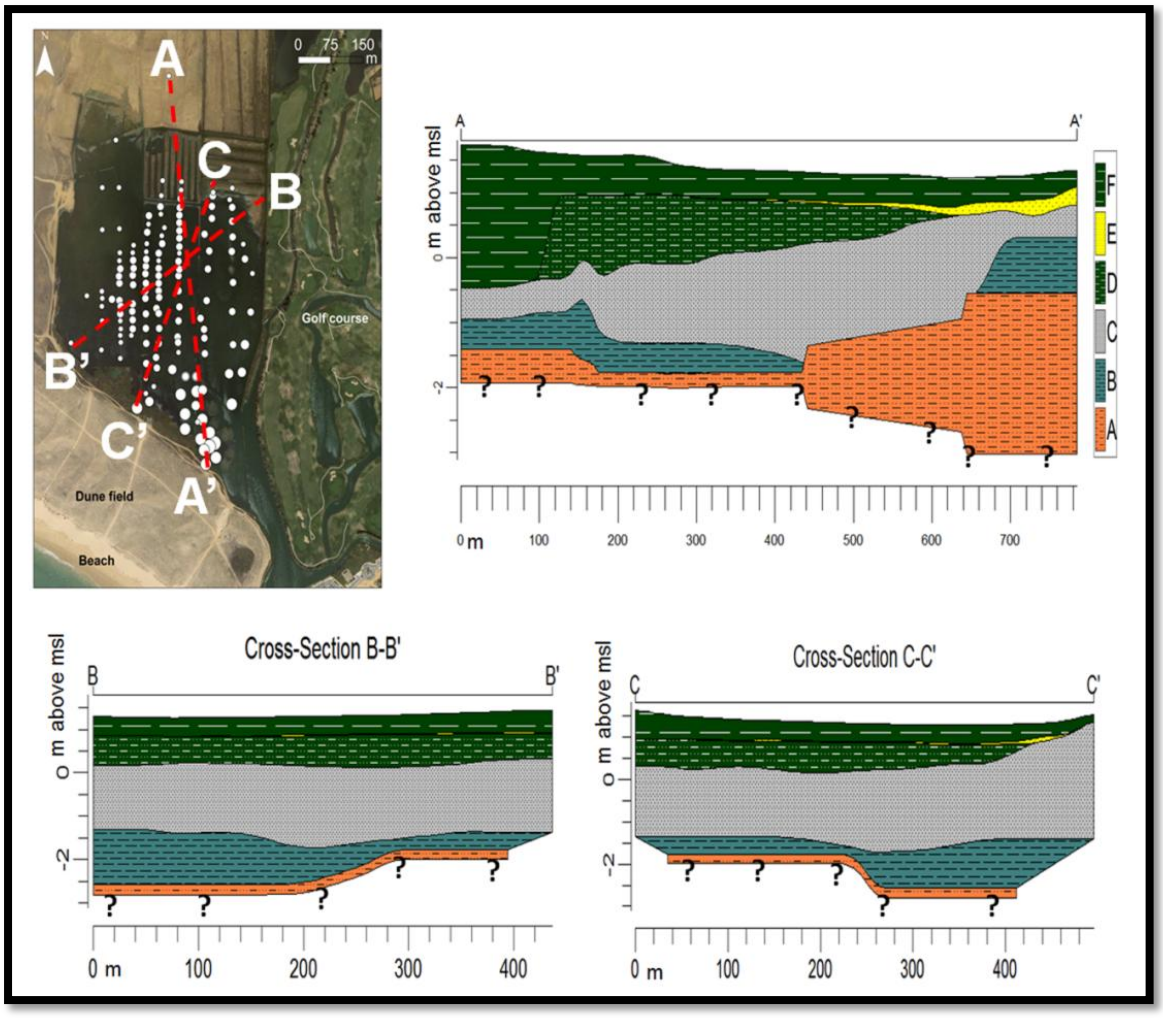

Figure 5.1.4 – Cross-sections based in the lithostratigraphical correlation of cores collected across the Salgados lowland. A-Profile N-S; B- Profile NE-SW; C- Profile NW-SE. See text for lithostratigraphic unit characterization.

Table 5.1.1 - Radiocarbon dates obtained for Lagoa dos Salgados Upper Holocene stratigraphic sequence.

Core	Lithostrat .Unit	Depth below surface (m)	Height above msl (m)	Material	$\delta^{13}C$ (‰)	Conv. ^{14}C age (yrs BP)	2 sigma calibrated result (yrs CAL BP)	Intercept Calibration Curve
LV12	D	0.77	0.65	organic sediment	-25.1‰	980±40	790-960	CAL AD 1030
SG92	D	0.46	0.82	organic sediment	-24.9‰	1300±40	1170-1300	CAL AD 680
SG37	D	0.58	0.74	organic sediment	-25.3‰	1380±40	1270-1340	CAL AD 650
LV7	D	0.59	0.68	organic sediment	-25.2‰	1420±40	1280-1380	CAL AD 640
SG39	D	0.62	0.69	organic sediment	-25.4‰	1610±40	1400-1570	CAL AD 420
SG1	B	2.43	-1.04	organic sediment	-22.5‰	2820±40	2850-3030	CAL BC 980
SG6	B	2.92	-1.61	organic sediment	-25.6‰	4710±40	5320-5580	CAL BC 3510
SG46	B	2.71	-1.39	organic sediment	-25.1‰	4760±40	5330-5590	CAL BC 3630 or 3580 or 3530
SG5	B	2.89	-1.52	organic sediment	-25.6‰	4850±40	5480-5650	CAL BC 3640
SG47	B	3.11	-1.37	organic sediment	-25.1‰	4940±40	5600-5740	CAL BC 3700
SG1	A	4.32	-2.93	organic sediment	-19.1‰	5920±50	6650-6880	CAL BC 4790

5.1.2. Textural features

The analysis of the geographical variation of a group of geometrical, compositional and textural features (*e.g.* thickness, percentage of sand, percentage of Ca carbonates, ϕ10, ϕ50, ϕ 90, mean, mode, standard deviation, kurtosis and skewness) of sediment from unit E was also conducted (Table 5.2). The percentage of sand (Figure 5.1.5A), decreases inland with maximum values (up to 100%) in the south-eastern areas of the basin and presents lowest values (up to 20%) in the northern and north-western sectors of the lowland. The lower values found closer to the landward edge of the deposit mirror the decreasing transport competence and capacity of a landward transport mechanism. However, it may, in cases, be also influenced by the very small thicknesses of the unit E in the more distal locations, where field subsampling could not avoid contamination of the sand by the over and underlying mud. The space distribution of mean grain size (Figure 5.1.5A) exhibits a pattern congruent with that of the proportion of sand. The largest values (460μm) occur in the south-eastern area and the lowest values in the north and northwest sectors. Similar patterns were also observed for median, mode, ϕ90 and ϕ10 parameters (Table 5.2).

The analysis of textural parameters indicates that unit E is coarser and thicker across the southern part of Salgados basin whereas the majority of the finer-grained sediment occurs in the northern to north-western part (Figure 5.1.5 and 5.1.6). These features point to a seaward source of unit E and dispersion path from seaward (coarser and thicker) to landward (finer and thinner). According to Friedman (1961) positive skewness in medium to fine sand could be the result of unidirectional flow or the result of rapid deposition preventing the washing out of finer particles. In our study (Figure 5.1.6B) a skewness pattern compatible with the above mentioned interpretation can be observed. The combination of textural results and geometrical data also suggest a north-south trending area (possibly a palaeo-channel) in the middle of the basin as a preferred route through which sediment was transported inland. It is also worth noting that regardless the distance to this channel, the plot of textural attributes in Figures 5.1.5 and 5.1.6 trend obliquely to the elongation of the barrier. In cores where unit E has more than 0.03m thick its mean grain size is *ca.* 1.5 ϕ (*i.e.* 370μm), it varies considerably with location within the lowland. When comparison is established between these sediments and their possible sources, represented by the studied present-day analogues, the widest variation in mean grain size is detected in sand from unit E, ranging from 1.05 ϕ to 3.5 ϕ (Table 5.2). The distal nearshore samples (collected between 11m and 19m below msl) and materials from unit D are slightly finer grained, presenting an average mean diameter of *ca.* 2.50 ϕ and 2.20 ϕ, respectively. By contrast, the beach and dune sedimentary environments exhibit lower values (*i.e.* coarser sediments) of 0.75 ϕ and 1 ϕ, respectively.

In the few cores that allowed the study of the vertical variation of textural attributes within unit E, the mean grain size (also the percentage of sand and percentage of Ca carbonate) remain virtually invariant or slightly decreasing up unit (Table 5.2).

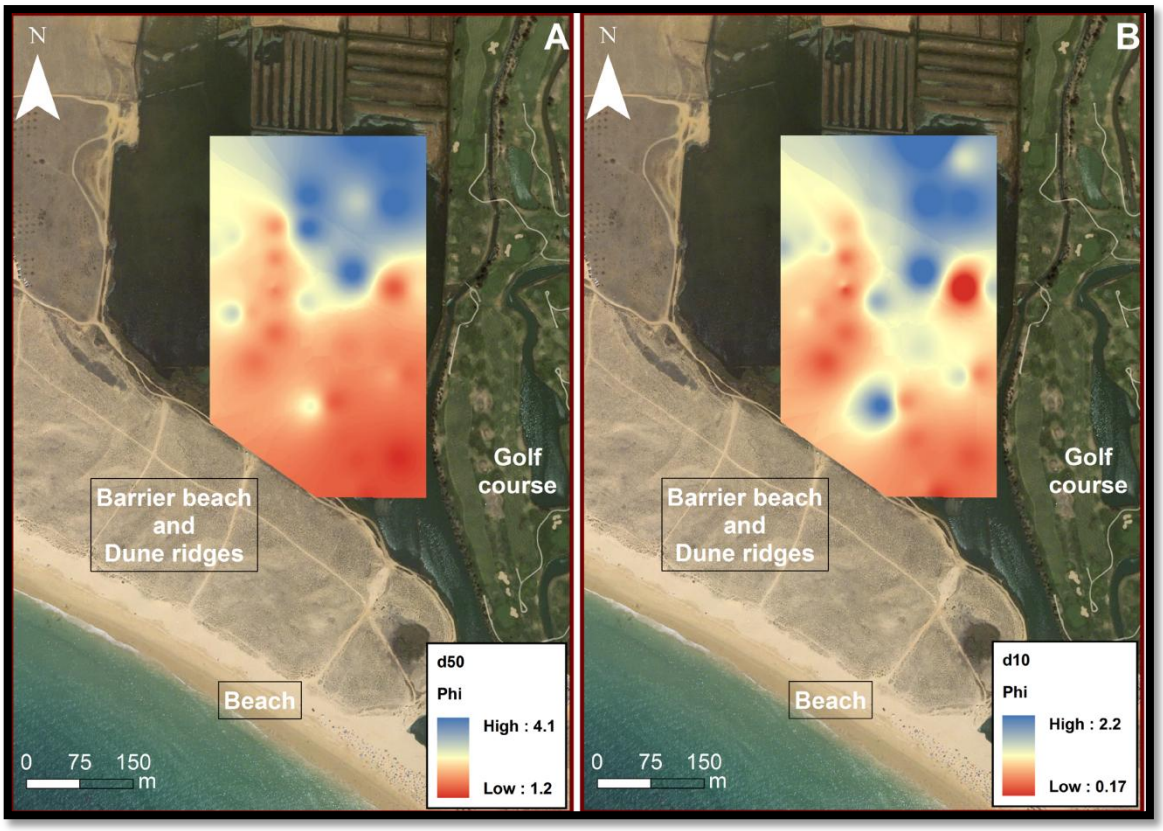

Figure 5.1.5 – A - Interpolated values of Unit E median grain size. B- Interpolated values of D10.

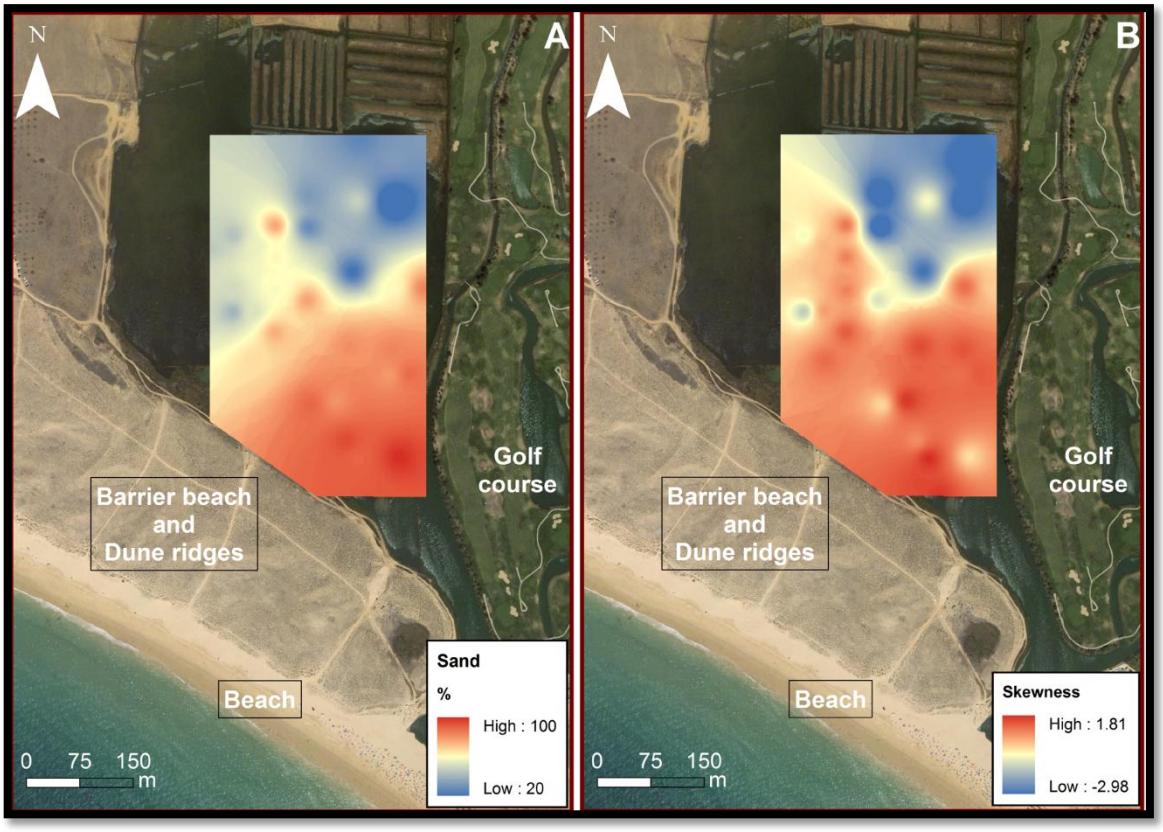

Figure 5.1.6 – A - Percentage of sand of unit E sediments. B – Simple skewness measure of unit E sediments.

Table 5.1.2 - Textural data from selected samples of Lagoa dos Salgados.

Sample	Sed. Env.	Depth (m)	1% Φ	10% Φ	90% Φ	Mean (MZ) Φ	Graphic Std Deviation (σ1)	Graphic Kurtosis (K_G)	Simple Sorting Measure (SSM)	Mode Φ	Median Φ
Praia_TdV	Beach	Sup	-0.30	0.45	1.81	1.15	0.53	1.04	0.89	1.25	1.16
Esc_Barra_Topo	Beach	Sup	-0.59	0.02	1.47	0.72	0.57	1.04	0.96	0.75	0.70
Esc_Barra_Base	Beach	Sup	-1.59	-0.60	1.44	0.47	0.79	0.99	1.31	0.75	0.50
Face_Praia	Beach	Sup	0.04	0.53	1.46	0.96	0.37	1.11	0.65	0.75	0.94
Barra	Beach	Sup	-1.98	0.01	1.71	0.88	0.73	1.14	1.29	1.25	0.90
Berma	Beach	Sup	-1.67	-0.82	1.65	0.35	0.96	0.98	1.56	0.25	0.29
Zona_Barra	Beach	Sup	-2.07	0.46	2.16	1.35	0.67	1.08	1.12	1.25	1.35
Crista_Duna	Dune	Sup	0.01	0.48	1.84	1.15	0.52	1.07	0.87	1.25	1.16
Duna2_Crista	Dune	Sup	-1.19	-0.08	1.58	0.77	0.65	1.07	1.11	0.75	0.78
Duna_R	Dune	Sup	-0.51	0.23	1.60	0.91	0.53	1.05	0.90	0.75	0.91
Duna_2R	Dune	Sup	-2.00	-0.25	1.39	0.63	0.64	1.18	1.14	0.75	0.62
Duna_2RR	Dune	Sup	-0.12	0.40	1.89	1.10	0.58	0.99	0.95	0.75	1.07
Duna	Dune	Sup	-1.30	0.01	1.85	0.96	0.77	1.09	1.34	1.25	1.01
Duna_F	Dune	Sup	0.00	0.52	2.01	1.22	0.57	0.98	0.94	1.25	1.18
Duna_2F	Dune	Sup	-1.31	0.19	1.71	0.95	0.60	1.07	1.02	1.25	0.98
D5	Dune	Sup	-0.71	0.22	1.93	1.08	0.66	0.97	1.08	1.25	1.09
SG_9m	Nearshore	Sup	-2.19	-1.52	2.48	0.72	1.43	1.29	2.47	1.25	0.88
SG_6m	Nearshore	Sup	0.34	1.32	2.89	2.18	0.61	1.00	1.00	2.25	2.26
SG_18_5	Nearshore	Sup	-2.30	-2.16	1.27	-0.84	1.36	0.74	2.11	-2.25	-1.17
SG_18	Nearshore	Sup	-2.03	-0.55	1.93	0.71	0.93	1.15	1.63	0.25	0.70
SG_15	Nearshore	Sup	-2.08	-0.80	1.31	0.37	0.83	1.06	1.40	0.75	0.44
SG_13_5m	Nearshore	Sup	-1.54	0.24	2.41	1.33	0.84	1.59	1.63	1.25	1.36
SG_12m	Nearshore	Sup	-1.69	-0.75	3.62	1.83	1.72	0.73	2.58	3.25	2.55
ArmP_16m	Nearshore	Sup				2.70					
ArmP_17.1m	Nearshore	Sup				2.41					
ArmP_17m	Nearshore	Sup				2.26					
ArmP_18m	Nearshore	Sup				2.91					
ArmP_13m	Nearshore	Sup				2.37					
ArmP_11m	Nearshore	Sup				2.84					
LV7	Unit E	0.40-0.41	0.62	1.15	4.06	2.46	1.16	1.01	1.02	1.75	2.05
LV7	Unit E	0.45-0.46	0.52	1.07	4.04	1.95	0.90	1.40	0.86	1.75	1.77

Sample	Sed. Env.	Depth (m)	1% ϕ	10% ϕ	90% ϕ	Mean (MZ) ϕ	Graphic Std Deviation (σ1)	Graphic Kurtosis (K_G)	Simple Sorting Measure (SSM)	Mode ϕ	Median ϕ
LV10	Unit E	0.46-0.47	-0.19	0.43	1.74	1.06	0.51	1.05	0.86	1.25	1.04
LV10	Unit E	0.56-0.57	-0.02	0.49	1.84	1.13	0.53	1.08	0.88	1.25	1.11
LV10	Unit E	0.64-0.65	-0.22	0.46	1.94	1.20	0.58	1.06	0.98	1.25	1.21
LV10	Unit E	0.80-0.81	0.13	0.62	1.85	1.22	0.48	1.02	0.79	1.25	1.21
LV10	Unit E	0.91-0.92	-0.44	0.44	1.85	1.10	0.56	1.18	0.99	1.25	1.06
7	Unit E	0.46-0.48	0.45	0.93	4.13	2.44	1.25	0.54	1.71	4.25	2.10
9	Unit E	0.43-0.77	-0.05	0.55	2.43	1.38	0.91	1.62	1.85	1.25	1.32
11	Unit E	0.445-0.70	0.16	0.77	2.94	1.61	0.89	1.49	1.73	1.25	1.53
13	Unit E	0.36-0.83	0.15	0.71	2.74	1.47	0.86	1.74	1.77	1.25	1.39
14	Storm ?	0.20-0.28	0.07	0.72	2.01	1.33	0.51	1.22	0.89	1.25	1.31
14	Unit E	0.40-0.82	0.08	0.68	2.17	1.40	0.58	1.04	0.97	1.25	1.38
15	Unit E	0.45-0.73	0.06	0.68	2.65	1.57	0.82	1.29	1.50	1.25	1.52
17	Unit E	0.39-0.665	0.31	0.78	4.05	2.14	1.30	1.28	1.76	1.25	1.50
20	Unit E	0.43-0.53	0.70	1.17	4.05	2.12	0.97	1.43	1.56	1.75	1.80
22	Unit E	0.57-0.58	1.13	1.80	4.20	3.42	0.94	0.68	1.37	4.25	4.05
24	Unit E	0.50-0.51	1.16	1.75	4.16	3.02	0.95	0.58	1.34	4.25	3.02
26	Unit E	0.495-0.50	1.56	2.20	4.19	3.53	0.79	0.67	1.14	4.25	4.03
31	Unit E	0.49-0.52	0.50	1.17	4.18	3.22	1.17	0.61	1.68	4.25	4.02
33	Unit E	0.49-0.53	0.49	1.68	4.23	3.52	0.96	8.61	1.57	4.25	4.09
35	Unit E	0.47-0.55	-0.19	0.17	4.12	1.99	1.56	0.52	2.11	4.25	1.49
37	Unit E	0.40-0.56	0.68	1.19	4.06	2.44	1.14	1.10	1.56	1.75	1.97
39	Unit E	0.42-0.59	0.05	0.75	3.45	1.64	0.90	1.61	1.78	1.75	1.59
41	Unit E	0.55-0.575	-0.26	1.28	4.04	2.53	1.01	1.18	1.59	2.25	2.41
52	Unit E	0.24-0.57	0.85	1.68	3.91	2.68	0.79	1.12	1.34	2.75	2.66
59	Unit E	0.36-0.42	-0.97	1.39	4.07	2.89	1.04	1.09	1.64	2.75	2.81
64	Unit E	0.44-0.455	0.35	1.18	4.19	3.24	1.17	0.64	1.70	4.25	4.03
66	Unit E	0.44-0.46	0.59	1.30	4.18	3.25	1.13	0.62	1.64	4.25	4.02
89	Unit E	0.43-0.45	0.68	1.16	4.14	2.61	1.17	0.56	1.63	4.25	2.34
91	Unit E	0.39-0.44	0.38	0.97	4.14	2.52	1.24	0.56	1.71	4.25	2.26
93	Unit E	0.415-0.445	0.19	0.78	4.15	2.37	1.34	0.54	1.82	4.25	2.03
95	Unit E	0.43-0.44	0.00	0.60	4.11	2.18	1.39	0.51	1.89	4.25	1.68

Sample	Sed. Env.	Depth (m)	1% ϕ	10% ϕ	90% ϕ	Mean (MZ) ϕ	Graphic Std Deviation (σ1)	Graphic Kurtosis (K_G)	Simple Sorting Measure (SSM)	Mode ϕ	Median ϕ
99	Unit E	0.44-0.48	0.23	0.67	4.08	2.16	1.35	1.04	1.83	1.75	1.63
101	Unit E	0.45-0.47	-0.04	0.59	4.13	2.22	1.41	0.52	1.92	4.25	1.77
103	Unit E	0.40-0.43	0.17	0.70	4.12	2.27	1.36	0.52	1.85	4.25	1.84
106	Unit E	0.45-0.465	0.43	0.89	4.07	2.32	1.26	0.98	1.71	1.75	1.88
115	Unit E	0.37-0.40	0.88	1.32	4.16	2.79	1.13	0.57	1.59	4.25	2.71
137	Unit E	0.42-0.45	0.34	0.95	4.15	2.58	1.25	0.56	1.73	4.25	2.41
139	Unit E	0.41-0.44	0.37	0.99	4.17	2.80	1.23	0.58	1.73	4.25	2.96
141	Unit E	0.46-0.465	0.59	1.18	4.16	2.77	1.17	0.57	1.65	4.25	2.74
11	Unit D	0.76-0.83				1.65					
52	Unit D	0.78-0.85				2.19					
56	Unit D	0.96-1.30				2.54					
59	Unit D	0.42-0.45				2.31					

5.1.3. Morphoscopic features

Morphoscopic analyses were conducted in a group of samples (unit E, dune, beach and nearshore). Sediment obtained from core SG14_(0.20-0.28) and possibly corresponding to a storm deposit was also studied. The samples were divided into three groups, each group corresponding to contrasting depositional environments: Unit E and sample SG14_(0.20-0.28), representing high-energy single events; dune and beach; nearshore. Samples from Unit E were observed: as a profile (with increasing distance from the coast) SG14_(0.40-0.82)-SG20-SG22-SG26; with samples within unit from 2 cores: LV7 and LV10; and a possible storm deposit sample SG14_(0.20-0.28). Dune samples also present a profile roughly corresponding to an outline from the coast-inland (with one dune crest sample – SG_Duna2_Crista). Nearshore samples were collected at different depths below msl offshore the Armação de Pêra bay. The basic morphoscopic data for each group is presented in the same order: composition (Figures 5.1.7, 5.1.10 and 5.1.13); roundness (Figures 5.1.8, 5.1.11 and 5.1.14); sphericity (Figures 5.1.9, 5.1.12 and 5.1.15). These results are complement by other morphoscopic data presented as histograms in: Figure 5.1.16 [Unit E and SG14_(0.20-0.28)], Figure 5.1.17 and Figure 5.1.18 (beach and dune) and Figure 5.1.19 (nearshore). In Figure 5.1.7 it is possible to observe the compositional characteristics of Unit E deposits and sample SG14_(0.20-0.28). The percentage of quartz grains, lithic material and bioclasts is shown. In terms of the percentage of quartz grains, Unit E samples are typically in the 60-75% range. This is in contrast with sample SG14_(0.20-0.28) that presents a value above 80% of quartz grains. Moreover, in terms of the percentage of lithic material it can be observed that all samples present values in the order of 10-15% with

the exception of LV10_(0.80-0.81), LV10_(0.90-0.91) and SG26 that present values of 6%, 18% and 18% respectively. In what concerns the percentage of bioclasts, it was observed that all samples from Unit E present values between 15% and 30%, while sample SG14_(0.20-0.28) presents a considerably lower value(5%).

In terms of roundness for the same group of samples (Figure 5.1.8) it is possible to perceive that the highest values for well-rounded and rounded grains (app. 50%) were detected in samples LV10_(0.46-0.47) and LV10_(0.90-0.91) respectively top and base of Unit E. Moreover, in core LV7 the base of unit E presents higher percentage of well-rounded and rounded grains when compared with the top of the unit. In all other samples values for well-rounded and rounded grains are in the 25%-40% range. In what concerns very angular and angular grains it was possible to visualize that most samples present values in the order of 40%-50%, the exception being cores LV7 and LV10. Furthermore, in core LV10 it was possible to establish a roughly decreasing upward trend on the presence of very angular and angular grains within Unit E (values ranging between 15 and 30%) whereas on core LV7 the base of the deposits presented values of 35% for very angular and angular grains and the top of the deposit presented higher values (44%).

Figure 5.1.9 presents the shape characteristics for the same group of samples. Spherical grains were observed in 20%-35% of the samples and the lowest sphericity values were detected in samples SG20 and LV7_(0.40-0.41). In what concerns prismatic and sub-prismatic shapes it was perceived that all samples typically presented values in the range 30%-40% with the exception of sample LV10_(0.46-0.47) that presented a value of 21% . The lowest value of spherical grains was observed in sample 14_(0.20-0.28) with 15%. In terms of discoidal and sub-discoidal grains no trend was possible to observe because all values were detected within the 35%-50% without any discernible peculiarity

Figure 5.1.10 presents the dune and beach samples compositional characteristics. All samples present quartz grains in the range of 50% to 60%. Regarding the percentage of lithic material it was observed that sample Dune_2RR (farther inland) presented the highest value, with 26% of lithic sediment while all the other samples presented lithics between 14% (*i.e.* Face_Praia – beach face) and 20% (*e.g.* Duna - dune). Bioclasts are present in all samples (25%-30%) with the exception of sample Duna_2RR with 16% of bioclasts. A slightly inland decreasing trend of the percentage of bioclasts was detected.

In terms of roundness, in the dune and beach samples from Lagoa dos Salgados (Figure 5.1.11), the well-rounded and rounded grains were present in the range 25%-50% in the dune samples (with a slight increasing inland trend) while the beach samples present values between 17% (*i.e.* Praia_TdV) and 45% (*e.g.* Berma). In what concerns very angular and angular grains, dune samples presented values ranging from 15% (*i.e.* Duna_2RR) to 34 % (*i.e.* Duna) whereas beach samples presented higher values ranging from 30% to 60%.

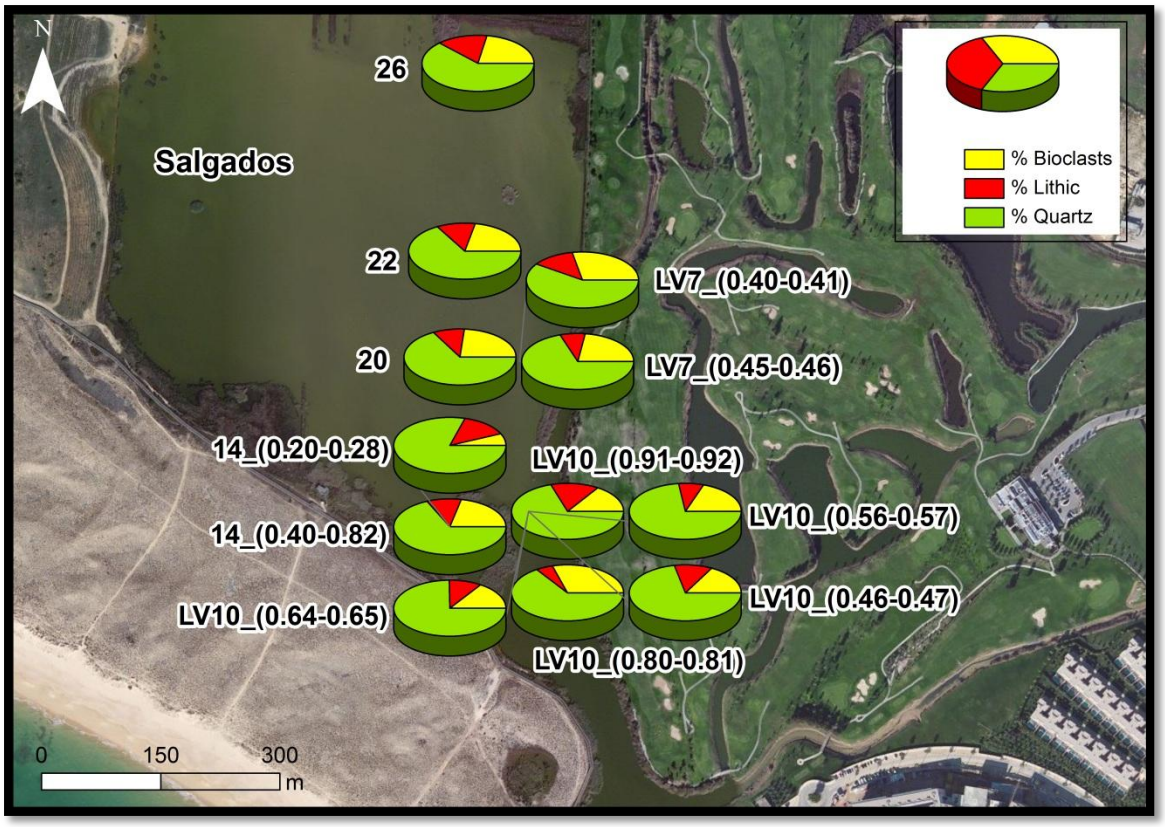

Figure 5.1.7 - Compositional characteristics of sample from unit E and sample 14_(0.20-0.28) from Lagoa dos Salgados, based in morphoscopic observation.

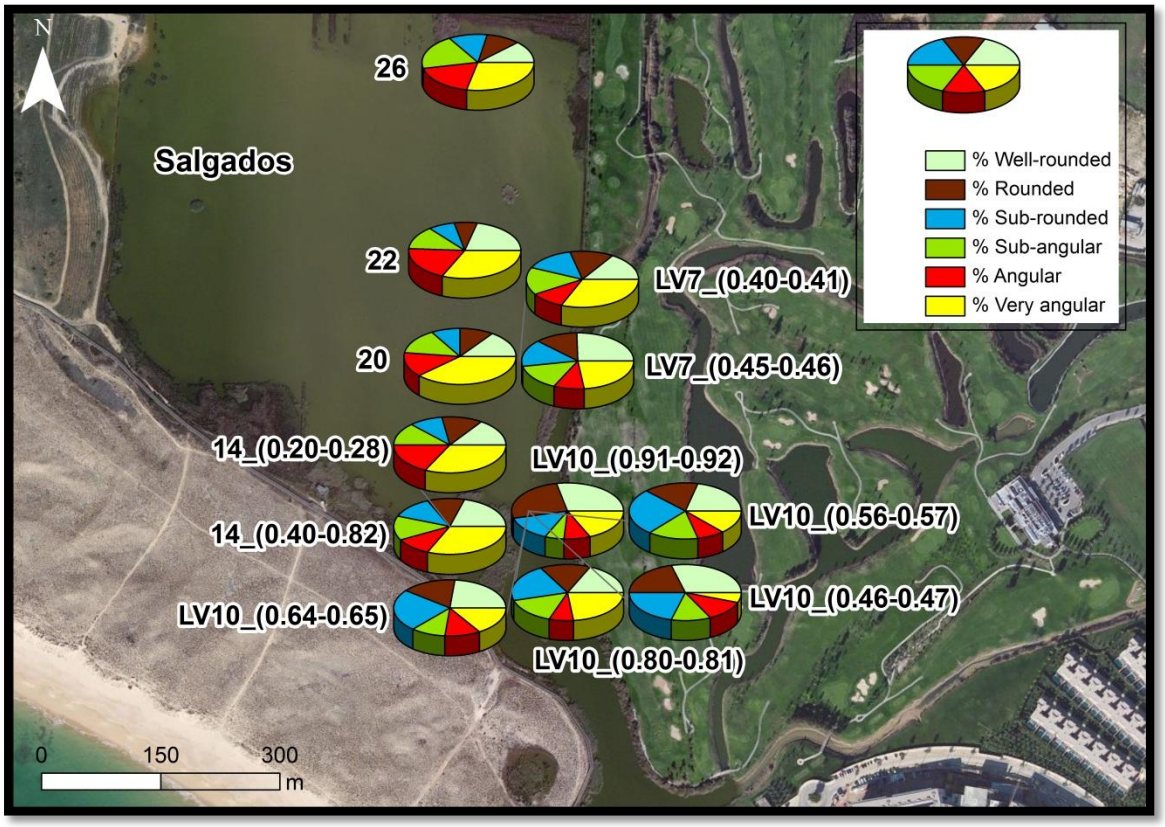

Figure 5.1.8 - Roundness classification of quartz grains from unit E and sample 14_(0.20-0.28) from Lagoa dos Salgados, based in morphoscopic analysis.

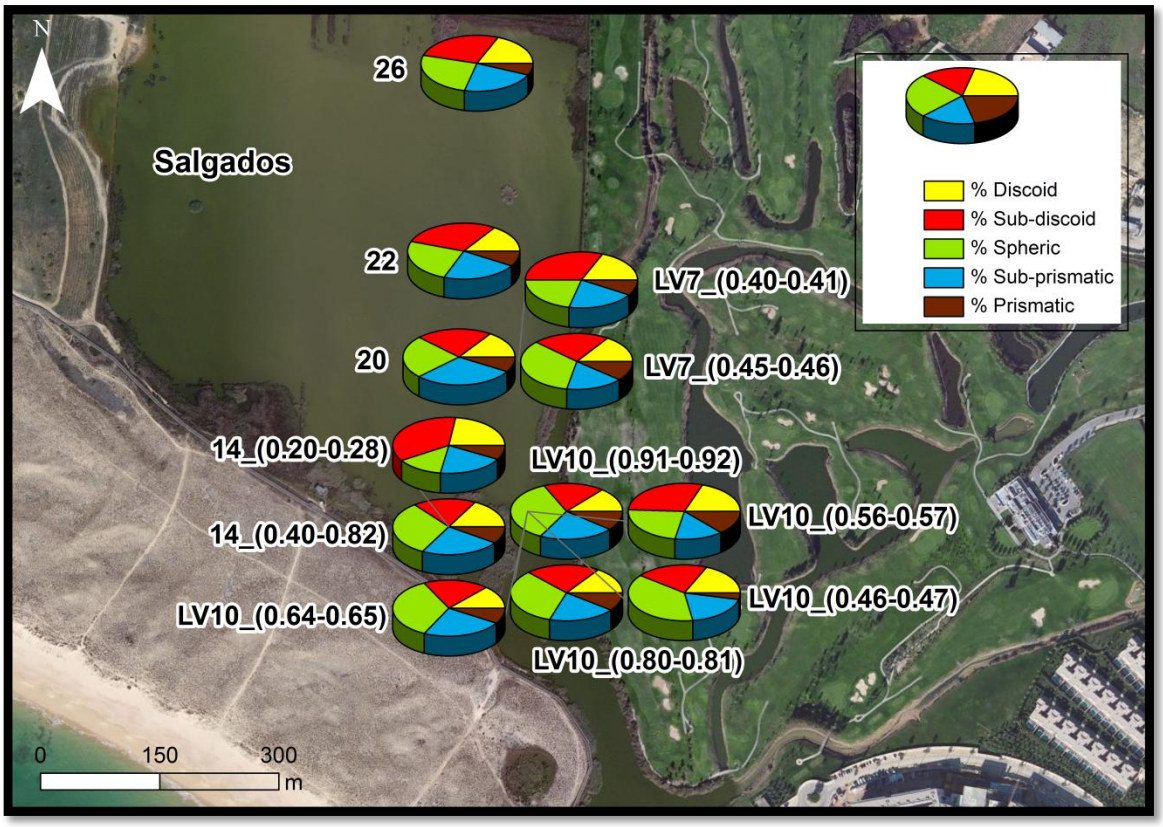

Figure 5.1.9 – Lagoa dos Salgados unit E and sample 14_(0.20-0.28) shape characteristics based in morphoscopic observation.

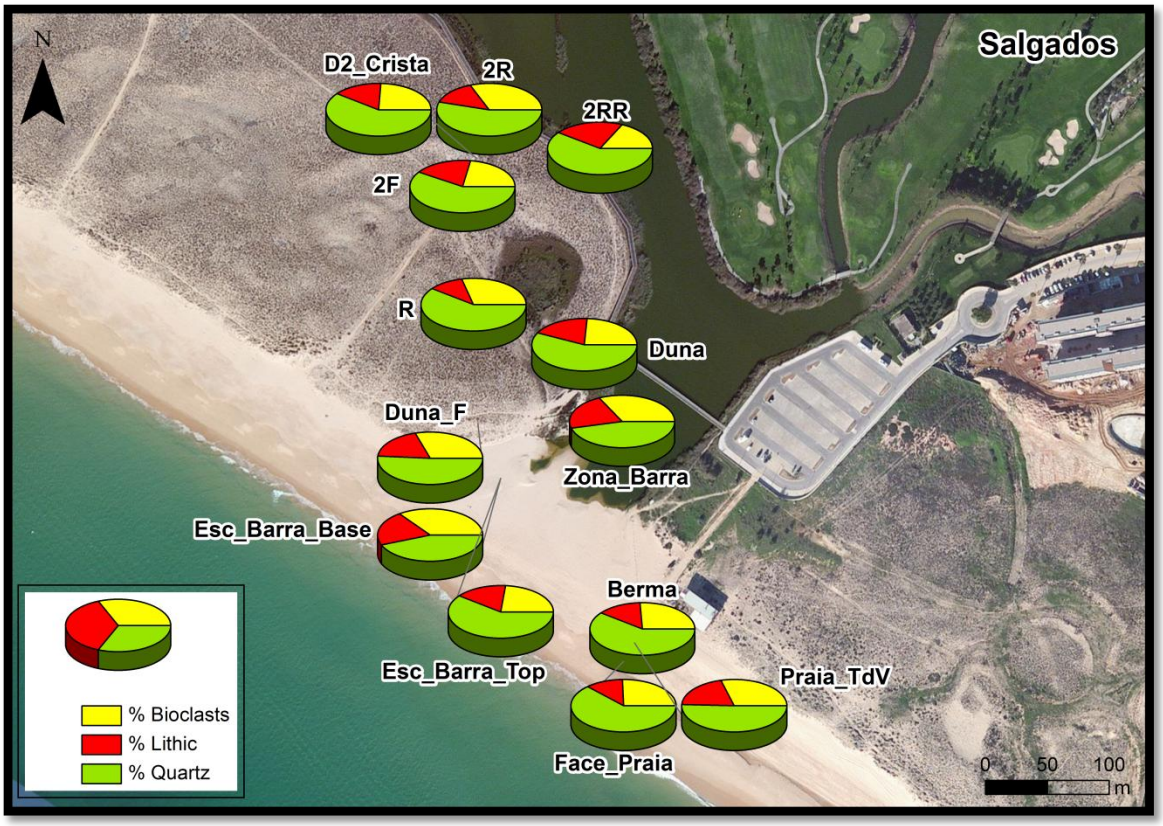

Figure 5.1.10 – Dune and beach samples (Lagoa dos Salgados) compositional characteristics based in morphoscopic observation.

Figure 5.1.12 presents the data obtained by analysing the shape of dune and beach samples from Lagoa dos Salgados. Spherical grains were observed in higher percentage in dune samples (20%-30%) than in beach samples (<20%) although sample Berma presented 29% of spherical grains. This result, coupled with higher proportion of spherical grains in the dune samples farther inland might suggest an increasing inland trend. In terms of discoidal and sub-discoidal grains it was observed that beach samples typically presented values of *ca.* 55% (except Berma with 40%) for these types of grain shape. By contrast, dune samples presented values that ranged from 28% (Duna_2F) to 54% (Duna_F). No clear spatial trend was identified. Regarding prismatic and sub-prismatic grains all samples presented values between 20% and 30% with no perceptible pattern.

Figure 5.1.13 presents the compositional features of the nearshore samples collected within the Salgados/Armação de Pêra bay. In compositional terms the nearshore samples are in contrast with other samples observed in Lagoa dos Salgados. In fact, they present very high percentages of bioclasts ranging from 50% to 70%, with the exception of ArmP_19m (sample farther offshore) with 34% of bioclasts. In what concerns lithic material all samples presented similar values within the 15%-30% interval. In none of the two above mentioned features a spatial trend was identified. Regarding the quartz percentage it was observed that the samples with higher percentage of quartz grains were ArmP_11m and ArmP_19m (which are the samples closest and farthest located from the coastline) with 36% and 47% respectively. All the other samples presented values between 10% and 25%.

The study of roundness of the nearshore samples (Figure 5.1.14) yieldied values for very angular and angular grains within the 20%-30% range with no observed spatial trend. The only two exceptions were samples ArmP_19 and ArmP_17.1 that present values of 16% and nil. Well-rounded and rounded grains presented percentage between 40% and 60% with no clear trend detectable.

The spherical character of the nearshore samples was measured (Figure 5.1.15) and it was possible to observe that all samples presented *ca.* 50% of spherical grains with the exception of sample ArmP_13m that presented a value of 35% of spherical quartz grains. Discoidal and sub-discoidal grains presented its higher percentage in sample ArmP_13m with 43% and its lower percentage in sample ArmP_17.1m with 21%. All other samples presented values between 30% and 40%. Prismatic and sub-prismatic grains presented results of *ca.* 20% with exceptions of samples ArmP_16m, ArmP_18m and ArmP_19m with values of 10%, 13% and 15% respectively. In terms of sphericity no spatial trend was established.

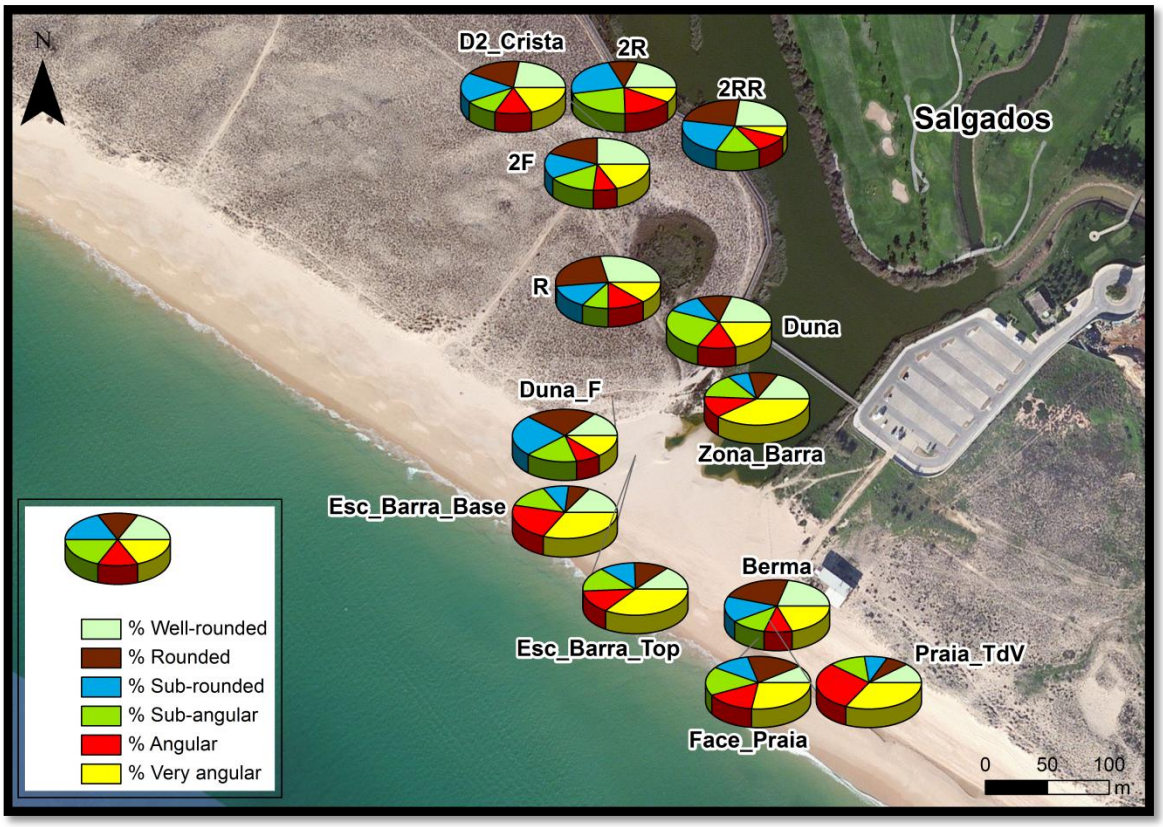

Figure 5.1.11 – Dune and beach samples from Lagoa dos Salgados and their roundness classification based in morphoscopic observation.

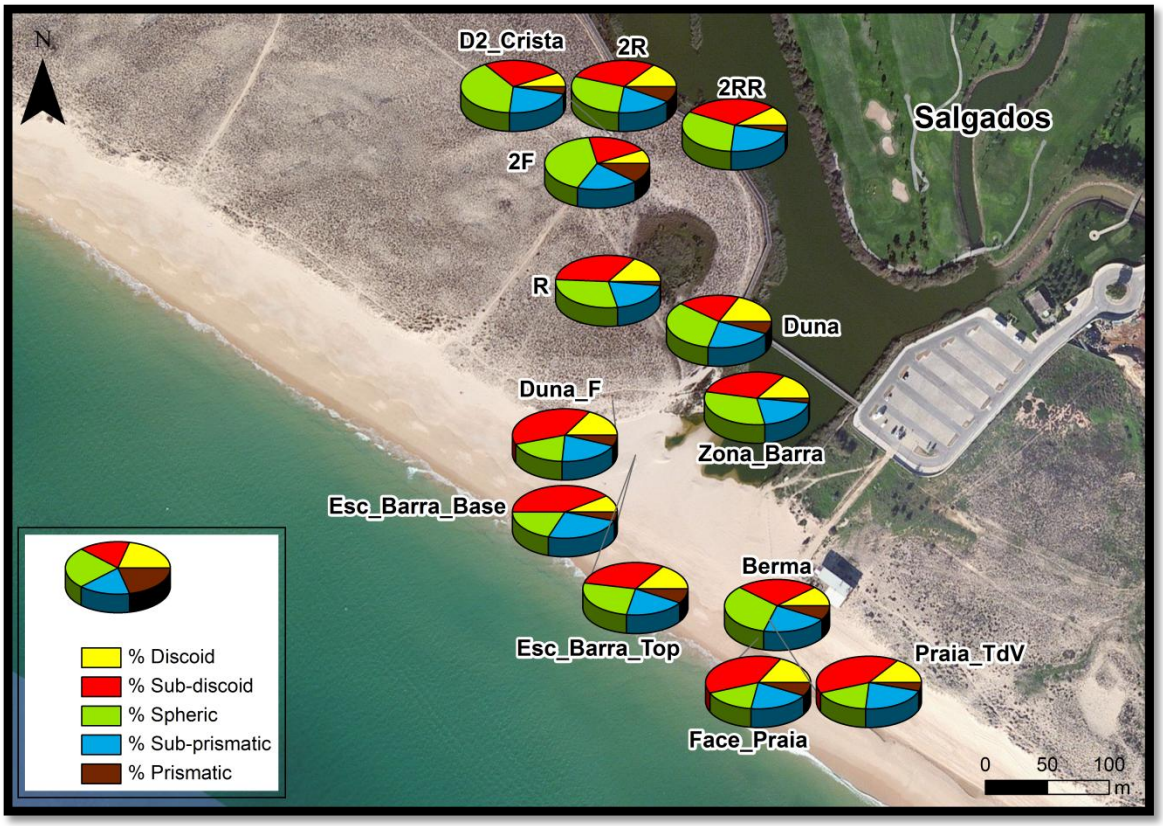

Figure 5.1.12 –Dune and beach samples (Lagoa dos Salgados) shape characteristics based in morphoscopic observation.

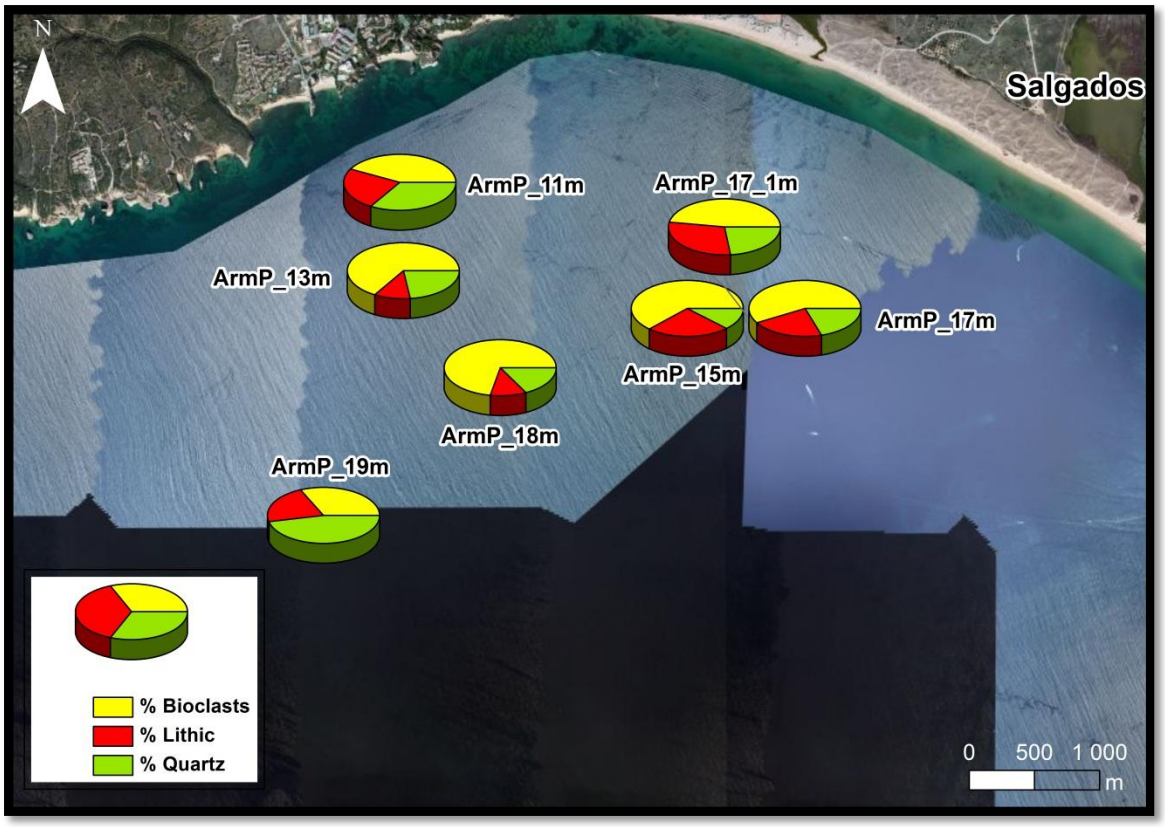

Figure 5.1.13 – Nearshore samples from Lagoa dos Salgados and their compositional aspects based in morphoscopic observation.

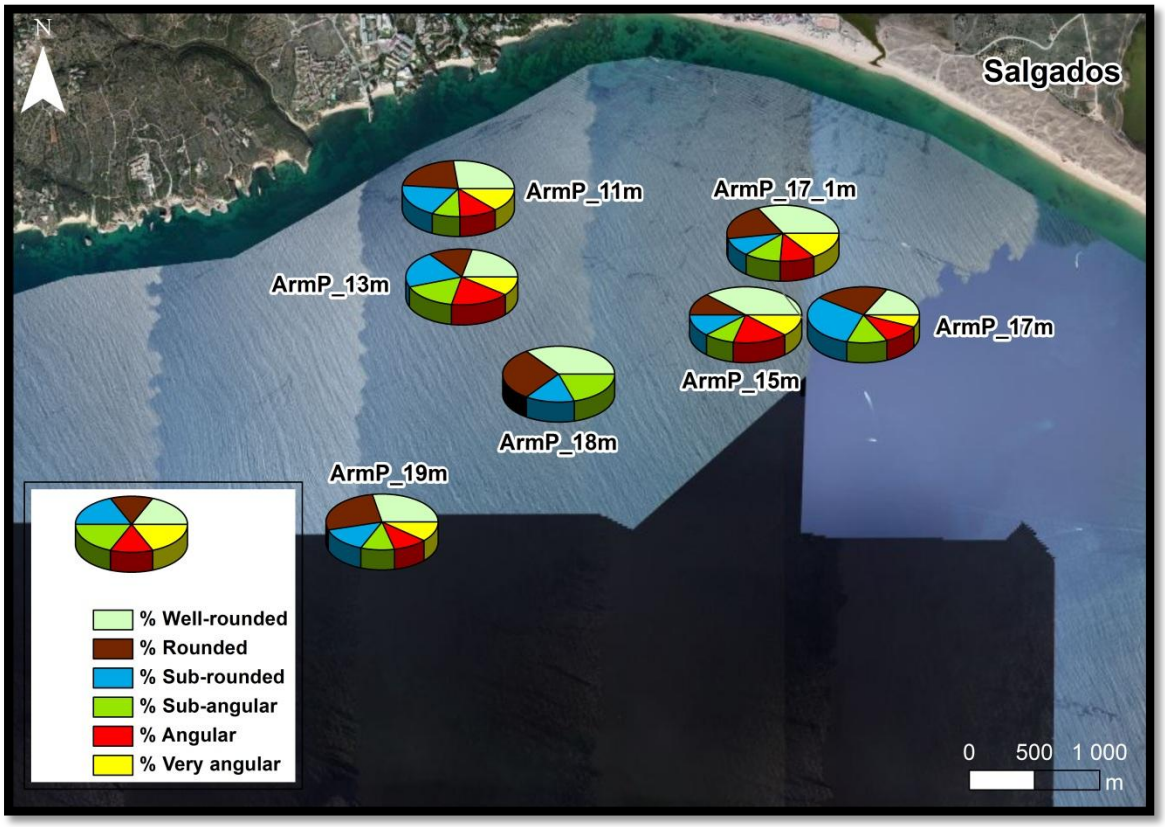

Figure 5.1.14 – Nearshore (Lagoa dos Salgados) samples roundness characteristics based in morphoscopic observation.

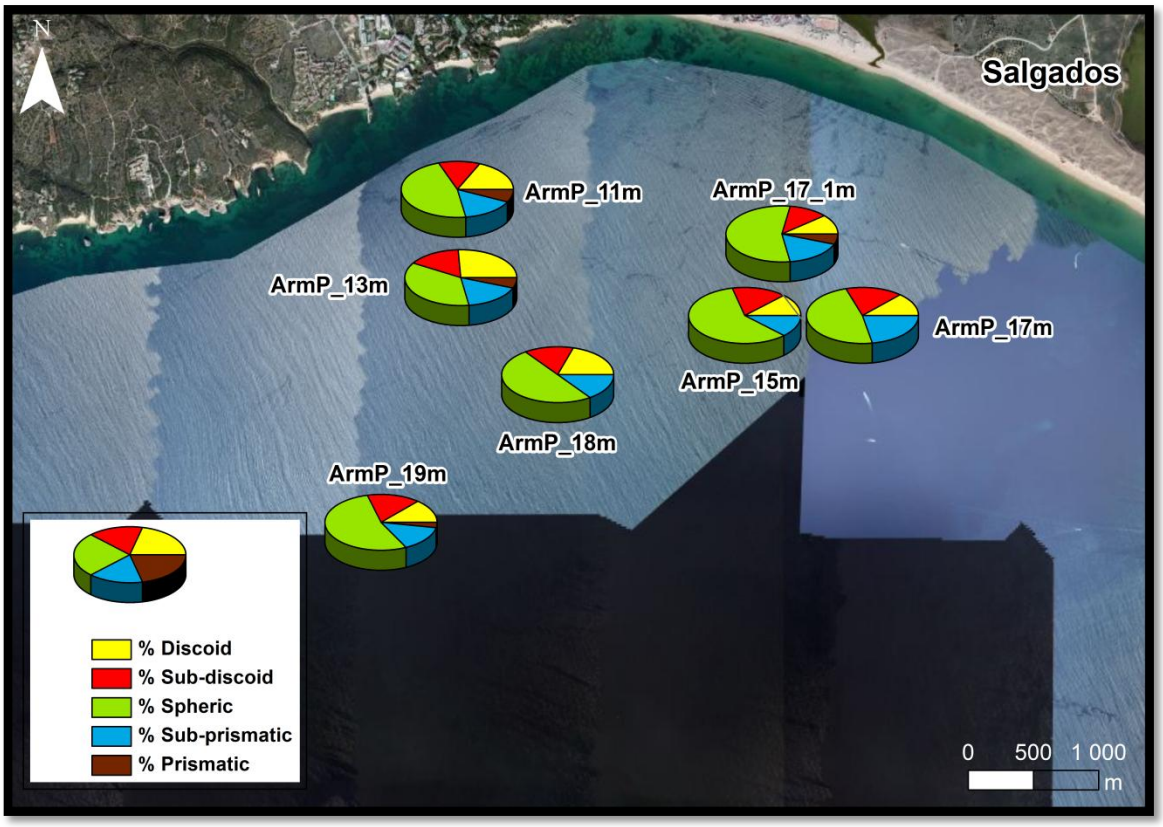

Figure 5.1.15 – Nearshore (Lagoa dos Salgados) samples shape characteristics based in morphoscopic observation.

Comparison of morphoscopic characteristics of grains from different sedimentary environments and lithostratigraphic units suggests that nearshore samples typically present more than 45% of well-rounded and rounded grains whereas, dunes present values of *ca.* 40%, beach samples exhibit values below 30%, unit E samples the widest range of values, varying from 20% to 50%, and finally sample 14_(0.20-0.28) presented a value of 25%. In what concerns very angular and angular grains, dune samples show values under 30% and beach samples above 50%; unit E presented about 40% (exception core LV10), nearshore samples also presented values of *ca.* 40% and sample 14_(0.20-0.28) a value of 45%. Regarding spherical grains it was observed that the highest percentage of these grains occurs in the nearshore samples (app. 50%). In contrast, the lowest values were observed in sample 14_(0.20-0.28) with 15% and in beach samples (*ca.* 20%). Unit E exhibited values of 20%-30%, whereas dunes presented higher values, varying between 30 and 40%.

5.1.4. Microtextural features

Microtextural features were analysed and quantified in samples from Lagoa dos Salgados. Figure 5.1.16 exhibits SEM images of quartz grains from Lagoa dos Salgados different sedimentary environments and from Unit E. In Annex 2 an atlas of quartz grain microtextural features is presented.

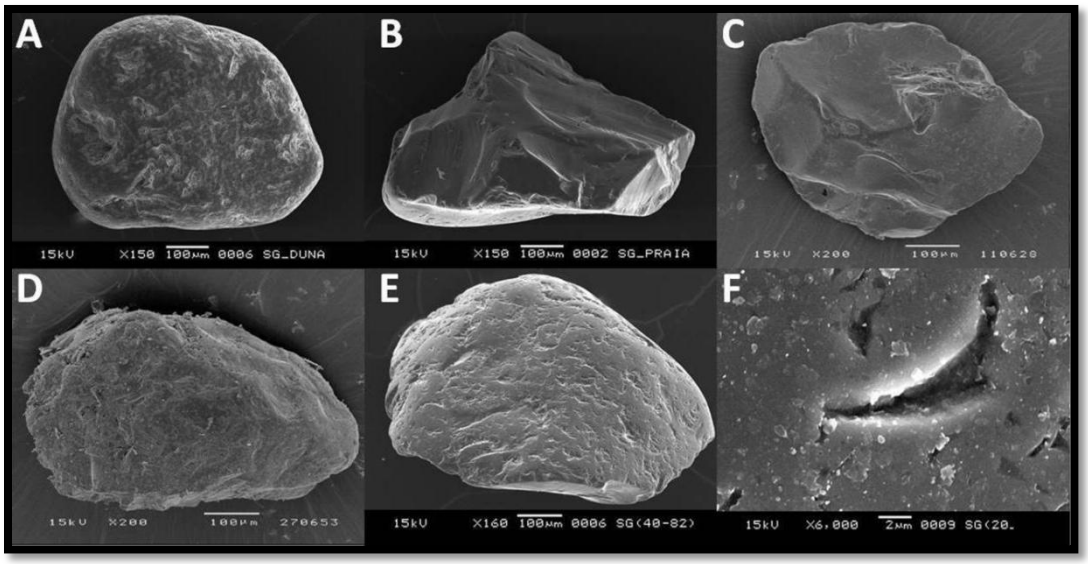

Figure 5.1.16 – SEM images of quartz grains from the Lagoa dos Salgados. A- Dune; B- Beach; C- Proximal nearshore; D- Distal nearshore; E- unit E, F- detail of percussion marks (approximately 12 microns in length) imprinted on the surface of a grain from unit E.

Figures 5.1.17 [samples from unit E and sample SG14_(0.20-0.28)], 5.1.18 (samples from dune and beach) and 5.1.19 (samples nearshore) and Table 5.1.3 (all samples) present the results obtained after microtextural classification of quartz grains collected in Lagoa dos Salgados. Furthermore, to verify grain-size influence (all samples were analysed in the 1-3 Φ fraction) two samples, one finer (*i.e.* SG20m) and another coarser (*i.e.* SG20M) than the fraction analysed (SG20) were also classified to establish if size conditioned the features observed and their frequency. In fact, if we compare the three samples from core SG20 we conclude that angularity and fresh surfaces are substantially higher in the finer fraction, while percussion marks and dissolution are higher in the coarser fraction. The sample that presented more balanced classificatory results was SG20 (*i.e.* 1-3 Φ fraction) thus supporting the choice of grain size to analyse.

Sample SG14_(0.20-0.28) can be compared to all samples from unit E presenting higher angularity, fresh surfaces (with the exception of SG26), the lowest expression of dissolution features in this group of samples and relevant presence of percussion marks [only comparable with SG14_(0.40-0.82)]. The two samples from LV7 did not indicate any pattern or trend when comparing base and top of unit E. In fact, both samples presented very similar values in all microtextural features with the only exception of adhering particles (higher values for the sample collected at the base of unit E). On the other hand, samples from core

LV10 revealed some peculiarities. In this case, it was possible to observe a decreasing trend in terms of angularity and fresh surfaces towards the top, although the highest values were observed in sample LV10_(0.80-0.81) with 2.921 and 3.134, respectively. However it is important to stress that the variation between all samples from this core was minor, between 1.892 and 2.921. In what concerns dissolution and adhering particles a mirror image of the described above can be observed, with the lowest value (*i.e.* 1.600 and 1.815, respectively) observed in sample LV10_(0.80-0.81). A foggy decreasing upward trend can be detected [with exception of sample LV10_(0.80-0.81)] in dissolution and adhering particles, as well as in percussion marks.

No spatial trend is readily detectable, although percussion marks tend to decrease inland, whereas fresh surfaces seem very slightly increase with distance from the coast (except sample SG20).

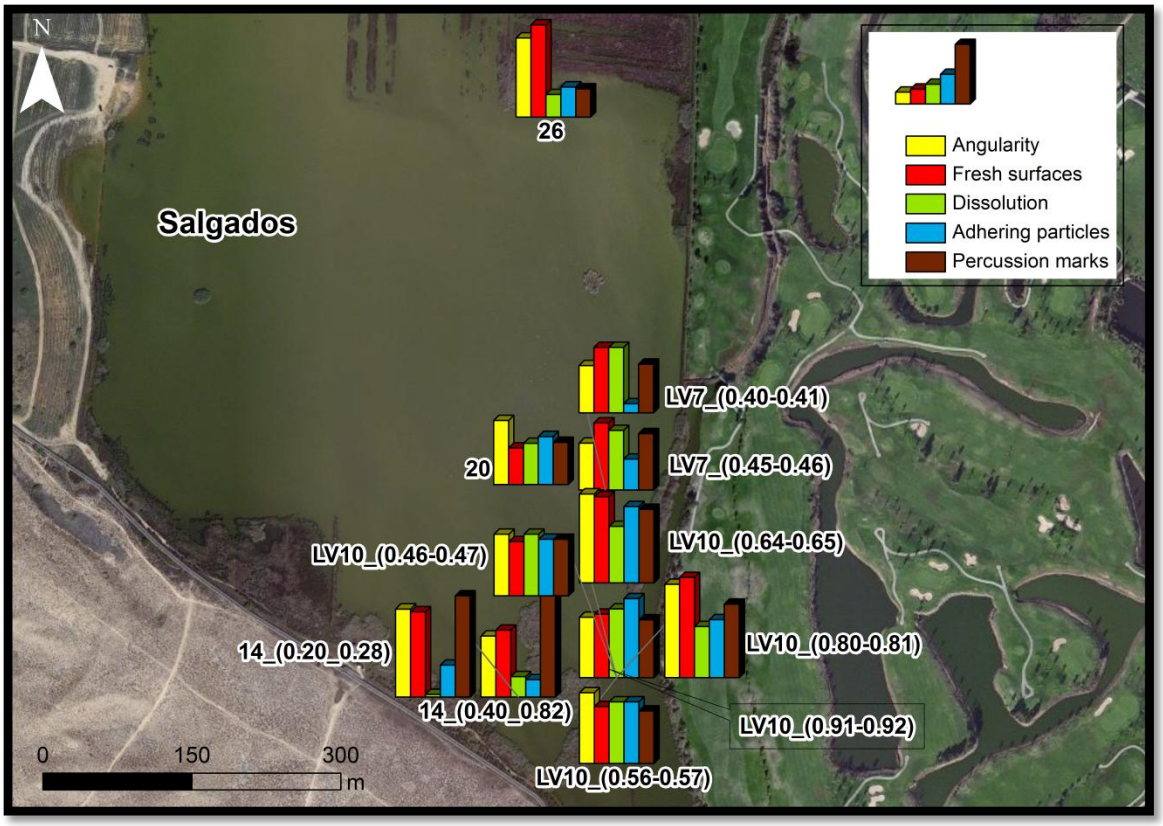

Figure 5.1.17 – Microtextural results and their spatial distribution in fraction 1-3 Φ of samples from unit E and 14_(0.20-0.28) from Lagoa dos Salgados.

Beach and dune samples revealed differences in microtextural attribute (Figure 5.1.18). Dunes presented values of angularity between 2 and 3, with higher values for dune crests (*i.e.* Crista_Duna and Duna2_Crista) and for the more recent dune ridge (DunaF). In the dune samples, fresh surfaces exhibit values varying from 1.25 to 2, with the exception of the higher value (*i.e.* 2.5) of one dune crest (*i.e.* Duna2_Crista) and the lower value (*i.e.* 0.75) for sample Duna_2RR (farther inland). Dissolution values for

the dune samples from Lagoa dos Salgados varied within the range 1.75 (*i.e.* Duna_R) and 3.3 (*i.e.* Duna). As regards to adhering particles the dune samples showed a narrower range (between 3 and 3.5) with two exceptions presenting values of 2.66 and 2.63 (Duna_R and Duna_F, respectively). In what concerns, percussion marks classification in dune samples, it was possible to determine that the values attributed to the samples varied between 1.0 (Duna2_Crista) and 2.36 (Duna_2F). In none of the microtextural features analysed a clear pattern or trend emerged in terms of distribution of values.

On the other hand, beach samples exhibited angularity values >2.75 with the exception of sample Praia_TdV (*i.e.* 1.80). It is also interesting to note that the sample corresponding to the beach berm (*i.e.* Berma) presented a lower value (when compared with Face_Praia and Barra). In terms of fresh surfaces observed in grains from the beach, the berm (*i.e.* Berma) presented the lower value (*i.e.* 2.0) whereas the other samples presented values above 2.6. In what regards dissolution features observed in the beach samples they occur in extremely low values, with the lowest value (0.33) observed in the beach face sample (*i.e.* Face_Praia) and the highest value (1.58) detected in the beach berm (*i.e.* Berma) sample. Adhering particles revealed the most striking difference between beach samples, with the berm (*i.e.* Berma) presenting a value of 2.41 whereas all the other samples exhibited values <0.66. Percussion marks were present especially in the beach face sample (*i.e.* Face_Praia) with a value of 2.75, while the other samples presented values within the interval 1.07-1.80.

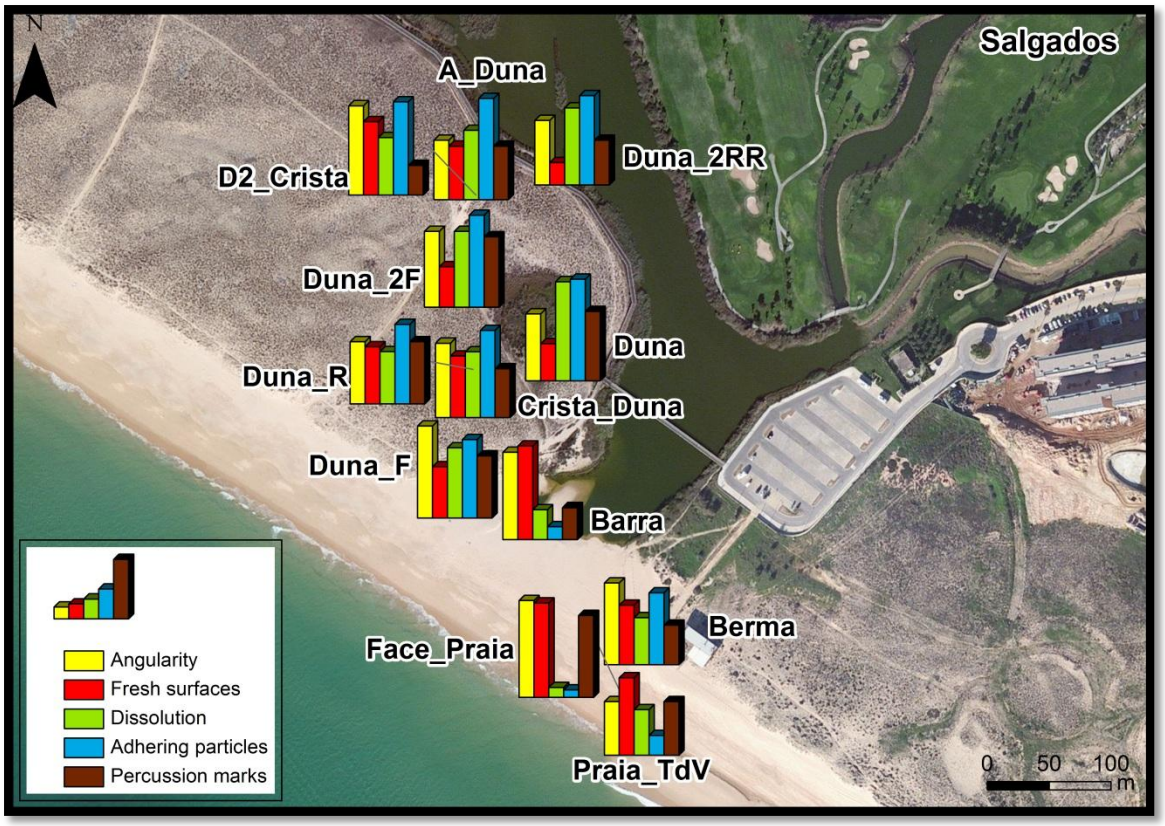

Figure 5.1.18 - – Microtextural results and their spatial distribution in samples from the dune and beach from Lagoa dos Salgados.

Nearshore samples can be divided in two groups: one composed of samples collected to the west of Lagoa dos Salgados inlet (identified with the ArmP acronym) and another group composed by samples collected immediately to the south of Lagoa dos Salgados (identified with the SG acronym). It was possible to observe that, in both groups, trends and spatial patterns are present (Figure 5.1.19). For instance, angularity and fresh surfaces decrease with increasing distance from coastline and depth. For example, ArmP samples range from 1.21 (*i.e.* ArmP_19m) to 3.0 (*i.e.* ArmP_11m) for angularity and from 0.21 to 1.81 for fresh surfaces in the exact same samples. On the other hand, adhering particles increase with distance to coastline, varying from 2.45 (*i.e.* SG-6m sample) to 3.80 (*i.e.* SG-18m sample). Regarding dissolution marks, a trend could only be recognized in one group of samples that presented decreasing values toward the coastal fringe, values varying from 1.70 (*i.e.* SG-6m sample) to 3.93 (*i.e.* SG-18m sample). Percussion marks did not present a clear spatial distribution, exhibiting values of 0.01 for sample SG-18m and values of 2.0 for sample SG-9m and SG-18m.

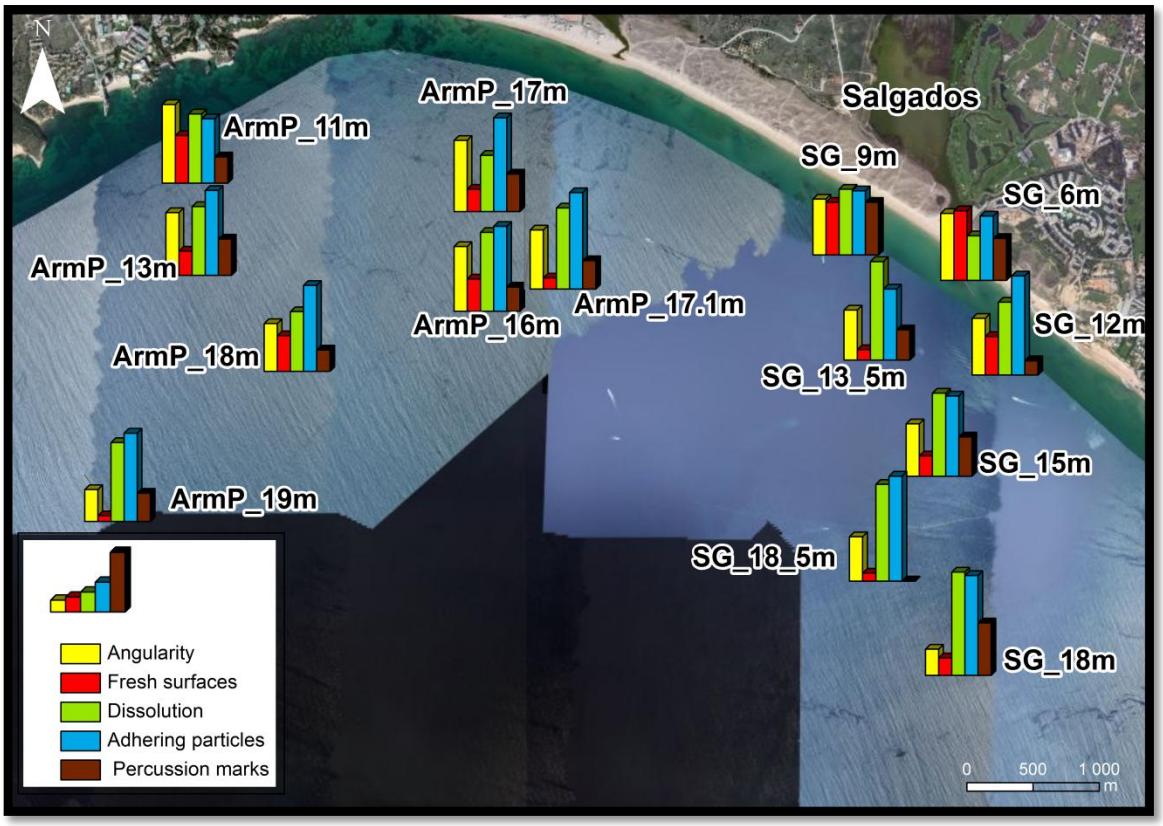

Figure 5.1.19 - – Microtextural results and their spatial distribution in the nearshore samples from Lagoa dos Salgados.

A summary characterization of microtextural features for every sedimentary environment studied, for unit E (tsunami samples) and for sample SG14_(0.20-0.28) (possible storm?) reveals that:

- Beach grains presented the highest values for fresh surfaces and strong presence of percussion marks. Dissolution and adhering particles are almost absent.
- Dune grains revealed a well balance representation of all the microtextural features.
- Nearshore samples presented high values of dissolution and adhering particles and moderate presence of percussion marks and fresh surfaces.
- Storm grains present many similarities with beach samples and unit E samples and can only be differentiated by the lower value of adhering particles.
- Tsunami-deposited grains (Unit E) presented the highest values of percussion marks and fresh surfaces (thus suggesting strong hydrodynamic processes before deposition). Tsunami grains can also be characterized by presenting the widest range of values observed in all the microtextural features.

Table 5.1.3 - Microtextural results obtained with the Lagoa dos Salgados samples.

Sample	Depth (m)	Sed. Env.	Number of grains	Angularity	Fresh surfaces	Dissolution	Adhering particles	Percussion marks
14	0.20_0.28	Storm (?)	12	2.750	2.667	0.083	1.000	3.167
14	0.40_0.82	Unit E	11	1.909	2.091	0.636	0.545	3.727
20	0.43-0.53	Unit E	27	2.000	1.143	1.286	1.500	1.321
20_M	0.43-0.53	Unit E	10	2.100	1.600	1.800	1.300	2.400
20_m	0.43-0.53	Unit E	27	3.481	3.778	1.444	2.667	0.963
22	0.57-0.58	Unit E	25	2.480	2.000	1.320	1.240	1.840
26	0.495-0.50	Unit E	17	2.471	2.882	0.706	0.941	0.882
LV10	0.46-0.47	Unit E	11	1.923	1.692	1.923	1.769	1.769
LV10	0.56-0.57	Unit E	24	2.214	1.785	1.928	1.928	1.642
LV10	0.64-0.65	Unit E	17	2.780	2.696	1.768	2.388	2.299
LV10	0.80-0.81	Unit E	25	2.921	3.134	1.600	1.815	2.300
LV10	0.91-0.92	Unit E	18	1.892	1.986	2.147	2.471	1.810
LV7	0.40-0.41	Unit E	21	1.476	2.048	2.048	0.286	1.524
LV7	0.45-0.46	Unit E	30	1.467	2.100	1.867	0.967	1.767
Praia_TdV	Sup	Beach	15	1.800	2.600	1.533	0.667	1.800
Face_Praia	Sup	Beach	12	3.250	3.167	0.333	0.250	2.750
Barra	Sup	Beach	14	2.929	3.143	1.000	0.429	1.071
Berma	Sup	Beach	12	2.750	2.000	1.583	2.417	1.333

Sample	Depth (m)	Sed. Env.	Number of grains	Angularity	Fresh surfaces	Dissolution	Adhering particles	Percussion marks
Crista_Duna	Sup	Dune	14	2.500	2.071	2.214	2.929	1.643
Duna2_Crist	Sup	Dune	15	3.000	2.467	1.933	3.133	1.000
A_Duna	Sup	Dune	15	2.000	1.800	2.333	3.400	1.800
Duna_R	Sup	Dune	12	2.083	1.917	1.750	2.667	2.083
Duna_2RR	Sup	Dune	12	2.167	0.750	2.583	3.000	1.500
Duna	Sup	Dune	12	2.250	1.250	3.333	3.417	2.333
Duna_F	Sup	Dune	11	3.091	1.727	2.364	2.636	2.091
Duna_2F	Sup	Dune	11	2.545	1.364	2.545	3.091	2.364
SG-6m	Sup	Nearshore	20	2.550	2.650	1.700	2.450	1.600
SG-9m	Sup	Nearshore	16	2.125	2.000	2.500	2.438	2.000
SG-12m	Sup	Nearshore	13	2.154	1.462	2.769	3.769	0.538
SG-13_5m	Sup	Nearshore	20	1.900	0.400	3.750	2.700	1.150
SG-15	Sup	Nearshore	18	2.000	0.778	3.167	3.056	1.500
SG-18_5m	Sup	Nearshore	13	1.692	0.308	3.692	4.000	0.010
SG-18m	Sup	Nearshore	15	1.000	0.667	3.933	3.800	2.000
ArmP_11m	Sup	Nearshore	11	3.000	1.818	2.636	2.455	1.000
ArmP_13m	Sup	Nearshore	13	2.385	0.923	2.615	3.231	1.385
ArmP_16m	Sup	Nearshore	13	2.462	1.231	3.000	3.231	0.923
ArmP_17_1m	Sup	Nearshore	12	2.250	0.417	3.083	3.667	1.083
ArmP_17m	Sup	Nearshore	7	2.714	0.857	2.143	3.571	1.429
ArmP_18m	Sup	Nearshore	11	1.818	1.364	2.273	3.273	0.818
ArmP_19m	Sup	Nearshore	14	1.214	0.214	3.000	3.357	1.071

5.1.5. Heavy mineral features

The heavy minerals assemblage was analysed in samples from the same environments as described above (Table 5.1.4). Samples from unit E and SG14_(0.20-0.28) revealed a percentage of heavy minerals in total sediment ranging from 0.25% to 0.45% with the exception of sample SG26 and LV7_(0.40-0.41) with extremely low values of 0.015% and 0.043% respectively. By contrast beach samples present a percentage of heavy minerals below 0.2% while dune samples present values around 0.25% with the exception of samples Duna2_Crista (0.075%), A_Duna (0.106%), Duna_2F (0.101%) and Duna_R (0.426). Furthermore, the nearshore samples present extremely low values of <0.092% of heavy minerals in total sediment.

Figure 5.1.20 and Table 5.1.5 exhibit the heavy mineral composition of samples from unit E and sample SG14_(0.20-0.28). These samples (as all collected in Lagoa dos Salgados) present mainly three different minerals (*i.e.* andalusite, staurolite and tourmaline) that typically correspond to *ca.* 85-90% of the heavy mineral population of the samples. Furthermore, other minerals were also identified from which amphiboles stand out with percentage that reached almost 6%.

Unit E heavy mineral assemblage did not revealed a clear horizontal or upward trend although in cores LV7 and LV10 the base of the deposit presents the lowest value (in each core) for andalusite and the highest for tourmaline. Values for these minerals varied between 23.1%-47.1% (andalusite) and 35.6%-58.95% (tourmaline). In what concerns amphiboles and other minerals (*e.g.* zircon; garnet, sphene, silimanite, epidote, pyroxene, rutile and brookite) percentages values, these were very low. In the case of amphiboles results were<1.1% [except sample LV10_(0.80-0.81) with 1.31%] and in the case of other minerals the sample presented the highest result with 4.6% while the other samples exhibited values <3.0%.

Sample SG14_(0.20-0.28) was differentiated from samples from unit E by the higher percentage of staurolite (*i.e.* 24%) while in unit E samples varied from 13.2%-19.1%.

Table 5.1.4 - Percentage of heavy minerals in total sediment in samples from Lagoa dos Salgados.

Sample	Depth (m)	Sedimentary Environment	% of Heavy minerals in total sediment
14	0.20_0.28	Storm (?)	0.248
14	0.40_0.82	Unit E	0.393
20	-	Unit E	0.251
26	-	Unit E	0.015
LV10	0.46-0.47	Unit E	0.319
LV10	0.56-0.57	Unit E	0.291
LV10	0.64-0.65	Unit E	0.335
LV10	0.80-0.81	Unit E	0.403
LV10	0.91-0.92	Unit E	0.451
LV7	0.40-0.41	Unit E	0.043
LV7	0.45-0.46	Unit E	0.357
Praia_TdV	Sup.	Beach	0.185
Face_Praia	Sup.	Beach	0.077
Barra	Sup.	Beach	0.192
Berma	Sup.	Beach	0.182
Crista_Duna	Sup.	Dune	0.245
Duna2_Crista	Sup.	Dune	0.075
A_Duna	Sup.	Dune	0.106
Duna_R	Sup.	Dune	0.426
Duna_2RR	Sup.	Dune	0.276
Duna	Sup.	Dune	0.229
Duna_F	Sup.	Dune	0.279
Duna_2F	Sup.	Dune	0.101
SG-6m	Sup.	Nearshore	0.075
SG-9m	Sup.	Nearshore	0.092
SG-13_5m	Sup.	Nearshore	0.091
SG-15m	Sup.	Nearshore	0.019
SG-18_5m	Sup.	Nearshore	0.029
SG-18m	Sup.	Nearshore	0.047

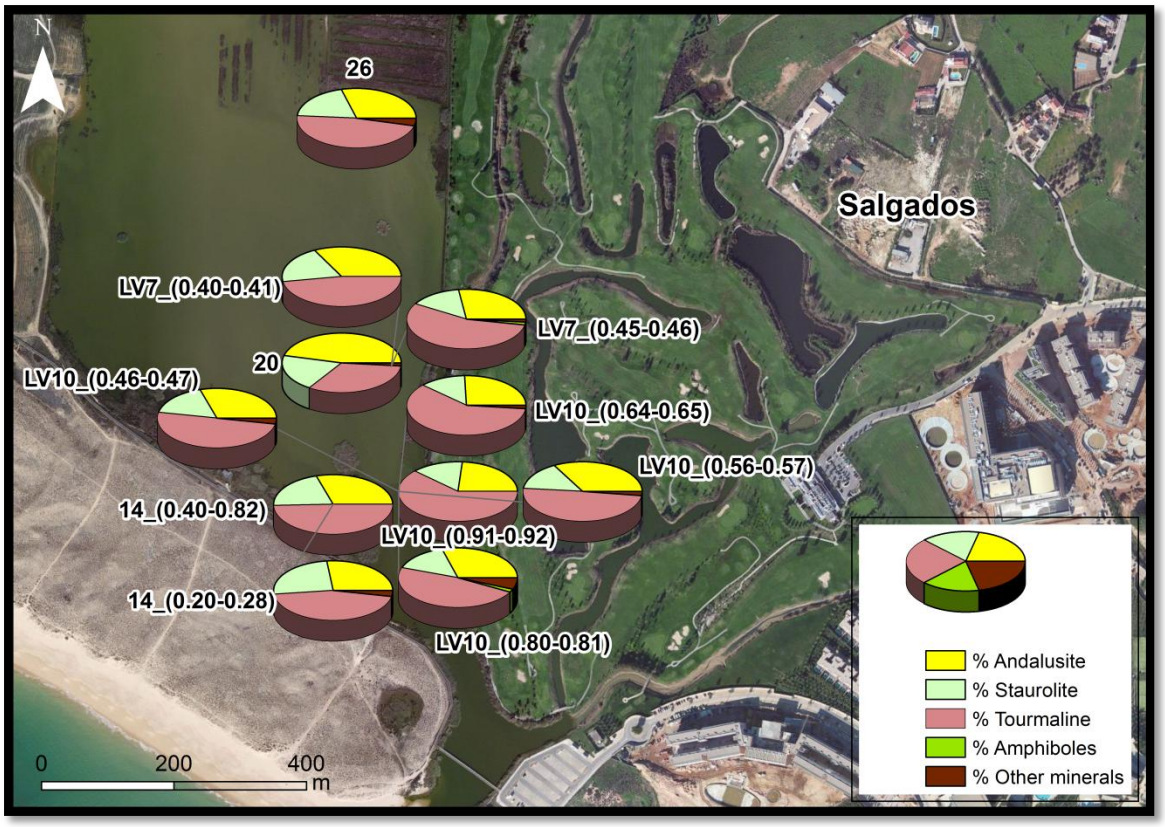

Figure 5.1.20 - – Heavy minerals results and their spatial distribution in samples from unit E and 14_(0.20-0.28) from Lagoa dos Salgados.

In what concerns beach samples (Figure 5.1.21 and Table 5.1.5), they presented percentages of andalusite varying from 27.4% (Barra) to 38.4% (*i.e.* Praia_TdV). Moreover, these samples exhibited values of staurolite of *ca.* 3.0% with the exception of the beach berm sample (*i.e.* Berma) that showed a value of 9.18%. The highest percentage value for tourmaline was observed in sample Face_Praia with a value of 67.2% while the lowest value was observed in sample Berma with 50%. Amphiboles were vestigial (*i.e.* 0.001%) with the exception of sample Berma with 2.0%. In the beach samples collected in Lagoa dos Salgados it was also possible to observe other minerals that summed percentages variying from 1.7% (*i.e.* Face_Praia) to 8.5% (*i.e.* Praia_TdV).

Regarding dune samples (Figure 5.1.21 and Table 5.1.5), no spatial trend could be established based in the heavy mineral composition. These samples presented values within the range 25.7%-41.8% of andalusite, of 6.79%-13.8% of staurolite and 46.7%-60.0% of tourmaline. The highest percentage (*i.e.* 2.85%) of amphiboles was observed in sample Duna_2F while the lowest value (*i.e.* 0.001%) was detected in samples Crista_Duna and Duna2_RR. The content in other minerals presented its lowest value (*i.e.* 0.011%) in the dune crest samples (*i.e.* Crista_Duna and Duna2_Crista) and the highest value of 6.18% in sample A_Duna.

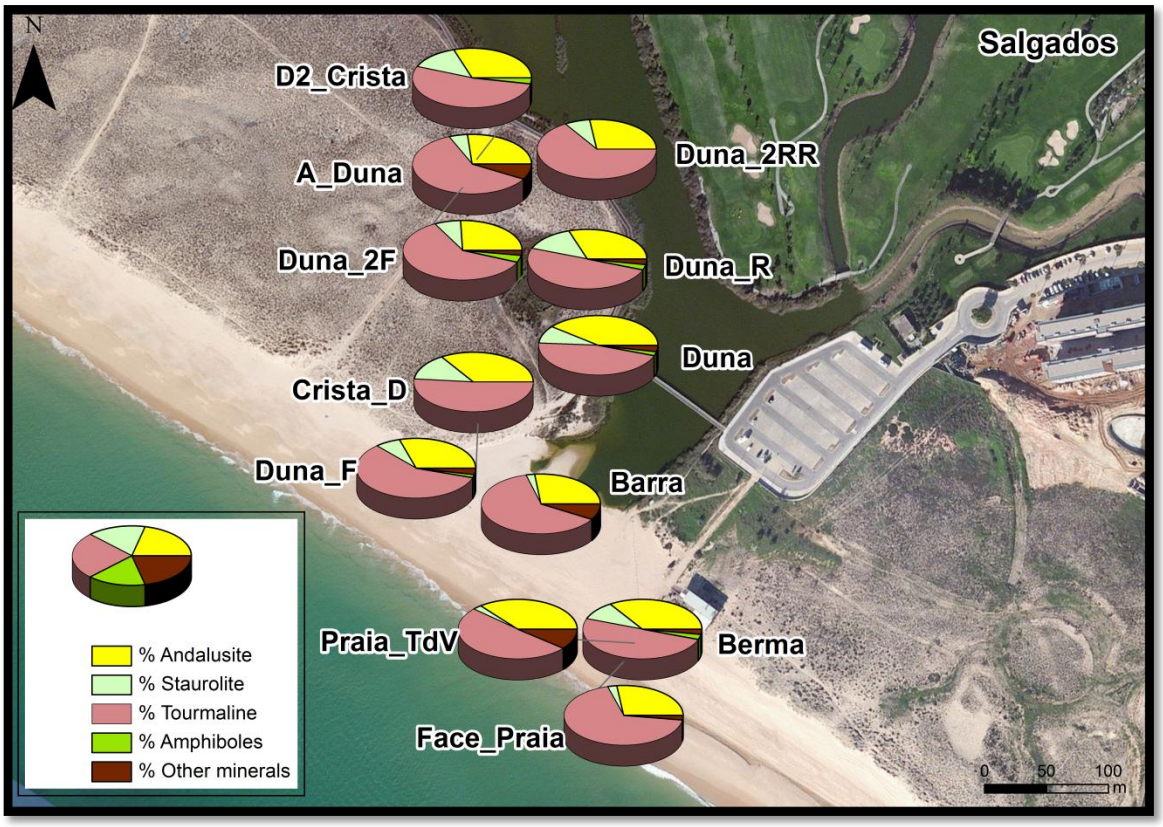

Figure 5.1.21 - Heavy minerals results and their spatial distribution in dune and beach samples from Lagoa dos Salgados.

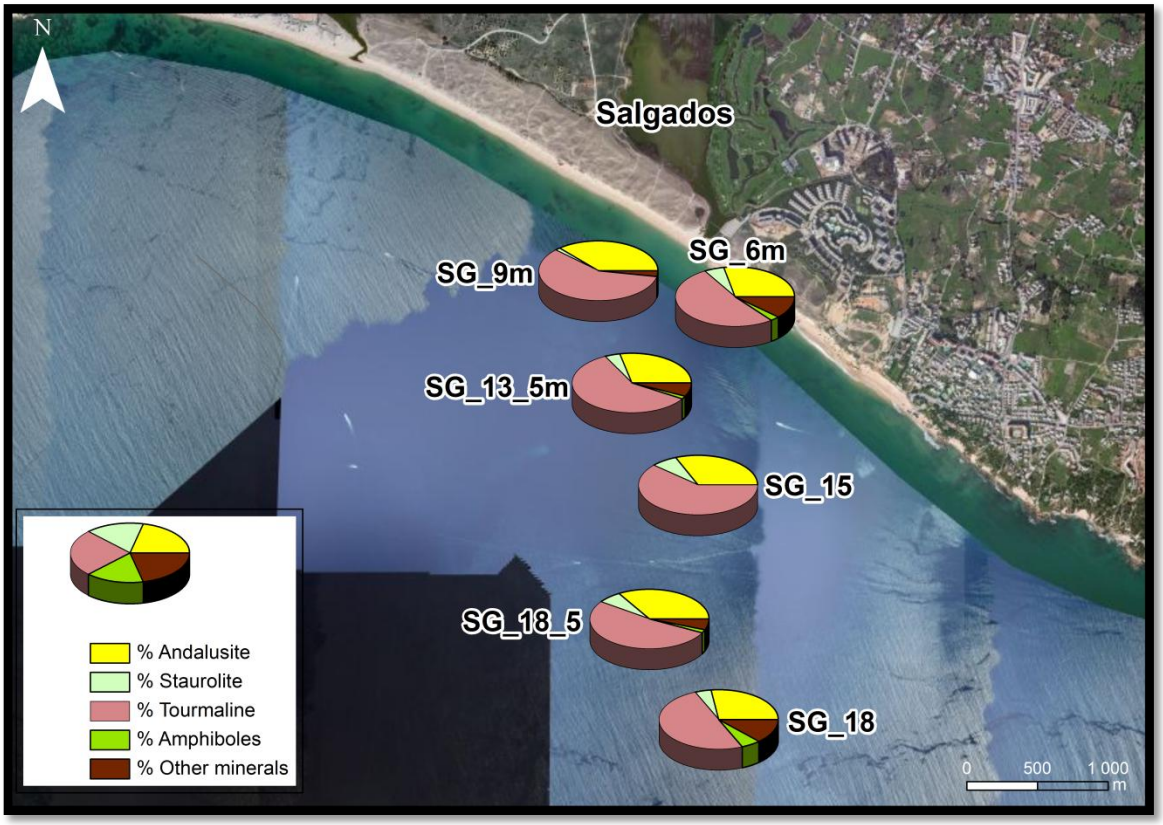

Figure 5.1.22 - Heavy minerals results and their spatial distribution in nearshore samplesfrom Lagoa dos Salgados.

Nearshore samples also did not allow the establishment of any distinguishable spatial pattern (Figure 5.1.22 and Table 5.1.5). In nearshore samples andalusite varied between 38.68% (*i.e.* SG-9m) and 27.58% (*i.e.* SG-18m), while ataurolite ranged from 1.46% to 7.69% (*i.e.* SG-9m and SG-15m, respectively). On the other hand, the highest value for tourmaline was observed in sample SG-15m with a value of 58.9% while the lowest value was detected in SG-18m with 49.4%. Nearshore samples present higher values for amphiboles (up to 5.7%) and for other minerals (up to 10.35%).

Comparison of heavy mineral assemblages from different sedimentary environments and lithostratigraphic units suggests that unit E samples present similar percentage values of heavy mineral assemblage as dune samples (*i.e.* andalusite, tourmaline, amphiboles and other minerals). Furthermore, the only exception is staurolite that presents its higher values (between 13.2% and 19.1% in samples from unit E and its highest value (*i.e.* 24.0%) in sample SG14_(0.20-0.28). Staurolite in dune samples varies from 6.79% to 13.8%. Beach samples were distinguishable by the higher percentage of other minerals and by the lowest percentage of staurolite. On the other hand, nearshore samples were differentiated by the higher content in amphiboles and other minerals.

Table 5.1.5 - Heavy mineral composition in samples from Lagoa dos Salgados.

Sample	Depth (m)	% Andalusite	% Staurolite	% Tourmaline	% Amphiboles	% Others
14	0.20_0.28	27.429	24.000	46.286	0.001	2.295
14	0.40_0.82	31.304	19.130	49.565	0.001	0.011
20	-	47.126	16.092	35.632	0.001	1.159
26	-	30.769	18.343	47.929	0.001	2.968
LV10	0.46-0.47	31.111	16.296	49.630	0.741	2.230
LV10	0.56-0.57	35.156	13.281	49.219	0.781	1.572
LV10	0.64-0.65	25.658	15.132	57.895	0.001	1.326
LV10	0.80-0.81	30.921	15.132	48.026	1.316	4.613
LV10	0.91-0.92	23.134	17.164	58.955	0.746	0.011
LV7	0.40-0.41	34.826	16.915	47.761	0.498	0.011
LV7	0.45-0.46	27.933	15.642	54.190	1.117	1.127
Praia_TdV	Sup.	38.415	2.439	50.610	0.001	8.545
Face_Praia	Sup.	27.586	3.448	67.241	0.001	1.734
Barra	Sup.	27.419	3.226	62.903	0.001	6.459
Berma	Sup.	36.735	9.184	50.000	2.041	2.050
Crista_Duna	Sup.	36.667	12.222	51.111	0.001	0.011
Duna2_Crista	Sup.	31.818	13.636	52.273	2.273	0.011
A_Duna	Sup.	26.543	6.790	59.877	0.617	6.181
Duna_R	Sup.	31.915	13.830	50.000	2.128	2.137
Duna_2RR	Sup.	27.536	8.696	63.043	0.001	0.735
Duna	Sup.	41.803	7.377	46.721	1.639	2.468
Duna_F	Sup.	31.288	7.975	57.055	1.227	2.462
Duna_2F	Sup.	25.714	9.524	60.000	2.857	1.914
SG-6m	Sup.	29.193	6.832	52.174	2.484	9.322
SG-9m	Sup.	38.686	1.460	56.934	0.730	2.198
SG-13_5m	Sup.	29.530	5.369	58.389	1.342	5.376
SG-15m	Sup.	33.333	7.692	58.974	0.001	0.011
SG-18_5m	Sup.	36.170	6.383	51.773	1.418	4.262
SG-18m	Sup.	27.586	5.747	49.425	5.747	10.352

5.2. Boca do Rio

5.2.1. Lithostratigraphic features

Boca do Rio sediment infilling has been studied by several authors (*e.g.* Dawson *et al.*, 1995; Hindson *et al.*, 1996; Hindson and Andrade, 1999; Oliveira *et al.*, 2009; Cunha *et al.*, 2010), which described a sandy deposit associated with the AD 1755 tsunami inundation sandwiched within estuarine mud. The top meter of the lithostratigraphy of the present-day alluvial plain has been described by other (see references above) and can be summarized by Figure 5.2.1. The uppermost layer of the sedimentary sequence consists of dark red/brown silty clay with an almost constant thickness of 0.80 - 1m. The underlying layer has been associated with the AD 1755 tsunami and has only been found within the main valley and the north-eastern (Ribeira de Vale Barão) tributary (Figure 5.2.2). It is present in the stratigraphic column up to *ca.*1500m from the coastline. The thickness of this sandy unit decreases from *ca.* 0.50m in the coastal edge of the alluvial plain to a few centimetres in the area where the tributary streams merge into the alluvial field. This unit presents a strong lateral variability and is sedimentologically complex. Five sedimentologically distinct sub-units were recognised by Hindson and Andrade (1999) within this unit in the seaward area of the lowland. These sub-units presented a distinguishable character varying from silty fine sand to clean marine sand, a dark brown layer, or a chaotic layer that also included boulders (in the southern sector of the alluvial plain). However, the sub-units were not consistently present throughout the alluvial plain and lateral variations in their appearance where frequent at short distances. Further inland, Hindson and Andrade (1999) state that the deposit is simpler and is reduced to a thin shelly sand layer before tapering out. The lower contact is clearly erosive and the upper contact with overlying unit is gradational, and in places difficult to establish. The altitude of the basal contact of the tsunamigenic unit rises gradually inland from *ca.* 1.0 to 1.6m. The layer underlying it is very similar to the topmost unit, consisting of the same brown mud with occasional organic material and charcoal. In some locations, the brown mud grades downwards into a black organic mud. The thickness of this unit varies between 0.5 and 1m. The base of this stratigraphic sequence consists of grey, marine sands with shells extending beyond a depth of 5m below ground surface without reaching the base.

Samples from tsunami sediment and present day analogues were collected in this area and used in this work (Figure 5.2.3). Three tsunami samples (SAO, SAM and SS3 – corresponding to a profile inland) were cored from the alluvial plain and crossing through the tsunamigenic unit, were studied. Furthermore, eleven other sediment samples (five nearshore, three dune, one beach and two alluvial) were also retrieved and utilized in this work to characterize present day sedimentary environments. The nearshore samples correspond to a profile from -20m below msl up to -5m below msl. The dune samples consist of aeolian material predating the AD 1755 event and preserved in karst hollows (P6 and P8) in the downwind slope of

the rock spur barring the lowland and one (pedogenised) sample of dune sand topping the spur crest, interpreted as the remnant of a climbing dune (Duna_Trep).

The chronology for the lithostratigraphy of Boca do Rio has been intensely debated (see references above).

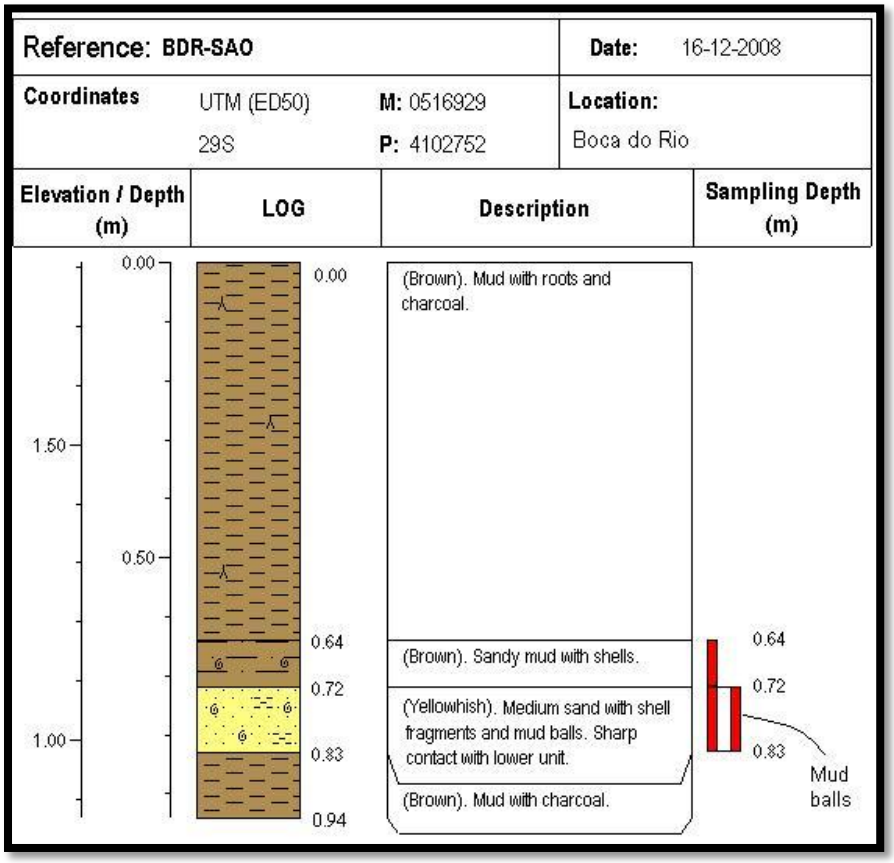

Figure 5.2.1 – Lithostratigraphic and macroscopic log description of sample-core SAO that roughly corresponds to the schematic lithostratigraphy of the alluvial plain topmost meter.

Figure 5.2.2 – Photographs of sampling in one trench within the alluvial plain of Boca do Rio. The yellowish sand is the unit associated with the AD 1755 tsunami. The plastic box is 0.30 m long.

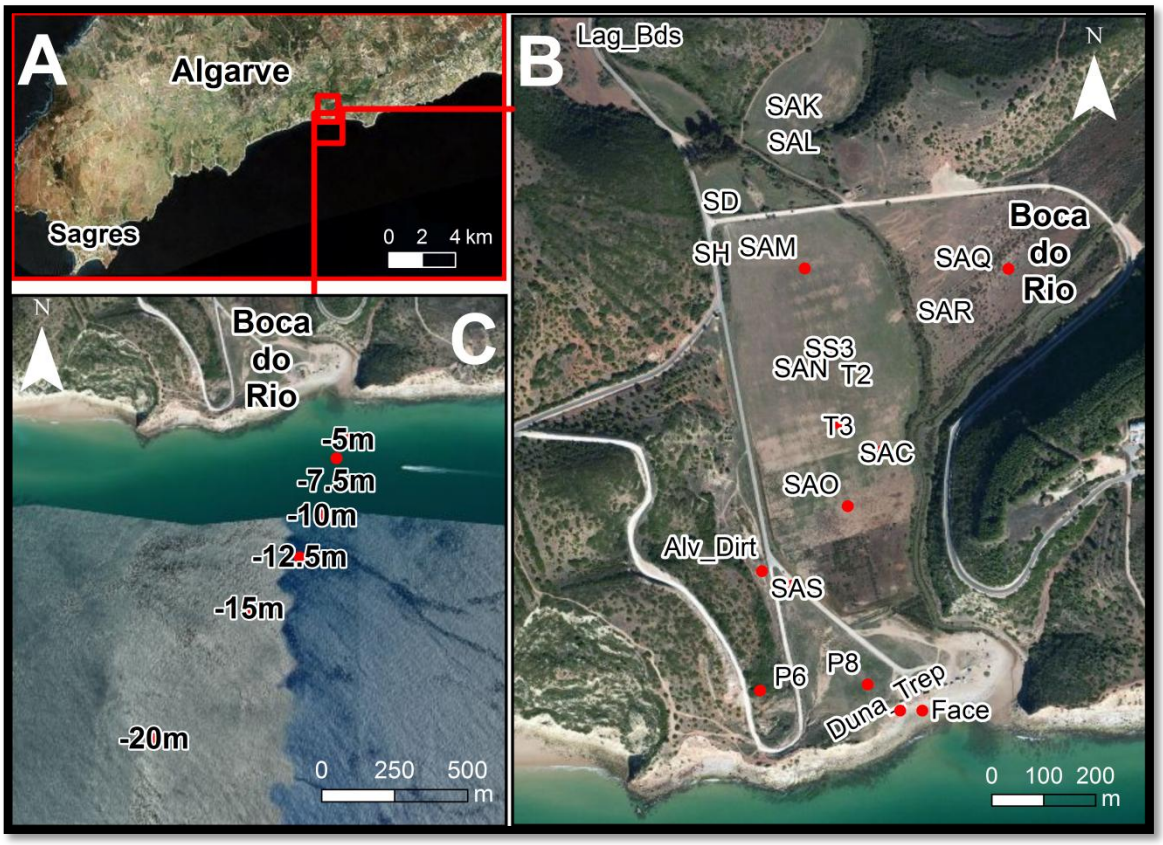

Figure 5.2.3 – Sampling locations within Boca do Rio area. A – Regional location. B - Samples collected within the alluvial plain. C- Samples collected in the nearshore of the Boca do Rio area.

5.2.2. Textural features

Grain-size parameters obtained for the group of samples used in this study are summarized in Table 5.2.1. With these results it is possible to recognise a decreasing inland trend for the 1%Φ and the 10% Φ in the tsunami samples. The standard deviation decrease inland while the remaining parameters did not revealed a clear trend. The beach sample (*i.e.* Face) presented a mean grain size of 1.66 Φ. The P6 and P8 dune samples presented many similarities in all textural aspects analysed while the dune sample Duna_Trep although sharing many resemblances, presented a slightly coarser overall grain-size. Within the nearshore samples one sample stands out (-10m) due to its remarkably coarser nature, its large standard variation (*i.e.* 1.60) and abrupt increase in size characterizing the 1 and 10 centiles; this is interpreted as resulting from bias introduced by a small number of large particles in an otherwise Gaussian size-distribution. The standard deviation in other samples remains under 0.55 Φ with the exception of the alluvial sediment. All the other nearshore samples presented mean values of approximately 1.75Φ (sample -10m presented a mean grain size value of 0.93Φ) and kurtosis between 1.11 and 1.21. The more heterometric sample is the alluvial sample (*i.e.* Alv_Dirt) presenting the lowest 90% and the highest 1% Φ with obvious consequences in the standard deviation value, by far the highest value observed (*i.e.* 2.83). Textural data allowed the clear

distinction of two samples (*i.e.* -10m and Alv_Dirt) among the ones analysed. The other entire group of samples share many of the aspects analysed and presented similar values that decreased the differentiation capacity solely based in the textural proxy.

Table 5.2.1 - Summary of textural attributes of samples collected in Boca do Rio.

Sample	Sed. Env.	1% Φ	10% Φ	90% Φ	Mean (MZ) Φ	Graphic Std Deviation (σ1)	Graphic Kurtosis (K_G)	Simple Sorting Measure (SSM)	Mode Φ	Median Φ
SAM	Tsunami	0.26	1.11	2.05	1.57	0.39	1.19	0.69	1.75	1.57
SS3	Tsunami	-1.19	0.70	1.82	1.26	0.43	1.05	0.72	1.25	1.26
SAO	Tsunami	-2.42	0.66	1.92	1.36	0.53	1.34	0.98	1.25	1.38
Face	Beach	0.67	1.17	2.22	1.66	0.40	1.13	0.70	1.75	1.66
Duna_Trep	Dune	0.67	1.26	2.26	1.75	0.39	1.10	0.66	1.75	1.74
P6	Dune	1.18	1.56	2.39	1.96	0.33	1.06	0.56	1.75	1.94
P8	Dune	1.10	1.40	2.26	1.80	0.34	1.08	0.56	1.75	1.79
-5m	Nearshore	-0.10	1.03	2.35	1.71	0.53	1.11	0.91	1.75	1.72
-10m	Nearshore	-3.62	-2.23	2.30	0.93	1.60	1.87	2.87	1.75	1.48
-12_5m	Nearshore	-1.39	1.17	2.44	1.82	0.51	1.21	0.90	1.75	1.82
-15m	Nearshore	-1.84	1.05	2.35	1.74	0.54	1.26	0.97	1.75	1.76
-20m	Nearshore	-1.91	1.03	2.31	1.69	0.52	1.26	0.93	1.75	1.71
Alv_Dirt	Alluvial	-3.77	-3.59	3.53	0.40	2.83	0.46	3.62	-3.75	1.37

An extrapolation of the percentage of sand and of the median grain size of the tsunamigenic unit is presented in Figure 5.2.4 (for sample location see Figure 5.2.3). In this figure it is possible to visualize the decrease in the proportion of sand with increasing distance from the coastline. The mean grain size (*i.e.* D50) revealed a somewhat more complex pattern with lower values in the centre of the alluvial plain close to its left embankment superimposed upon a general trend of decrease in median grain size with increasing distance inland.

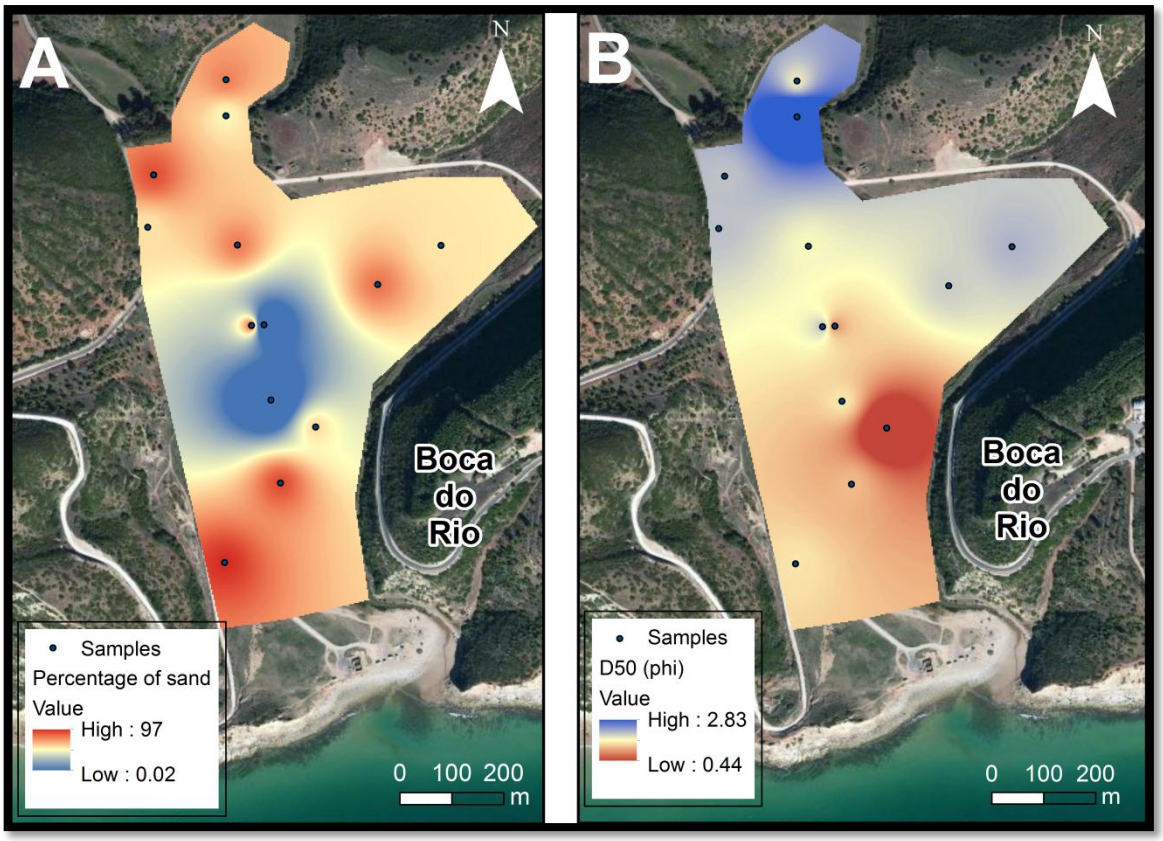

Figure 5.2.4 – Inverse Distance Weighting extrapolation for percentage of sand (A) and median grain size (b) for samples retrieved from the tsunamigenic unit in Boca do Rio.

In terms of micromorphological studies it was possible to analyse a sample from BDR_T2_97_105 that included the contact between the tsunamigenic sandy unit and the underlying layer (Figure 5.2.5). In compositional terms no major contrast was registered from the base to the top of the sand in the thin section. Quartz was present throughout the thin section in percentage around 75-90%, Calcite was also common (app. 10%), Mica was detected in low percentage but many shell fragments (up to 15 %) where identified in the thin section. Rounded mud clasts show out distinctively in the thin section and one of the major changes observed was the presence of rip-up clasts solely on the basal 4 cm of the unit. Other major change observed was related with the size of mud clasts and grains (smaller to the top of the unit), together with the decrease of abundance in shell fragments towards the top; in addition, the compaction of the sediment is higher at the base of the deposit.

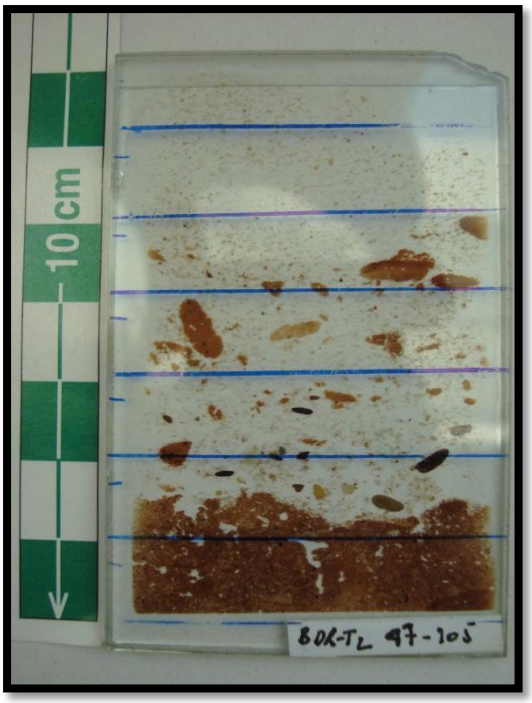

Figure 5.2.5 - Image of a 7.5x4.5 cm thin section from the tsunamigenic layer and underlying mud (sample BDR_T2_97_105).

5.2.3. Morphoscopy features

Morphoscopic analyses were conducted in samples from Boca do Rio (Figure 5.2.6). In compositional terms it was possible to verify that the nearshore samples (Figure 5.2.6A) presented a percentage of quartz grains in the range of 50% to 70% (*i.e.* samples -5m and -20m). In terms of the percentage of lithic material little variation was noted in the nearshore samples, which presented values of *ca.* 25%. Bioclasts presence varied between 9.52% (-10m) and 27.72% (*i.e.* -12.5m).

The beach sample presented values of 44.79% for quartz grains, 31.25% for lithic material and 23.96% for bioclasts. On the other hand, dune samples present the overall lowest value for lithic material (*i.e.* P6-15.50% and P8-18.81%) although these samples presented contrasting percentages for quartz (P6- 61.39%; P8- 42.20%) and bioclasts (P6- 19.80%; P8- 42.20%; respectively). The alluvial sample presented the following percentages: 63% for quartz grains; 25% for lithic material and 12% for bioclasts. The tsunami samples (*i.e.* SAM and SAO) presented similar values for quartz but contrasting values for lithic material (higher in sample SAM - farther inland) and for bioclasts (higher in sample SAO – closest to the coast line).

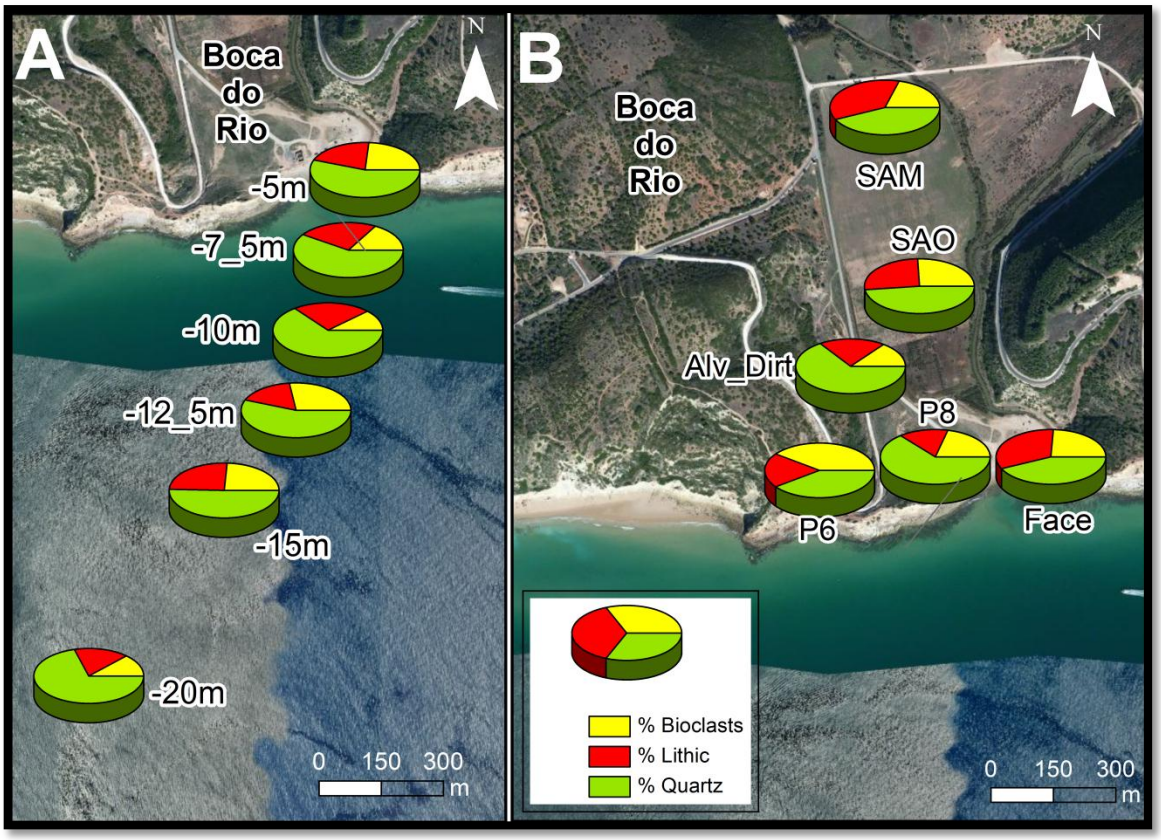

Figure 5.2.6 - Morphoscopic compositional characteristics of samples from Boca do Rio. A – Nearshore samples. B – Beach, dune, alluvial and tsunami samples.

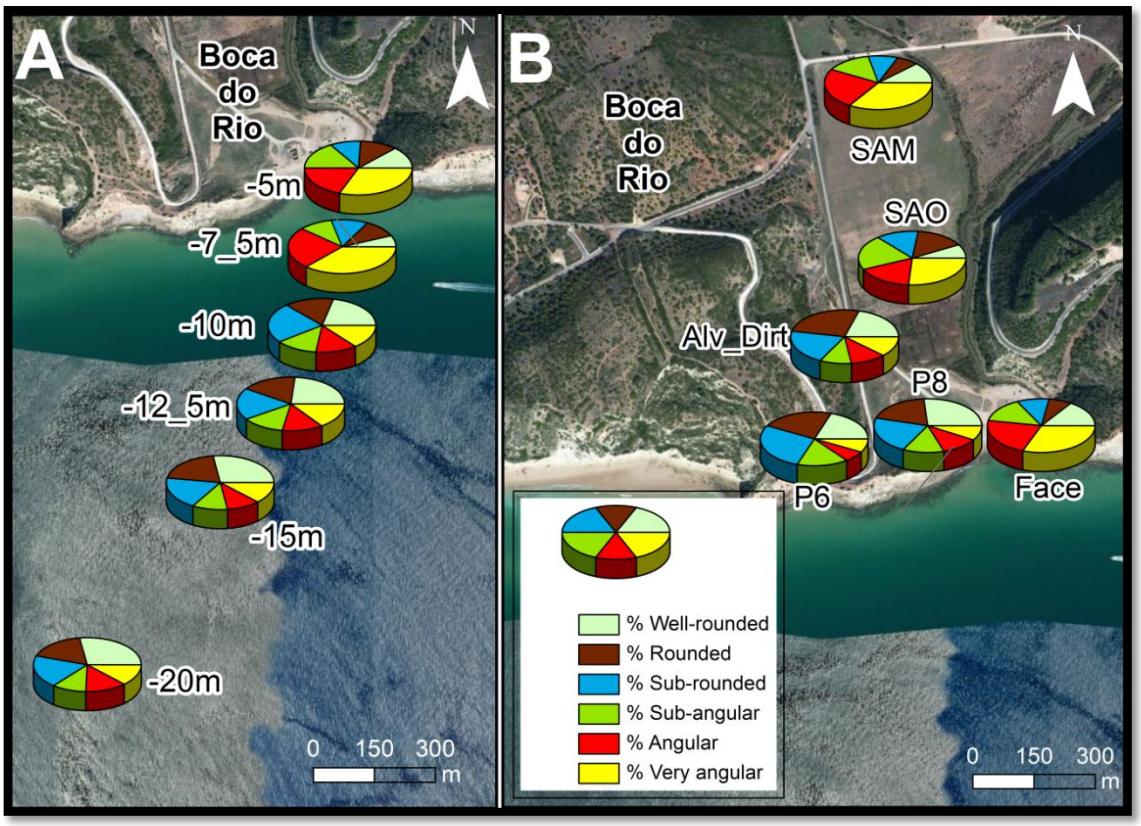

Figure 5.2.7 – Roundness classification of nearshore samples (A) and beach, dune, aluvial and tsunami samples (B) from Boca do Rio.

Regarding roundness of the quartz grains observed (Figure 5.2.7) it is visible that the nearshore samples present a higher percentage of angular and very angular grains in the samples closer to the coast (maximum value of 59.20% and 50.00% for samples -7.5m and -5m respectively). In contrast the well-rounded and rounded grains were present in higher percentage in the samples farther away from the coast (*i.e.* 46.15% and 48.00% for samples -20m and -15m respectively). The high values observed for the proximal nearshore samples (*i.e.* -5m and -7.5m) were also observed in the beach sample (*i.e.* Face) with a percentage of 52.17% for very angular and angular grains. The dune samples presented a large predominance of well-rounded, rounded and sub-rounded grains with values of 68.00% for sample P6 and of 65.00% for sample P8, respectively. On the other hand, tsunami samples show high values for very angular and angular grains (*i.e.* SAM-56.10 % and SAO-44.90%) with the higher values observed farther inland.

The shape of quartz grains was also analysed in Boca do Rio (Figure 5.2.8). The nearshore samples presented a decreasing trend towards the coast of spherical grains with values of 34.62 % for sample -20m and of 13.85% for sample -7.5m. Sample -5m presented a value of 25.86% in contrast with the tendency described above. The beach and dune samples showed values of *ca.* 25% of spherical grains. The alluvial samples exhibited a value of 30.77% for spherical grains and the highest value of all samples for prismatic grains (*i.e.* 23.08%). On the other hand, tsunami samples (*i.e.* SAM and SAO) revealed percentage of *ca.* 17% of spherical grains and *ca.* 55% for discoid and sub-discoid grains (sample SAM-farther inland- with the higher value – 58.14%).

The morphoscopic results allowed the differentiation of sedimentary environments mainly based in the roundness and sphericity characteristics of grains (*i.e.* well-rounded and rounded grains are more present in the distal nearshore samples while more angular grains are present in the proximal, beach and tsunami samples). In terms of spatial variation of morphoscopic characteristics in the tsunami samples, the low number of samples constrains interpretations but it is important to note an increase inland of lithic material.

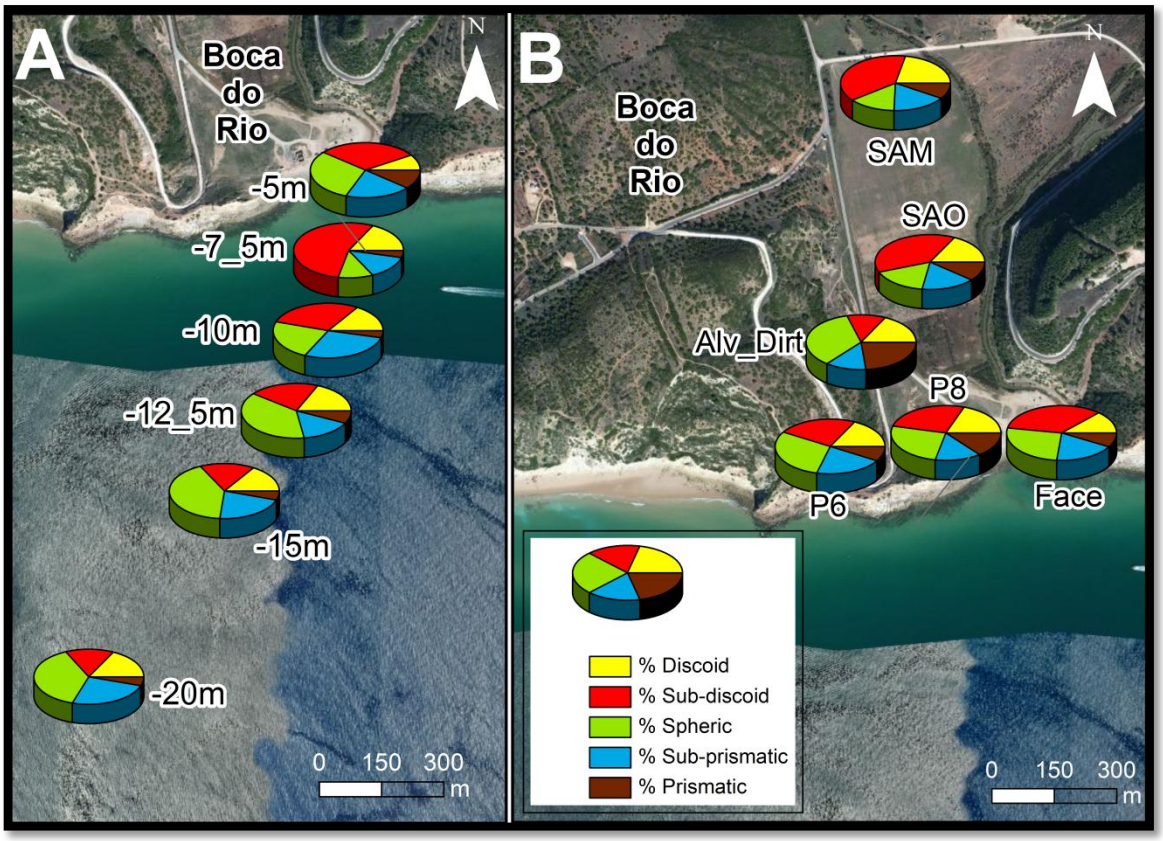

Figure 5.2.8 - Sphericity classification of nearshore samples (A) and beach, dune, aluvial and tsunami samples (B) from Boca do Rio.

5.2.4. Microtextural features

The microtextural results obtained for Boca do Rio are summarized in Figure 5.2.9 and Table 5.2.2.

In terms of angularity, all samples present values in the range between 2.2 and 2.5, except higher values yielded by beach and two proximal nearshore samples (3.000, 3.462 and 3.417, respectively) and lower values by two nearshore samples -15m and -20m (1.455 and 1.909, respectively) and one dune sample (Duna_Trep - 1.667). On the other hand, fresh surfaces present highest values in nearshore samples -5m and -7.5m (4.385 and 4.250, respectively); the beach sample exhibits a result of 2.700, while tsunami samples show results within the 1.920 to 2.800 range; the dunes present values of 1.524 and 1.560 (P6 and P8 respectively) while Duna_Trep (and all other remaining samples) show values under 1.15. In what concerns dissolution features, it was observed that samples with values < 1 are tsunami sample SS3 and proximal nearshore samples (-5m and -7.5m). Moreover, the other tsunami samples (SAM and SAO) present values for dissolution of 1.500 and 1.520, respectively. The highest values registered for dissolution were obtained in one nearshore (-10m) and two alluvial samples, with values above 3.5. Regarding adhering particles, dunes showed results around 2, while tsunami and beach samples exhibited values between 1.100 and 1.560. Alluvial samples, Duna_Trep and all nearshore sediments (except -5m and -7.5) present results for adhering particles above 3.0. Furthermore, percussion marks are present in all tsunami samples above

ca. 3 with the highest value obtained for sample SS3, (3.600). Beach and proximal nearshore samples (-5m and -7.5m) exhibit values of 2.800, 3.000 and 2.545, respectively. Moreover, dune samples show values around 1.250, except sample Duna_Trep with a value of 0.833. Alluvial samples present the lowest values observed, with 0.333 (*i.e.* Lag_Bds) and 0.400 (Alv_Dirt).

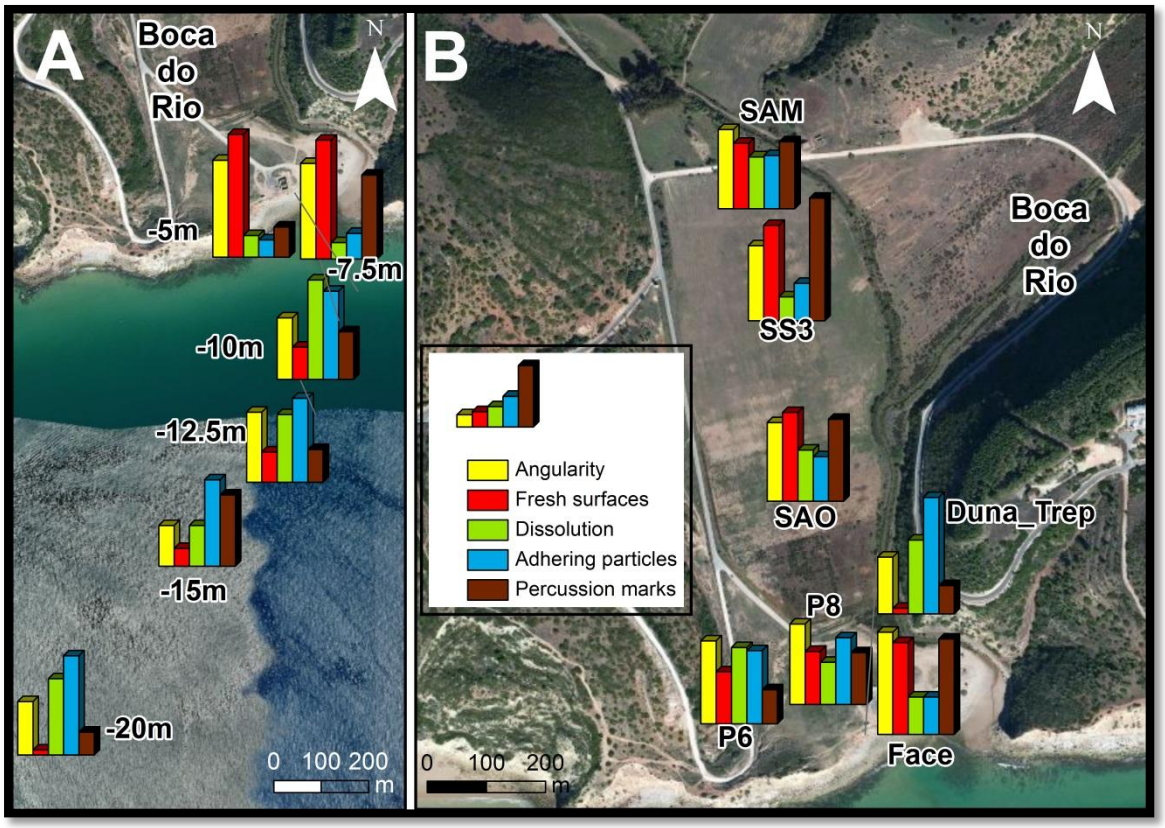

Figure 5.2.9 – Microtextural results and their spatial distribution in Boca do Rio. A- Nearshore samples. B- Beach, dune and tsunami samples.

Table 5.2.2 - Microtextural results of samples from Boca do Rio.

Sample	Depth (m)	Sedimentary Environment	Number of grains	Angularity	Fresh surfaces	Dissolution	Adhering particles	Percussion marks
SAM	1.04-1.17	Tsunami	25	2.320	1.920	1.520	1.560	1.960
SS3		Tsunami	10	2.200	2.800	0.700	1.100	3.600
SAO	0.87-0.98	Tsunami	20	2.300	2.600	1.500	1.300	2.400
Face	Sup	Beach	10	3.000	2.700	1.100	1.100	2.800
Duna_Trep	Sup	Dune	12	1.667	0.167	2.167	3.417	0.833
P6	Sup	Dune	21	2.429	1.524	2.238	2.143	1.000
P8	Sup	Dune	25	2.360	1.560	1.240	1.960	1.520
-5m	Sup	Nearshore	13	3.462	4.385	0.769	0.615	1.077
-7_5m	Sup	Nearshore	12	3.417	4.250	0.583	0.917	3.000
-10m	Sup	Nearshore	20	2.200	1.150	3.550	3.150	1.700
-12_5m	Sup	Nearshore	12	2.500	1.083	2.417	3.000	1.167
-15m	Sup	Nearshore	11	1.455	0.636	1.455	3.091	2.545
-20m	Sup	Nearshore	11	1.909	0.182	2.727	3.545	0.818
Lag_Bds	Sup	Alluvial	9	2.444	0.222	3.556	4.222	0.333
Alv_Dirt	Sup	Alluvial	10	2.400	0.300	3.500	3.900	0.400

In terms of microtextural analysis, results described above can be summarized as follows:

- Nearshore samples can be divided in two groups (proximal and distal samples). The latter presents very high values for angularity and fresh surfaces and extremely low values for adhering particles and dissolution, whereas distal samples present exactly the opposite.
- Beach sample revealed high values for angularity, fresh surfaces and percussion marks.
- Dune samples presented a well-balanced range of values for all characteristics studied although sample Duna_Trep revealed a higher content of dissolution and adhering particles, thus suggesting a different (older) age or more intense pedogenetic reworking when compared with the two other dune samples (P6 and P8).
- Tsunami samples presented angularity corresponding to *ca.* 2.250, very high results for fresh surfaces and the highest value for percussion marks.
- Alluvial samples presented low values for fresh surfaces and percussion marks but exhibited the highest values for dissolution and adhering particles.

No unequivocal spatial trend could be established except among the nearshore samples.

5.2.5. Heavy mineral features

Heavy mineral content in samples from Boca do Rio was analysed (Table 5.2.3). Tsunami samples presented values of 0.168% (*i.e.* SAM), 0.212% (*i.e.* SS3) and 0.070% (*i.e.* SAO) thus not allowing the establishment of any spatial trend. The beach sample (*i.e.* Face) and the Duna_Trep sample presented values of *ca.* 0.35% and 0.38% (the highest observed), respectively. All the remaining samples (all nearshore samples and two dune samples – P6 and P8) presented much lower percentage (<0.07%) for heavy mineral fraction in total sediment.

In compositional terms all samples presented more than 75% of andalusite, staurolite and tourmaline with pyroxene and amphiboles also present (Figure 5.2.10 and Table 5.2.4). All nearshore samples presented more than 25% of andalusite with the exception of sample -10m (*i.e.* 19.737%). Beach and dune samples presented results in the range 22% to 24%, except sample Duna_Trep with a result of 31.21%. Tsunami samples exhibited values in the range of 22% to 28% while alluvial samples showed a result of 19.12%. Staurolite results allowed a more clear differentiation due to the fact that all nearshore samples presented values above 15%, alluvial sample has 22.794% while face and dune samples presented values of *ca.* 14.5% (except Duna_Trep with 17.197%). On the other hand tsunami samples revealed values within the range 10.156% and 15.172%. In the case of tourmaline spatial trends could be inferred: in the nearshore samples it is visible a decrease in the percentage of tourmaline with decreasing distance to the coast while in the tsunami samples the percentage of tourmaline increases inland. In fact, all nearshore samples exhibited results below 50% while beach and dunes (except Duna_Trep with 42%) displayed values around *ca.* 50% which are similar to the percentage obtained for tourmaline in tsunami samples.

Table 5.2.3 - Percentage of heavy mineral composition in total sediment of samples from Boca do Rio.

Sample	Depth (m)	Sedimentary Environment	% of Heavy minerals in total sediment
SAM	1.04-1.17	Tsunami	0.168
SS3	-	Tsunami	0.212
SAO	0.87-0.98	Tsunami	0.070
Face	Sup	Beach	0.350
Duna_Trep	Sup	Dune	0.378
P6	Sup	Dune	0.036
P8	Sup	Dune	0.053
-5m	Sup	Nearshore	0.010
-10m	Sup	Nearshore	0.026
-12_5m	Sup	Nearshore	0.053
-20m	Sup	Nearshore	0.068
Alv_Dirt	Sup	Alluvial	0.013

Alluvial sample presented a value of 40.441% of tourmaline. In what regards pyroxene it was observed that all nearshore samples presented results above 7% while beach and dune exhibited values in the 4.45%-5.50% range. Tsunami samples seem to decrease its content in pyroxene inland with values varying from 4.138% to 8.462%. Amphiboles are rare in nearshore samples and absent in beach sample. Amphiboles present its maximum value in the alluvial sample with a 3.676% presence. In what concerns other minerals (*e.g.* zircon, garnet, olivine, epidote, monazite, rutile and sphene), it can be observed that dune, beach and tsunami samples presented similar values (*i.e.* dune and beach *ca.* 3.5% while tsunami exhibited values in the range of 3.454% to 5.390%). Nearshore samples presented values below 1.761% except sample -5m that displayed a result of 3.156% for the presence of other minerals. Alluvial sample revealed the highest value for the presence of other minerals with a result of 5.886%.

As a summary, it can be perceived that tsunami samples share more similarities in terms of heavy mineral percentage compositional content (*i.e.* andalusite, staurolite, tourmaline and other minerals) with dune and beach samples than with any other group of samples (i.e nearshore or alluvial samples). Staurolite apparently allowed the differentiation of environments except for sample Duna_Trep.

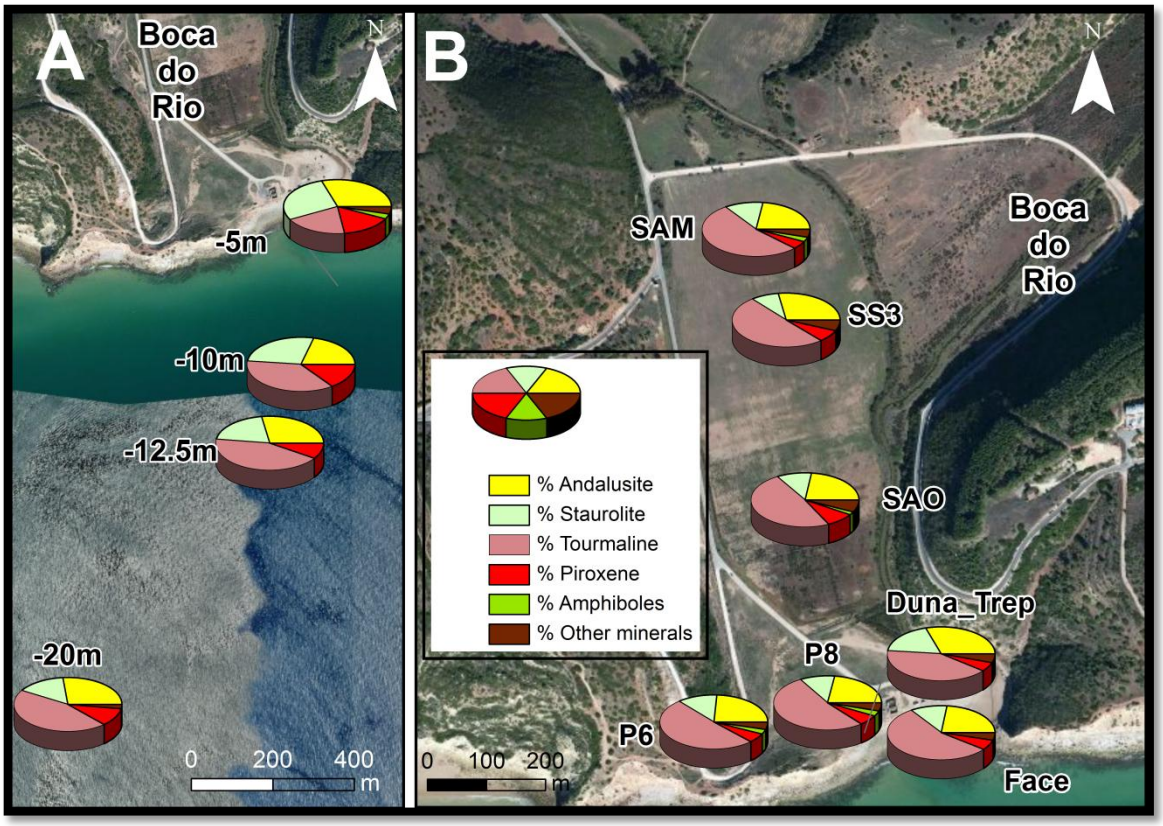

Figure 5.2.10 – Heavy mineral composition of nearshore samples (A) and beach dune and tsunami sample (B) from Boca do Rio.

Table 5.2.4 - Results from heavy mineral assemblages in the Boca do Rio samples.

Sample	% Andalusite	% Staurolite	% Tourmaline	% Pyroxene	% Amphibole	% Others
SAM	22.069	15.172	53.103	4.138	2.069	3.454
SS3	28.125	10.156	50.000	6.250	0.781	4.695
SAO	22.308	13.846	48.462	8.462	1.538	5.390
Face	22.581	14.516	54.839	4.839	0.001	3.235
Duna_Trep	31.210	17.197	42.675	4.459	0.637	3.828
P6	23.784	15.135	50.811	4.865	2.162	3.250
P8	22.000	14.000	52.500	5.500	2.500	3.505
-5m	31.496	24.409	22.047	16.535	2.362	3.156
-10m	19.737	28.947	38.816	12.500	0.001	0.010
-12_5m	28.205	19.872	44.231	7.051	0.001	0.650
-20m	26.901	16.374	45.614	8.772	0.585	1.761
Alv_Dirt	19.118	22.794	40.441	8.088	3.676	5.886

5.3. Voe of Scatsta

5.3.1. Lithostratigraphic features

In the location of Voe of Scatsta, the erosion of peat by the sea exposed along the coast a cliffed outcrop of *ca.* 2m high. Within the lower part of that peat, there is an approximately 0.10m thick, wide-spread massive sand layer, which overlies 0.30m of peat. The sand layer is more or less continuous for more than 150m both alongshore and inland. Several cores were collected in this region and two of those cores SHT_1 and SHT_3, taken from the walls of trenches located less than 50m apart and aligned cross shore, were studied in more detail (Figure 5.3.1 and 5.3.2). Two samples from each core were analysed; one correspondent to the base of the sandy deposit and a second sample (in each core) located above the previous one and close to the top contact of the sand unit but still within it.

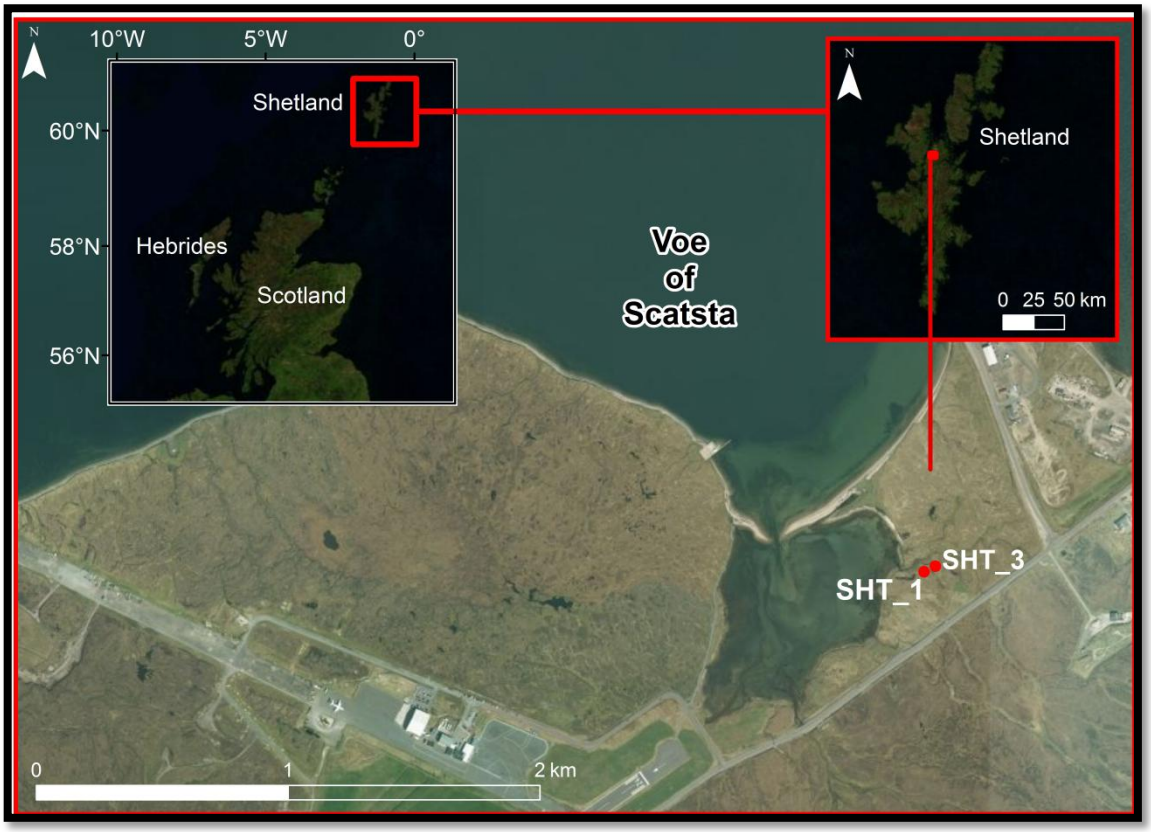

Figure 5.3.1 – Location of cores obtained in Voe of Scatsta, Shetland Islands.

Both studied cores presented similar lithostratigraphies (Figure 5.3.3). The exposed trench walls revealed a basal peat unit of *ca.* 0.30m. This unit is overlaid by a medium to coarse sand layer with an erosional contact at the base and an uncorformity at the top of the unit. Moreover, this unit also exhibited

some centimetric pebbles and rare cobbles although it did not present very rich shell content. On top of this sandy unit, a peat layer, sharing many of the characteristics of the basal unit, is present. The top 0.10m are composed of dark brown soil with many roots and plant fragments.

Figure 5.3.2 – Photo of the trench wall (left image) were sample SHT_1 was collected. Detail of the tsunamigenic unit (right image; blue rectangle is app. 0. 10 m).

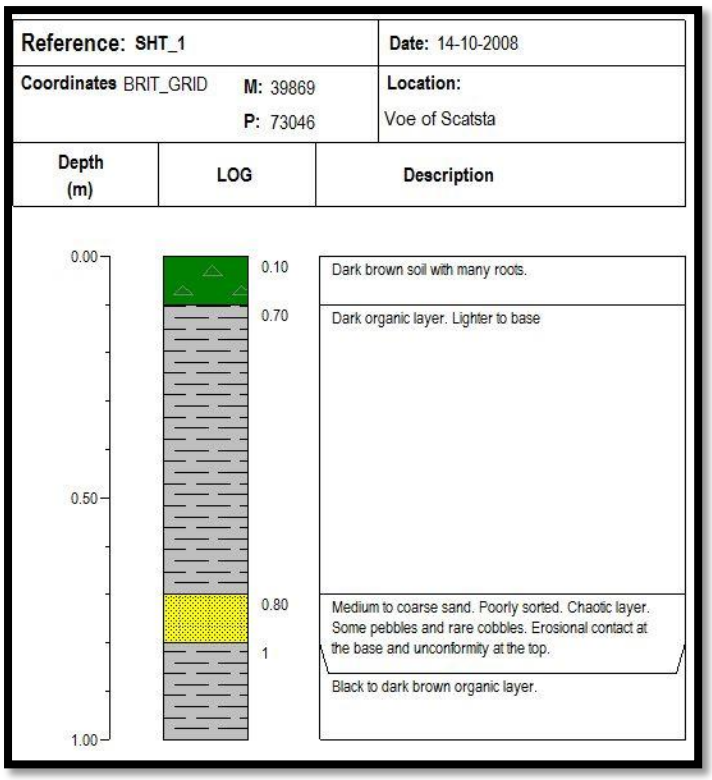

Figure 5.3.3 – Lithostratigraphy of core SHT_1 retrieved in Voe of Scatsta.

The proposed chronology for this sandy layer and its association with a specific tsunamigenic event will be discussed in the following chapter based in radiocarbon dates obtained by other authors (Bondevik *et al.*, 2005; Dawson *et al.*, 2006).

5.3.2. Textural features

Grain-size distribution and parameters were measured and the vertical and horizontal variation in textural propertied were measured in all samples (Table 5.3.1). The coarse sediment consists of medium to coarse, moderately sorted, quartziferous sand. Samples reveal contrasting behaviour in terms of vertical trends for 1%ϕ, 10% ϕ, 90% ϕ, mean, mode and median. While the sediment in core SHT_1 display a fining upward trend, core SHT_3 reveals a coarsening upward sequence, although the low number of samples constrains further interpretations and extrapolations of these results. On the other hand, only kurtosis exhibits an identical pattern in both cores (SHT_1 and SHT_3), the values being higher at the base of the unit.

In terms of horizontal variation, the sample closest to the shoreline (SHT_1) is slightly coarser at the base and also when averaging the mean values obtained for each sample pair, but the top sand in each core shows an opposite trend. Standard deviations are almost identical in all samples. Thus, textural data did not allow the establishment of any consistent trend of vertical or horizontal variation in grain size.

Table 5.3.1 - Summary from the textural results obtained for samples collected in Voe of Scatsta.

Sample	Depth (m)	1% ϕ	10% ϕ	90 % ϕ	Mean (MZ) ϕ	Graphic Std Deviation (σ1)	Graphic Kurtosis (K_G)	Simple Sorting Measure (SSM)	Mode ϕ	Median ϕ
SHT_1	0.22-0.24	-0.83	-0.02	2.69	1.24	1.06	1.01	1.76	0.75	1.17
SHT_1	0.26-0.28	-1.51	-0.68	2.23	0.64	1.13	1.13	1.89	0.25	0.57
SHT_3	0.22-0.25	-1.15	-0.37	2.47	0.99	1.07	1.13	1.87	0.25	0.88
SHT_3	0.25-0.28	-0.97	-0.18	2.59	1.20	1.07	1.44	1.80	1.25	1.28

In terms of micromorphological changes (Figure 5.3.4) the major changes observed were related with the size of clasts and grains (consistently smaller towards the top of the unit), this trend being accompanied by the decrease in abundance of plant fragments and by decrease in the voids (higher compaction of the sediment at the base of the deposit).

Figure 5.3.4 – Image of a 7.5x4.5 cm thin section from sample SHT_3 (22-30).

5.3.3. Morphoscopy features

Morphoscopic characteristics were measured in samples from core SHT_1 and SHT_3. Results are summarized in Figures 5.3.5, 5.3.6 and 5.3.7. In compositional terms it was possible to observe that a very high percentage of quartz was detected [*i.e.* from 50% in sample SHT_3_(23-25) up to 65% in sample SHT_1_(22-24)]. Moreover, one should take into account that (contrary to the cases of Lagoa dos Salgados and Boca do Rio) the bioclasts observed were essentially (>90%) plant fragments and not carbonate shells. Samples from core SHT_3 presented less bioclasts (*ca.* 10%) than samples from core SHT_1 (*ca.* 25%). Moreover, it was also possible to detect that the percentage of lithic material is higher at the base of the unit when compared with overlying samples (the difference between base and top varying between 6% and 12%).

In terms of roundness of the quartz grains observed (Figure 5.3.6) it was possible to observe that the well-rounded and rounded grains are typically present in percentages around 60% to 65% and are more frequent at the base of the sand in both cores. Very angular and angular grains are more frequent at the top samples in each core, with values between 15% and 20%.

Regarding shape (Figure 5.3.7), the results show that spherical grains were more frequently found (7% in SHT_1 and 3% in SHT_3) at the base of the sand unit, whereas more discoid grains showed more frequently at the top. In terms of shape all samples presented values within a narrow range.

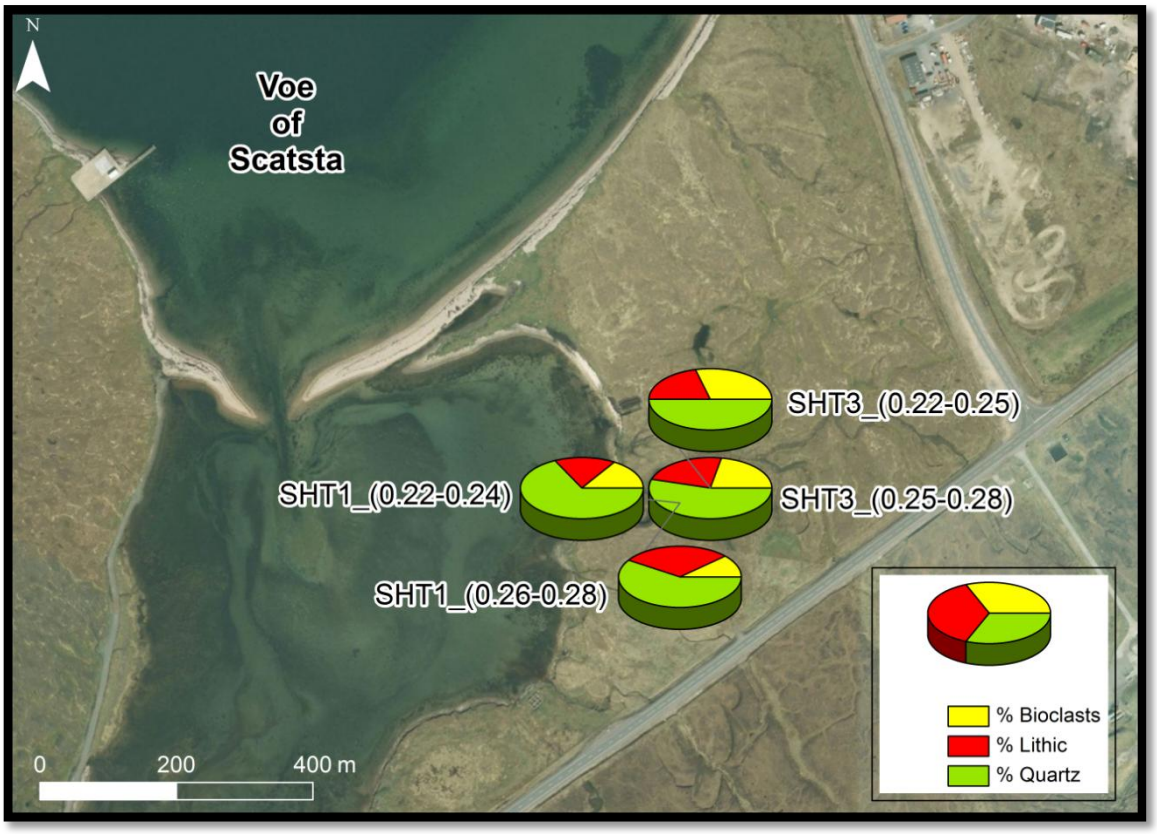

Figure 5.3.5 – Morphoscopic compositional features of samples retrieved from Voe of Scatsta.

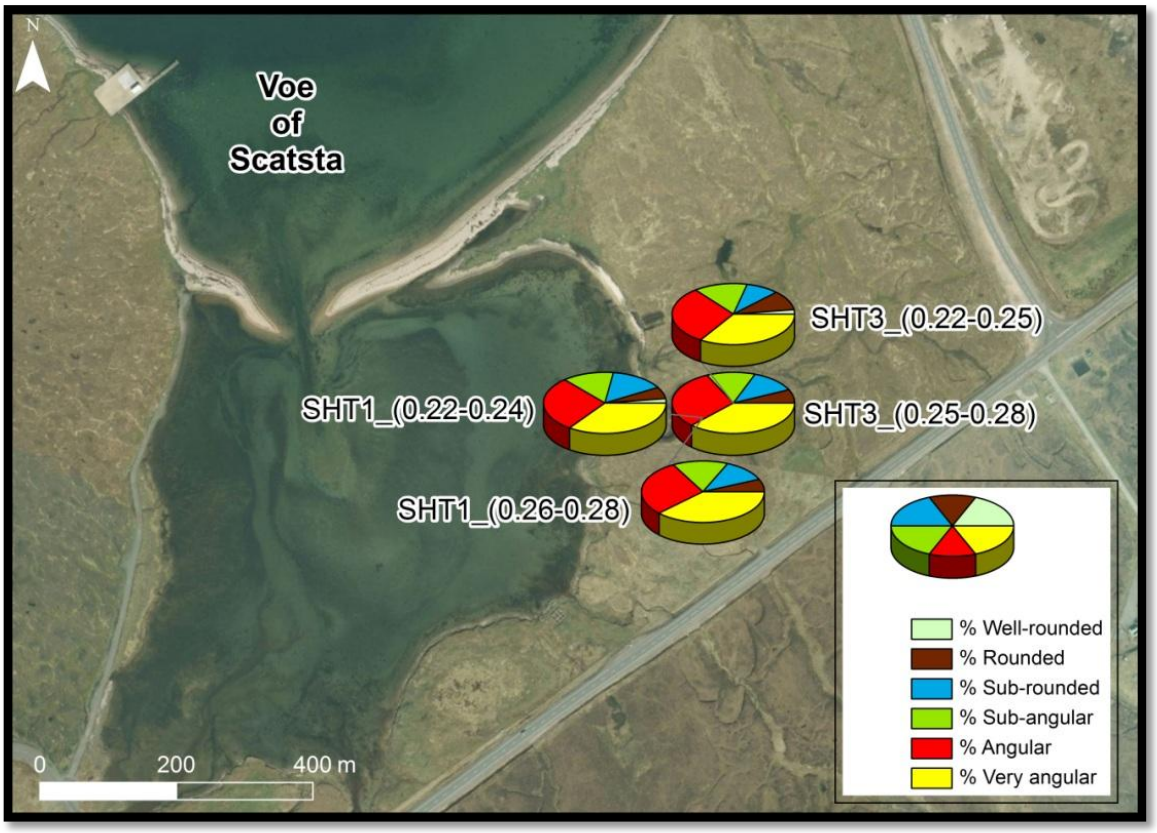

Figure 5.3.6 – Roundness classification for quartz grains from samples collected in the Voe of Scatsta.

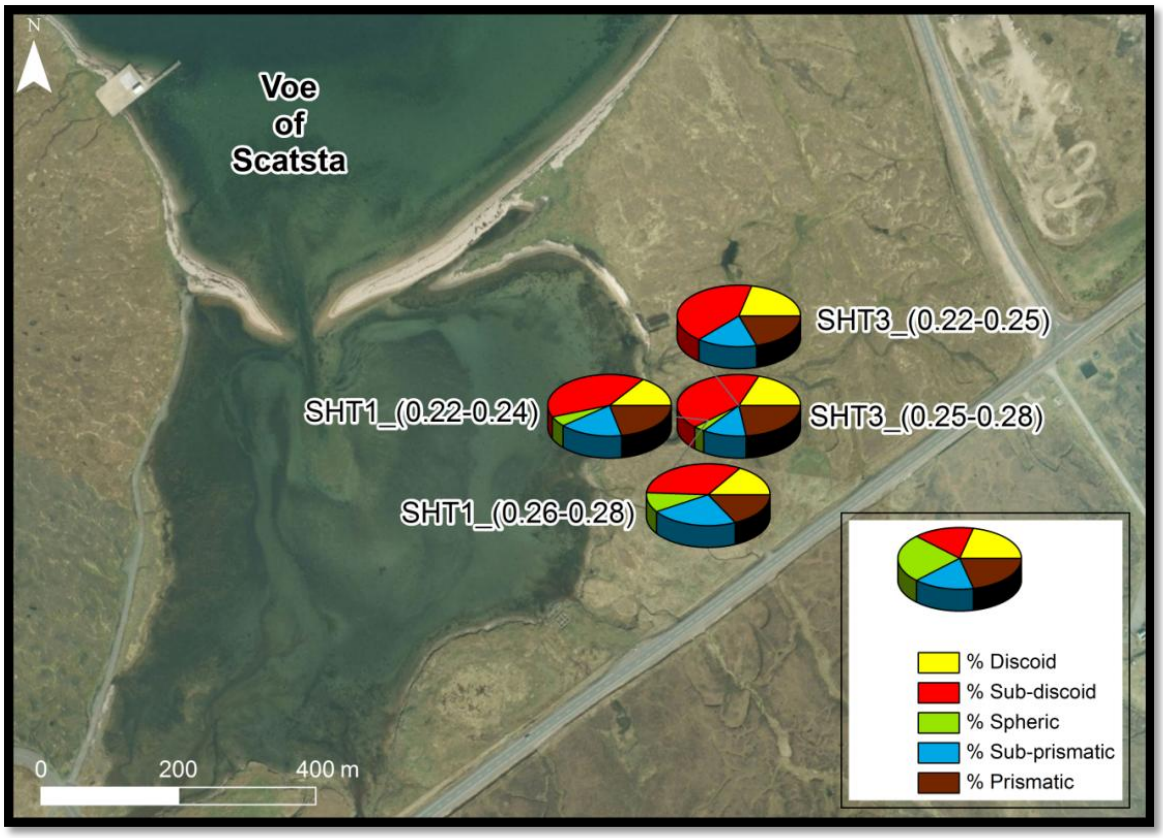

Figure 5.3.7 - Shape classification for quartz grains from samples collected in the Voe of Scatsta.

As a summary, it can be said that morphoscopy was not totally conclusive in the establishment of vertical or horizontal trends with the exception of the presence of more lithic material at the base of the high-energy sandy deposit and more angular grains at the top.

5.3.4. Microtextural features

The vertical variation in microtextural features was assessed in tsunamigenic sediment from the Voe of Scatsta (Figure 5.3.8 and Table 5.3.2). It was possible to detect that angularity increases towards the top, particularly in core SHT_3. In terms of fresh surfaces the samples studied displayed values in the range 2.0 [SHT_1_(22-24)] to 3.3 [*i.e.* SHT_3_(22-25)]. Dissolution features are higher at the base than at the top of the tsunamigenic unit in both cores (1.2 to 3.3 in core SHT_1 and 1.8 to 2.5; top and base respectively). Regarding adhering particles the values obtained were very high in sample SHT_1_(22-24, with 4.4) while the other samples yielded results in the range of 1.4 to 1.1 for adhering particles. On the other hand, results obtained for percussion marks results were similar within each core but contrasting between core SHT_1 and SHT_3, with the latter presenting significantly lower values.

The microtextural analysis of the four samples retrieved from the Voe of Scatsta shows that these proxies are to some extent useful to highlight vertical variation of features within the tsunamigenic unit.

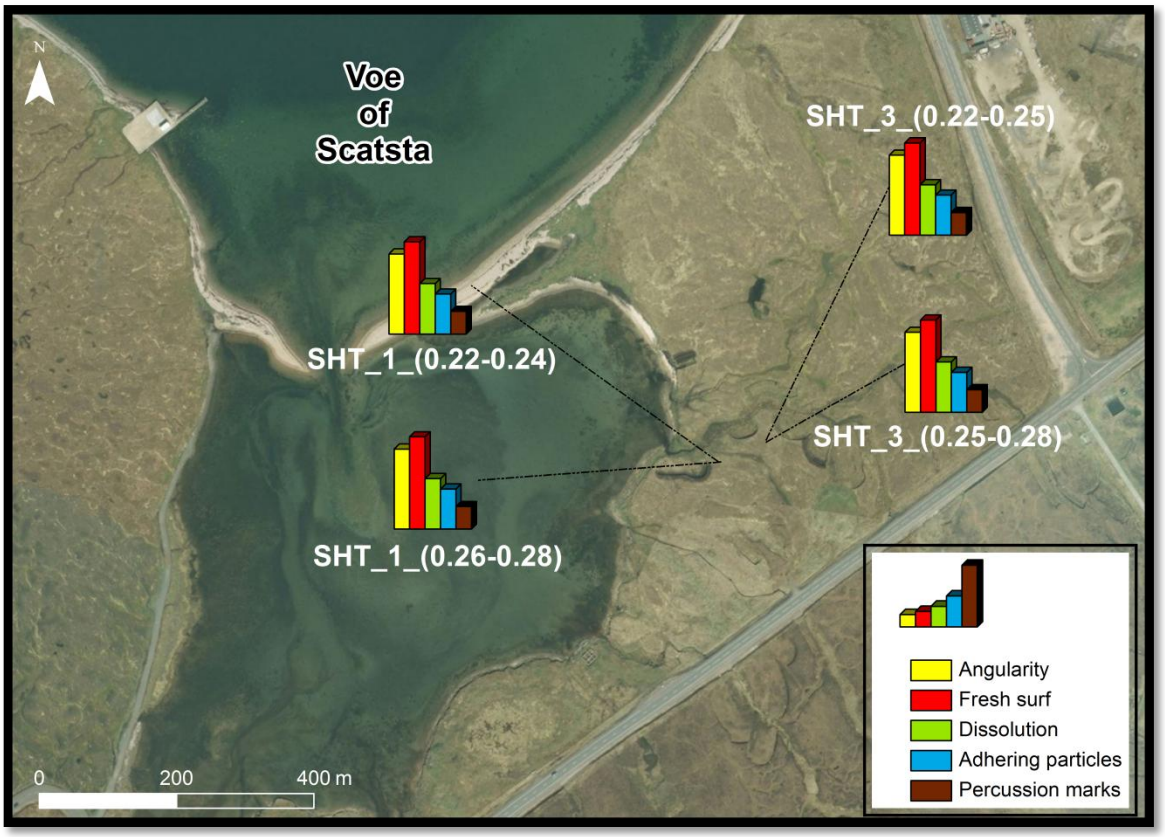

Figure 5.3.8 - Microtextural features results and spatial distribution in samples retrieved from the Voe of Scatsta.

Table 5.3.2 - Summary of microtextural results obtained in samples from Voe of Scatsta.

Sample	Depth (m)	Number of grains	Angularity	Fresh surfaces	Dissolution	Adhering particles	Percussion marks
SHT_1	0.22-0.24	12	3.217	2.000	1.217	4.435	0.174
SHT_1	0.26-0.28	12	3.167	2.667	3.250	2.083	0.010
SHT_3	0.22-0.25	16	2.875	3.313	1.813	1.438	0.813
SHT_3	0.25-0.28	15	1.867	2.733	2.533	2.200	0.800

5.3.5. Heavy mineral features

Heavy mineral assemblage was studied in four samples from cores SHT_1 and SHT_3. In terms of the percentage of heavy minerals in total sediment it was possible to differentiate the two cores SHT_1 (values of 0.52% to 0.59%) and SHT_3 (values of 0.826% and 0.827%- virtually identical) (Table 5.3.3).

Table 5.3.3 - Percentage of heavy mineral content in total sediment of samples from Voe of Scatsta.

Sample	Depth (m)	% of Heavy minerals in total sediment
SHT_1	0.22-0.24	0.527
SHT_1	0.26-0.28	0.585
SHT_3	0.22-0.25	0.826
SHT_3	0.25-0.28	0.827

The heavy mineral assemblages of samples from cores SHT_1 and cores SHT_3 are strongly dominated by amphiboles with a presence of more than 88.95% (Figure 5.3.9 and Table 5.3.4). This mineral is also more frequent at the basal samples in each core. By contrast, andalusite exhibited smaller results for the basal samples (3.302% and 2.941%, for SHT_1 and SHT_3, respectively) when compared with overlying samples (5.233% and 5.128%, for SHT_1 and SHT_3, respectively). Pyroxene and garnet did not demonstrate any clear vertical trend and showed very low values of less than 1.80%. Other minerals (*e.g.* zircon, silimanite and staurolite) revealed presence of around 2.3% with the exception of sample SHT_3_(25-28) with 1.291%.

Heavy mineral assemblages contributed to the establishment of vertical trends within the sandy deposit, although the low number of samples might constrain generalizations.

Table 5.3.4 - Heavy mineral assemblages in sand samples of Voe of Scatsta.

Sample	Depth (m)	% Andalusite	% Pyroxene	% Amphibole	% Garnet	% Others
SHT_1	0.22-0.24	5.233	1.744	88.953	1.744	2.361
SHT_1	0.26-0.28	3.302	1.415	92.453	0.472	2.366
SHT_3	0.22-0.25	5.128	1.282	91.667	0.641	2.334
SHT_3	0.25-0.28	2.941	0.588	92.941	1.176	1.291

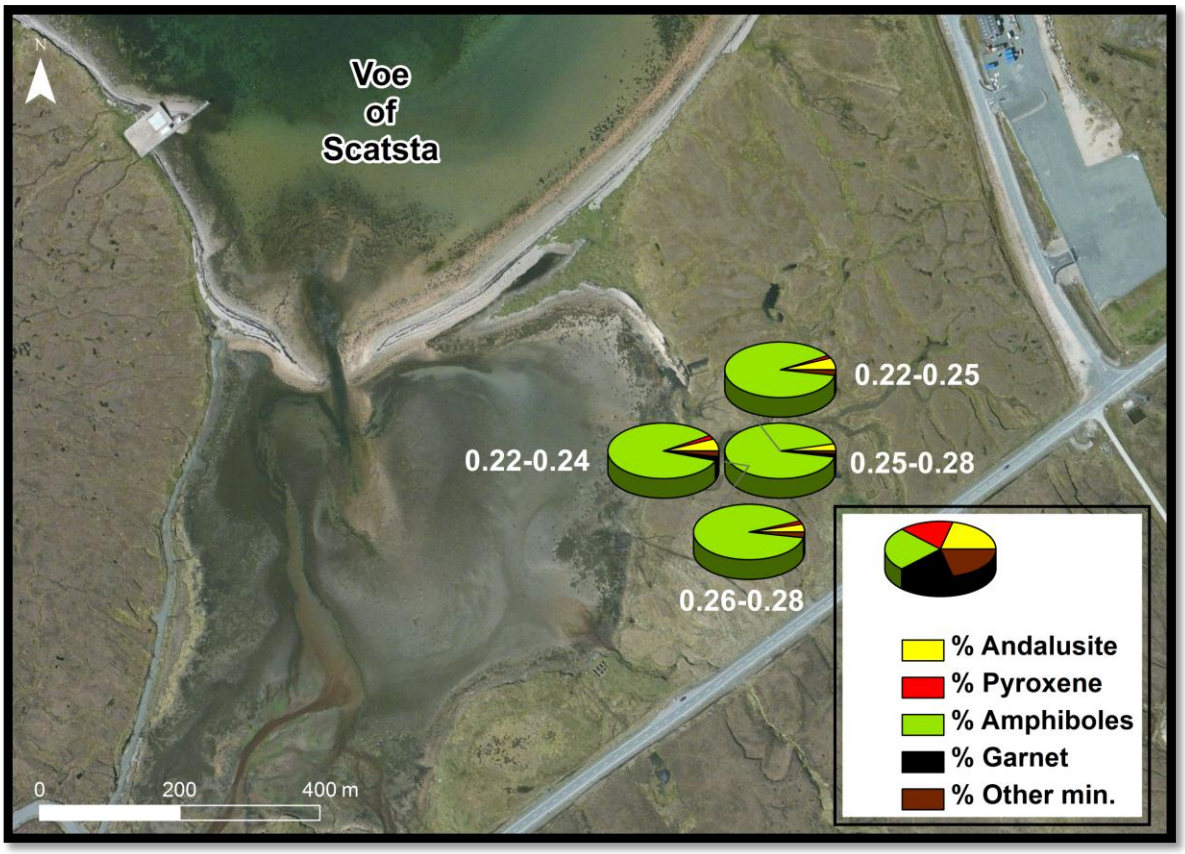

Figure 5.3.9 - Heavy mineral composition of tsunamigenic samples collected in Voe of Scatsta.

5.4. Lhok Nga

5.4.1. Lithostratigraphic features

Samples used in this study were collected a few weeks after the tsunami event of 26 December 2004. Figure 5.4.1 illustrates the spatial distribution of the samples retrieved: two samples from present-day analogues (*i.e.* nearshore and beach) and four locations corresponding to a sampling profile inland (NGA_2, NGA_7, NGA_9 and NGA_18). It is important to note that locations NGA_2 and NGA_7 yielded more than one sample of the tsunamigenic sediment and were collected to assess vertical variations within it.

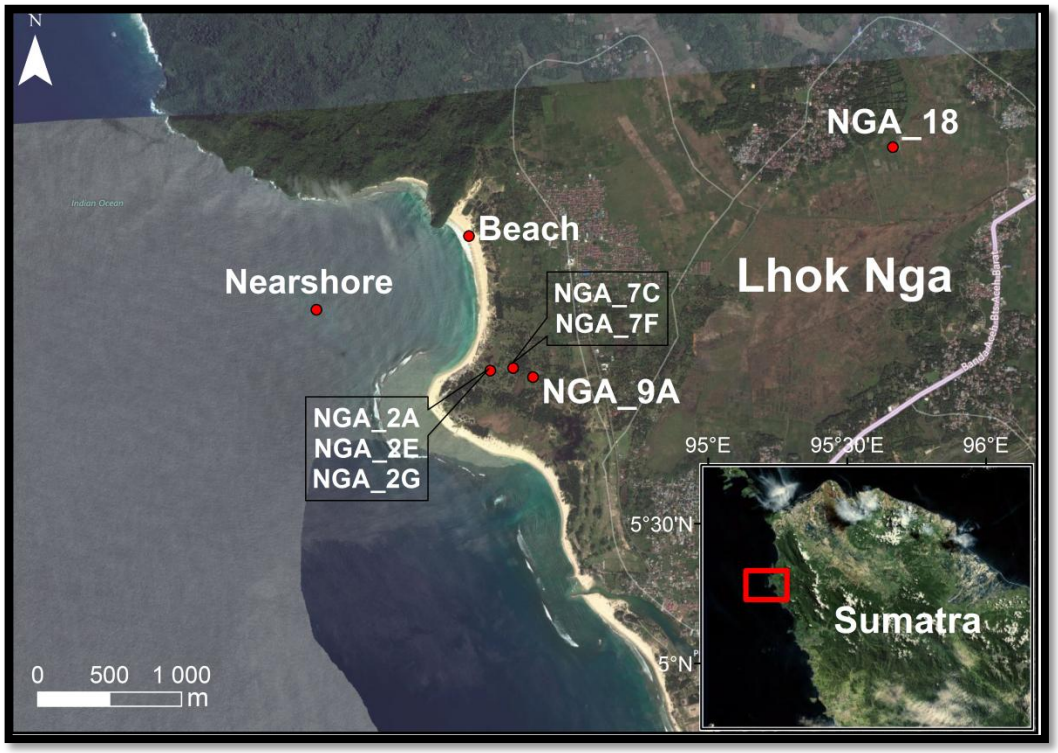

Figure 5.4.1 - Location maps of the Lhok Nga Bay and collected samples (Paris *et al.*, 2007).

The 2004 tsunami deposits in this area consist of medium to coarse, greyish to yellowish sands, which display lateral variations in thickness and grain-size and vertical variations in texture. The deposits settled on top of brown sandy soils, dune sands or beachrock near the coast, reddish fluvial sands in the rivers, and dark brown silty soil in the rice paddies (Paris *et al.*, 2007). The lower contact of the tsunami unit is abrupt or erosional when in contact with underlying sand. The thickness of the tsunami deposits decreases landward.

In Lhok Nga, the tsunami deposit displayed stratification into distinct layers in some sampling locations, and in cases up to 15 layers could be distinguished in the field. Typically, the basal layers are coarser and massive and separated by thin mud lines (in cross section) from the upper part that is usually finer. A landward increasing content of rip-up clasts of the locally underlying soil, roots, wood, leaves and anthropic clasts (glass, brick, metal, plastic, *etc.*) was detected.

In some trenches the topmost layer was considered as the backwash deposit, when it is coarser than the lower normally-graded couplet of layers (*e.g.* NGA_2G and NGA_7F).

The schematic lithostratigraphy (including all the samples used in this study) is described in Figure 5.4.2.

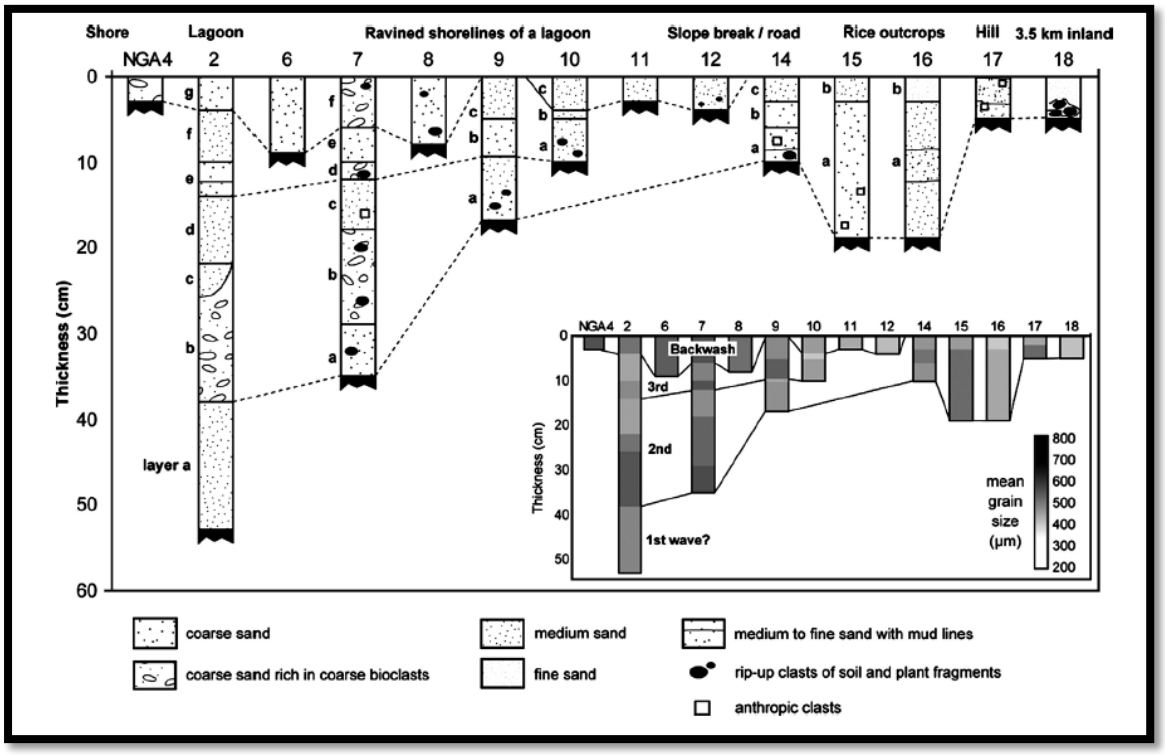

Figure 5.4.2 - Sequence stratigraphy and interpretation of the vertical trends along the Lhok Nga transect (Paris *et al.*, 2007).

5.4.2. Textural features

Based in the mean grain size (Table 5.4.1), all samples are within the medium to coarse sand interval (except NGA_18). Furthermore, using samples NGA_2A, NGA_7C, NGA_9A and NGA_18 is possible to establish a decreasing inland grain-size trend. For the same samples it can also be observed that NGA_18 (farther inland) presents the smaller mean grain size 2.10 ϕ.

The backwash samples NGA_2G and NGA_7F exhibit an opposite trend with finer material (NGA_2G = 0.78 ϕ; NGA_7F = 0.42 ϕ) closer to the coast.

Table 5.4.1 - Mean grain size of samples retrieved from Lhok Nga (data provided by R. Paris).

Sample	Sed. Env.	Mean (MZ) Φ
NGA_2A	Tsunami	1.03
NGA_2E	Tsunami	1.08
NGA_2G	Tsunami	0.78
NGA_7C	Tsunami	1.02
NGA_7F	Tsunami	0.42
NGA_9A	Tsunami	1.19
NGA_18	Tsunami	2.10

5.4.3. Morphoscopy features

Morphoscopic analysis was conducted in samples from Lhok Nga and results are shown as figures to visualize spatial distribution (Figure 5.4.3, 5.4.4 and 5.4.5).

In compositional terms (Figure 5.4.3), samples from Lhok Nga, reveal quartz content in the range of 35% to 45%, except samples NGA_2G with the higher value of 50.0% and NGA_7F with the lower value of 28.1%; interestingly both samples represent backwash sediment. Regarding lithic material, the values are consistently within the 15%-20% range, except for samples NGA_7C and NGA_18 with 8.57% and 11.61% respectively. The carbonate bioclasts are present typically in percentage of *ca.* 45% with two exceptions, both backwash samples, presenting contrasting values (55.2% for sample NGA_7F and 33.7% for sample NGA_2G, respectively the highest and the lowest values observed).

Quartz grains from samples studied were classified in terms of roundness (Figure 5.4.3) and sphericity (Figure 5.4.4). Sediment deposited by backwash presented the higher values of well-rounded and rounded grains (11% and 37%, respectively NGA_2G and NGA_7F) whereas all other samples presented results of less than 9%. In terms of very angular and angular grains the highest values were observed in sand at the base of trench 2 (NGA_2A), 9 (NGA_9A) and 18 (NGA_18) with values of 83.3%, 78.4% and 87.2% respectively. On the other hand spherical grains represent less than 6% in all samples, except the backwash sediment (NGA_2G and NGA_7F) with 10.9% and 20.0%, respectively. The grains also revealed a well-balanced distribution between prismatic and discoid shapes.

As a summary it can be concluded that morphoscopic results slightly contributed to the differentiation of samples of the base of the tsunamigenic unit (roundness characteristics) and of the backwash (percentage of bioclasts and sphericity characteristics).

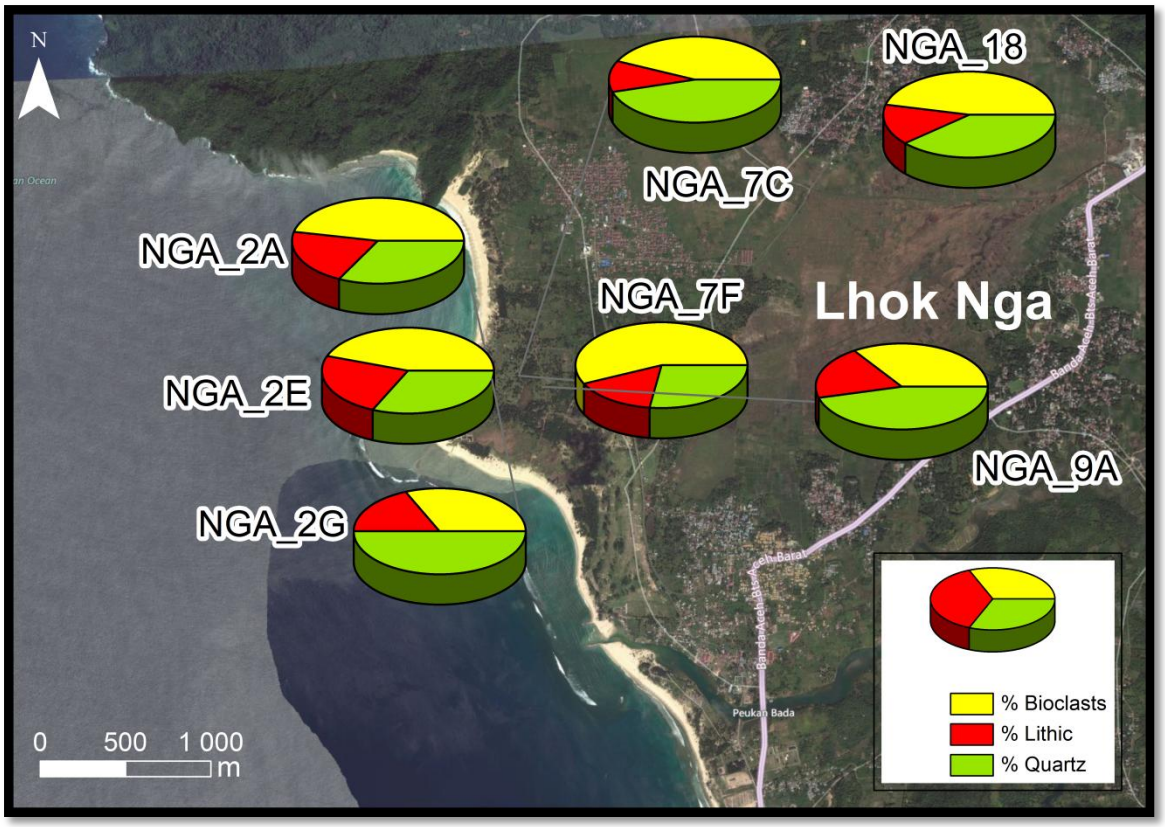

Figure 5.4.3 - Morphoscopic compositional features of samples retrieved from Lhok Nga.

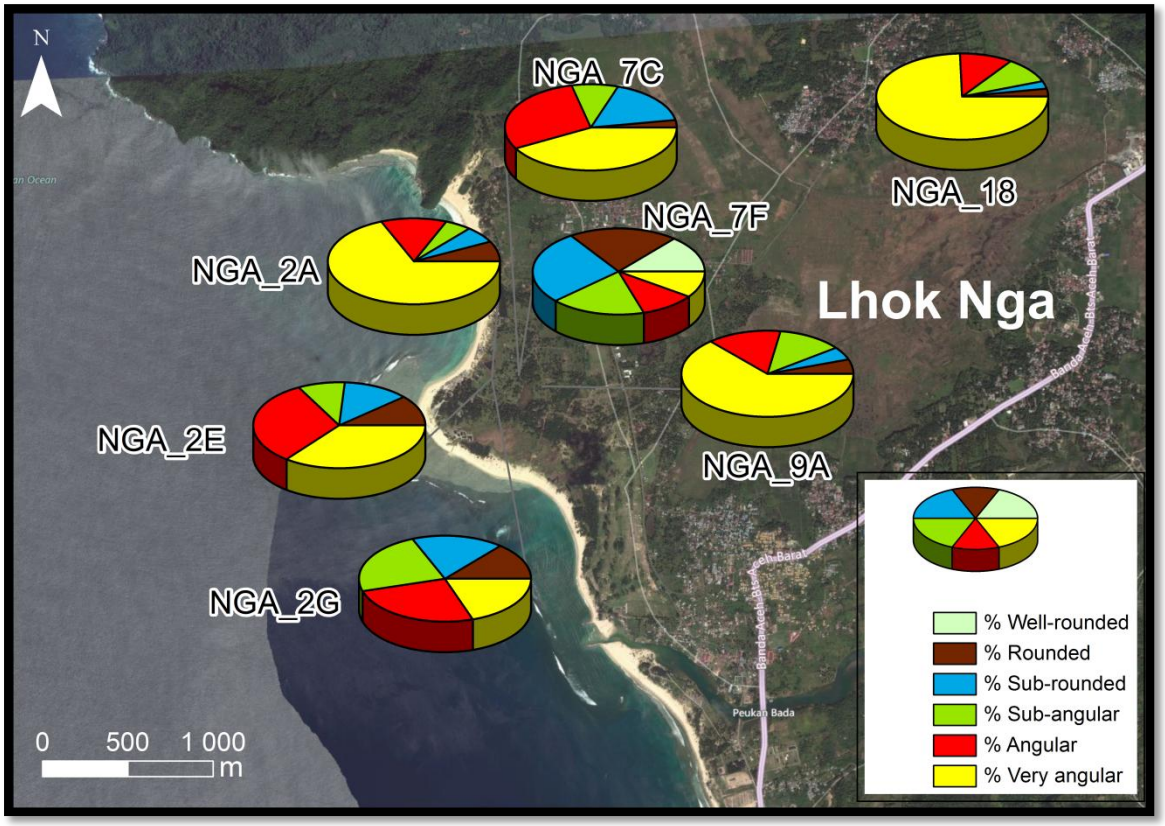

Figure 5.4.4 - Roundness classification for quartz grains from samples collected in Lhok Nga.

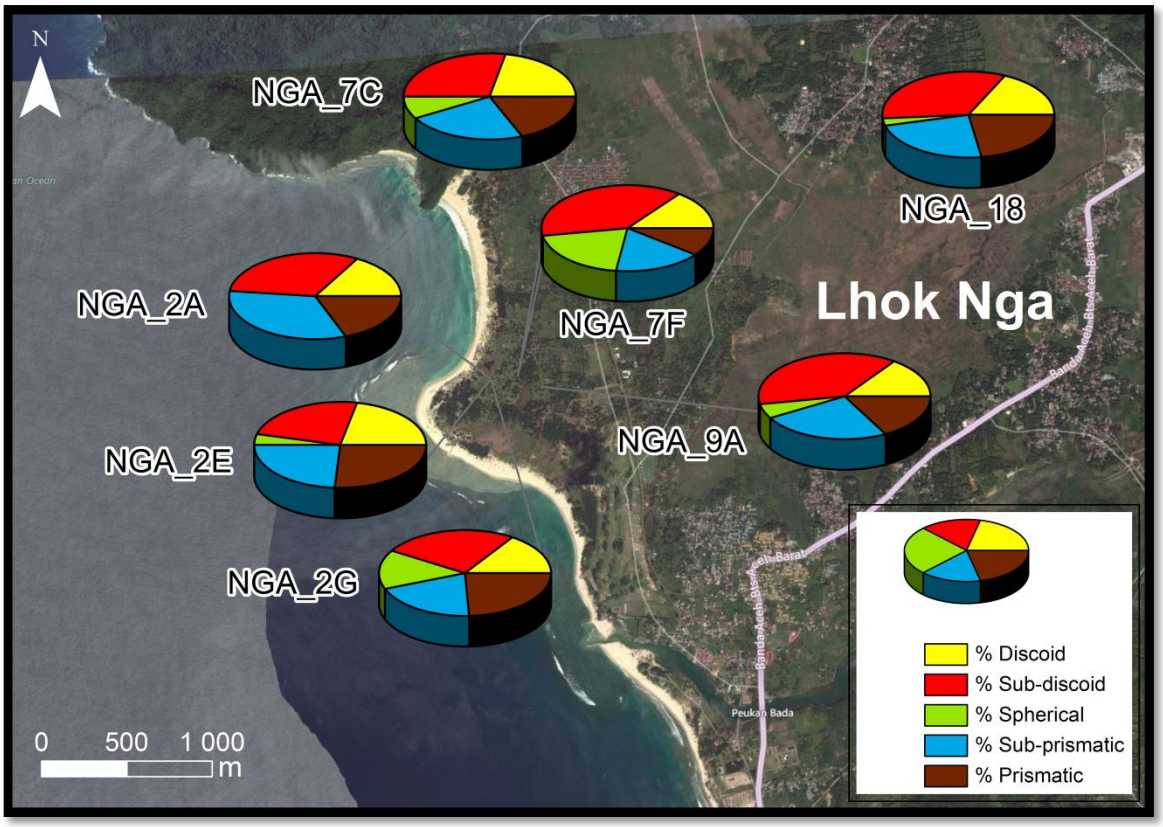

Figure 5.4.5 - Shape classification for quartz grains from samples collected in Lhok Nga.

5.4.4. Microtextural features

Microtextural features were observed and classified in samples from Lhok Nga. Regarding angularity, the samples present higher values inland (*e.g.* NGA_9A=4.00) but no consistent spatial trend could be established. Samples from trench NGA_2 exhibit increasing values towards the top of the tsunamigenic unit but the same pattern is not present in trench NGA_7. In terms of fresh surfaces, it was observed that all samples displayed results < 3, except in the case of backwash sediment (NGA_2G, with a result of 3.571 and NGA_7F with a result of 3.429) and sample NGA_7C with a result of 3.276. In trenches NGA_2 and NGA_7 it was observed that fresh surfaces increase towards the top of the tsunamigenic unit. Values of dissolution features are extremely low (*i.e.* <1.6) in all cases, except for samples NGA_18 and NGA_nearshore (the latter presenting the highest value). In what respects adhering particles it was observed that the highest values (above 4.3) were noticed in the nearshore and beach sample with the lower values being obtained in the NGA_2A and NGA_2F samples (1.938 and 1.357, respectively). Percussion marks increase to the top in trenches NGA_2 and NGA_7, and the highest value was observed in sample NGA_7F (backwash, result of 1.643), while the lowest value was yielded by sample NGA_18 (0.010).

Microtextural results solely reveal vertical variations within the tsunamigenic unit in fresh surfaces and percussion marks (increasing to the top) and that the highest values were identified in the sediment deposited by backwash.

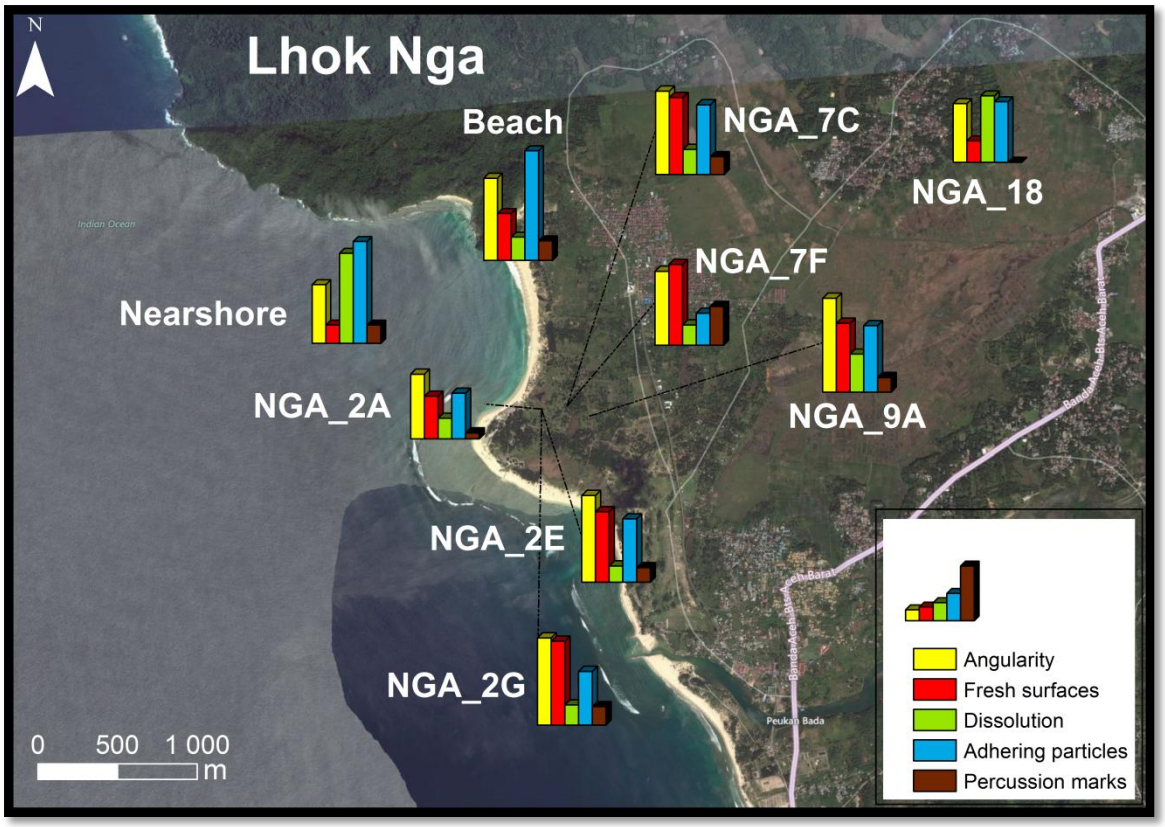

Figure 5.4.6 - Spatial distribution of microtextural results in sediments retrieved from Lhok Nga.

Table 5.4.2 - Summary of microtextural results obtained in samples from Lhok Nga.

Sample	Depth	Sed. Env.	Number of grains	Angularity	Fresh surfaces	Dissolution	Adhering particles	Percussion marks
NGA_2A	Sup	Tsunami	16	2.750	1.813	0.875	1.938	0.250
NGA_2E	Sup	Tsunami	13	3.692	3.000	0.692	2.692	0.615
NGA_2G	Sup	Tsunami	14	3.714	3.571	0.857	2.286	0.786
NGA_7C	Sup	Tsunami	29	3.552	3.276	1.069	2.966	0.759
NGA_7F	Sup	Tsunami	14	3.143	3.429	0.857	1.357	1.643
NGA_9A	Sup	Tsunami	29	4.000	2.931	1.621	2.828	0.621
NGA_18	Sup	Tsunami	24	2.500	0.917	2.833	2.583	0.010
Ind_nearshore	Sup	Nearshore	19	2.500	0.778	3.833	4.333	0.778
Ind_beach	Sup	Beach	6	3.500	2.000	1.000	4.667	0.833

5.4.5. Heavy mineral features

In terms of heavy mineral content in total sediment (Table 5.4.3) the studied samples from Lhok Nga exhibited extremely low values (<0.001%) in all samples.

Table 5.4.3 - Percentage of heavy mineral content in total sediment of samples from Lhok Nga.

Sample	Sedimentary Environment	% of Heavy minerals in total sediment
NGA_2A	Tsunami	<0.001
NGA_2G	Tsunami	<0.001
NGA_7C	Tsunami	<0.001
NGA_9A	Tsunami	<0.001
NGA_18	Tsunami	<0.001

In terms of heavy mineral assemblage (Figure 5.4.7 and Table 5.4.4), it was observed that amphiboles is the more frequent mineral specimen although presenting a wide range of values from 47.500 (*i.e.* NGA_18) up to 85.976% (*i.e.* NGA_7C). In what concerns andalusite, it was observed that the highest results were observed in the sample closest to the coastline (*i.e.* NGA_2A) and in the sample farther inland (*i.e.* NGA_18) with 35.294% and 38.750%, respectively. The minimum value observed in percentage of andalusite was in sample NGA_7C. Regarding pyroxene, presented its higher values in samples NGA_2A (*i.e.* 7.843%) and NGA_18 (*i.e.* 2.500%) while its lower results were registered in samples NGA_7C (*i.e.* 0.610%) and NGA_9A (*i.e.* 0.962%). Samples NGA_2G (backwash sample) presented more zircon (*i.e.* 4.065%) and garnet (*i.e.* 2.439%) than the other samples that exhibited values of less than 3% and 2%, with the exception of sample NGA_18 that showed values of 2.500% and 7.500% for garnet and zircon, respectively. Other minerals were not observed in this group of samples. No peculiar vertical or horizontal heavy mineral assemblage trend was evident in this group of samples.

Table 5.4.4 - Results from heavy mineral assemblages in Lhok Nga samples.

Sample	% Andalusite	% Pyroxene	% Amphibole	% Garnet	% Zircon	% Others
NGA_2A	35.294	7.843	51.961	0.001	2.941	0
NGA_2G	13.821	1.626	76.423	2.439	4.065	0
NGA_7C	7.927	0.610	85.976	0.001	1.829	0
NGA_9A	12.500	0.962	74.038	1.923	1.923	0
NGA_18	38.750	2.500	47.500	2.500	7.500	0

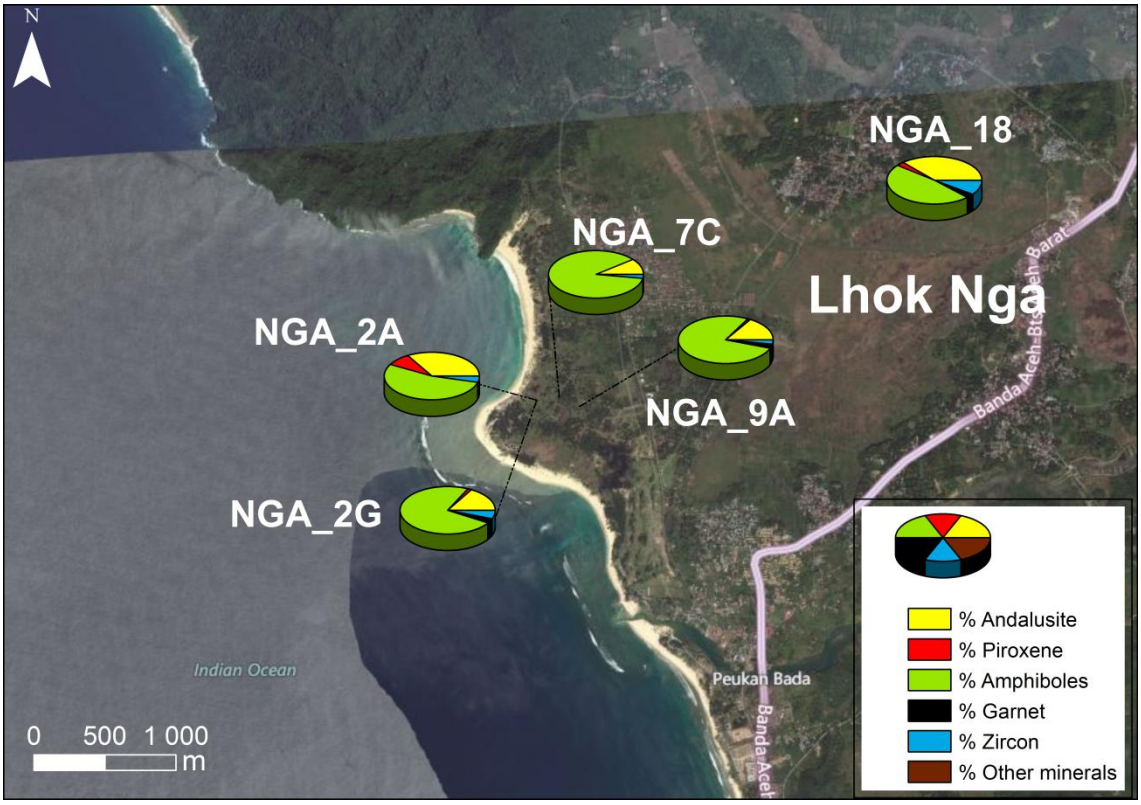

Figure 5.4.7 - Heavy mineral composition of tsunamigenic samples collected in Lhok Nga.

5.5. Stoneybridge

5.5.1. Lithostratigraphic features

A tempestite sandy deposit retrieved immediately after the Great Storm of the 11th of January of 2005 was used in this research. The storm damage was particularly felt by the south-facing coastal areas in South Uist and Benbecula (Hebrides Islands) which experienced the severest storm wave activity during this January 2005 storm. Near Stoneybridge (Figure 5.5.1), a beach ridge was breached by the waves, resulting in widespread flooding inland together with the deposition of fans of gravel and sand some of which are up to 35 cm in thickness (Angus and Rennie, 2007). This discontinuous (medium to fine sand) unit, with varying thickness, was recognised up to 150m landward of the coastal dunes and are draped over the machair.

In the core used in this study (Figure 5.5.2) a 0.10m thick sand layer was recovered and four samples (at different depth in that core) were used in all sedimentological analyses that are presented below.

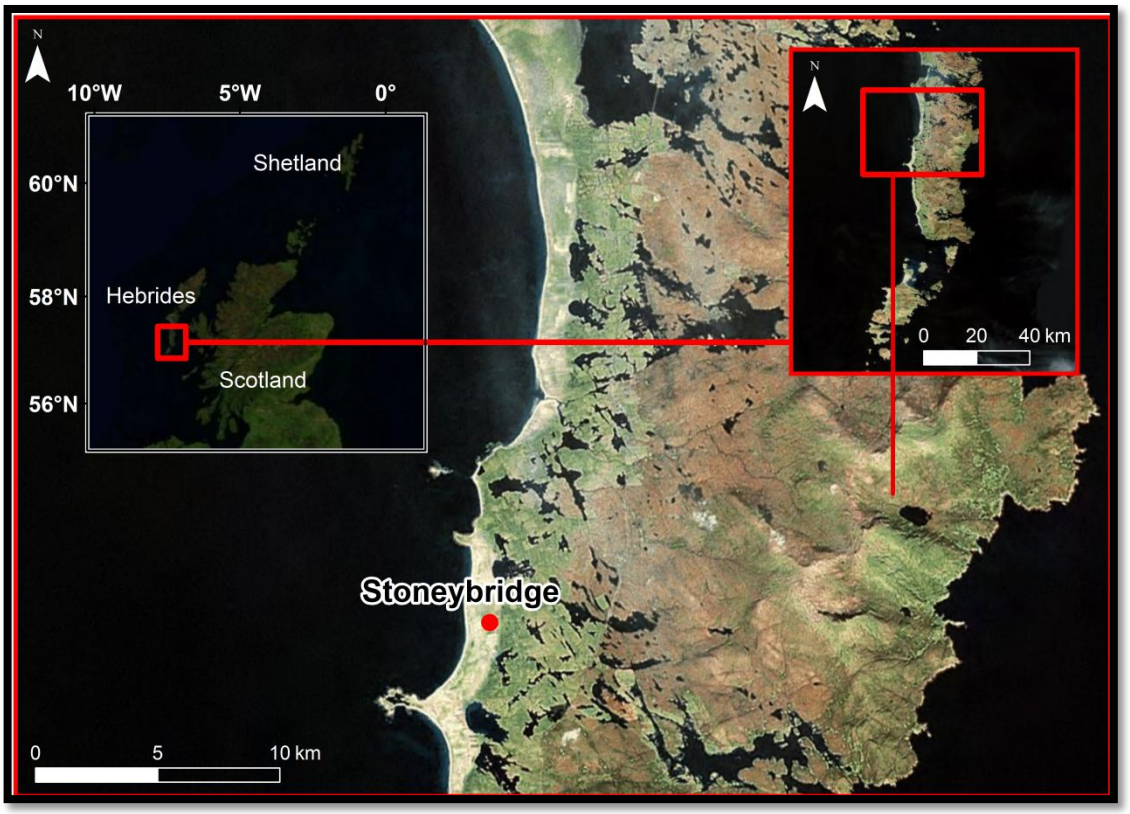

Figure 5.5.1 - – Location of samples obtained in Stoneybridge, Hebrides Islands

Figure 5.5.2 - Image of the sandy storm deposit retrieved from Stoneybridge.

5.5.2. Textural features

Grain-size parameters were measured in the four samples collected in Stoneybridge (Table 5.5.1). The samples are all composed of fine sand and the mean grain-size is of *ca.* 2.45 ϕ, except sample HB_(0.05-0.06) that is slightly coarser (2.1 ϕ). The standard deviation is similar in all samples with the lowest value of 0.36 ϕ in the top sample and the highest value of 0.58 ϕ in sample HB_(0.05-0.06). Kurtosis revealed decreases towards the top of the unit. It was also noticed that base and top of the tempestite present identical median values.

Table 5.5.1 - Summary of textural characteristics of samples retrieved from Stoneybridge.

Sample	Depth (m)	1% ϕ	10% ϕ	90% ϕ	Mean (MZ) ϕ	Graphic Std Deviation (σ1)	Graphic Kurtosis (K_G)	Simple Sorting Measure (SSM)	Mode ϕ	Median ϕ
HB	0.02-0.03	1.29	2.02	2.91	2.49	0.36	1.09	0.62	2.75	2.51
HB	0.05-0.06	0.54	1.23	2.73	2.08	0.58	1.01	0.95	2.25	2.18
HB	0.07-0.08	0.89	1.80	2.92	2.44	0.44	1.18	0.78	2.75	2.48
HB	0.09-0.10	0.77	1.72	2.99	2.46	0.52	1.28	0.95	2.75	2.51

5.5.3. Morphoscopy features

Morphoscopic characteristics were observed in four samples from the tempestites retrieved from Stoneybridge (Figure 5.5.3, 5.5.4, 5.5.5 and 5.5.6). The samples are dominated by variable but generally high abundance of bioclasts, around 45% (mainly dominated by plant fragments but also with infrequent shell material). The top presented 60% of bioclasts wheareas the base yielded 70% of bioclasts. On the

other hand, quartz occurs in proportions of *ca.* 30%, except in the base of the unit with 15%. All samples present low percentage of lithic materials (app. 20%) although the base of the unit displayed 7% and the top 14% in lithics. Figure 5.5.4 shows the roundness classification of grains from the storm deposit. The samples yielded low values for well-rounded and rounded grains, with 23.5% at the base and less than 6.7% in every other case. In what concerns very angular and angular grains they are especially abundant in samples HB_(0.05-0.06) and HB_(0.07-0.08) with 72% and 75%, the remaining samples exhibiting values above 53%. Figure 5.5.5 displays the sphericity results obtained for the same group of samples. It is possible to observe that spherical samples are rare (less than 10% of grains) in two samples, HB_(0.05-0.06) and HB_(0.09-0.10), this type of shape being absent in all remaining samples. The grains from the storm deposit are typically discoid or sub-discoid, occurring from base to top in percentages of 68%, 68%, 60% and 63%.

In the case of the tempestite retrieved from the Hebrides no vertical trend was recognized solely based in this proxy.

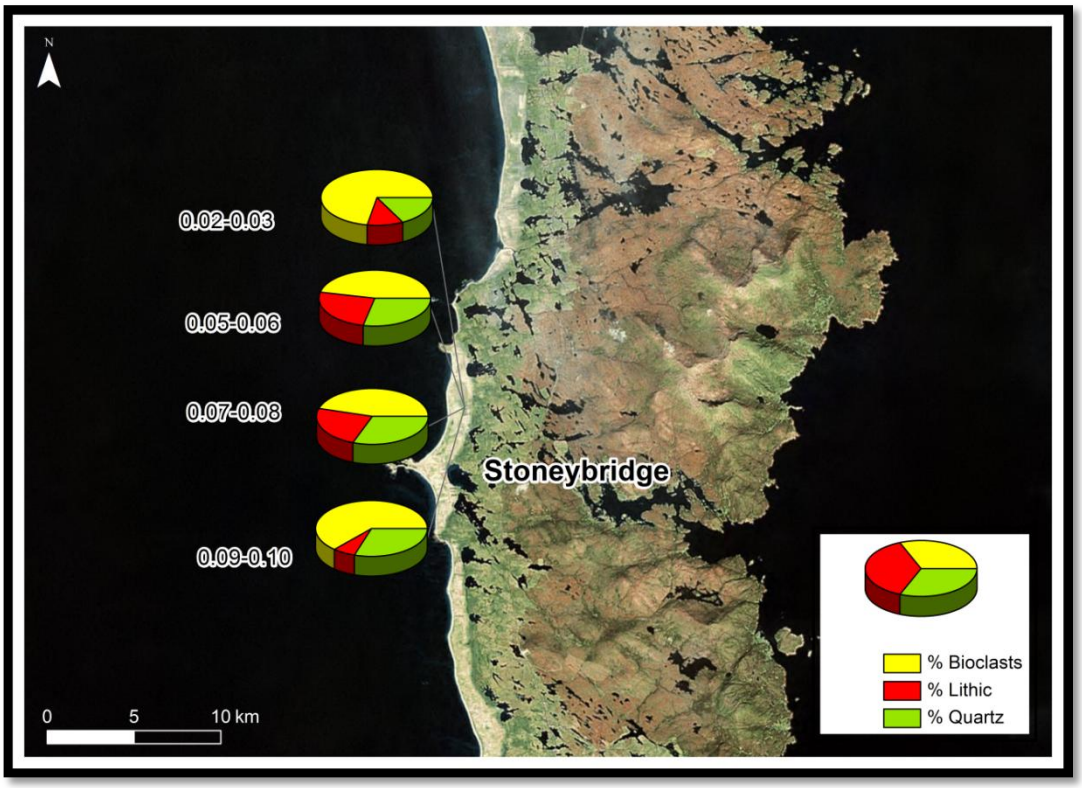

Figure 5.5.3 - Morphoscopic compositional features of samples retrieved from Stoneybridge.

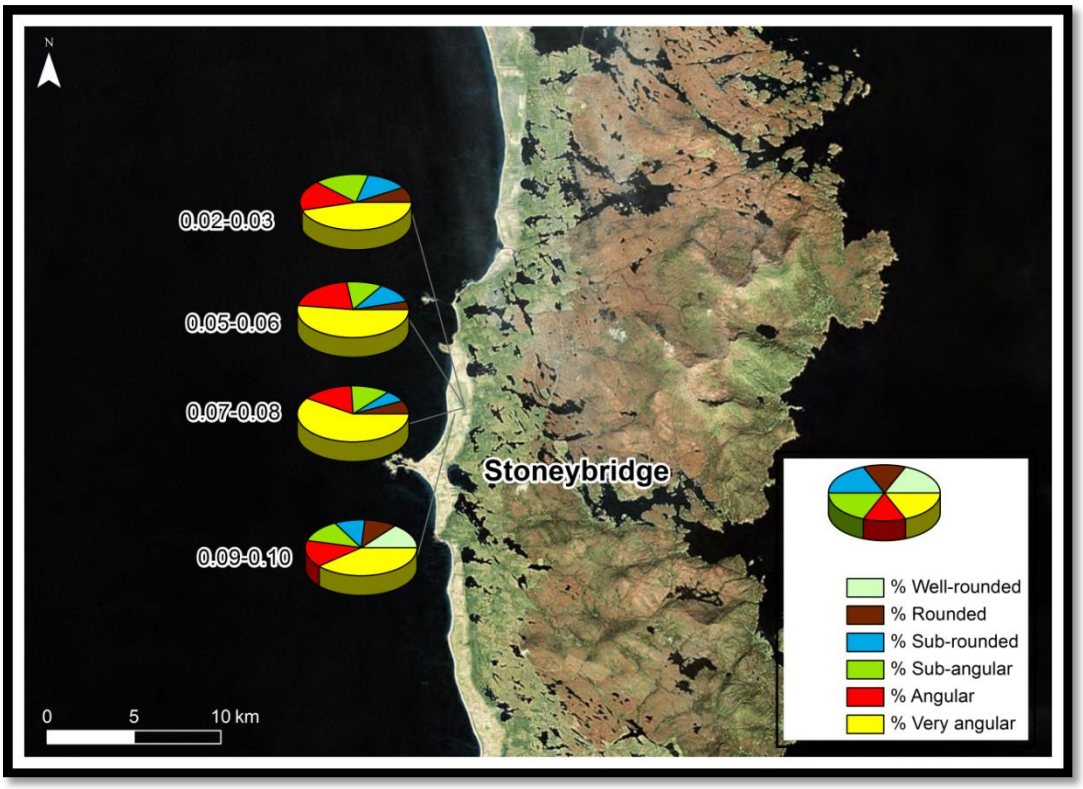

Figure 5.5.4 - Roundness classification for quartz grains from samples collected in Stoneybridge.

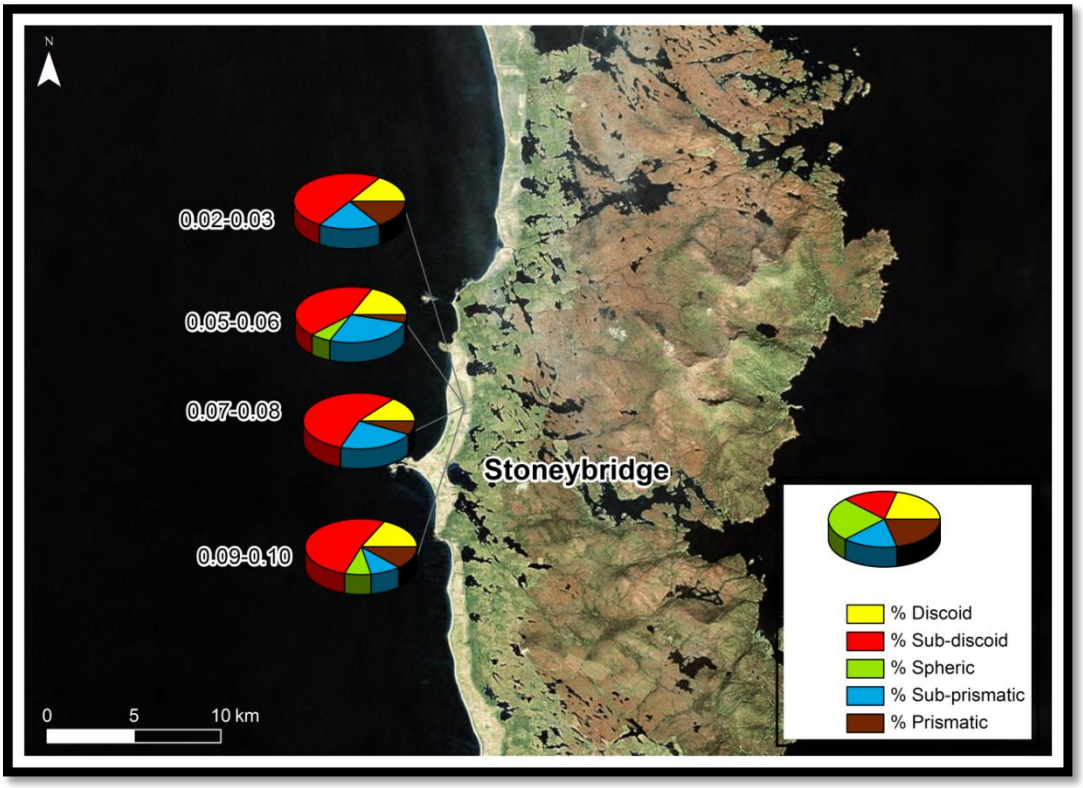

Figure 5.5.5 - Shape classification for quartz grains from samples collected in Stoneybridge.

5.5.4. Microtextural features

Microtextural classification was conducted in samples from the storm deposit that was collected in Stoneybridge (Figure 5.5.6 and Table 5.5.2). Angularity exhibited high values (*ca.* 3.143 to 3.643) except the base of the unit that displayed a result of 2.212. In terms of fresh surfaces the highest values were observed in samples HB_(0.05-0.06) and HB_(0.07-0.08) with results of 2.500 and 2.000 respectively while the fewer fresh surfaces were measured in the basal sample. On the other hand, dissolution presented very high values (highest at the top and base of tempestite) and the lowest of 3.000 for sample HB_(0.07-0.08). Regarding adhering particles they present values of *ca.* 3.5 in the middle samples while the top and base of the deposit revealed values around 4.5. In what concerns, percussion marks the highest values of 0.643 was detected in sample HB_(0.05-0.06) while the lowest result of 0.083 was observed in sample HB_(0.07-0.08).

Microtextural data was not advantageous in establishing a vertical trend for the tempestite although it was clear that the base and top of the deposit exhibited contrasting results with the other tempestite samples (except for percussion marks).

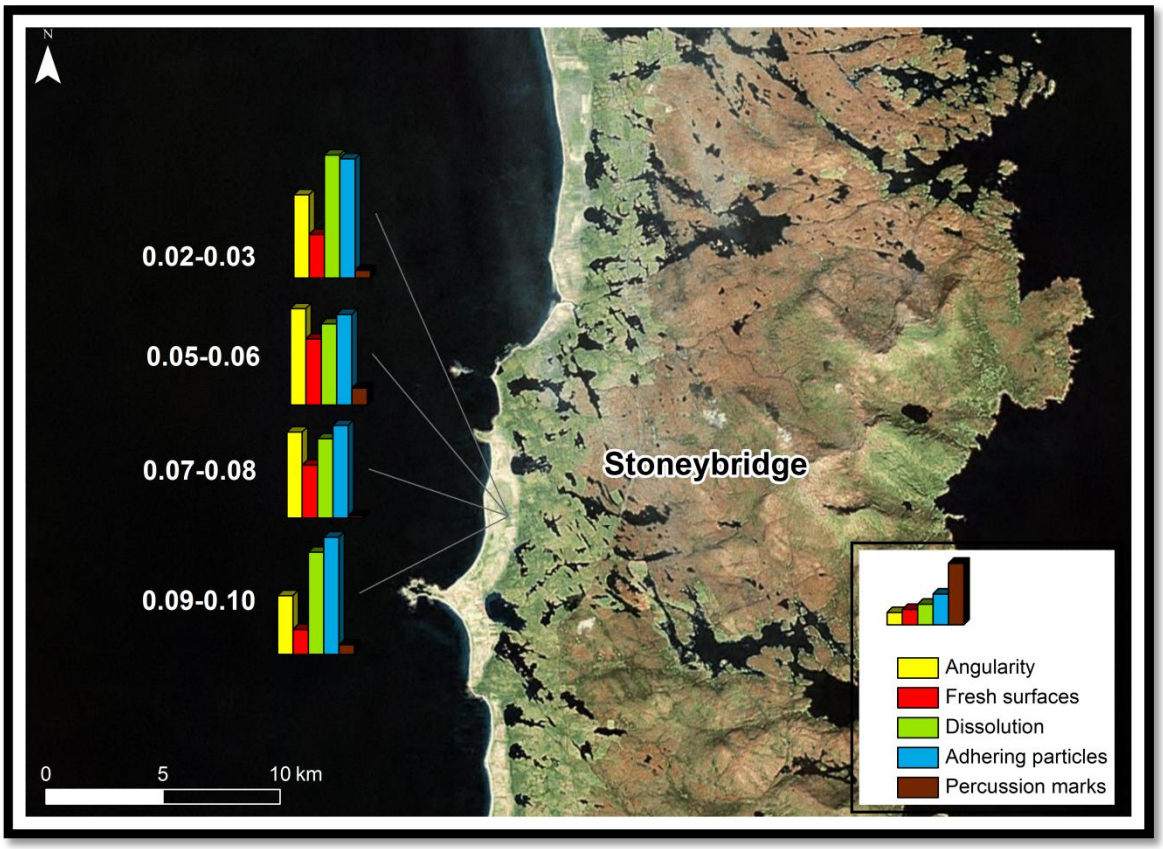

Figure 5.5.6 - Microtextural features results and their distribution across the storm layer retrieved in Stoneybridge.

Table 5.5.2 - Summary of microtextural results obtained in samples from Stoneybridge.

Sample	Depth (m)	Number of grains	Angularity	Fresh surfaces	Dissolution	Adhering particles	Percussion marks
HB	0.02-0.03	14	3.143	1.643	4.643	4.500	0.286
HB	0.05-0.06	14	3.643	2.500	3.071	3.429	0.643
HB	0.07-0.08	12	3.250	2.000	3.000	3.500	0.083
HB	0.09-0.10	14	2.214	0.929	3.857	4.429	0.357

5.5.5. Heavy mineral features

Heavy mineral assemblages for the tempestite were studied with the purpose of establish, if possible, vertical trends. In terms of the percentage of heavy minerals in total sediment it was clear an increase to the top of the unit (varying from 0.257%, at the top, to 2.604%, at the base) (Table 5.5.3).

Table 5.5.3 - Percentage of heavy mineral content in total sediment of samples from Stoneybridge.

Sample	Depth	Sedimentary Environment	% of Heavy minerals in total sediment
HB	0.02-0.03	Storm	0.257
HB	0.05-0.06	Storm	0.716
HB	0.07-0.08	Storm	1.029
HB	0.09-0.10	Storm	2.604

In compositional terms (Figure 5.5.7 and Table 5.5.4) no trend was established based in percentage variation of the main mineralogical components of these samples. The tempestite samples were mainly composed by amphiboles (>79.352%) with the highest result obtained for sample HB_(0.05-0.06) with 86.555% of the sample. Andalusite exhibited its highest value (*i.e.* 6.047%) for the base of the deposit and its lowest value (*i.e.* 1.619%) for sample HB_(0.07-0.08). In what concerns pyroxene, the highest value was displayed by sample HB_(0.07-0.08) with 11.741% and the lowest value by sample HB_(0.05-0.06) with 5.882%. Garnet and other minerals (*e.g.* monazite, epidote, staurolite, silimanite and zircon) were also detected in percentages ranging respectively between 2.521%-4.858% and 0.475%-2.436%, respectively.

Heavy mineral assemblages were not successful in the establishment of clear patterns within the whole deposit.

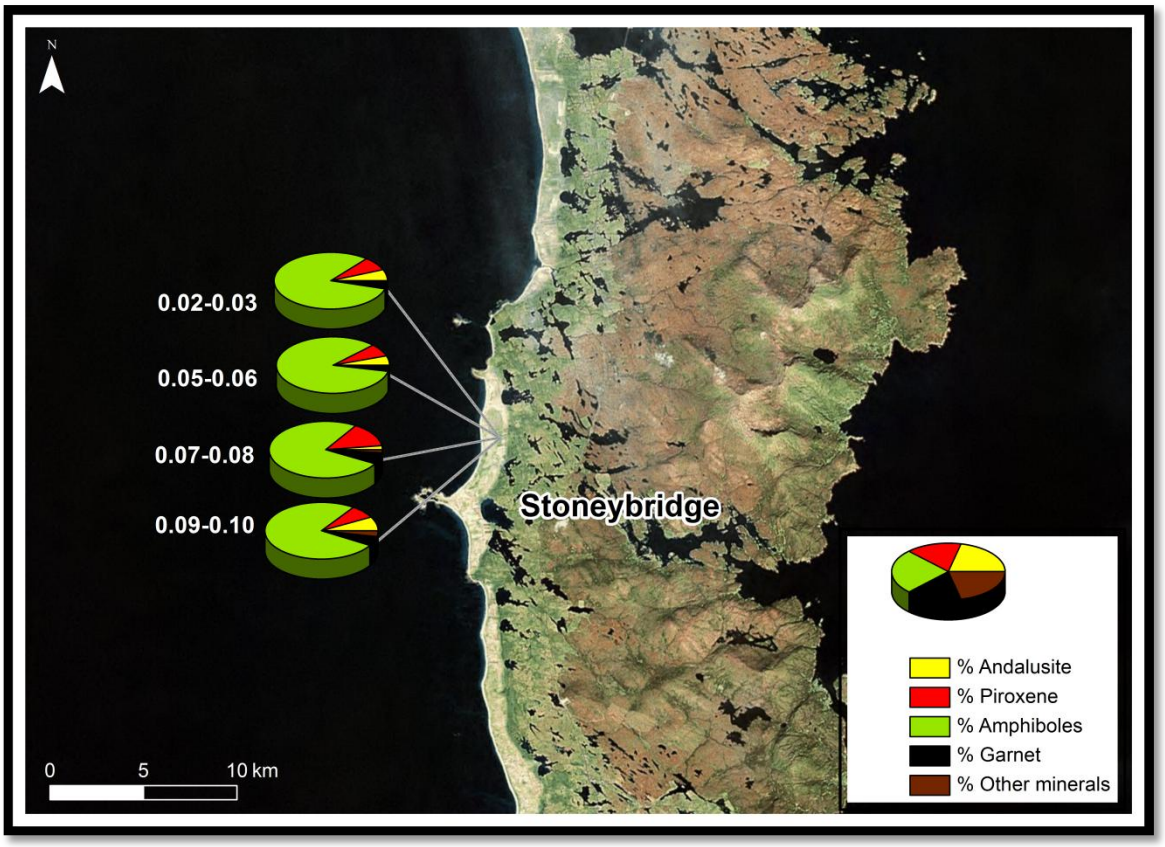

Figure 5.5.7 - Heavy mineral composition of tempestite samples collected in Stoneybridge.

Table 5.5.4 - Results from heavy mineral assemblages in the Stoneybridge samples.

Sample	Depth (m)	% Andalusite	% Pyroxene	% Amphibole	% Garnet	% Others
HB	0.02-0.03	4.603	6.695	84.519	3.347	0.847
HB	0.05-0.06	3.782	5.882	86.555	2.521	0.475
HB	0.07-0.08	1.619	11.741	79.352	4.858	1.271
HB	0.09-0.10	6.047	6.977	82.326	4.186	2.436

6. Discussion

6.1. Textural signatures of extreme marine inundations

All studied areas present a peculiar/unique lithostratigraphic signature in the top of each sites Holocene sequence. These signatures are found in sediment units that are correlatable with specific extreme marine inundations that affected each location. The dates of inundations were obtained through the extrapolation of radiocarbon ages, the computation of sedimentation rates based in radionuclides decay rate or in previous work conducted in the studied or nearby areas.

A conspicuous erosional/unconformity basal contact, generally observed in tsunamigenic deposits reported in the literature and indicative of the energetic character of the events responsible for their deposition, was observed in all studied areas and was also detected in the tempestite storm deposit of Stoneybridge, thus in accordance with Switzer (2008) that also recognized a sharp basal contact in storm deposits in Australia. Moreover, and also revealing the high energy involved, rip-up clasts were detected in all tsunamigenic units but were absent in the storm deposit. In cases, the amount of erosion of the underlying layers may have been considerable (*e.g.* in Salgados, erosion may have removed sediment accumulated throughout at least 800 cal years, calculated after radiocarbon dates of top unit D and base of unit F). These observations are in agreement with the findings of Minoura and Nakaya (1991), Bondevik *et al.* (1997), Nanayama *et al.* (2000) and Dawson and Stewart (2007) that correlate the presence of intraclasts ripped from soft underlying units with the enormous erosive capacity associated with a tsunami inundation. In agreement with Phantuwongraj and Choowong (2011), rip-up clasts are rare or absent in storm deposits probably due to the dominance of the inflow sedimentation and especially the constrasting intensity and duration of each inundation pulse.

The enrichment in broken shells of marine bivalves and also of tests and valves of both foraminifera and ostracods, which is another peculiar feature commonly observed in tsunamigenic deposits (*e.g.* Moore and Moore 1988; Bryant *et al.* 1992; Albertão and Martins 1996; Imamura *et al.* 1997; Clague *et al.*, 1999; Donato *et al.*, 2008), was only clearly perceived in the Portuguese and Indonesian samples and was not detected in the Scottish case, probably due to contrasting specific biological associations, taphonomical constrains and hydrodynamic conditions. In fact, the interpretation of the Scottish sedimentary sequences (from sediments of the tsunami and characterizing the permanent regime) relies essentially upon diatom proxies, which are extremely rare in the Portuguese case.

All deposits addressed exhibited a clear inland-thinning trend although conditioned by specific palaeotopographic characteristics, reaching distances in the order of 3 km away from the coast. In agreement with the findings of Gelfenbaum *et al.* (2007), tsunami deposits in Salgados, Boca do Rio and Lhok Nga were thicker in topographic lows (areas of spatial flow deceleration) and thin over topographic

highs (areas of spatial flow acceleration). Furthermore, in all studied sites, macroscopic observations performed in the field at the scale of the outcrops or exposures remarked fining upward tendencies although, in cases, the laboratory processing of samples failed to confirm this feature, probably due to the presence of scattered gritt, large shell and/or plant fragments, occasionally captured in the small subsamples used for lab analyses.

Although turbulent flows such as the ones associated with tsunami inundations are intrinsically chaotic and, by consequence, the associated processes of deposition and erosion are complex and varied at short time and spatial scales, it is possible to find some consistency in assess the grain-size characteristics of the depositional product and attempt to establish likely source materials.

In Salgados, the sediment grain size of the tsunami layer decreases inland and upwards typically within one Φ interval, in all samples where that layer is thicker than 0.03m. At the inland edge of the deposit, the sediment thickness is typically less than 0.03m; here, the sand is finer and shows poorer sorting (larger standard deviations); the mean grain-size of the whole sediment markedly drops, mainly due to three reasons: decrease in size of the coarser fraction, enrichment in mud (either contemporaneous of the depositon or induced by post-deposition illuviation) and sampling limitations, *i.e.* difficulty in retrieving a very thin layer of tsunami sediment with ghosty contacts preventing contamination by the framing muddy sediment. The same difficulty applies to other locations worldwide, though it has rarely been made explicit by the authors, and should be taken in consideration in interpretations of existing and future studies.

A pronounced contrast in the content of sand and consequently of the mean grain size (see Figure 6.1 for example) is detectable at the very base of all studied units laid down by extreme marine inundations, when compared with the underlying materials. Moreover, further upward in the high-energy sandy units, the sediment is virtually homogeneous in size or normally graded (with the exception of Lhok Nga, see below). This fact leads to the absence or to difficulties in identifying sedimentary structures besides a massive/chaotic character that is common to many tsunami deposits, hence in accordance with the suggestions previously forwarded by Dawson *et al.*(1995) and Dahanayake and Kulasena (2008).

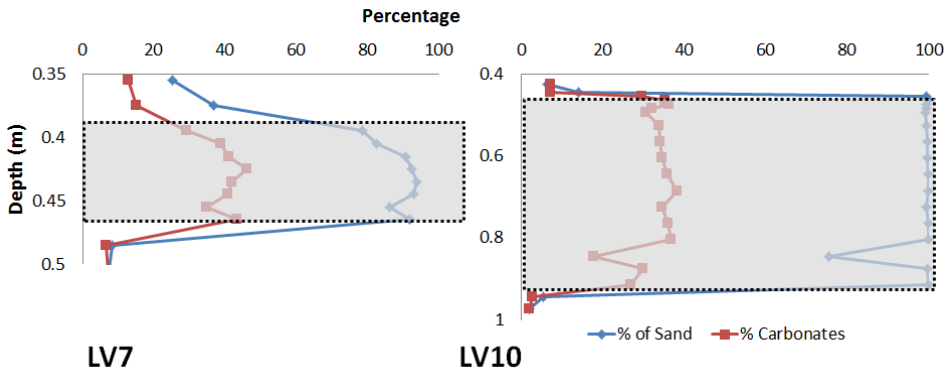

Figure 6.1 - Percentage of sand and calcium carbonate within the tsunamigenic unit E on cores LV7 and LV10 (Salgados).

The Indonesian tsunamigenic unit presented a complex stratigraphy with multiple coarser and finer *laminae* and layers correspondent to several waves of the 2004 tsunami. Furthermore, in Lhok Nga, very fine sediments were deposited as extremely thin mud drapes during periods of lower flow velocities, separating coarser sub-units associated with different wave pulses or backwashes. In the case of Lhok Nga, as discussed by Paris *et al.* (2007), normally-graded couplets or triplets of layers were used to identify the run-up of each wave. Furthermore, the topmost layer was interpreted as backwash deposition (presenting a seaward decrease in mean grain-size). This very recent tsunamigenic deposit is unique in that, it exhibits clear textural constrasts and accumulated texturally-distinguishable sub-units throughout the depocenter region, in contrast with many other tsunamigenic deposits, either the ones studied here or others reported in the literature; this fact might suggest that sedimentary structures and sub-units such as the ones preserved in Lhok Nga may actually have formed elsewhere but were rapidly degraded or homegeneized, thus contributing to enhance the massive character of the deposits. This is in agreement with the findings of Szczucinski (2011) who observed the progressive disappearence of sedimentary structures and features from the same locations and sediment layers in 5 consecutive yearly campaigns in a study of the 2004 Indian Ocean tsunami deposition. The reasoning above should be present when inferences on the number of waves or vectorial properties of the flow are straightforwardly taken from sedimentary units deposited by old inundation events.

Tsunami deposits can vary immensely from location to location, mainly due to regional to local geological, geomorphological and climate constrains, all of which play a part in determining differences in sediment sources. Grain-size variation in tsunamiites is determined by the dimensional range of sediment available for transport, rather than by flow capacity (Bourgeois, 2009), maybe with the only exception of gigantic megaclats, which require exceptional flow conditions. In the sedimentary units addressed in this study (Table 6.2) the mean grain size roughly correspond to fine to medium sand although, as mentioned above, sampling limitations, occasional shell or plant fragments may have influenced the laboratory results, due to the fact that they are not hydraulic equivalents of the lithic or mineralogical grains with which they coexist in the sediment. The tsunamiite from Salgados (once more where its thickness exceeds 0.03m) presents essentially an unimodal grain size distribution, which suggests predominance of one sedimentary source. The same pattern was observed in all other studied areas, except Lhok Nga. Indeed, Paris *et al.* (2007) used textural data to suggest that in Lhok Nga the 2004 Indian tsunami deposit may have been nourished from the beach with relevant contributions from the shallow shelf, the coral reef, the lagoons and the dunes.

All sites addressed in this study other than Lhok Nga yielded high energy sediment with standard deviation roughly below 1 Φ thus suggesting that the source material was probably well sorted and normally distributed. This is in accordance with Bahlburg and Weiss (2007) that analysed the grain-size distributions of tsunami materials deposited by the 2004 tsunami in the Indian and Kenyan coasts. Moreover, those deposits were essentially characterized by symmetrical or slightly positively-skewed size distributions and

this was interpreted as confirming that the tsunami sediment was entrained from well sorted pre-tsunami materials available in the nearshore and beach environments. In the case of Lagoa dos Salgados, a similar pattern was detected in the size distribution of sediments from both unit E and dune/beach material from present-day analogues. Tsunamiites and tempestite from Portugal and Scotland exhibit a slightly positive kurtosis (leptokurtic curves), which, according to Bahlburg and Weiss (2006), might suggest a limited size-interval of the source material, in contrast with a platykurtic kurtosis reported by Paris *et al.* 2007 indicating multiple sediment sources in Lhok Nga.

Numerous authors attempted to use textural parameters to differentiate sedimentary environments or transport mechanisms with controversial results (*e.g.* Mason and Folk, 1958; Friedman, 1961; Shepard and Young, 1961; Visher, 1969; McLaren, 1981; McLaren and Bowes, 1985). In the case of Salgados (where a larger number of samples were collected from nearshore, beach and dune) this was crudely achieved using the 10% Φ and 90% Φ percentiles and skewness (Table 6.1) of the grain size distribution. Nearshore samples presented the largest standard deviation thus exhibiting larger differences between values for 10% Φ and 90% Φ percentiles. As a result of their study of sediments in Brazos River bar, Texas, Mason and Folk (1958) concluded that skewness is sensitive to transport and depositional environment. In their study case, beach samples were negatively skewed while dunes were positively skewed. Friedman (1961) confirmed these findings. Our results in Salgados do not corroborate those conclusions (Table 6.1). Moreover, McLaren (1981) concluded that mean grain size, sorting and skewness are dependent of the source of the deposit and independent of transportation process or sedimentary environment. Our results validate this conclusion due to higher similarities found between tsunamiites and dune and beach samples. In the case of Salgados and Boca do Rio it is also evident that the eroded underlying (finer-grained) unit was also a relevant sedimentary contributor for the tsunamigenic layer in both studied areas.

On the other hand, McLaren and Bowles (1985) concluded that sedimentary deposits may become either: a) coarser, better sorted, and more positively skewed (in high energy transport) or finer, better sorted; or b) more negatively skewed (in low energy regime). In the Salgados case, tsunami samples are more positively skewed (mean value of 0.167) than their likely source material (Table 6.1); thus, according to McLaren and Bowles (1985) model, this textural shift indicates a source-deposit relation and confirms the high energy character of the transport agent responsible for the emplacement of the tsunamigenic unit.

Friedman (1967) questioned if grain size analysis will ever be helpful in environmental interpretation. Our conclusion is that if a given deposit is related to more than one source, it is extremely difficult to use mean grain size, sorting or skewness as useful sedimentological tools in the differentiation of the parental material source. Our textural data confirmed what has been commonly reported elsewhere for sediment entrained, transported and deposited by tsunami waves: they transport essentially sediment that is available in the coastal fringe (*e.g.* Dawson 1994; Moore *et al.* 1994; Atwater and Moore, 1992; Clague and Bobrowsky, 1994; Hindson *et al.*, 1996; Dawson, 2004; Kortekaas and Dawson, 2007; Oliveira *et al.*, 2009;

Paris *et al.*, 2010b; Goff *et al.*, 2010a; Costa *et al.*, 2012a,b); the concept of coast being restricted the closure depth.

Table 6.1 - Mean values for textural data from present day analogues from Salgados.

	10% Φ	90% Φ	Mean (Φ)	Standard deviation (Φ)	Kurtosis	Skewness
Beach (n=7)	0.006	1.66	0.84	0.66	1.05	1.11
Dune (n=9)	0.192	1.75	0.98	0.61	1.05	1.04
Nearshore (n=7)	-0.602	2.27	0.90	1.10	1.08	1.83

Table 6.2 - Summary of sedimentological data by studied site. Note n= number of samples analysed.

	Salgados (n=40)	Boca do Rio (n=17)	Voe of Scatsta (n=4)	Lhok Nga (n=7)	Stoneybridge (n=4)
Erosional/abrupt/sharp/unconformity basal contact	Present	Present	Present	Present	Present
Massive/chaotic unit	Present	Present	Present	Absent	Present
Unit with several *laminae*	Absent	Absent	Absent	Present	Absent
Stratigraphic peculiarity	Present	Present	Present	Present	Present
Finning upward	Absent	Absent	Absent	Absent	Absent
Thins inland	Present	Present	Present	Present	Present
Max. distance inland (deposit)	App. 850 m	App. 1500 m	App. 1500m	App. 3500 m	App. 150m
Rip-up clasts	Present	Present	Present	Present	Absent
Broken shells	Present	Present	Absent	Present	Absent
Mud drapes	Absent	Absent	Absent	Present	Absent
D50 (Φ)	1.05 to 3.53	0.44 to 1.96	0.64 to 1.24	0.42 to 2.10	2.08 to 2.49
Standard deviation	0.48 to 1.56	0.39 to 0.53	1.06 to 1.13	Not calculated	0.36 to 0.58
Kurtosis	0.51 to 1.74	1.05 to 1.34	1.01 to 1.43	Not calculated	1.01 to 1.28

6.2. Morphoscopic signatures of extreme marine inundations

Every sedimentary environment is characterized by specific energy conditions, which vary in time and space, those fluctuations representing temporary shifts, departures, from modal conditions that define the permanent regime. The results obtained in this study show that the contrasting energetic character and transport mechanisms associated with tsunamigenic events and the nearshore hydrodynamics, including occasional high energy storm events, translate into compositional characteristics, roundness and sphericity attributes of sediment particles. In the case of Salgados, principal component analysis reveals that it is possible to distinguish nearshore and tsunami sediments in compositional terms. In Figure 6.2, tsunamis samples are positively correlated with the percentage of quartz (right hemisphere) whereas, by contrast, nearshore samples are grouped in association with larger representation of bioclasts and lithic material. This indicates that the coastal dune and beach were the main sedimentary source of the tsunami sediments in contrast with the nearshore environment which, despite the sand abundance, contributed with little material to that particular deposit.

Roundness varies with the size-class considered within the same detritic sediment, so by concentrating the analysis in one size fraction, common to different samples, comparability between data was maintained. Results obtained in this study from Salgados and Boca do Rio are not in agreement with Hails (1967) which state that it is impossible to distinguish between beach and dune sands exclusively by considering roundness. In fact, the differentiation of these two sedimentary environments (*i.e.* beach and dune) is illustrated by higher roundness characteristics of dune samples (right quadrants – Figure 6.3 and 6.5) in contrast with more angular grains in beach sediment (left quadrants – Figures 6.3 and 6.5). In accordance with Beal and Shepard (1956) the difference in roundness between dune and beach sediments is only relative rather than absolute, which recommends caution in the interpretation of results if this proxy is solely used in reconstructing paleoenvironments in stratigraphic studies. The latter authors also concluded that quartz grains in dunes were more rounded than in adjacent beaches and attributed that difference mainly to selective sorting by wind transport rather than abrasion, as inferred by many other authors.

Kumbrein (1941) suggested that in Nature there is a close correlation between sphericity and roundness of clastic particles, although these attributes are conceptually independent. With a given distance of transport, roundness changes more significantly than sphericity because roundness is more sensitive to small-scaled features (*i.e.* edges of grains) whereas sphericity is more dependent of the major dimensional ratio, which requires much more energy to change, hence being a function of source (Mason and Folk, 1958). In Salgados and Boca do Rio (Figure 6.4 and 6.6), sphericity was only able to be of practical use in the former case, nearshore samples tending to group in the right quadrant, in opposition with all remaining samples.

In conclusion, based in morphoscopic features of quartz grains studied, it was possible to establish likely sources and differentiate sedimentary environments. However, the differences are essentially qualitative and critical reserve should be applied when analysing and interpreting results elsewhere. In

Salgados (Figure 6.2 and 6.4), it was clear both through the compositional pattern, as well as considering sphericity, that nearshore samples share the less affinity with tsunamiite samples. Furthermore, in Salgados it was also possible to use roundness (Figure 6.3) to differentiate more angular (beach, nearshore, storm, tsunami) from more rounded (nearshore and dune) samples, thus allowing distinction between dune and beach samples. In Boca do Rio (Figure 6.5) it was possible to discriminate samples using roundness: samples with more angular grains [beach, tsunami, one proximal nearshore (-7.5 m)] cluster and plot separately from the rest of the studied sediments. On the other hand, sphericity (Figure 6.6) allowed separating nearshore from tsunami sands. Thus, these results suggest similar conclusions to the ones obtained in Salgados in terms of parental materials for the tsunami sediment: the nearshore region was the less likely sedimentary source of the AD 1755 tsunami that strongly affected these two coastal areas of the Algarve.

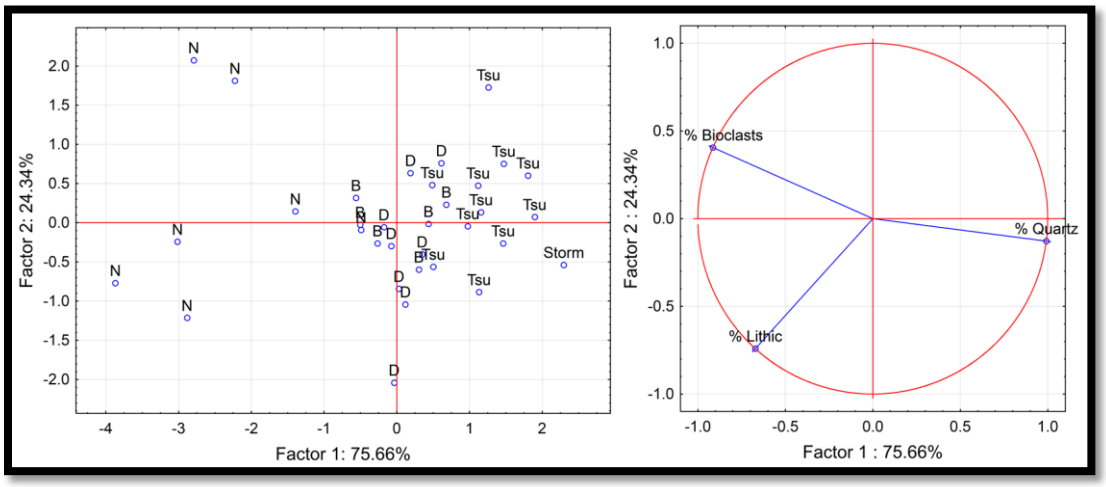

Figure 6.2 – Principal component analysis; morphoscopic compositional study of Salgados samples. Note: left image - B- beach samples; D- dune samples; N-nearshore samples; Tsu – tsunami samples.

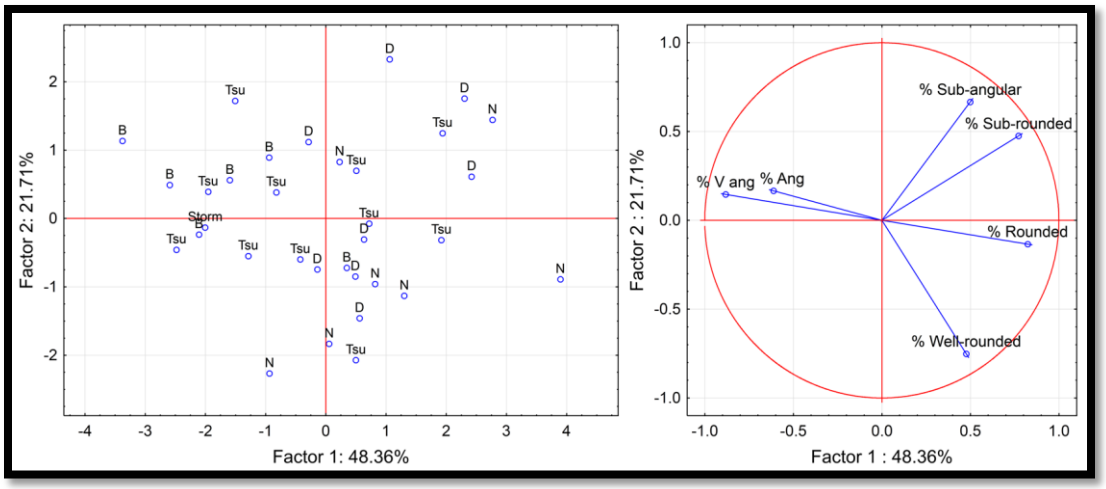

Figure 6.3 – Principal component analysis; roundness of Salgados samples. Note: left image - B-beach samples; D- dune samples; N-nearshore samples; Tsu – tsunami samples.

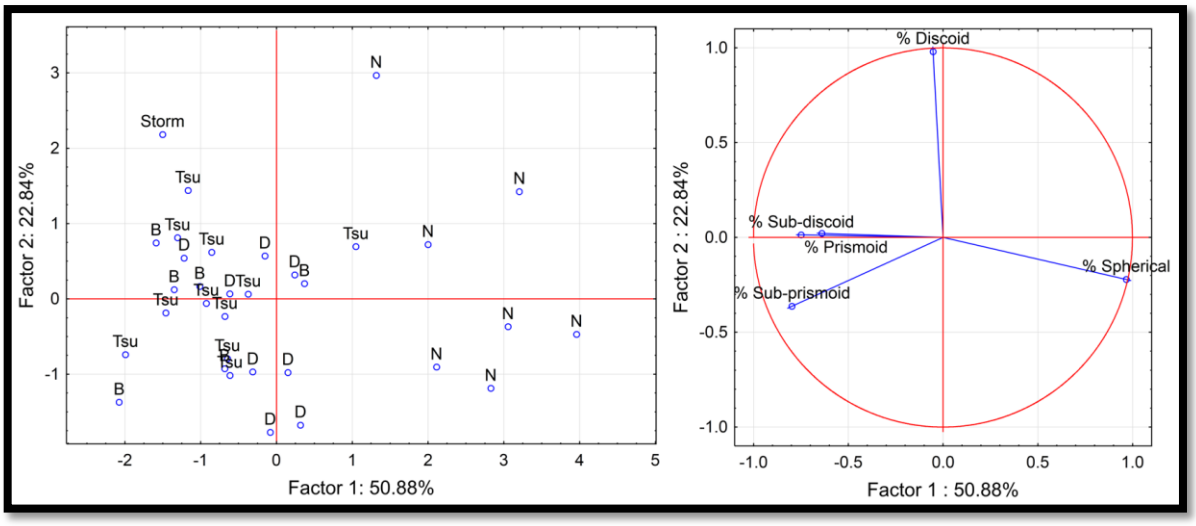

Figure 6.4 – Principal component analysis; sphericity of Salgados samples. Note: left image - B-beach samples; D- dune samples; N-nearshore samples; Tsu – tsunami samples.

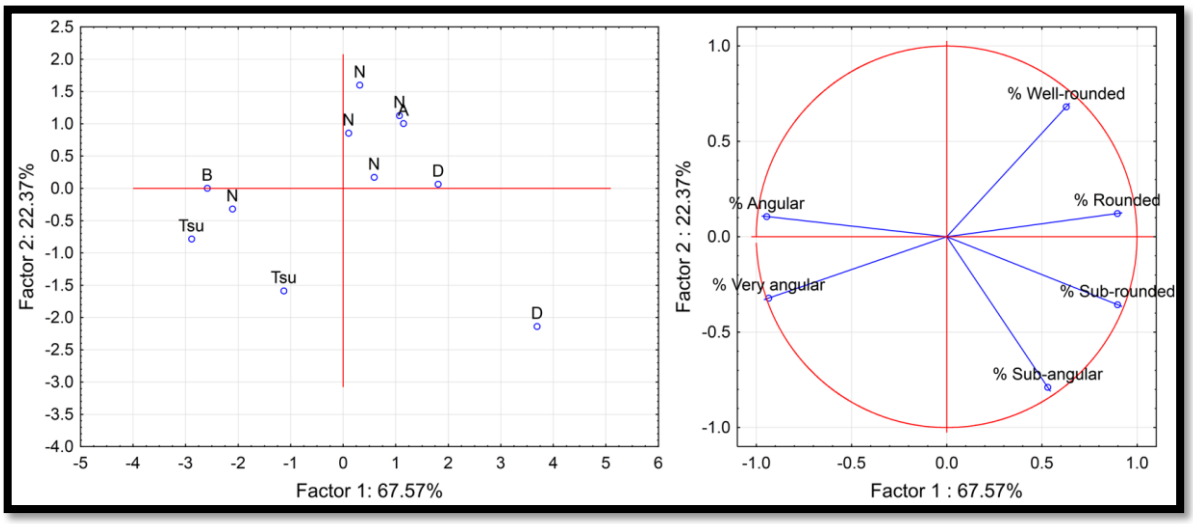

Figure 6.5 – Principal component analysis; roundness of Boca do Rio samples. Note: left image – A – alluvial sample; B - beach sample; D- dune samples; N-nearshore samples; Tsu – tsunami samples.

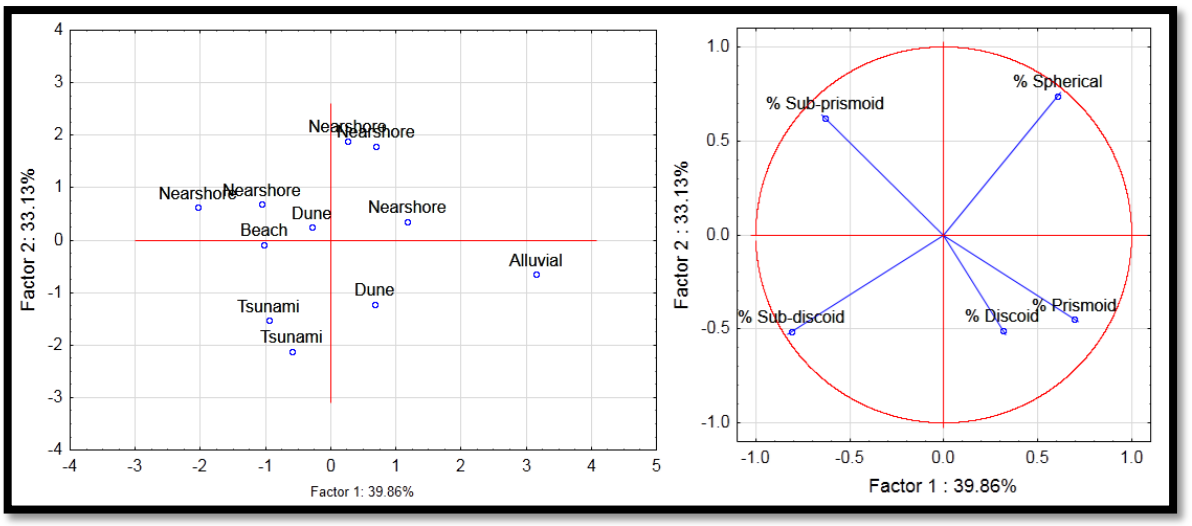

Figure 6.6 – Principal component analysis; sphericity of Boca do Rio samples.

In the Scottish areas, roundness and sphericity were not valid tools for discriminating sub-units within the tsunamiite or tempestite sediment layer, hence demonstrating that either the deposit was massive or that these proxies were not useful in these areas. Both arguments are effective, especially if considering the low number of samples used. By contrast, in Lhok Nga, roundness allowed clear differentiation of the sediment samples deposited by the tsunami backwash (see Figure 6.7 - left quadrants, backwash samples) whereas sphericity allowed discriminating the base of the deposit (Figure 6.8 - top quadrants). These results suggest that time played an important role in the rounding of grains because at the base of the deposit (inrushing water and sediment) they are more angular than in the backwash samples. This rounding could have occurred because of difference in sources (the backwash could have added an extra source supplying mature grains located inland) or by rapid smoothening or removal of edges and corners induced by effective grain-grain collisions during transport. The latter hypothesis raises questions in terms of the transport duration necessary to transform sand-sized angular quartz grains in more rounded ones. The issue has been debated for larger particles and there is a wide consensum that high-energy and turbulent transport is actually able to produce rapid changes of surface features in quartz particles (*i.e.* short-distance and evolution of roundness); however, in shallow marine environments, the roundness and luster characterizing quartz sand may essentially be acquired by pressure-induced near-bottom vibration induced by travelling waves, rather than impact between particles moving alongshore or cross shore and entrained, re-suspended and deposited by coastal currents. To what extent a high-density extremely turbulent flow saturated with suspended sand and moving inland at high speed, such as a tsunami, can be effective in producing similar reworking patterns of the grains surface, in a very short time-span, remains an open question. Although departing a bit from the central objectives of this dissertation, the question above is further discussed in the following sub-chapter of this thesis and the rationale, results and conclusions of an experiment addressing that issue may be found in Costa *et al.* (2012c). In three of the five studied areas, morphoscopic analysis proved to be a useful tool in the discrimination of environments and/or in the establishment of likely source material for extreme marine inundations.

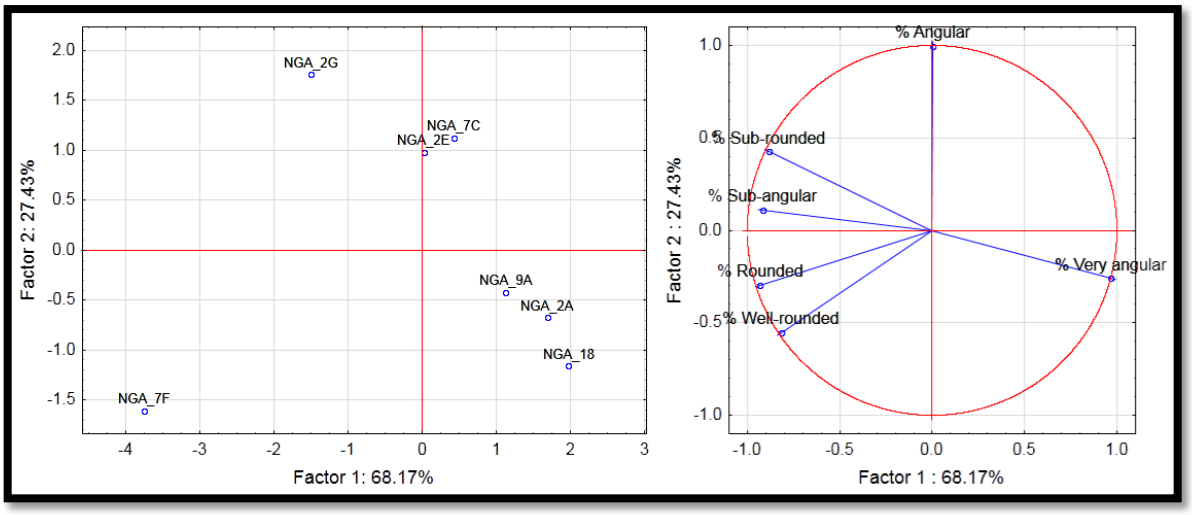

Figure 6.7 – Principal component analysis; roundness of Lhok Nga samples.

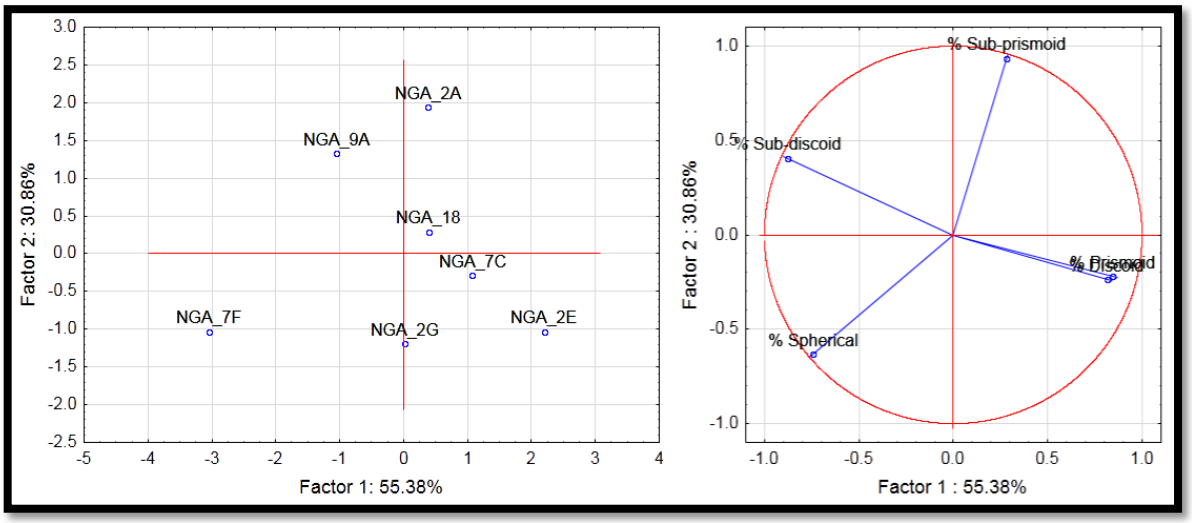

Figure 6.8 – Principal component analysis; sphericity of Lhok Nga samples.

6.3. Microtextural signatures of extreme marine inundations

Several attempts (*e.g.* Krinsley and Margolis, 1969; Bettencourt *et al.*, 1989; Pyokari, 1997; Abu-Zeid *et al.*, 2001; Mahaney *et al.*, 2001; Bull and Morgan, 2006; Costa *et al.*, 2009; Deane, 2010) have been made in order to characterize surface microscopic signatures in quartz grains from distinct sedimentary environments. The results proposed have been controversial and far from unanimous in the identification of features, interpretation of inprinting mechanisms or processes, and association of specific microtextural signatures with specific sedimentary environments.

Mahaney (2002) characterized a group of 41 microtextural features and suggested the association of some features with specific environments (*e.g.* percussion marks in aqueous environments; bulbous edges in aeolian environments); however, no grains associated with high energy inundation events were analysed in this study. By contrast, Krinsley and Donahue (1968) established that specific differences exist depending on the environment of transportation and deposition; however, they also suggested that river transport and turbidity current movement do not impress characteristic surface textures on quartz sand grains.

Recently, Madhavaraju *et al.* (2009) examined quartz grains under the scanning electron microscope and defined thirty two distinct microtextures that they grouped into three modes of origin, *i.e.*, mechanical (eighteen features), mechanical and/or chemical (five features) and chemical (seven features). Even in the same sedimentary environment, changes were detected. In agreement with these findings, Manickam and Barbaroux (1987) observed that in the Loire River (France) chemical features are dominant during winter while mechanical features dominate during the summer. Furthermore, Lisá (2004) detected that in the case of typical aeolian sediments; about 10% of the fraction studied will not show any surface microtextures typical of aeolian transport.

One of the main problems in addressing these issues is the subjectivity and the discrepancy of observations made by different observers. In one attempt to verify operator variance, Culver *et al.* (1983) tested through five different observers the classification of eight samples and thirty two surface microtextural features and concluded that differences, although considerable in the recognition of individual surface features, were negligible in discrimination/grouping of samples. Although much has been done, one of the requirements that need to be addressed in the future is to standardize the definitions of microtextural features and in that sense the work by Mahaney (2002) should be used as the best available reference. Moreover, one tool that should be used to minimize the inter-observer incongruity is the use of wide-range statistical analyses. Mahaney *et al.* (2001) concluded that statistical measurements show the importance of grain overprinting and, in the opinion of the author, their use should be mandatory in grain surface microscopic studies.

The analysis of microtexture box-plot diagrams (Figure 6.9) for each group of samples adressed in this study allowed identificating the characteristic features associated with each sedimentary environment.

The angularity parameter, although not being *per se* a distinctive microtextural differentiator (*e.g.* majority of grains are either sub-angular or sub-rounded), provides interesting data, with the highest median values for storm and beach grains but the highest values (more angular) are observed in tsunami grains that also present a wide range of values.

Nearshore samples and alluvial samples exhibit the lowest median values of fresh surfaces, while the highest, as well as the broadest array values, have been observed in dune, beach and tsunami grains.

Adhering particles and dissolution features present similar patterns with the highest median values for alluvial grains, although storm deposits also exhibit high values. Tsunami and beach presented lower median values and tsunami, storm and beach, once more, presented the widest range of values.

In respect to percussion marks, the highest median values were observed in tsunami, dune and beach grains. However, tsunami grains yielded the highest values (above 3.5) suggesting a major resurfacing of the grain by this microtextural signature.

The data analysed strongly suggest that a geographical signature is also present in sample grouping, thus indicating, at least partially, the permanency of a source signature, which may exhibit a considerable variation between the different coastal environments addressed.

The tsunami grains are generally characterized by a large number of fresh surfaces (Indonesian samples presenting highest median values for fresh surfaces and angularity) (Figure 6.10). Moreover, the Scottish tsunami samples present strong dissolution (interpreted as post-depositional and favoured by a long post-event burial period) but the number of fresh surfaces that can be identified is still considerable. On the other hand, the Portuguese samples are characterized not only by larger numbers of fresh surfaces (when compared with potential source material: nearshore, beach, dune and alluvial) but also by the extremely abundant percussion marks including near total resurfacing of some grains. The Portuguese samples present a strong dominance of percussion-marks on grain surfaces (up to 50% of the population analysed), with an almost complete resurfacing of the grain. The Scottish (storm and tsunami) and Indonesian tsunami samples show clear dominance of fresh surfaces, even if masked by post-event dissolution (Shetland samples).

Bivariate and ternary plots reveal differences and relationships between the samples studied in what relates microtextural imprints. One example is Figure 6.11, where percussion marks and dissolution are plotted. In this figure it is noticed that the vast majority of nearshore samples presented low values of percussion marks and high values of dissolution. The same pattern is observed in alluvial samples. On the other hand, beach samples show low dissolution and few percussion marks. By comparison, dunes present slightly higher values of dissolution and percussion marks. As observed in Figure 6.11, tsunami and storm samples exhibit a strong regional imprint. The Portuguese tsunami samples present high values of percussion marks and low values of dissolution, while tsunami samples from Indonesia and Shetland do not

present significant values of percussion marks but share low values of dissolution with the Portuguese tsunami samples.

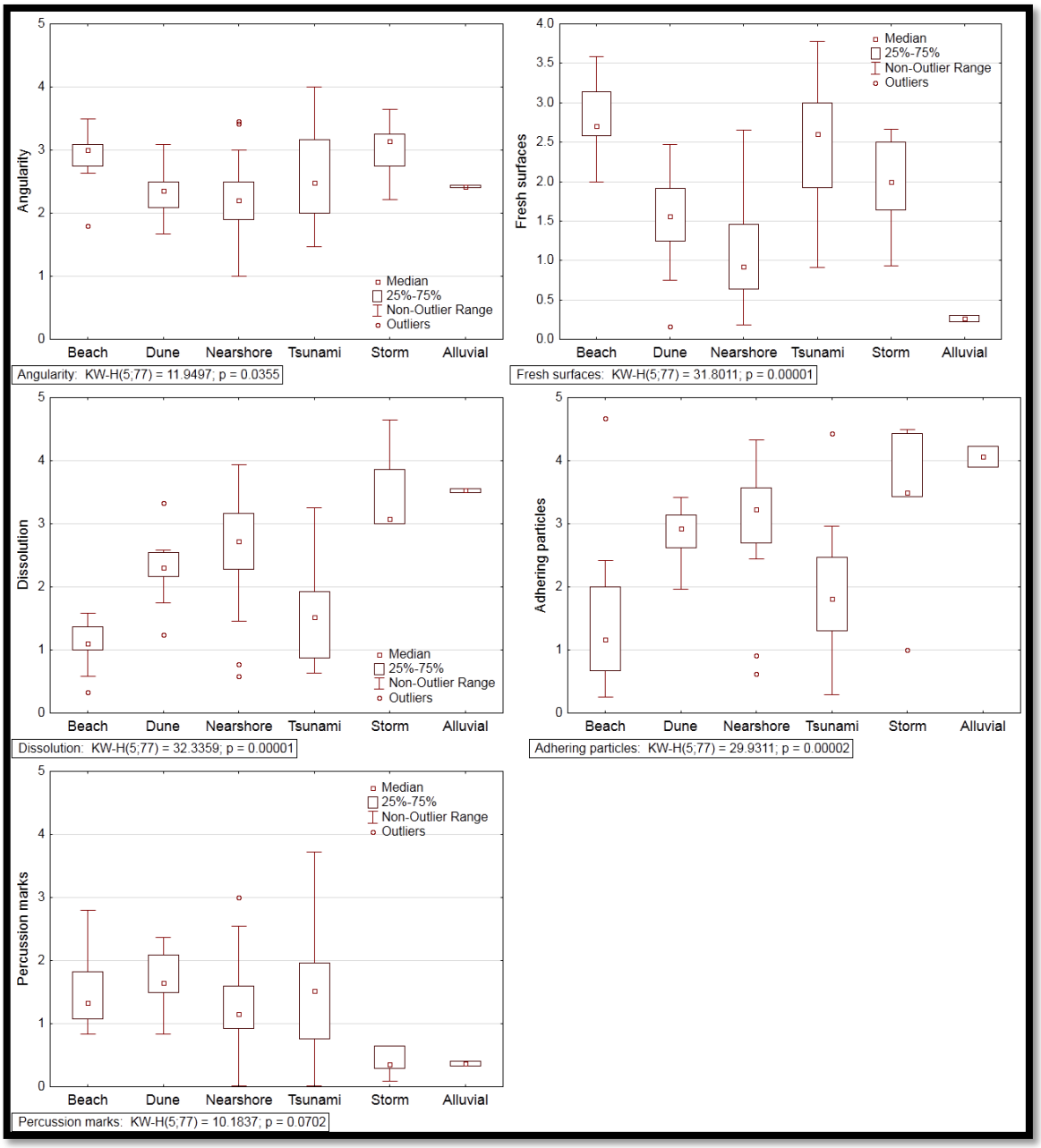

Figure 6.9 – Analysis of microtexture features in box-plot diagrams for each group of samples (extreme marine inundations and sedimentary environments).

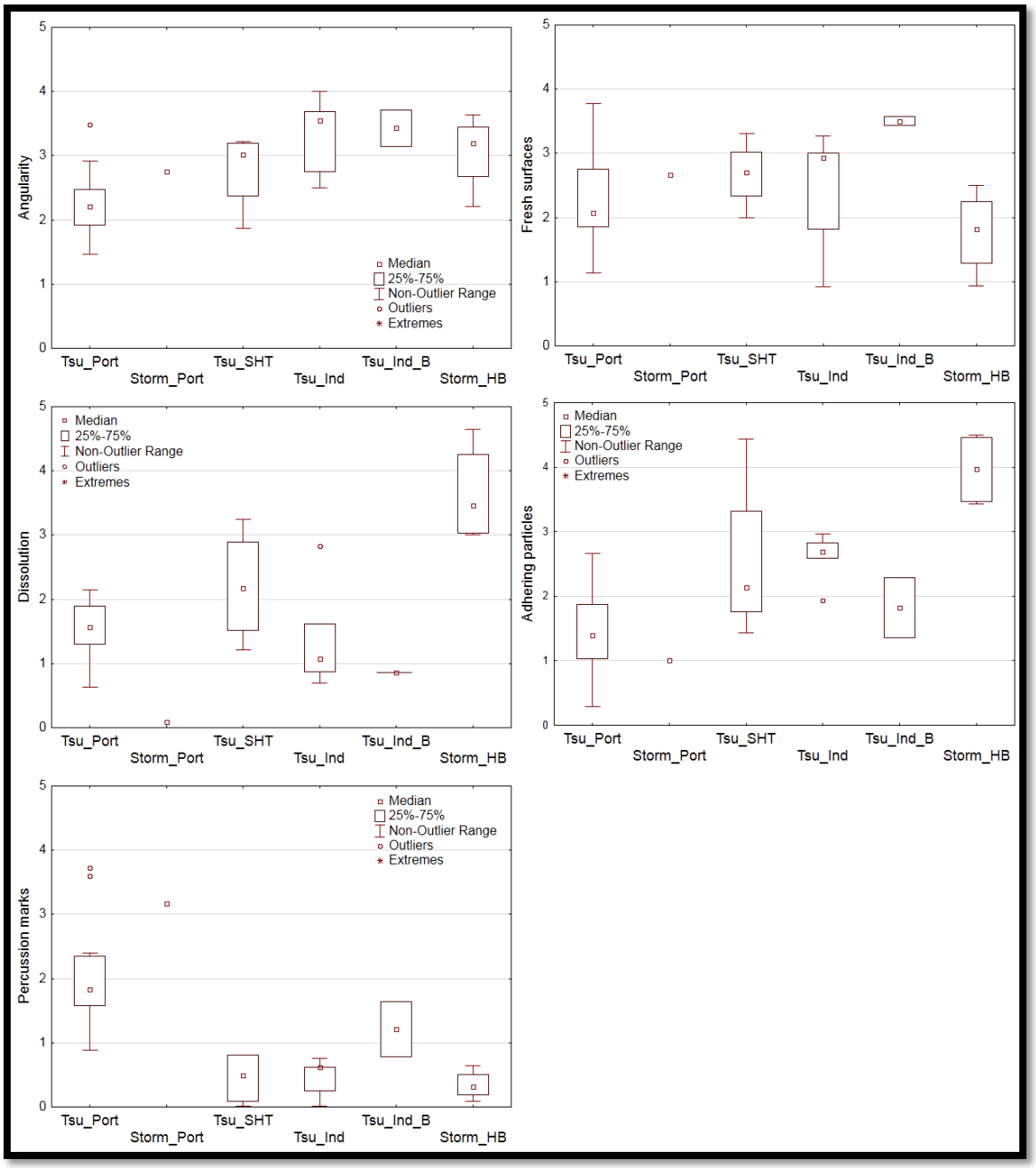

Figure 6.10 – Comparison of microtextural (angularity; fresh surfaces; dissolution; adhering particles; percussion marks) results according to the location where the tsunami or storm samples were collected.

In Figure 6.12 ternary plots were drawn and relationships between fresh surfaces, percussion marks, adhering particles or dissolution are observed. The relationship between fresh surfaces, percussion marks and dissolution is plotted in Figure 6.12A and it is possible to note that alluvial and nearshore samples typically present low values of fresh surfaces and percussion marks, but are characterized by high values of dissolution. By contrast, beach and tsunami samples present high values of fresh surfaces and low values of dissolution. The highest values of percussion marks can be observed in the Portuguese tsunami and storm samples. Moreover, in Figure 6.12B relationships between fresh surfaces, percussion marks and dissolution

features are apparent. This figure replicates the pattern exhibited by Figure 6.12A but is important to stress that nearshore and alluvial samples present high values of adhering particles and tsunami and beach samples present lower values. Dune samples (visible in both figures 6.12A and 6.12B) presented typical mean values in the microtextures observed.

Principal components analysis allowed extracting the two main factors representing more than 80% of the total variability. Indeed, the orthogonal axes observed in Figure 6.13 are related with 4 major groups of microtextural features. Their association with the sedimentary samples can be observed in Figure 6.12. It is noted that Component 1 (x-axis in Figure 6.13) indicates opposition between dissolution/adhering particles (component 1, positive values) and percussion marks and fresh surfaces (component 1, negative values), thus being a good indicator of the (hydro)dynamic conditions in the sedimentary environment. On the other hand, Component 2 (y-axis in Figure 6.13) depicts the opposition between percussion marks (top sector, positive values) and angularity (lower sector, negative values). Component 1 allows a clear differentiation between the two sets of microtextural families; one, more related with mechanical features (angularity, fresh surfaces and percussion marks, related with mechanical reworking processes) and another group of microtextures related with chemical processes (dissolution and adhering particles). As one can observe in Figure 6.13, in terms of sedimentary discrimination of environments, although a large majority of samples can be inserted in one specific quadrant (*e.g.* nearshore and alluvial samples on the top right quadrant; beach and tsunami samples are mostly present in the left quadrants; dune samples are mostly in the centre of the chart) there still is considerable variation of samples within each quadrant.

From the above, we suggest that the use of only one microtexture to determine sedimentary environment is probably an invalid approach. After completing the analysis of our dataset we recommend that in the future one should use, at least, five microtextural features and a considerable number of grains. It is important to note geographical variations and to keep in mind that no sole microtexture can be applied worldwide to a unique sedimentary environment, although in the majority of environments there are some microtextural associations that are dominant. The group of five microtextural features described above allowed the characterization of several sedimentary environments as summarized below:

Alluvial- High values of dissolution and adhering particles. Moderate presence of percussion marks.

Beach- Highest percentage of fresh surface and strong presence of percussion marks. Dissolution and adhering particles are almost absent.

Dune- Presents a well balance representation of all the microtextural features.

Nearshore- High values of dissolution and adhering particles and moderate presence of percussion marks and fresh surfaces.

Storm- Although a regional factor might influence the data (4 out 5 samples are from the Hebrides, Scotland), storm grains present many similarities with beach samples and can only be differentiated from those by the broadest variety of values observed.

Tsunami- Presents the highest values of percussion marks and fresh surfaces (thus suggesting strong hydrodynamic processes before deposition). Tsunami grains can also be characterized by presenting the widest range of values observed in the microtextural features.

Although the number of samples is not perfectly balanced (lower number of samples for alluvial and storm samples; higher number of tsunami) these results suggest that it is possible to differentiate quartz grains from different sedimentary environments as long as it is possible to compare them to a representative set of grains from a specific study area.

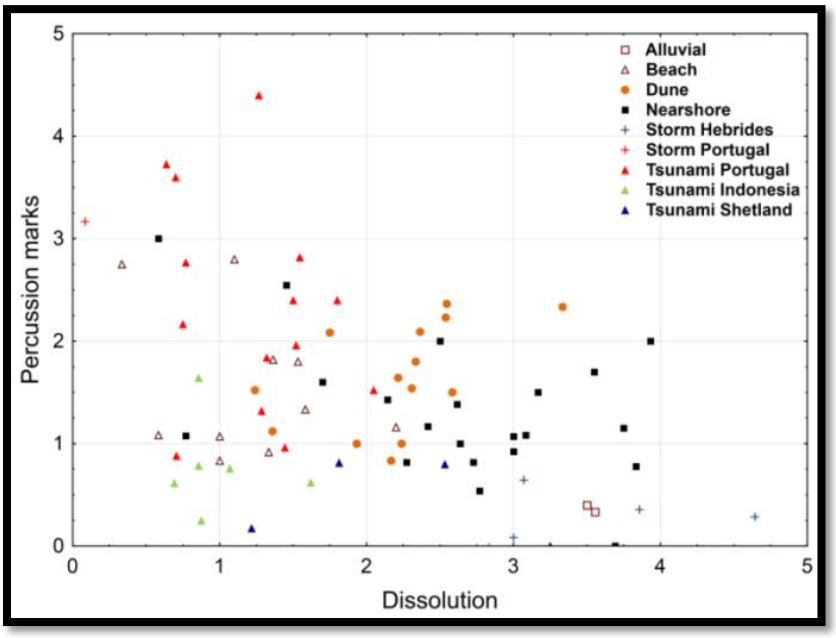

Figure 6.11 – Bivariate plot of percussion marks vs dissolution on all samples analysed.

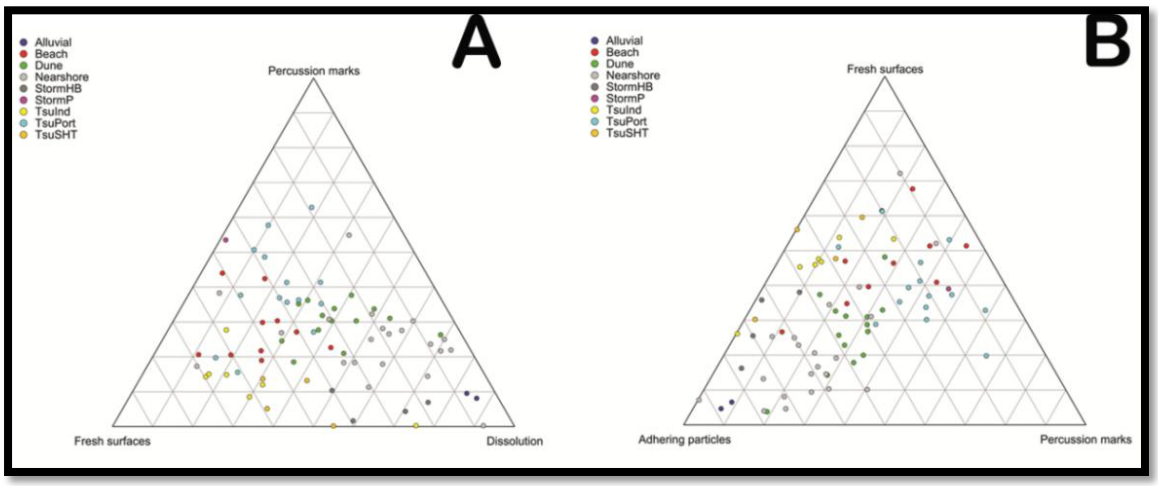

Figure 6.12 – Ternary plots of percussion marks, fresh surface and dissolution (left image) and percussion marks, fresh surface and adhering particles (right image) on all samples analysed. (Note: StormHB- storm sample from Hebrides; StormP- storm sample from Portugal; TsuInd- tsunami sample from Indonesia; TsuPort- tsunami sample from Portugal; TsuSHT- tsunami sample from Shetland).

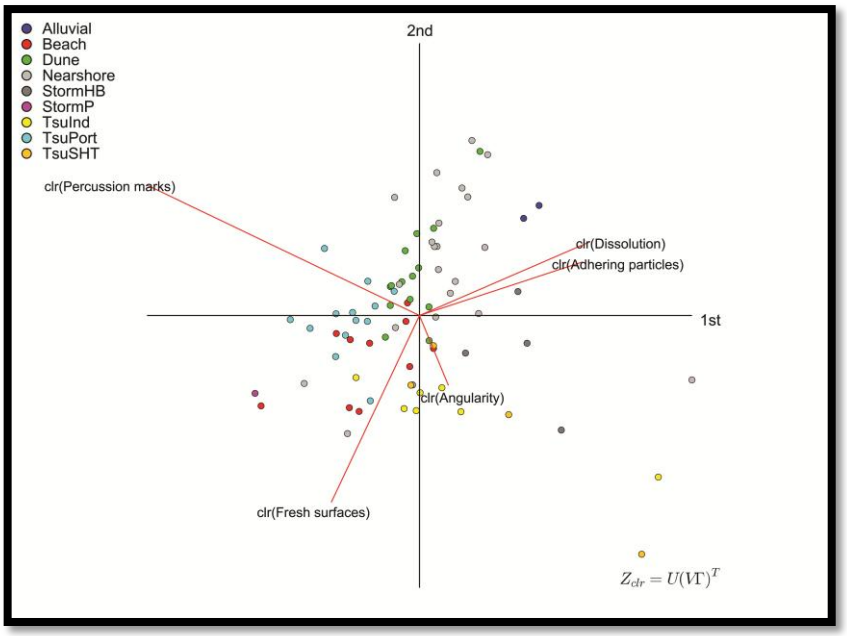

Figure 6.13 – Principal components analysis of the microtextures analysed and samples based in the two main factors identified. (Note: StormHB- storm sample from Hebrides; StormP- storm sample from Portugal; TsuInd- tsunami sample from Indonesia; TsuPort- tsunami sample from Portugal; TsuSHT- tsunami sample from Shetland). (Clr –centered log-ratio transformation; Z – random vector; T – variation matrix; ɼ – covariation matrix; V – matrix used in clr transformation; U – random vector).

In two of the study cases (Boca do Rio and Salgados) the main feature of tsunami grains was the high value of percussion marks, with no comparable value within their inferred source of sediment. However, this feature was not observed in other tsunami and storm deposits (Scotland and Indonesia) where fresh surfaces dominated and increased when compared with possible source material. The difference can be explained by the presence of an extra sedimentary source (*e.g.* dunes), which is the case of the Portuguese study areas. This fact would increase the sediment concentration and likely would cause more impacts between grains although with less kinetic energy involved in the impacts because they would have less space to gain velocity before collision. Furthermore, this fact suggests that the sediment concentration control the presence/increase of specific microtextural signatures in tsunami and storm grains. The increase in the energy involved in deposition of high energy events, when compared with permanent-regime sedimentation, tends to be represented in quartz grains as an increase in percussion marks or fresh surfaces. Although grains tend to maintain some inherited microtextural characteristics, total resurfacing of grains may occur but mainly in areas closer to the coast.

The origin of percussion marks has been a contentious matter. For instance, Campbell (1963) indicated that little evidence can be found to support the thesis that percussion markings on sand-size particles can be done in an aqueous environment. On the other hand, Mahaney (2002), Madhavaraju *et al.* (2009) and Deane (2010) suggested that V-shaped patterns of mechanical origin mainly originate in subaqueous medium with high-energy conditions. Lindé and Mycielska-Dowgiałło (1980) tested grains (in sedimentary environments and experimentally) and noted that there are differences in the occurrence of the

V-shaped forms found on natural and experimental sand grains, but their similarity nevertheless proves that the grains were subjected to mechanical abrasion in aqueous environment. So, it is manifest that although the origin of percussion marks is still a matter under discussion it is typically associated with aqueous high energy conditions of grain mobilization.

The approach addopted, both with field and experimental data, suggests that the generation of percussion marks is strongly linked with high sediment concentration and transport by grain flow. As Bagnold (1962) stated, sediment with a volume concentration greater than 9% would, as a rule, not move in suspension and Hsu (2004) suggested that concentrated dispersions of grains tend to move by grain collision. Furthermore, Mulder and Alexander (2001) suggested that in sediment mixtures with 40% or more sediment-volume concentrations are not physically turbidity currents, as in such high concentrations they are no longer supported by fluid turbulence, because grain interactions play the dominant role. Hanes (1986) modelled water flow as two fluid regions with continuous stress, velocity and granular concentration overlying a stationary bed: a collision-dominated granular fluid region and a wall-bounded turbulent-fluid shear region with saltating grains.

It is argue here that grain interaction, within an aqueous environment with high sediment concentration (*i.e.* typical in tsunami evens - Gelfenbaum *et al.*, 2007; Paris *et al.*, 2009, 2010b), is the main process responsible for the abundance in percussion marks detected in our dataset.

In order to answer that question one experiment was conducted using a magnetic stirrer within a container with water and sediment. The purpose of the experiment was to test the microtextural implications of aqueous transport at different time scales (6 and 60 minutes), different velocities (700 and 1100 magnet rotations per minute) and different sediment concentrations (2, 20 and 40%). The proportion of sand and glass microspheres (chosen because of their similarity with quartz, economical cost and clean surfaces) used was 1/3 of microspheres and 2/3 of beach sand. After each run, microspheres were selected and SEM images obtained. Furthermore, the microtextures detected in each microsphere, were counted and were later compared with features photographed in pre-experiment (non-used) microspheres (Figure 6.14).

The results obtained show a higher number of shallow mechanical imprints (e. g. percussion-like marks) at the higher sediment concentration (40%) range. In contrast, larger areas of a single sphere were affected at the lower concentration regime (2%) and the marks presented high relief, thus suggesting stronger impacts. Velocity and time increases translated in intensifications in the frequency of microtextural features.

The experiment proved that a relatively short period of time is enough to imprint significant abrasion marks in microspheres, thus strongly suggesting that short-lived events can produce strong imprints in quartz grains. However, they do not produce significantly shallow (percussion mark like) impacts. In fact, the microtextures produced were fresh surfaces, fractures and abrasion affecting areas of different sizes.

The laboratory experiments confirmed the data collected and observed in a wide range of sedimentary environments establishing that short lived events are capable of imprinting the surface of quartz grains and also demonstrating that sediment concentration and velocities of the water flow are conditioning factors of type, frequency and incision-depth of microtextural features sculptured in the surface of clastic particles.

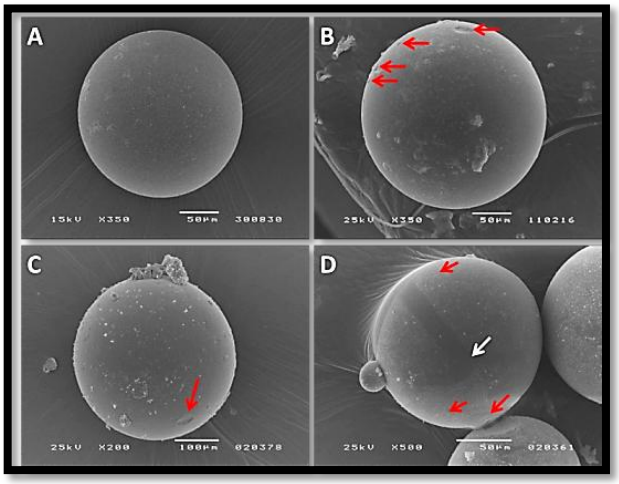

Figure 6.14 – Glass microsphere image. A – Microsphere image before experiments. B – Microsphere image after 60 minutes at 1100 rpm with a sediment concentration of 20%. Red arrow marks fresh surface. C – Microsphere image after 6 minutes at 1100 rpm with a sediment concentration of 2%. Red arrow marks fresh surface. D - Microsphere image after 60 minutes at 700 rpm with a sediment concentration of 40%. Red arrows mark percussion marks and white arrow marks long abrasion mark.

This experiment suggests that time plays an important role in terms of the frequency of microtextural signatures, but the energy-level involved and sediment concentration associated with each event are the main factors that control which and how much microtextural imprints are observed in the grains. Based in our results we argue that short lived high-energy events of coastal inundation are undoubtedly capable of resurfacing, totally or partially, quartz grains sourced in the vicinity of the deposition place.

The experimental results indicate that when entrained in a low-concentration regime, the microtextural signatures developing and affecting the particle surface are mainly deep impact features and fresh surfaces, while percussion marks are only present in higher concentration regimes (Figure 6.14C and 6.14D). This suggests that the sediment concentration plays a significant role in the microtextural features that are produced during high energy aqueous events. The experimental results suggest that lower sediment concentration allows the grains to reach higher velocities upon impact which is put in evidence by the deeper imprints in the grains surface in the lower sediment concentration regime. Furthermore, the different velocities tested indicate that the main microtextural difference is the frequency of microtextures observed, also implying a relationship between velocity of transport and frequency of imprints in the grains surface.

One example that supports the arguments presented is the findings of Wang *et al.* (1982) that analysed grains from turbidites in the Canadian continental margin. The authors concluded that the grains maintained their original shape, even if their edges appeared to be slightly rounded, but the microtextural features were superimposed by "an abundance of collision-induced marks, particularly mechanical V-forms".

Some of the previous SEM studies on tsunami deposits did not focus in quartz but ilmenite grains - Babu *et al.*, 2007 and Lakshmi *et al.*, 2010 - and showed that the high intensity of tsunami wave action caused severe deformation of ilmenite particles. The comparability of the results presented here with these results is constrained by the different minerals (and characteristics) used. Studies that used quartz (Bruzzi and Prone, 2000; Costa *et al.*, 2009) presented evidences that high-energy events (in both cases the AD 1755 tsunami) were essentially characterized by source-inherited features. However, a few features were specifically associated with tsunami transport, such as upturned plates, fractures and marks of considerable size.

Nevertheless, the present findings provide further evidence that even though the exact source is somewhat difficult to establish with clear-cut precision, that is primarily due to the fact that tsunami waves transport grains from a wide range of environments, and they are capable of carving microtextural signatures in the grains. A tsunami-transported grain population should thus reflect the sedimentary environments crossed by the tsunami waves (when they are close to the coast and capable of eroding, transporting and depositing sediments, *i.e.*, within the closure depth of the coastal zone) and the imprints that are marked in the surface of grain during that event. The dominance of contemporaneous or pre-event signal depends not only on the duration and energy of the event but also on the sediment concentration that controls the inter-grain collision.

A model of transport is proposed based in the microtextural features observed (Figure 6.15). In this model we suggest that the microtextural signatures observed in the surface of quartz grains are conditioned by the transport mechanism involved in each sedimentary environment. Thus, in the nearshore area (below depth of closure) the dominant transport mechanism is the oscillatory movement of waves, in the beach (submerged and emerged) area the breaking of waves is the transport agent that dominates. On the other hand, in the dunes the wind is the transport agent that causes the movement of grains. Furthermore, in the alluvial plains the movement of grains is caused by occasional flooding episodes of fluvial origin. These mechanisms of transport of grains conditioned decisively the quantity and types of microtextural imprints observed in the grains (cf. Figure 6.15A).

When tsunami waves invade the coastal area, they are capable of eroding, transport and deposit large sediment masses. The type of microtextural signatures observed in quartz grains is, in our opinion, conditioned by the type of transport and sediment concentration during tsunami run-up. In Figure 6.15B a conceptual model is exhibited presenting the geographical areas where it is believed grain flow transport dominates (*i.e.* the slip face of the dune) and were the grains are subject to more percussion marks imprints. The suspension and saltation mechanisms also occur but are present during the whole tsunamigenic

invasion, while grain flow is constrained to a specific area where gravity and sediment concentration play decisive roles. In the study areas where stable dunes are not present, the microtextural signatures to be observed should present a complete lack or reduced number of microtextural features associated with grain flow (*i.e.* percussion marks) and a more clear dominance of fresh surfaces (associated with saltation and suspension).

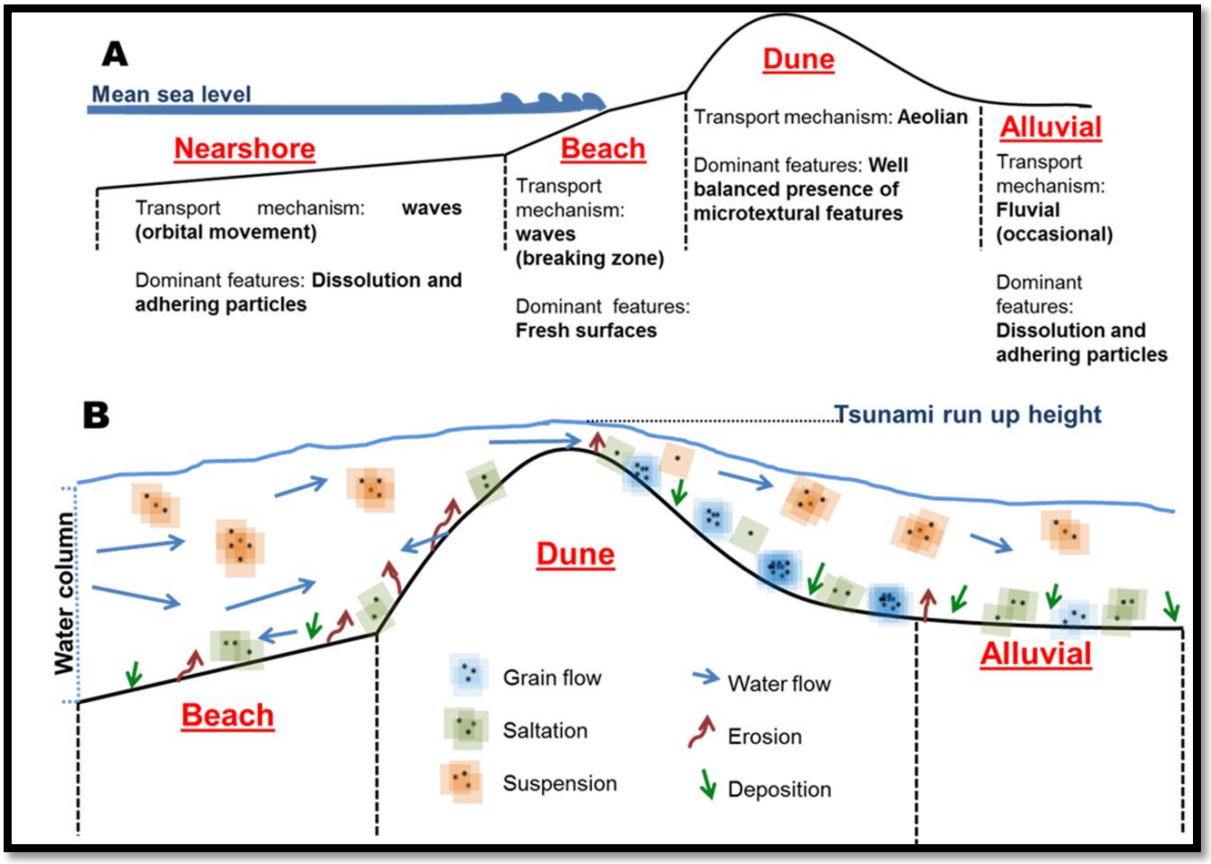

Figure 6.15 - Conceptual transport model for sedimentary environments and high energy events based in microtextural features of quartz grains analysed. A – Sedimentary environments and associated dominant microtextures. B – Grain transport during a tsunami wave incursion.

6.4. Heavy mineral signature of extreme marine inundations

The use of heavy minerals to establish provenance of tsunamigenic deposits has been sparsely attempted (*e.g.* Switzer *et al.*, 2005; Bahlburg and Weiss, 2007; Szczucinski *et al.*, 2006; Babu *et al.*, 2007; Morton *et al.*, 2007; Narayana *et al.*, 2007; Higman and Bourgeois, 2008; Morton *et al.*, 2008; Switzer and Jones, 2008). Generally, local specificities in the assemblages of geological nature constrain extrapolation of inferences between field sites and, so far, the only feature commonly observed in all locations is a higher heavy mineral content in the basal part or basal sub-units (when the layer is stratigraphically complex) of tsunamigenic deposits and yet, the reason explaining this concentration is still not well understood.

The results obtained are in agreement with the above. In fact, as demonstrated for the tsunamiites and tempestites studied, the sampling region prevails as a grouping factor (Figure 6.16) when the whole of the sample set is studied, thus demonstrating a regional conditioning factor as responsible for up to 75% of the variance in tsunamigenic and storm deposits assemblages. Hence, samples need to be considered and analysed by geographical regions if further discrimination is wanted to be extracted from the samples. Otherwise, when analysed overall, the regional character will prevail.

In the Portuguese studied areas the heavy mineral assemblages are dominated (>90%) by andalusite, tourmaline and staurolite. In Lhok Nga, about 90% of the heavy mineral population is composed of amphiboles and andalusite. In Scotland, in Voe of Scatsta, heavy minerals are almost exclusively (*ca.* 90%) made of amphiboles; whereas in Stoneybridge the assemblage is dominated by amphiboles and pyroxenes (>90%). The highest concentration of heavy minerals was detected in tempestites of Stoneybridge mainly due to richer source material (*i.e.* Lewisian gneiss).

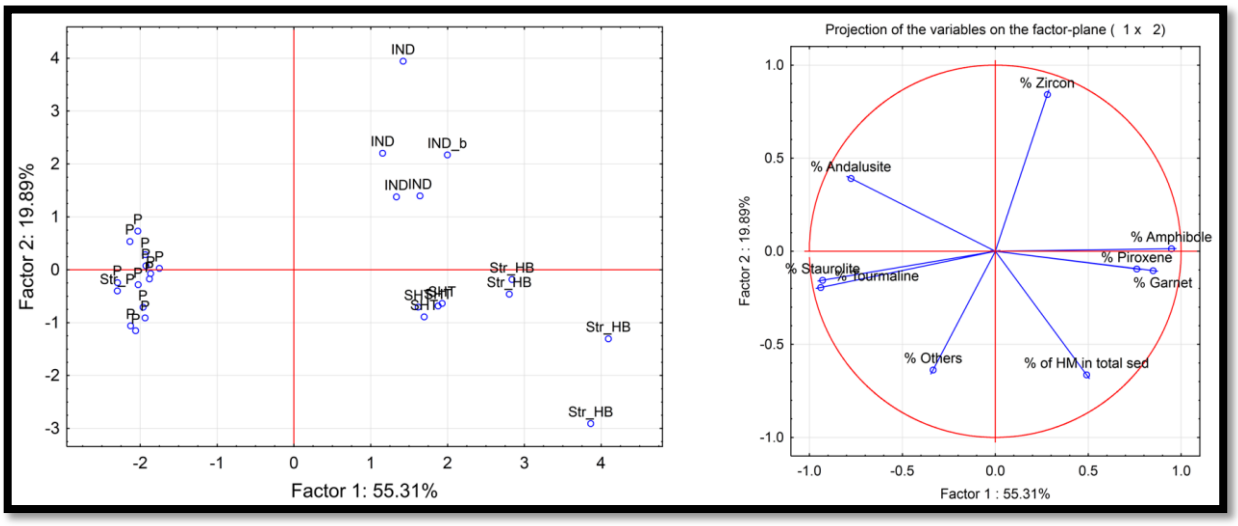

Figure 6.16 – Principal component analysis of extreme marine inundations samples and their heavy mineral assemblage. Note: left image – IND – tsunami samples Indonesia; P – tsunami samples Portugal; Str_P – storm sample Portugal; Str_HB – storm sample Hebrides; SHT – tsunami samples Shetland.

The Indonesian samples presented lower values of heavy mineral content in total sediment fraction and no trend was detectable. However, while Lhok Nga's tsunami samples exhibited a complex stratigraphy, other deposits analysed elsewhere were in essence massive. This is reflected in the heavy mineral results by the maximum horizontal and vertical variation in the proportion charecterizing each heavy mineral species (although without alterations in the assemblage) having been found in Indonesia and attributed to preservation of distinct depositional episodes including run-in and backwash and selective density controlled transport. By contrast, the Portuguese and Scottish tsunami sediments are more homogenous, reflecting preservation of one sedimentation pulse or mixing promoted by multiple waves within a confined accommodation space.

Thus, the results are in accordance with Bahlburg and Weiss (2007) that detected higher heavy-mineral concentrations at the base of individual sand layers inferred to have been laid down by different waves from the same event, and also in line with Morton *et al.* (2007), who concluded that storm and tsunami deposits can contain heavy-mineral *laminae* at the base and within the deposit because the heavy mineral assemblage is source dependent.

To facilitate the discussion below, Table 6.3 summarizes the range of specific gravities for the minerals observed in the studied areas. It is possible to perceived that staurolite is the densest mineral in the Portuguese assemblages, while zircon and garnet were the denser minerals detected in Lhok Nga. In fact, in the Lhok Nga's samples, it was observed that the higher values for zircon and garnet were detected in the backwash sample and in the most inland sample, which suggest that the source of those minerals was situated farther inland.

Table 6.3 – Specific gravity for main minerals studied.

Mineral	Specific gravity (g/cm^3)
Staurolite	3.65-3.75
Andalusite	3.16-3.20
Tourmaline	3.00-3.25
Pyroxene	3.03-3.96
Amphiboles	2.85-3.60
Garnet	3.10-4.30
Zircon	4.60-4.70
Quartz	2.60-2.70

In the cases of Salgados and Boca do Rio, principal component analysis shows that the first 2 components explain more than 2/3 of the total variance in heavy mineral assemblages (Figure 6.19 and

6.22); tsunami samples share fewer similarities with nearshore materials and more resemblances with dune and, to a less extent, with beach sediment, thus indicating dune and beach as the more likely sources.

In Salgados and Boca do Rio, results of heavy mineral studies allowed discriminating tsunami sediments from all possible source materials, the former generally showing higher proportions of heavy minerals in total sedimentand selective concentration of staurolite (densest heavy mineral identified in the assemblage). The discrepancies between the percentages of staurolite in the Portuguese studied areas might be related with the more complex stratigraphy of Boca do Rio (*cf.* Hindson and Andrade, 1999) indicating that backwash sedimentation was present and conditioned the results obtained for that location. In the studied samples of Boca do Rio, the stratigraphical contrast was not evident but heavy minerals suggest that heavy mineral assemblage was probably conditioned by possible backwash.

Figure 6.17 presents a ternary plot diagram (andalusite, staurolite and tourmaline) with samples from Salgados that demonstrates that all present-day analogues, tsunamiites and tempestite samples share many similarities in terms of assemblages although with more similarities between dune and tsunami, thus, once more suggesting the dune as the more likely (or relevant) sediment source for the tsunami deposit.

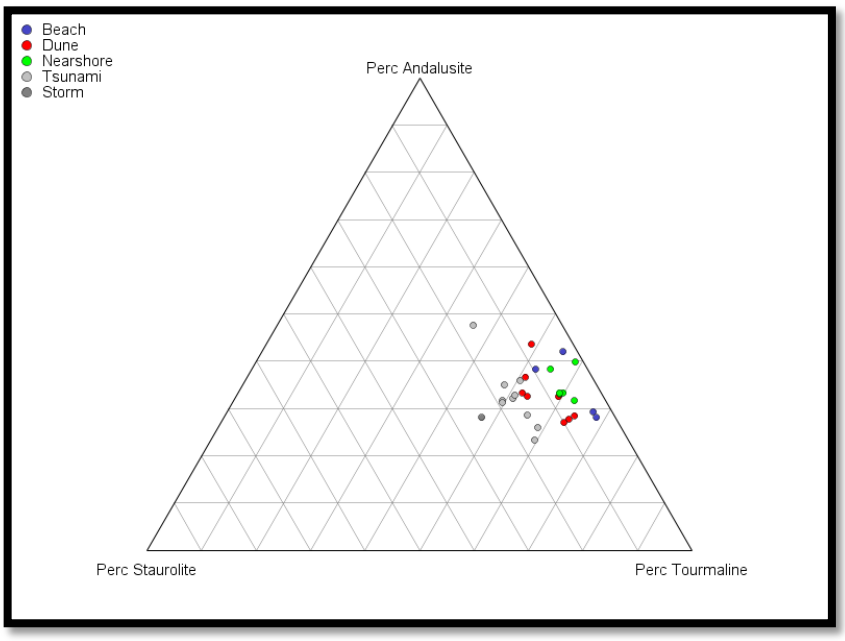

Figure 6.17 – Ternary plot of staurolite, andalusite and tourmaline assemblages in Salgados.

In agreement with the above, Figure 6.18 demonstrates that tsunami samples from Salgados present the highest percentage of heavy minerals and highest percentage of staurolite. These two facts combined suggest a higher or selective transport capacity during this tsunami event.

Sample SG_14_(0.20-0.28), a likely storm deposit, present the highest concentration of staurolite (the densest heavy mineral of the assemblage), which might be related to what Mange and Wright (2007)

described about swash on beaches during storms that are typically ideal for carrying away the quartz and feldspar, while leaving behind the concentrated heavy minerals. However, the fact that this tempestite sample is a single example limits the robustness of the conclusion.

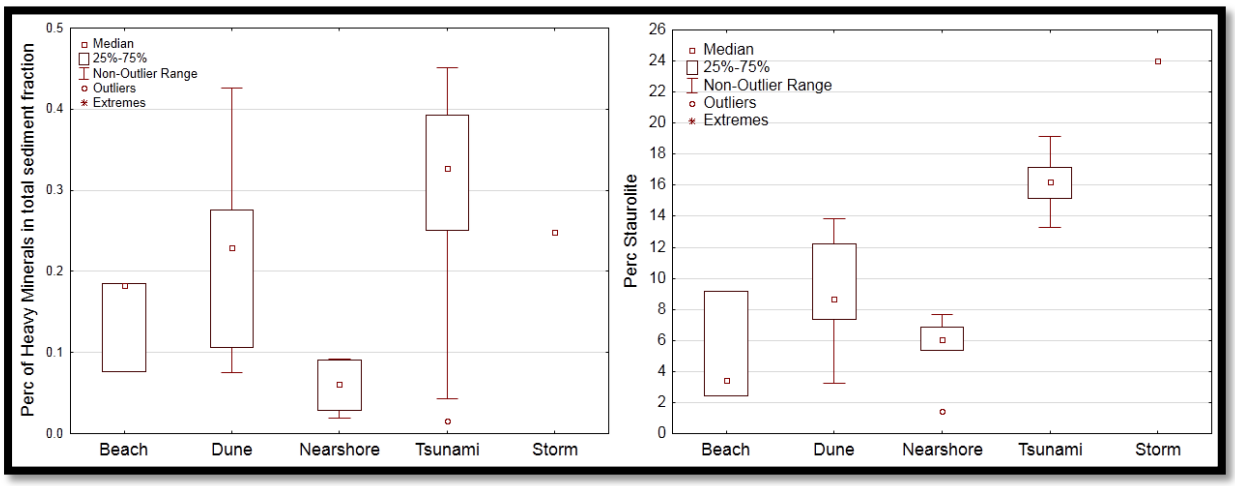

Figure 6.18 – Percentage of heavy mineral in total sediment fraction (left image) and percentage of staurolite (right image) observed in beach, dune, nearshore, tsunami and storm samples retrieved from Salgados.

Komar and Wang (1984) documented on the Oregon coast the development of small black-sand deposits during single storm events, the concentrating processes taking place within the zone of wave swash on the beach face. Swash processes are ideal for the development of heavy-mineral concentrates by the selective winnowing of low-density quartz and feldspar, the heavy minerals lagging behind. However, there is a marked enhancement of swash motions having periods >20 sec, the approximate upper limit of wave periods directly attributable to the storm. This long-period swash action, referred to as related with infragravity waves, must obtain its energy indirectly from the storm, since it does increase with storm intensity and offshore wave height. These long-period swash motions are a major factor in producing erosion of the beach face and the increase in the long-period infragravity swash on beaches during storms is ideal for selectively winnowing away lighter minerals and while leaving behind sediment concentrated in heavy minerals; thus, a functional analogy can be established with our results, that detected higher heavy mineral concentration in tsunamiites, in association with the inrrush of a long-period wave reworking local sandy sediment.

The waves and currents in the outer portions of beaches are not as conducive to mineral sorting as in the swash zone. The breaker zone is characterized by high levels of turbulence, which carry sand in suspension, thus having the effect of mixing of the sediments rather than sorting them according to their densities. Particles having low settling rates will tend to drift offshore from the breaker zone, and this may result in some degree of concentration of heavy minerals on the beach as a whole.

The model proposed by Kudrass (1987) invoke something of a ‘‘sweeping’’ action of the waves, selectively pushing the heavy-minerals landward to concentrate them in the beach sands, depleting their concentrations in the offshore shelf sands. Part of this sweeping action may result from the orbital motions of the waves acting on the seafloor sand in the offshore, thus again in agreement with the results presented here that indicate lower heavy mineral concentrations in the nearshore samples.

In samples where it was possible to conduct vertical analysis of variation in the percentage of heavy minerals in total sediment, the results disagree with Morton *et al.* (2008), who identified an overall upward increase in heavy mineral laminations at some locations. In fact, samples from Salgados, Voe of Scatsta and Stoneybridge present a clear pattern of decreasing the percentage of heavy minerals upwards in the high-energy sediment unit, thus suggesting a decrease in energy associated with the event(s) responsible for their deposition and this is in total agreement with textural data.

In what concerns horizontal patterns, it was not possible to establish a clear variation in Boca do Rio, whereas in Salgados a very slight decrease inland was identified.

In Boca do Rio, dune and beach are the more likely sources for the tsunamigenic deposit as illustrated in Figure 6.20 and 6.21. In the ternary plot diagram (andalusite, staurolite and tourmaline) all samples exhibit compositional similarities although nearshore samples slightly differ from all others. This and the results displayed in Figure 6.21 – showing strong similarities between dune and tsunami samples and prominent contrast with nearshore samples – clearly point to the establishment of dune as the most relevant sedimentary source of the tsunamigenic unit. Furthermore, the same pattern is highlighted in the principal component analysis (Figure 6.22) that, once more, demonstrates the grouping of tsunami, beach and dune samples and the differentiation from nearshore samples.

In fact, this result (dune as the main source of tsunamigenic sediment) is in agreement with inferences taken from the historical record (Silva Lopes, 1841) and geomorphological analysis (Oliveira *et al.*, 2009) in Boca do Rio, where the erosion of the dunes by the AD 1755 tsunami and textural relations between aeolian and tsunami sediment in this location are further discussed.

Actually, Bahlburg and Spiske (2011) in their study of the sedimentary record of the February 2010 tsunami at Isla Mocha (Chile), observed that the tsunamigenic unit was produced essentially (*i.e.* >90%) by the backflow. These authors suggest that due to the lack of sedimentary structures, many previous studies of modern tsunami sediments assumed that most of the detritus were deposited during inflow and an uncritical use of this assumption may lead to erroneous interpretations of palaeotsunami magnitudes and sedimentary processes, if unknowingly applied to backflow deposits. It is hypothesized by this work, that this statement may apply to part of the previous studies focusing the AD 1755 deposit at Boca do Rio. Results obtained in this study suggest that in some locations of that lowland a signal from the backwash has been preserved and is still detectable in the heavy mineral assemblage of the tsunami sediment layer.

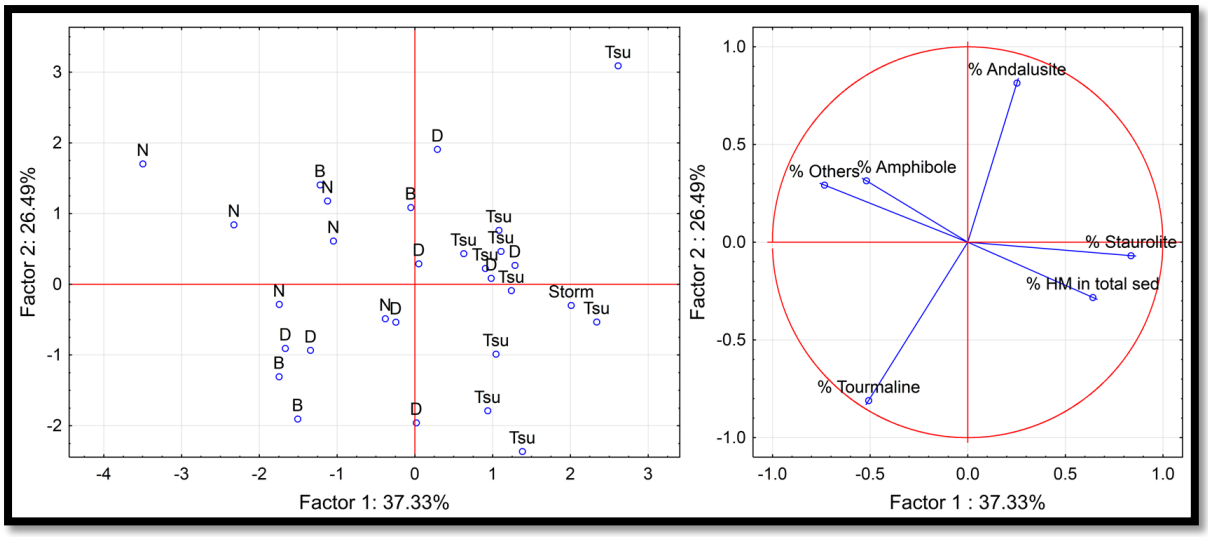

Figure 6.19 – Principal component analysis of heavy mineral assemblage retrieved from Salgados. Note: left image - B- beach samples; D- dune samples; N-nearshore samples; Tsu – tsunami samples.

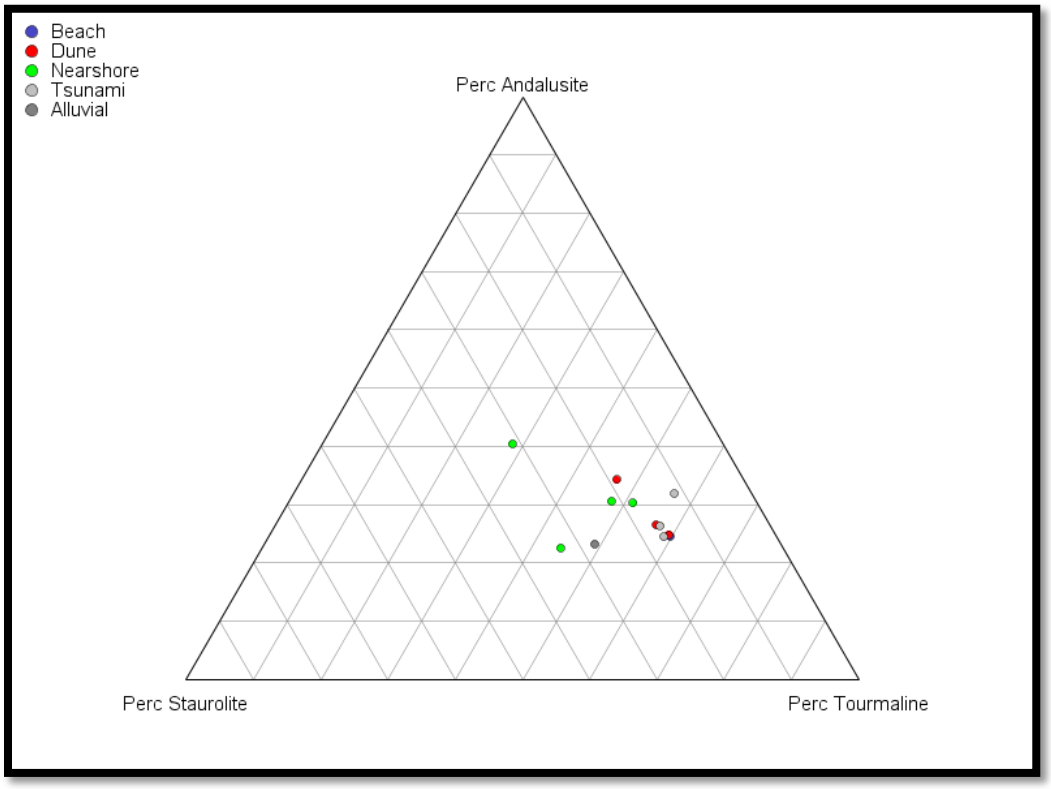

Figure 6.20 – Ternary plot of staurolite, andalusite and tourmaline assemblage from Boca do Rio samples.

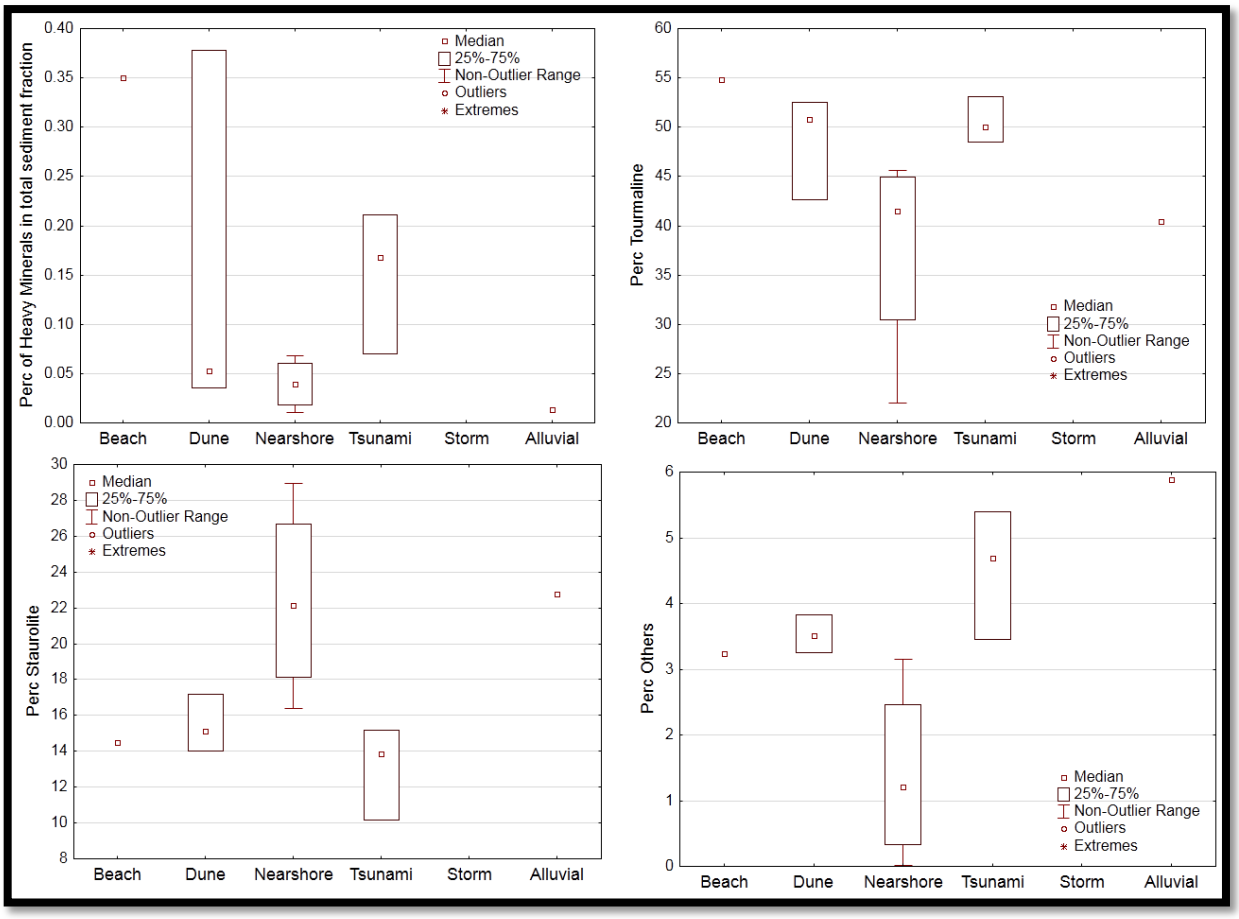

Figure 6.21 – Box-plot diagrams of heavy mineral assemblages from samples retrieved in Boca do Rio.

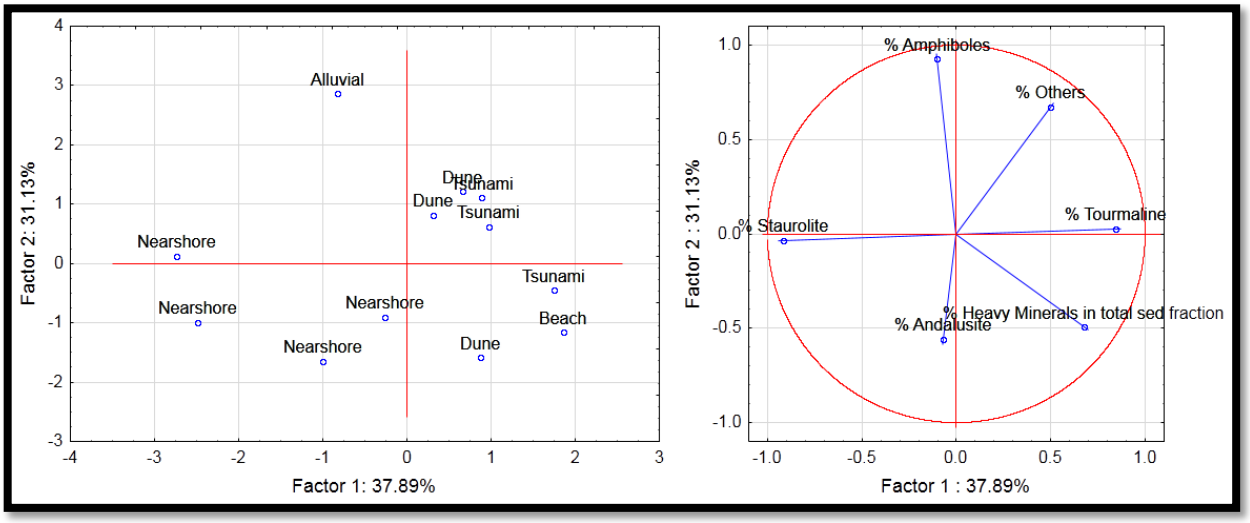

Figure 6.22 – Principal component analysis of heavy mineral assemblages from samples retrieved in Boca do Rio.

This results strongly suggest that tsunami samples in Salgados and Boca do Rio were mainly sourced in dune material and to a lesser extent to beach samples. However, in Boca do Rio, backwash

signal is present in the heavy mineral assemblages due to lower content in staurolite and proportion of "other minerals" (suggesting seaward sediment input).

The comparison of our results with the data reported by Jagodzinski *et al.* (2009) - which also tried to compare tsunami deposits, beach sediments and pre-tsunami soils in Thailand – is limited by the constrains associated with regional variance. While Jagodzinski *et al.* (2009) detected differences in the proportions of mica and tourmaline and attributed those differences to the mode of sediment transport and deposition (with mica, due to its low density, being more abundant in the topmost part of the tsunami deposit) on the assemblages studied in Salgados, Boca do Rio, Voe of Scatsta and Lhok Nga it was possible to associate variations in staurolite (Salgados and Boca do Rio) and in zircon and garnet (backwash Lhok Nga) – the denser minerals of the respective assemblages - to tsunamiites and those variations are attributed to likely source and run-in and backwash interchange.

In Stoneybridge, the pattern that emerged was a robust decrease upward in terms of the heavy mineral percentage in total sediment, which is in agreement with the description by Mange and Wright (2007) for storm heavy mineral concentration. The assemblage remains stable although with minor and irregular percentage variations in garnet, pyroxenes and amphiboles, which are insufficient for interpretations beyond inter-sample disparities.

6.5. Sedimentary environments and sedimentological differentiation

The differentiation between sedimentary environments using proxies other than ecological has been attempted many times in the past and no worldwide criteria have been undisputedly accepted. Based in the cases studied in Portugal and in agreement with the data obtained in this study, it was possible to establish specific criteria to differentiate a number of sedimentary environments (Table 6.4). However, limitations on the number of representative samples and locations should be considered, this summary beying a first approach that should be tested elsewhere.

It was concluded that alluvial samples tend to be more heterometric and poorly sorted when compared with dune and beach samples. Alluvial samples also presented a richer heavy mineral assemblage in terms of "other minerals" indicating a different (inland) relevant source.

On the other hand, grains of beach sediment are more angular and present more abundant fresh surfaces (both in the morphoscopic and microtextural analyses). By contrast, dune sediment yielded more rounded and spherical particles and present more adhering particles than beach samples.

Mason and Folk (1958) were able to distinguish beach, dune and aeolian flat sediments by size analysis (using standard deviation, kurtosis and skewness of the grain size distributions). In their study case, dune and beach presented the lower and higher standard deviation, respectively, and these sedimentary environments were not distinguishable using kurtosis and skewness. The same authors also concluded that there is a very high inter-location variation in size distribution parameters, that variation constraining some of the conclusions. In the presented studied cases, textural analysis, by itself, did not allow a clear differentiation of sedimentary environments.

These results are partly in agreement with Shepard and Young (1961) (74 locations worldwide) that demonstrated that dune sands are generally rounder, have a larger silt content and higher content in heavy minerals. If dune sands are more rounded than beach samples because of the abrasion between grains produced during wind transportation, very little rounding would have occurred in transporting sand to the bordering dunes. That being the case it would be necessary to collect samples at considerable distances inland, within the dune field, in order to get appreciable differences. If, on the other hand, the principal difference comes from the sorting action of the wind in picking up rounder grains from the beach, the difference should be immediate. Beal and Shepard (1956) showed that there was no progressive change with distance inland.

Shepard and Young (1961) concluded that a greater degree of roundness in dune samples in almost all cases studied. 80% of sand grains in beach berms are more rounded than in the foreshore, either by action of wind or action of waves. They determined increasing roundness for beach, berm and dune. These contrasting results reflect the high specific character of each group of samples, which should be reflected in caution when analysing the results from these proxies. In the field areas addressed in this study, dune grains, in agreement with Shepard and Young (1961), were more rounded inland and the berm

presented more angular particles. An increasing inland profile/trend in roundness was just about discernible in Salgados and in Boca do Rio the oldest dune (known as Roman dune, due to roman ruins that it covers) presented higher values for roundness and dissolution, thus suggesting longer periods subjected to mechanical and/or chemical processes, hence indicating an older age.

According to the obtained results, nearshore samples should be divided in two groups: proximal and distal nearshore samples. The first group (situated between the closure depth and the surf zone) shares many similarities with beach samples and, in the case of Boca do Rio grains from the latter were more angular than from the former. Distal nearshore samples (situated beyond the closure depth) presented typically higher percentage of bioclasts, rounded grains with strong and abundant dissolution features and the higher values for adhering particles. In fact, Samsuddin (1986) discussed a marked variation in size distribution in the foreshore and breaker zone that occurs due to a variation in wave energy reaching the point of sampling and extent of turbulence affecting this environment. The plunge point just seaward of the backwash is considered as the point of maximum turbulence and high energy conditions. This zone is of primary importance in forming the final sediment pattern in the beach environment. We argue that this plunge point correspond to the higher values for angularity and fresh surfaces that were observed in our grains. Our conclusions are supported by Iversen (1951) that demonstrated that the internal motion of breaking waves is a highly turbulent flow condition that is capable of keeping large amounts of particles in suspension, which might justify an increase in collision between grains with consequent increase of angularity, mechanical marks and fresh surfaces.

From the proxies tested in the present research it was able to apply morphoscopy, microtextural analysis and heavy mineral assemblages as tools for sedimentary environment differentiation, although caution should be used in the extrapolation of these results elsewhere.

6.6. Single event signatures: the spatial contrast

The tsunami deposits of AD 1755 that accumulated along the Algarve coastline mostly consist of a laterally extensive layer of shell-rich sand displaying an erosive base and a gradual and irregular upper boundary, which ramps and thins landwards. In some locations, the tsunami deposit is entirely composed of sand (*e.g.* Salgados). In other areas, the tsunami deposits are characterized by sand sheets containing isolated (also referred to as "floating") cobbles (*e.g.* Boca do Rio).

The Lagoa dos Salgados is actively accreting and this coastal depositional environment exhibits significant potential as a sedimentary archive of palaeoenvironmental changes that occurred throughout the Holocene. In this case, the data described above suggests that the lagoonal infill accumulated essentially after 7000 Cal BP, in progressively lower-energy conditions, favoured by sheltering offered by the presence of a coastal barrier. Sediments of units A to C exhibit a neater marine signature when compared with the topmost deposits of units D and F, which correspond to terrestrial-sourced, mud-dominated sedimentation that persisted throughout the last *ca.* 1500 years across the whole lowland. This later sedimentation pattern was disrupted by a unique event responsible for the deposition of unit E, a single laterally continuous and thin *laminae* of coarser material carrying abundant marine ecological proxies, which suggests a brief return to higher-energy conditions and marine sourced sedimentation, affecting most of the lowland. Although the Lagoa dos Salgados is subject to occasional breaching of the barrier promoted by marine overwash, providing water and sediment exchange with the ocean, the textural signature of these events is, at present, as it was in the recent past, confined to the inlet and flood shoals, where marine sand reaches the top of the stratigraphic column. Further inland and at a short lateral distance from the channel, the top sedimentary unit is solely represented by mud of unit F.

Within the upper mud-dominated units D and F (global thickness of 0.70-1.90 m) the conspicuous medium sand lamina (unit E) occurs at *ca.* 0.40 m below the surface and consists essentially of quartz sand with marine bivalve shell fragments and mud intraclasts (rip-up clasts). The thickness of this layer decreases from *ca.* 0.80 m close to the barrier to a few mm *ca.* 850 m at its landward limit, well beyond normal overwash, storm and tidal influence.

The sandy tsunami layer in Boca do Rio consisted of several distinct sub-units that vary greatly in both vertical and horizontal sections. This unit is in contrast with the mud-dominated sedimentation of terrestrial source observed in the under and overlying units. The highly variable nature of the horizon appears to be due to rapid variation in the hydrodynamic characteristics of the depositional event (run-in, backwash and periods mediating both processes where mud could settle) and diversity in source materials. The tsunami deposit detectable at *ca.* 0.80 m below the surface wedges out and becomes discontinuous, but it can be traced for more than 1 km inland.

Mapping of the *laminae* in Salgados suggests a wide, thin and fan-shaped feature, wedging out within the lagoonal basin, implying an exceptionally large inundation of marine origin. The erosive base together with the presence of rip-up clasts and grain size contrast with the framing sediment favours an

emplacement mechanism governed by an abrupt single high-energy marine inundation, rather than a positive increment in the sea level rise rate.

The spatial distribution of characteristics of sediment from unit E and the inferred vectorial properties of flow and associated sediment dispersion path are compatible with a massive inflow of marine water and sediment. This is in clear contrast with the outflow that must have followed the inundation and apparently failed to leave a distinct sedimentary record. Moreover, the sedimentary signature of the inundation demonstrates that the inflow path of water and sediment was essentially conveyed through the inlet rather than extensive overtopping of the barrier, thus providing an objective limit to the maximum elevation of the water level at the time of inundation. In the case of Boca do Rio, according to coeval sources (Pereira de Sousa, 1919), the tsunami waves overtopped the existing foredune. 11-13 m for the elevation of tsunami waves at the coast are mentioned, as well as the destruction of the large foredune by the incoming waves. A detailed description of the effects of the backwash was also made, referring to the uncovering of Roman ruins in the beach area. Since AD 1755, the coastal system has not been capable of rebuilding a robust foredune.

The comparison of the textural, morphoscopic, microtextural and heavy mineral assemblage of unit E from Salgados sediments and of possible sources, suggest that the coarser fraction of unit E was mainly derived from beach and dune sediments, whereas the underlying unit D may have contributed to the finer fractions. The beach comes out as a very likely source in terms of angularity and fresh surfaces of the grains, whereas dunes are suggested as a major source by percussion marks and heavy mineral assemblages. Most probably both environments have contributed as primary and essential sources for materials washed inland and deposited as unit E. This is in line with Sato *et al.* (1995), who found that two Japanese tsunami deposits (1983 and 1993) were mainly sourced from the beach sediments, using limited textural data.

As suggested by Goff *et al.* (1998; 2001) the shell richness is one of the attributes characterizing tsunami sediments, and a good marker of the high-energy involved in the sediment transport. In Lagoa dos Salgados, unit E is characterized by a sharp increase in the carbonate content associated with shells, mostly represented by fragments of thick-shelled marine bivalves. In Boca do Rio, within the tsunamigenic unit, the nannoplankton, foraminifera and ostracoda assemblages are diverse, containing a variety of predominantly marine species (Hindson *et al.*, 1996; Hindson and Andrade, 1999), which is in contrast with the assemblages observed for the under and overlying units, which were dominated by a small number of species that were able to tolerate the variable salinity conditions typical of estuarine and salt marsh environments.

The heavy mineral assemblage in places sampled at Boca do Rio might suggest incorporation of material from backwash, although the massive facet of the deposit constrained the clear identification of sub-units that could reinforce that conclusion. In the studied cases of Salgados and Boca do Rio, differences in heavy mineral assemblages of tsunamiites allows speculation about the relevance of the backwash

sedimentary contribution. In the case of Boca do Rio it may have been larger and probably fuelled by the geomorphological setting – enclosed valley. In contrast, the wide flat area of Salgados lagoon apparently dismissed any relevant contribution of backwash deposition, which was not perceived in any of the proxies used. The influence of contrasting geomorphology of the accommodation space offered by both lowlands in what regards sedimentary signatures left by the same flooding episode is further illustrated by Hindson and Andrade (1999) detailed stratigraphic analysis of the trenches excavated in Boca do Rio; they found a complex stratigraphy and interpreted that complexity as indicative of more than one episode of sedimentation being represented within the tsunamigenic unit, at least in the more seaward portion of the lowland. Further inland, they remarked that the deposit was texturally more consistent, and transformed into a single homogeneous sand layer, indicating that the processes of deposition were simpler. This is in clear contrast with Salgados, where a more spatially consistent deposit (*i.e.* single sandy layer) was observed, suggesting that the depositional story preserved in the sedimentary archive is proportionally simpler.

The likely source for the tsunami deposit is Boca do Rio has been discussed by other authors (Hindson *et al.*, 1996; Hindson and Andrade 1999 and Oliveira *et al.*, 2009) and all implied the dune as the main sedimentary contributor for the tsunamiite. Our morphoscopic, textural, microtextural and heavy mineral results are in agreement with this, especially by demonstrating that nearshore was the unlikeliest source and implying the dune as the main source (if not the only) relevant source. The backwash signal is relevant, at least in some locations, and should deserve consideration in future studies.

Immediately to the east of Salgados, in the Alcantarilha lowland, Dinis *et al.* (2010) observed geomorphological features extending inland from the lee slope of the coastal dune ridge associated with the deposition of a thining inland sandy layer that extended in the adjacent alluvial plain, and interpreted these features as the result of a tsunami event; due to its chronostratigraphic characteristics it can be correlated with the same event responsible for the deposition of unit E in Lagoa dos Salgados (*i.e.* the AD 1755 tsunami).

Similarly, in Martinhal (immediately to the east of Sagres), the AD 1755 tsunami breached the barrier and deposited an extensive sheet of sand. The tsunami origin for this deposit was supported by several features, such as incorporation of rip-up clasts from the underlying layer, basal erosive contact and contrast between increased content of marine Foraminifera in the tsunamigenic unit and the essentially brackish assemblages yielded by the under and over lying layers (Kortekaas and Dawson, 2007).

In other areas of the Algarve sedimentary evidences of the AD 1755 deposits were also discussed by Andrade (1990, 1992) in Ria Formosa, central Algarve; and Costa *et al.* (2011) in Barranco and Furnas (east of Martinhal). In the case of Ria Formosa severe damage of the barrier chain and extensive overwash of two of the eastern barrier islands (Armona and Tavira) was detected.

In the Barranco and Furnas alluvial plains a group of uncommon size-range particles [0.3 - 1m (a-axis diameter)] were observed a few hundred meters inland. The radiocarbon dates obtained from *in situ* endolithic bivalve shells suggested that transport was contemporary with the AD 1755 tsunami.

Although the documentary record indicates that the Algarve coast has been affected by other tsunamis in the last two millennia (Baptista and Miranda, 2009), no clear sedimentary record of their activity has been found, until present. If the time window is extended further back, a single reference to a peculiar layer, inferred as tsunamigenic and dated from *ca.* 6th century BC, was described by Schneider *et al.* (2009) in a central Algarve lowland.

The lack of correspondence between historical and sedimentary record of tsunami events in the Late Holocene can be attributed to: a) eventual predominance of erosional patterns, as discussed by Szczucinski (2011) in the case of the 2004 Indian Ocean tsunami, thus inhibiting the preservation and deposition of tsunamigenic signature; b) lack of textural contrast hindering distinction between tsunami and framing sediments; c) tsunami waves incapable of overtopping dunes, thus limiting their sedimentary signature further inland of the coastline; d) extensive seaward shift in the location of the land-sea interface promoted by the forced regression that accompanied intensive silting of formerly drowned lowlands.

This study shows that the sedimentary signature recognized in unit E from Lagoa dos Salgados shares many stratigraphic and chronological characteristics with the nearby deposits detected in Boca do Rio (and elsewhere in the Algarve), thus suggesting a regional and synchronous event as responsible for its deposition. This conclusion is in agreement with the documentary record of this particular inundation in the Algarve coast. The spatial characteristics of the tsunami layer at Lagoa dos Salgados suggests that the barrier was effective in preventing extensive overtopping by the waves and this provides grounds to infer the maximum elevation of the sea surface in this coastal stretch of *ca.* 10m at the time of inundation.

A similar pattern was observed in Boca do Rio. The pre-existing dune was washed away by the AD 1755 tsunami waves (Silva Lopes, 1841). Based in historical records (Silva Lopes, 1841), archaeological data and GIS-assisted geomorphological reconstructions (Oliveira *et al.*, 2009) the estimated elevation of that dune is compatible with values obtained for Salgados (*ca.* 10m), thus indicating a similar tsunami wave height at the coast between the two locations (separated by approximately 50 km).

The uniqueness of this record within the top low-energy sedimentary sequence lasting for about 1500 years in Lagoa dos Salgados, Alcantarilha, Boca do Rio and elsewhere in Algarve lowlands might be used, with caution, to extrapolate a recurrence interval for similar high magnitude tsunami-borne inundations of this coast, suggesting that such interval may be of millennial scale.

6.7. Multiple event signatures

The deposits studied here share many of the sedimentological diagnostic criteria of tsunamiites and a summary is presented in Table 6.4.

The Salgados tsunamigenic unit is composed of medium to fine sand, contrasting markedly with the underlying sediment and is separated from it by an unconformity. The tsunamiite in Salgados presents a decreasing thickness inland up to its oblivion approximately 800 m from the present day coastline. This unit presents a strong lateral variance in terms of its sedimentary characteristics although it is commonly observed as a massive sandy deposit with no identifiable laminations and without sedimentary structures. Numerous mud rip-up clasts from the underlying unit were found in this unit.

In Boca do Rio the studied tsunamiite studied is present in the alluvial plain Holocene sequence, up to *ca.*1200 m from the coastline. The thickness of this unit also decreases inland. The study of this deposit revealed a strong lateral variation and a complex sedimentological characterization. In some locations it was possible to differentiate sub-units within this unit, mainly in the seaward area. However, the sub-units disappear inland and the deposit becomes a massive-like deposit before its wedging out inland. The lower contact of this unit is erosive and it also showed very abundant broken shells of marine organisms, rip-up clasts and, in some locations, cobbles and boulders.

The tsunami sediments associated with the Storegga slide consist of fine or medium sand, often containing rip-up clasts both of organic material or peat. They basal contact is erosive and the unit has a massive-like appearance even if cobbles could be observed within the unit.

In Lhok Nga the tsunamiite is composed of greyish to yellowish coarser to medium sand, with relevant variations in thickness, grain-size and vertical trends. The contact between the tsunamigenic units and the underlying soil is abrupt or erosional. The thickness of the tsunami deposits varied and reached its maximum values in the topographic lows. Lamination was visible and corresponded to distinct layers associated with the sequence of run-in and backwash phases of successive tsunami waves.

The fact that different size-ranges were observed within the tsunamigenic unit might suggest that the sediment material was transported through a combination of rolling, saltation and suspension.

Age-estimation calculations allowed the association of the deposits observed in Salgados, Boca do Rio and Voe of Scatsta with specific events that affected the Portuguese and Scottish coasts (AD 1755 Lisbon tsunami and the Storegga Slide). The Lhok Nga deposit was associated with the 2004 Indian Ocean tsunami.

Common aspects to the occurrences briefly characterized above include an erosional/sharp basal contact, thinning inland, fining upwards, the presence of rip-up clasts and a higher concentration of heavy minerals (decreasing upward) when compared with source material. These characteristics reflect the suddenness of a unique high-energy marine inundation responsible for the deposition of the studied units. One further pattern common to all deposits studied is that they may show contrasts in sediment texture,

vertical size-grading, thickness of the deposit, neatness of boundaries with over and underlying units, presence of transitional grading to the overlying sediments and other macroscopic features (*e.g.* alignment of prolate mud clasts, platy shell fragments or whole valves embedded in sand, number of rip-up clasts at a certain distance from the basal contact, "floating" bouders or cobbles) in observation points located at very short distances. This is more apparent in deposits showing more complex lithostratigraphic arrangements, which, in turn, may reflect, to some extent, entrapment of the inundation in semi-enclosed spaces, a feature determined by geomorphological constrains.

Although sedimentological similarities between the different studied deposits were salient, several differences were noted. Only the deposit of Lhok Nga presented stratification/laminations distinctly separating depositional entities, which were associated with the different waves and backwash. The other deposits essentially revealed a massive aspect, which is probably associated with either depositional specificity associated with turbulent flow or with the lack of conservation of the sedimentary structures, as reported to have been observed within a 5-year interval following the 2004 tsunami – see above. Related with this is the presence of mud-drapes in the unit studied in Lhok Nga and their absence in the deposits of Salgados, Boca do Rio and Voe of Scatsta. The deposition and preservation of mud drapes on sand waves is favoured by a large sand-wave asymmetry, a high bottom concentration of suspended mud and large time-velocity asymmetry (Allen, 1982) conditions that were likely registered in Lhok Nga but apparently did not prevail in the other locations studied.

Broken shells (of both macro and microscopic organisms) are a common presence in tsunami deposits. In our studied cases, the tsunamiites revealed a significant occurrence of broken shells within the units analysed and attributed to tsunamis. However, in the Voe of Scatsta samples macroscopically it was not possible to observe the presence of shells within the deposit.

In terms of grain size distribution all the massive-like deposits presented a unimodal distribution, while the Lhok Nga samples presented a bimodal distribution, thus representing a substancial difference in terms of source origin. In the case of Salgados, Boca do Rio and Voe of Scatsta the unimodal distribution is simply explained by the similar grain-size characteristics of the possible source materials.

Morphoscopic and microtextural imprints were discussed in detail in section 6.2.and 6.3. Some local specifies constrain extrapolations of the results, although they demonstrated the relevance of these techniques in the differentiation of tsunamigenic units and in the establishment of their likely sedimentary sources.

All tsunamiites studied revealed an increase in the percentage of heavy minerals and a decreasing upwards concentration of denser minerals.

The establishment of source was possible for Salgados and Boca do Rio where it was clear that the tsunamigenic sediments share less similarities with both alluvial and nearshore materials and more

(morphoscopic, microtextural and heavy mineral assemblages) similarities with dune and beach deposits, thus suggesting the latter as the probable sedimentary source of the tsunamigenic units.

Table 6.4 – Comparison of sedimentological features of the tsunamiites studied in this work.

Criteria	Salgados	Boca do Rio	Voe of Scatsta	Lhok Nga
Age	AD 1755	AD 1755	*ca.* 8000 yrs BP	AD 2004
Basal contact	Erosional/sharp/ unconformity	Erosional/ sharp/ unconformity	Erosional/sharp/ unconformity	Erosional/sharp/ unconformity
Max. distance inland (deposit)	*ca.* 850m	*ca.* 1500m	*ca.* 1500m	*ca.* 3500m
Structure of unit	Massive	Massive	Massive	Unit with several laminae
Thins inland	Present	Present	Present	Present
Sedimentary structures	Not observed	Not observed	Not observed	Parallel lamination or cross-lamination
Mud-drapes	Not observed	Not observed	Not observed	Present
Rip-up clasts	Present	Present	Present	Present
Broken shells	Present	Present	Not observed	Present
Grain size distr.	Unimodal	Unimodal	Unimodal	Bimodal
Fines upwards	Present	Present	Present	Present
Microtextural characteristics	Percussion marks	Percussion marks	Fresh surfaces	Fresh surfaces
Heavy mineral assemblage	Highest percentage and more denser minerals	Highest percentage and dilution of denser minerals (backwash signal).	Rich in heavy minerals (more at base)	Rich in heavy minerals (more at base). Backwash signal present.
Sediment source	Dune and beach	Dune and beach	Undetermined	Undetermined

6.8. Storm vs tsunami deposits

To compare tsunami and storm deposits it would be preferable to compare events and their sedimentological signatures in the same location. However, due to sedimentary and sampling constrains this was only possible in the case of Salgados, even though only one storm sample was studied in detail, it constrains interpretations and precludes extrapolations. Though the limitations above, comparison was possible between the Stoneybridge storm samples and the tsunamiites of Salgados, Boca do Rio, Voe of Scatsta and Lhok Nga (Table 6.5). Furthermore, the Salgados storm deposit was compared with the tsunamiite and present-day analogues retrieved from the same location.

Both tsunami and storm deposits can appear to be massive, lacking sedimentary structures, but most storm deposits exhibit at least some sub-horizontal planar stratification (Schwartz, 1975; Morton 1978; Leatherman and Williams, 1983; Tuttle *et al.*, 2004). Where present, the number of layers or lamina sets in both tsunami and storm deposits depend partly on the thickness of the deposit. Both deposits studied at Salgados did not present lamination or differentiation in layers, thus revealing a more massive-like structure. In the case of Stoneybridge and their comparison with tsunamiites, it was noted the absence of rip-up clasts and of broken shells in the former case, which was attributed to local characteristics. Another differentiator factor was the presence of more angular and less spherical grains which could be ascribed to either characteristics of source sediment or to the energy and timing involved in the storm event. The latter assumption is valid if we consider that the rounding of grains is a process that requires longer time to be completed (in comparison with sharpening of edges – as previously discussed in section 6.2). Another factor that allowed differentiation between storm and tsunami deposits was the distinct inland penetration in Salgados. The storm deposit is registered at shorter distances from the coast while the tsunami imprint extends for almost 1 km inland. It is quite plausible that the inland penetration distance of the sedimentological signatures of a large tsunami exceeds that of a storm when the same location (*i.e.* same morphological constrains) and similar time windows (thus excluding significant changes in the above-mentioned constrains) are considered. It is however questionable if this contrast in dimension is a universal criterium for distinction of storms and tsunami deposits.

At Stoneybridge the vertical variation of the storm deposit was observed with the presence of more bioclasts at top and base of the deposit (fact explained by the proximity with under and overlying layers). In fact, more lithic material was observed in the middle section of this deposit, which reflects more clearly the high-energetic character of the event and the sediment source. Moreover the grains revealed more angular features and fresh surfaces, which is clearly related with the more energy involved and the possible higher sediment concentration. However, it is important to stress that the base of the unit presented low angularity values, possibly the result of long term action on the initially available sediment. The fact that percussions marks were present in a reduced percentage is most likely related with source characteristics.

The tempestite grains in the Stoneybridge deposit were mostly sub-discoid and spherical grains were nearly absent and the percentage of heavy minerals decreases to top, which is a common aspect of

storm deposits (Mange and Wright, 2007). Moreover, it was also observed a decrease in the percentage of "other (heavy) minerals" towards the top which might reflect the decreasing capacity of transportation or, more probably, the selective transport of heavy minerals (which was discussed in section 6.4).

In Salgados the fact that only one possible tempestite sample was used in this study limits some analysis and interpretations. Results obtained in this case show that the tempestite presented lowest percentage of bioclasts compared with both the tsunami and possible source materials. Hence, the storm deposit present the highest percentage (*ca.* 80%) of quartz, followed by tsunami (75%-55%) and present-day analogues (<60%). The tempestite in Salgados shared many similarities with beach samples, such as the lower percentage of well-rounded grains and high content in discoid grains, although it presented similar values to tsunami grains in terms of angularity and percussion marks. The storm deposit in Salgados presented high percentage of heavy minerals (higher than possible sources but lower than tsunami samples), a maximum value for staurolite (densest mineral of the assemblage) - which was followed by the rest of tsunami samples. Furthermore, it also presented the lowest value for tourmaline (similarly to tsunami samples). These heavy mineral features are indicative of similarities between the two events (*i.e.* storm and tsunami) even though tsunamis seem to present a higher concentration of heavy minerals probably due to their higher transport energy (*i.e.* higher turbulence of the flow).

Table 6.5 – Sedimentological characteristics of storm deposits from Salgados and Stoneybridge and their differentiation from tsunami deposits.

Criteria	Salgados	Stoneybridge	Differences to tsunami deposits
Stratigraphical	Erosional abrupt contact Massive unit without laminations No rip-up clasts Broken shells Thins inland	Erosional basal contact Massive unit lacking laminations No rip-up clasts Broken shells No vertical grain-size trend	No lateral variations Less extension inland Absence of rip-up clasts
Textural	No clear differentiator	No clear differentiator	No clear differentiator
Morphoscopic	No clear differentiator	More bioclasts in base and top More lithic – middle of unit More angular Mostly sub-discoid; spherical nearly absent	No clear differentiator
Microtextural	More similar to beach High percussion marks	Base of unit lower values of angularity Fresh higher in mid dep HB -Low percussion marks (source-related)	Lower frequency of percussion marks
Heavy minerals	Increase in heavy mineral percentage Salgados more Staurolite	% of heavy minerals decreases to top Less "other minerals" to the top	Higher percentage of HM

7. Conclusions

7.1. Achievements and future work

Numerous studies of sediments recording extreme marine inundations have aimed to characterize and distinguish such sedimentary materials, thus contributing to extend the available database on coastal inundation further back in time, well beyond the historical record, and also estimate event recurrence. This work further contributed to these objectives by focusing on the application of textural, morphoscopic, microtextural and compositional analysis and features, to identify deposits of extreme marine inundations and their likely source materials. The work presented here results from a variety of locations (Salgados and Boca do Rio - Portugal; Lhok Nga – Indonesia; Voe of Scatsta and Stoneybridge - Scotland) and considers events of different chronologies and sources (AD 1755, 26 December 2004 and the Storegga Slide tsunamis; the Great Storm of 11 January 2005) that affected contrasting coastal settings with different regional oceanographic conditions.

The methods used on samples from the studied sites were: lithostratigraphic interpretation, grain-size analysis and interpretation of size-distribution patterns; morphoscopic characterization of selected particle populations under the microscope; microtextural characterization of quartz grains using Scanning Electron Microscope imagery and study of heavy mineral assemblages.

The storm and tsunami deposits studied consisted of essentially sand-sized sediment. The typical lithostatigraphic setting of these peculiar deposits is of one high-energy layer or *laminae* sandwiched within low-energy sediment, presenting an abrupt basal contact, thinning and fining inland until wedging out within the low-energy materials, which correspond to the signature of the permanent sedimentation regime. Tsunami deposits typically exhibited a noticeable lateral variation in all sedimentary and geometric features, even at short distances, and all presented a massive internal structure, with the exception of the most recent event (2004 tsunami and deposit in Lhok Nga – Indonesia).

Results obtained from the morphoscopic study of sand-sized particles (e.g. roundness and shape) indicate that in Salgados (Portugal), Boca do Rio (Portugal) and Lhok Nga, these attributes are useful in discriminating coastal sedimentary environments and/or in the establishment of likely source material for materials deposited by extreme marine inundations. For instance, in Salgados it was clear both through the compositional pattern, as well as considering sphericity, that the nearshore samples share the less affinity with the tsunamiite samples.

Results from grain surface microtextural analysis revealed that this proxy is a valuable complementary sedimentological technique to be applied in the discrimination of coastal sedimentary

environments and is relevant in the identification of extreme marine inundation deposits, especially when considered within the regional sedimentological and geomorphological context. Tsunami- and storm-transported grains presented a more frequent surface reworking by percussion marks and fresh surfaces when compared with potential source materials and with grains representing present-day active coastal depositional environments. Heavy mineral assemblages were typically site-specific. Generally, the concentration of heavy minerals in total sediment decreases up-unit in the high-energy layer and, in one of the studied sites (Salgados, southern Portugal) the content in heavy minerals (e.g. staurolite) presented qualitative and quantitative similarities with dune samples. In that case, it was also possible to use heavy mineral assemblages to differentiate tsunami and storm deposits. In Lhok Nga (Indonesia) and Boca do Rio (Portugal) it was also possible to identify a mineralogical signature specific of the tsunami backwash.

The recognition of the same sedimentary signature of the AD 1755 tsunamigenic event, in several lowlands of the Algarve coast of Portugal and its integration in the sedimentary history preserved in its long-term sedimentary archive provides grounds to suggest a millennial-scale time for the return period of this type of events, with similar intensity, in this region. However, constrains on our present-day ability to pick and identify all the geological evidences of extreme marine inundations in the sedimentary record (*e.g.* associated with preservation of deposit, existence of lithological and textural contrasts, *etc.*) need to be further addressed to establish return periods more confidently. Similarities between deposits studied in Salgados and Boca do Rio were compiled and facilitated interpretations at a regional scale. Differentiation between tsunami and storm deposits was evidenced by the incorporation of rip-up clasts in tsunamigenic deposits while they were absent in the storm deposits analysed. Furthermore, the dimensions and strong lateral variation in features of tsunamigenic units was in strong contrast with the smaller size and more consistent spatial distribution of sedimentary features within storm-deposited sedimentary units.

Overall results revealed that site-specific effects precluded clear-cut extrapolations on a storm *vs* tsunami emplacement mechanism of worldwide application, although they demonstrated that the use of multiple proxies, such as textural, morphoscopic, microtextural and compositional, data, enhances the possibility of using sedimentological criteria to recognize and differentiate tsunami from storm deposits and, in both cases, determine source-deposits relations, if the regional context is sufficiently constrained.

The initial goals established for this thesis were achieved:

a) Coastal sediments deposited by Holocene extreme marine inundations were identified, described, characterized, dated and related with single high-energy events of abrupt marine inundation;

b) Sediment exposures and samples were analysed using a multidisciplinary and multi-proxy approach that included characterization and interpretation of lithostratigraphic, geometric, dimensional, textural, microtextural and compositional features of the sediment, addressed at contrasting spatial scales (ranging from the scale of the outcrop or sedimentary column to the ultramicroscopic imagery of single particles) to achieve an interpretation of processes controlling the entrainment, transport and deposition of terrigenous sediment during high-energy single events of coastal flooding;

c) Textural and microtextural analysis was applied in order to establish the source material or/and to identify specific signatures of extreme marine inundations in coastal sediments;

d) The value of heavy mineral assemblages in coastal sediments in establishing source materials or/and in building compositional signatures specific of extreme marine inundations was tested with encouraging results;

e) Return periods for extreme marine inundations (*i.e.* tsunamis) were conjectured for the Algarve coast of Portugal;

f) Overall, this thesis contributed to the development of the current knowledge on criteria used to characterize sediments deposited by high-energy events of coastal flooding, such as tsunamis and storms, and to increase our ability to distinguish deposits related with each type of oceanographic forcing. This is especially true in what regards the study of factors controlling microtextural features imprinted in the surface of quartz grains and the value of those features in reconstructing the nature and energy-level of the transport agent.

The work presented in this thesis, although contributing to the enhancement of sedimentological criteria presently available to recognize and differentiate extreme marine inundation deposits, revealed areas where additional research should be conducted in order to better understand the complex processes involved in extreme marine inundations and how they translate into the sediment. In fact, additional and more detailed provenance studies should be conducted with the purpose of establishing tsunami- and storm-deposit sedimentary sources and, through this, improve understanding on the physical and sedimentary mechanisms of extreme marine inundations. For instance, the backwash process and its influence in the arrangement of tsunamigenic units, is at the present state of knowledge, scarcely understood. To conduct these studies the widespread use of microtextural and heavy mineral analysis on samples obtained from both observed and fossil deposits is recommended; revisiting classic reference locations and deposits, such as the ones of Boca do Rio (Portugal) or Voe of Scatsta (Scotland), re-sampling and re-interpreting these "classical" deposits incorporating the developments achieved on backwash signatures learned from the Sumatra and Japan events may result in significant advances in the comprehension of the geological record. Furthermore, the increase in the number of research sites will facilitate generalization of conclusions and perception on which proxies or features may be used independently of regional to local specificities; thus diminishing the influence of site-specific constrains that normally (at the present state of knowledge) modulate inferences obtained from the study of extreme marine inundations departing from the geological archive. These approaches will provide more tools and data to comprehend depositional and erosional processes involved in tsunami and storm sediment flow and transport.

In some cases, where tsunami or storms present significant sedimentary erosive patterns (volume of sediment remobilized exceeding the total volume of the sediment unit inland) it would be challenging and

innovative to focus on the sediment deposited at the nearshore area, beyond the closure depth, where some of these deposits are most probably immobilized and in a state of “non-equilibrium” with the prevailing oceanographic conditions; if that section of the inner shelf is accreting, the potential of a short core containing record of multiple events is high.

In this study no major differences between tsunami deposits caused by different origins (i.e earthquake and landslide) were detected. However, further studies should address this issue with the ambitious aim of increasing our ability to distinguish sedimentary columns containing multiple events generated by the same source (even if separated in space) from sections containing signatures of multiple-source events, both cases being of different significance in geodynamic and hazard terms. Furthermore, the relationship between distant and local tsunami origins will most probably (at least, at a regional scale) be reflected in the tsunami deposit. The application and development of more accurate age-estimation techniques (direct or indirect) will also facilitate the establishment of return periods of extreme marine inundations with obvious positive consequences for the study and assessment of hazard/risk for any specific coastal area. It is essential that future research contributes to the increase of the accuracy of the sedimentological criteria to recognize and differentiate sedimentary products laid down by extreme marine inundations.

References

Abe, K., (1979) Size of earthquakes inferred from tsunami data. *Journal of Geophysics Research*, 84, 1561-1568.

Abe, K., (1981) Physical size tsunamigenic earthquakes of the, north-western pacific. *Phys. Earth Planet. International*, 27, 194-205.

Abramson, H., (1998) Evidence for tsunami and earthquakes during the last 3500 years from Lagoon Creek, a coastal freshwater marsh, Northern California, *MSc*, pp. 76. Humboldt State University.

Abrantes, F., Alt-Epping, U., Lebreiro, S., Voelker, A., Schneider, R., (2008) Sedimentological record of tsunamis on shallow-shelf areas: The case of the 1969 AD and 1755 AD tsunamis on the Portuguese Shelf off Lisbon. *Marine Geology*, 249(3-4), 283-293.

Abrantes, F., Lebreiro, S., Rodrigues, T., Gil, I., Bartels-Jónsdóttir, H., Oliveira, P., Kissel, C., Grimalt, J.O., (2005) Shallow-marine sediment cores record climate variability and earthquake activity off Lisbon (Portugal) for the last 2000 years. *Quaternary Science Reviews*, 24(23-24), 2477-2494.

Abu-Zeid, M.M., Baghdady, A.R., El-Etr, H.A., (2001) Textural attributes, mineralogy and provenance of sand dune fields in the greater Al Ain area, United Arab Emirates. *Journal of Arid Environments*, 48(4), 475-499.

Aitken, M.J., (1990) Science-based dating in archaeology, pp. 1335-1373. Longman, London.

Aitken, M.J., (1992) Optical dating. *Quaternary Science Reviews*, 11, 127-131.

Albertão, G.A., Martins, P.P., (1996) A possible tsunami deposit at the Cretaceous-Tertiary boundary in Pernambuco, northeastern Brazil. *Sedimentary Geology*, 104(1-4), 189-201.

Allen, J.R.L., (1982) Sedimentary Structures: Their Character and Physical Basis, *2*, pp. 593. Elsevier, Oxford.

Almeida, L.P., Ferreira, O., Vousdoukas, M.I., Dodet, G., (2011) Historical variation and trends in storminess along the Portuguese South Coast. *Nat. Hazards Earth Syst. Sci.*, 11, 2407-2417.

Ambraseys, N.N., (1962) Data for the investigation of seismic sea waves in the Eastern Mediterranean. *Bulletin Seismological Society America*, 52, 895-913.

Andrade, C., (1990) O Ambiente de barreira da Ria Formosa (Algarve, Portugal). In: *Departamento de Geologia*, *PhD*, pp. 645. Lisboa.

Andrade, C., (1992) Tsunami Generated forms in the Algarve Barrier Islands (South Portugal). *Science of Tsunami Hazards*, 10, 1, 21-34.

Andrade, C., Andrade, A., Kortekaas, S., Dawson, A., (1997) Sedimentological traces of tsunamigenic overwash of the Martinhal lowland (Western Algarve – Portugal). In: *Seminário sobre a Zona Costeira do Algarve* (Ed. by A. Eurocoast-Portugal), pp. 11-18, Faro, Portugal.

Andrade, C., Freitas, M.C., Miranda, J.M., Baptista, M.A., Cachão, M., Silva, P., Munhá, J., (2003) Recognizing possible tsunami sediments in the ultradissipative environment of the Tagus estuary (Portugal). In: *Coastal Sediments'03 - The 5th International Symposium on Coastal Engineering and Science of Coastal Sediment Processes*, *CD-ROM (ISBN: 978-981-238-422-5 CD)* (Ed. by A.S.a.P.H. Richard A. Davis), pp. 14, Clearwater Beach, Florida.

Andrade, C., Freitas, M.C., Moreno, J., Craveiro, S.C., (2004) Stratigraphical evidence of Late Holocene barrier breaching and extreme storms in lagoonal sediments of Ria Formosa, Algarve, Portugal. *Marine Geology*, 210(1-4), 339-362.

Andrade, C., Munhá, J.M., Paulino, J., (1998) Geochemical signature of extreme marine flooding in the Boca do Rio lowland (Algarve, Portugal). *Com. V Congresso Nacional de Geologia*, Lisboa, IGN, SGP, 84(1), 51-54.

Andrade, C., Trigo, R.M., Freitas, M.C., Gallego, M.C., Borges, P., Ramos, A.M., (2008) Comparing historic records of storm frequency and the North Atlantic Oscillation (NAO) chronology for the Azores region. *The Holocene*, 18(5), 745-754.

Angus, S., Rennie, A.F., (2007) An Ataireachd Ard: The Great Sea Surge. The Natural Heritage Impact of the Storm of 11 January 2005 in the Uists and Barra, Outer Hebrides. In: P.S.N. Heritage (Ed.), *Scottish Natural Heritage commissioned Report* (Ed. by P.S.N. Heritage).

Apotsos, A., Jaffe, B., Gelfenbaum, G., (2011) Wave characteristic and morphologic effects on the onshore hydrodynamic response of tsunamis. *Coastal Engineering*, 58(11), 1034-1048.

Appleby, P.G., Oldfield, F., (1983) The assessment of ^{210}Pb data from sites with varying sediment accumulation rates. *Hydrobiologia*, 103, 29-35.

Atwater, B.F., (1987) Evidence for great Holocene earthquakes along the outer coast of Washington State. *Science*, 236, 942-944.

Atwater, B.F., Moore, A.L., (1992) A tsunami about 1000 years ago in Puget Sound, Washington. *Science*, 258, 1614-1617.

Babu, N., Suresh Babu, D.S., Mohan Das, P.N., (2007) Impact of tsunami on texture and mineralogy of a major placer deposit in southwest coast of India. *Environ. Geol.*, 52(71-80).
Bagnold, R.A., (1962) Auto-suspension of transported sediments. *Proc. Royal Society*, Series A 236, 315-319.
Bahlburg, H., Spiske, M., (2011) Sedimentology of tsunami inflow and backflow deposits: key differences revealed in a modern example. *Sedimentology*, DOI: 10.1111/j.1365-3091.2011.01295.x.
Bahlburg, H., Weiss, R., (2007) Sedimentology of the December 26, 2004, Sumatra Tsunami deposits in eastern India (Tamil Nadu) and Kenya. *International Journal of Earth Sciences*, 96(6), 1195-1209.
Banerjee, D., Murray, A.S., Foster, I.D.L., (2001) Scilly Isles, UK: optical dating of a possible tsunami deposit from the 1755 Lisbon earthquake. *Quaternary Science Reviews*, 20, 715-718.
Baptista, M.A., Miranda, J.M., (2009) Revision of the Portuguese catalog of tsunamis. *Nat. Hazards Earth Syst. Sci.*, 9, 25-42.
Baptista, M.A., Miranda, P.M.A., Miranda, J.M., Mendes Victor, L., (1998) Constrains on the source of the 1755 Lisbon tsunami inferred from numerical modelling of historical data on the source of the 1755 Lisbon tsunami. *Journal of Geodynamics*, 25, 159-174.
Barber, A.J., Crow, M.J., (2005) Chapter 4: pre-Tertiary stratigraphy. In: A.J. Barber, M.J. Crow, J.S. Milsom (Eds.), *Sumatra: Geology, Resources and Tectonic Evolution*, *Memoir, 31* (Ed. by A.J. Barber, M.J. Crow, J.S. Milsom), pp. 24-53. Geological Society, London.
Bardet, J.-P., Synolakis, C.E., Davies, H.L., Imamura, F., Okal, E.A., (2003) Landslide tsunamis: Recent findings and research directions. *Pure Appl. Geophys.*, 160, 1793-1809.
Beal, M.A., Shepard, F.P., (1956) A use of roundness to determine depositional environments. *Journal of Sedimentary Petrology*, 26, 49-60.
Beget, J., (2000) Volcanic Tsunamis. In: H. Siguardsson (Ed.), *Encyclopedia of Volcanoes* (Ed. by H. Siguardsson), pp. 1005-1013.
Bengtsson, L., Enell, M., (1986) Handbook of Holocene Palaeoecology and Palaeohydrology. In: B.E. Berglund (Ed.), *Chemical analysis* (Ed. by B.E. Berglund), pp. 423-451. John Wiley & Sons Ldt, Chichester.
Benner, R., Browne, T., Brueckner, H., Scheffers, A., Kelletat, D., (2010) Boulder transport by waves: progress in physical modelling. *Annals of Geomorphology*, 3, 127-146.
Bettencourt, P., J.M., J., P.H., L., (1989) Origine sédimentaire du système d'îles barrières de L'Algarve: Apport de l'exoscopie des quartz. *An. Inst. Hidrogr.*, 10, 51-57.
Blair, T.C., McPherson, J.G., (1999) Grain-size and textural classification of coarse sedimentary particles. *Journal of Sed. Research*, 69, 6-19.
Boldt, K.D., Lane, P., Woodruff, J.D., Donnelly, J.P., (2010) Calibrating a sedimentary record of overwash from southeastern New England using modeled historic hurricane surges. *Marine Geology*, 275, 127-139.
Bondevik, S., (2003) Storegga tsunami sand in peat below the Tapes beach ridge at Harøy, western Norway, and its possible relation to an early Stone Age settlement. *Boreas*, 32(476-483).
Bondevik, S., Mangerud, J., Dawson, S., Dawson, A., Lohn, Ø., (2005) Evidence for three North Sea tsunamis at the Shetland Islands between 8000 and 1500 years ago. *Quaternary Science Reviews*, 24, 1757-1775.
Bondevik, S., Mangerud, J., Dawson, S., Dawson, A., Lohne, Ø., (2003) Record-breaking height for 8000-year-old tsunami in the North Atlantic. *Eos (Transactions, American Geophysical Union)*, 84, 289-293.
Bondevik, S., Svendsen, J.I., Mangerud, J., (1997) Tsunami sedimentary facies deposited by the Storegga tsunami in shallow marine basins and coastal lakes, western Norway. *Sedimentology*, 44, 1115-1131.
Bourgeois, J., (2009) Geologic records and effects of tsunamis: in The Sea, *Volume 15: Tsunamis*, pp. 53-91. Harvard University Press.
Bourgeois, J., Hansen, T.A., Wiberg, P.L., Kauffman, E.G., (1988) A tsunami deposit at the Cretaceous-Tertiary boundary in Texas. *Science*, 241, 567-570.
Bourgeois, J., Petroff, C., Yeh, H., Titov, V., Synolakis, C., Benson, B., Kuroiwa, J., Lander, J., Norabuena, E., (1999) Geologic Setting, Field Survey and Modeling of the Chimbote, Northern Peru, Tsunami of 21 February 1996. *Pure and Applied Geophysics*, 154, 513-540.
Bourrouilh-Le Jan, F.G., Beck, C., Gorsline, D.S., (2007) Catastrophic events (hurricanes, tsunami and others) and their sedimentary records: Introductory notes and new concepts for shallow water deposits. *Sedimentary Geology*, 199(1-2), 1-11.
Bowman, S., (1990) Radiocarbon dating, pp. 64. British Museum Press, London, United Kingdom.
BP, E., (1995) Report No: XFE/030/95 (Ed. by B.D. Management), pp. Unpublished, London.
Bruzzi, C., Prone, A., (2000) A method of sedimentological identification of storm and tsunami deposits: Exoscopic analysis, preliminary results. *Quaternaire*, 11, no.3-4., 167-177.
Bryant, E., Nott, J., (2001) Geological indicators of large tsunami in Australia. *Natural Hazards*, 24, 231-249.
Bryant, E., Young, R., Price, D., (1992) Evidence of tsunami sedimentation on the southeastern coast of Australia. *Journal of Geology*, 100, 753-765.
Bryant, E.A., Young, R.W., Price, D.M., (1996) Tsunami as a major control on coastal evolution, southeastern Australia. *Journal of Coastal Research*, 12(4), 831-840.

Bryn, P., Berg, K., Lien, R., Solheim, A.O., D., Rise, L., (2002) The Storegga geomodel and its use in slide risk evaluation: geological and geotechnical site investigations in the Storegga area. In: *Society for Underwater Technology*, pp. 219-232.

Bull, P.A., Morgan, R.M., (2006) Sediment Fingerprints: A forensic technique using quartz sand grains. *Science & Justice*, 46(2), 107-124.

Bussert, R., Aberhan, M., (2004) Storms and tsunamis: evidence of event sedimentation in the Late Jurassic Tendaguru Beds of southeastern Tanzania. *Journal of African Earth Sciences*, 39(3-5), 549-555.

Cailleux, A., (1942) Les actions eoliennes periglaciaires en Europe. *Soc. Geol., France. Mem. Nouv. Sec.* , 21(1-2), 176.

Campbell, D.H., (1963) Percussion marks on quartz grains. *Journal of Sedimentary Petrology*, 33(4), 855-859.

Cantalamessa, G., Di Celma, C., (2005) Sedimentary features of tsunami backwash deposits in a shallow marine Miocene setting, Mejillones Peninsula, northern Chile. *Sedimentary Geology*, 178(3-4), 259-273.

Caron, V., (2011) Contrasted textural and taphonomic properties of high-energy wave deposits cemented in beachrocks (St. Bartholomew Island, French West Indies). *Sedimentary Geology*, 237(3-4), 189-208.

Carvalho, C., (1998) GranGraf v2B (Ed. by U.o.L. Grain-size software developed at Science Faculty, Portuga).

CERC, (1992) Automated Coastal Engineering System. In: C.o. Engineers (Ed.), *Volume I: Technical Reference and Vol II: User's Guide* (Ed. by C.o. Engineers). Department of the Army Waterway Experiment Station, Mississippi.

Chagué-Goff, C., Dawson, S., Goff, J.R., Zachariasen, J., Berryman, K.R., Garnett, D.L., Waldron, H.M., Mildenhall, D.C., (2002) A tsunami (ca. 6300 years BP) and other Holocene environmental changes, northern Hawke's Bay, New Zealand. *Sedimentary Geology*, 150(1-2), 89-102.

Chagué-Goff, C., Schneider, J.-L., Goff, J.R., Dominey-Howes, D., Strotz, L., (2011) Expanding the proxy toolkit to help identify past events - Lessons from the 2004 Indian Ocean Tsunami and the 2009 South Pacific Tsunami. *Earth-Science Reviews*, 107(1-2), 107-122.

Chandrasekar, N., (2005) Tsunami of 26th December 2004: Observation on Inundation, Sedimentation and Geomorphology of Kanyakumari coast, South India. In: *22nd Intl. Tsunami Symposium* (Ed. by P.a. Satake), pp. 49-56, Xania, Greece.

Chappell, J., Chivas, A., Wallensky, E., Polach, H., Aharon, P., (1983) Holocene palaeo-environmental changes, central to north Great Barrier Reef inner zone. *J. Aust. Geol. Geophys.*, 8, 223-235.

Chivas, A., Chappell, J., Head, J., Wallensky, E., (1986) Radiocarbon evidence for the timing and rate of island development, beach rock formation and phosphatization at Lady Elliot Island, Queensland. *Marine Geology*, 69, 273-287.

Choowong, M., Murakoshi, N., Hisada, K.-i., Charoentitirat, T., Charusiri, P., Phantuwongraj, S., Wongkok, P., Choowong, A., Subsayjun, R., Chutakositkanon, V., Jankaew, K., Kanjanapayont, P., (2008) Flow conditions of the 2004 Indian Ocean tsunami in Thailand, inferred from capping bedforms and sedimentary structures. *Terra Nova*, 20, 141–149.

Choowong, M., Phantuwongraj, S., Charoentitirat, T., Chutakositkanon, V., Yumuang, S., Charusiri, P., (2009) Beach recovery after 2004 Indian Ocean tsunami from Phang-nga, Thailand. *Geomorphology*, 104(3-4), 134-142.

Cita, M.B., Camerlenghi, A., Rimoldi, B., (1996) Deep-sea tsunami deposits in the eastern Mediterranean: New evidence and depositional models. *Sedimentary Geology*, 104(1-4), 155-173.

Clague, J.J., Bobrowsky, P.T., (1994) Tsunami deposits beneath tidal marshes on Vancouver Island, British Columbia. *Geological Society of America Bulletin*, 106(10), 1293-1303.

Clague, J.J., Bobrowsky, P.T., Hamilton, T.S., (1994) A sand sheet deposited by the 1964 Alaska tsunami at Port Alberni, British Columbia. *Estuarine, Coastal and Shelf Science*, 38(4), 413-421.

Clague, J.J., Bobrowsky, P.T., Hutchinson, I., (2000) A review of geological records of large tsunamis at Vancouver Island, British Columbia, and implications for hazard. *Quaternary Science Reviews*, 19, 849-863.

Clague, J.J., Hutchinson, I., Mathewes, R.W., Petterson, R.T., (1999) Evidence for late Holocene tsunamis at Catala Lake, British Columbia. *Journal of Coastal Research*, 15(1), 45-60.

Collins, E.S., Scott, D.B., Gayes, P.T., (1999) Hurricane records on the South Carolina coast: can they be detected in the sedimentary record? *Quaternary International*, 56, 15-26.

Corrochano, A., Merino, S.G., Barba, P., Bernardes, C., (2000) Los sedimentos del canal de Mira (Aveiro, Portugal): propriedades texturales, procedencia y modelo paleogeografico. *Studia Geologica Salmanticensia*, 36, 143-160.

Costa, M., (1994) Agitação marítima na costa portuguesa. *Anais do Instituto Hidrográfico*, 13, 35-40.

Costa, M., Silva, R., Vitorino, J., (2001) Contribuição para o estudo do clima de agitação marítima na costa portuguesa. In: *2ª Jornadas Portuguesas de Engenharia Costeira e Portuária*, pp. 20. Associação Nacional de Navegação, Sines.

Costa, P.J.M., (2006) Geological recognition of abrupt marine invasions in two coastal areas of Portugal. In: *Geography and Earth Sciences*, *MPhil*, pp. 139. Brunel University, London.

Costa, P.J.M., Andrade, C., Dawson, A.G., Mahaney, W.C., Paris, R., Freitas, M.C., Taborda, R., (2012b) Microtextural characteristics of quartz grains transported and deposited by tsunamis and storms. *Sedimentary Geology*, 275–276, 55-69.

Costa, P.J.M., Andrade, C., Freitas, M.C., Oliveira, M.A., Jouanneau, J.M., (2009) Preliminary Results of Exoscopic Analysis of Quartz Grains Deposited by a Palaeotsunami in Salgados Lowland (Algarve, Portugal). *Journal of Coastal Research*(SI 56), 39-43.

Costa, P.J.M., Andrade, C., Freitas, M.C., Oliveira, M.A., Lopes, V., Dawson, A.G., Moreno, J., Fatela, F., Jouanneau, J.-M., (2012a) A tsunami record in the sedimentary archive of the central Algarve coast, Portugal: characterizing sediment, reconstructing sources and inundation paths. *The Holocene*, 22(8), 899-914.

Costa, P.J.M., Andrade, C., Freitas, M.C., Oliveira, M.A., Silva, C.M.d., Omira, R., Taborda, R., Baptista, M.A., Dawson, A.G., (2011) Boulder deposition during major tsunami events. *Earth Surface Processes and Landforms*, 36, 2054–2068

Costa, P.J.M., Andrade, C., Mahaney, W.C., Marques da Silva, F., Freire, P., Freitas, M.C., Janardo, C., Oliveira, M.A., Silva, T., Lopes, V., (2012c) Aeolian Microtextures in Silica Spheres Induced in a Wind Tunnel Experiment: Comparison with Aeolian Quartz. *Geomorphology (in press)*.

Crichton, D., (2003) The Shetland Islands, pp. 11. Esure insurance services Ltd.

Culver, S.J., Bull, P.A., Campbell, S.S., R.A. Whalley, W.B., (1983) Environment descrimination based in quartz grain surface textures: a statistical investigation. *Sedimentology*, 30, 129-136.

Cundy, A.B., Kortekaas, S., Dewez, T., Stewart, I.S., Collins, P.E.F., Croudace, I.W., Maroukian, H., Papanastassiou, D., Gaki-Papanastassiou, P., Pavlopoulos, K., Dawson, A., (2000) Coastal wetlands as recorders of earthquake subsidence in the Aegean: a case study of the 1894 Gulf of Atalantiearthquakes, central Greece. *Marine Geology*, 170(1-2), 3-26.

Cunha, P.P., Buylaert, J.P., Murray, A.S., Andrade, C., Freitas, M.C., Fatela, F., Munhá, J.M., Martins, A.A., Sugisaki, S., (2010) Optical dating of clastic deposits generated by an extreme marine coastal flood: the 1755 tsunami deposits in the Algarve (Portugal). *Quaternary Geochronology*, 5(2-3), 329-335.

Dahanayake, K., Kulasena, N., (2008) Recognition of diagnostic criteria for recent- and paleo-tsunami sediments from Sri Lanka. *Marine Geology*, 254, 180-186.

Davis, J.C., (1986) Statistics and data analysis in geology, pp. 646. Wiley, New York.

Davis, R.A.J., Knowles, S.C., Bland, M.J., (1989) Role of hurricanes in the Holocene stratigraphy of estuaries: examples from the Gulf Coast of Florida. *Journal of Sedimentary Petrology*, 59, 1052-1061.

Dawson, A., Dawson, S., Bondevik, S., (2006) A Late Holocene Tsunami at Basta Voe, Yell, Shetland Isles. *Scottish Geographical Journal*, 122(2), 100-108.

Dawson, A., Napier, I., Davies, N., McIlveny, J., (2011) A review of SOTEAG monitoring data and other long term environmental series from Shetland, pp. 118.

Dawson, A.G., (1994) Geomorphological effects of tsunami run-up and backwash. *Geomorphology*, 10(1-4), 83-94.

Dawson, A.G., (1999) Linking tsunami deposits, submarine slides and offshore earthquakes. *Quaternary International*, 60(1), 119-126.

Dawson, A.G., (2004) Tsunami hazards in Europe. *Environment International*, 30, 577-585.

Dawson, A.G., Dawson, S., Ritchie, W., (2007) Historical climatology and coastal change associated with the 'Great Storm' of January 2005, South Uist and Benbecula, Scottish Outer Hebrides. *Scottish Geographical Journal*, 123(2), 135-149.

Dawson, A.G., Foster, I.D.L., Shi, S., Smith, D., Long, D., (1991) The identification of past tsunamis in coastal sediment sequences. *Science of Tsunami Hazards*, 9, 73-82.

Dawson, A.G., Hindson, R., Andrade, C., Freitas, C., Parish, R., Baterman, R., (1995) Tsunami sedimentation associated with the Lisbon earthquake of 1 November AD 1755: Boca do Rio, Algarve, Portugal. *The Holocene*, 5(2), 209-215.

Dawson, A.G., Long, D., Smith, D.E., (1988) The Storegga Slides: Evidence from eastern Scotland for a possible tsunami. *Marine Geology*, 82(3-4), 271-276.

Dawson, A.G., Shi, S., (2000) Tsunami deposits. *Pure and Applied Geophysics*, 157, 875-897.

Dawson, A.G., Shi, S., Dawson, S., Shuto, N., Takahashi, T., (1996a) Coastal sedimentation associated with the June 2nd and 3rd tsunami in Rajegwesi, Java. *Quaternary Science Reviews*, 15, 901-912.

Dawson, A.G., Smith, D.E., Dawson, S., (2001) Potential Impacts of Climate Change on Sea Levels around Scotland. Scottish Natural Heritage, Edinburgh.

Dawson, A.G., Smith, D.E., Long, D., (1990) Evidence for a tsunami from a mesolithic site in Inverness, Scotland. *Journal of Archaeological Science*, 17(5), 509-512.

Dawson, A.G., Stewart, I., (2007) Tsunami deposits in the geological record. *Sedimentary Geology*, 200(3-4), 166-183.

Dawson, A.G., Stewart, I., (2008) Offshore Tractive Current Deposition: The Forgotten Tsunami Sedimentation Process. In: T. Shiki, Y. Tsuji, T. Yamazaki, K. Minoura (Eds.), *Tsunamiites - Features and implications* (Ed. by T. Shiki, Y. Tsuji, T. Yamazaki, K. Minoura), pp. 153-161. Elsevier, Amsterdam.

Dawson, S., (2007) Diatom biostratigraphy of tsunami deposits: Examples from the 1998 Papua New Guinea tsunami. *Sedimentary Geology*, doi:10.1016/j.sedgeo.2007.01.011, 8.

Dawson, S., Smith, D.E., (2000) The sedimentology of Middle Holocene tsunami facies in northern Sutherland, Scotland, UK. *Marine Geology*, 170(1-2), 69-79.

Dawson, S., Smith, D.E., Jordan, J., Dawson, A.G., (2004) Late Holocene coastal sand movements in the Outer Hebrides, NW Scotland. *Marine Geology*, 210, 281-306.

Dawson, S., Smith, D.E., Ruffman, A., Shi, S., (1996b) The diatom biostratigraphy of tsunami sediments: Examples from recent and middle holocene events. *Physics and Chemistry of The Earth*, 21(1-2), 87-92.

Deane, S.M., (2010) Quartz Grain Microtextures and Sediment Provenance: Using Scanning Electron Microscopy to Characterize Tropical Highland Sediments from Costa Rica and the Dominican Republic. *Master's Thesis, University of Tennessee*, 122 pp.

Delany, C., Devoy, R., (1995) Evidence from sites in western Ireland of late Holocene changes in coastal environments. *Marine Geology*, 124, 273-287.

Dengler, L., Preuss, J., (2003) Mitigation Lessons from the July 17, 1998 Papua New Guinea Tsunami. *Pageoph*, 160(10-11), 2001-2031.

Dezileau, L., Sabatier, P., Blanchemanche, P., Joly, B., Swingedouw, D., Cassou, C., Castaings, J., Martinez, P., Von Grafenstein, U., (2011) Intense storm activity during the Little Ice Age on the French Mediterranean coast. *Palaeogeography, Palaeoclimatology, Palaeoecology*, 299(1-2), doi:10.1016/j.palaeo.2010.11.009.

Dinis, J., Andrade, C., Oliveira, M.A., Freitas, M.C., Cunha, P.P., Martins, A., Costa, P., (2010) Geomorphological constraining of tsunami (?) run-up in the Alcantarilha coastal lowland (Central Algarve, Portugal). In: *Conferência Coastal Hope - Iberian Coastal Holocene Paleonvironmental Evolution*, *Proceedings*, pp. 40-41, Lisbon.

Dominey-Howes, D., (2007) Geological and historical records of tsunami in Australia. *Marine Geology*, 239(1-2), 99-123.

Dominey-Howes, D., Cundy, A., Croudace, I., (2000) High energy marine flood deposits on Astypalaea Island, Greece: possible evidence for the AD 1956 southern Aegean tsunami. *Marine Geology*, 163, 303-315.

Dominey-Howes, D., Dawson, A., Smith, D., (1998) Late Holocene coastal tectonics at Falasarna, western Crete: a sedimentary study. *Geological Society of London*, Stewart, I., Vita-Finzi, C. (Eds.)(Coastal Tectonics), 343-352.

Dominey-Howes, D., Humphreys, G., Hesse, P., (2006) Tsunami and palaeotsunami depositional signatures and their potential value in understanding the Late-Holocene tsunami record. *The Holocene*, 16(8), 1095-1107.

Donato, S.V., Reinhardt, E.G., Boyce, J.I., Rothaus, R., Vosmer, T., (2008) Identifying tsunami deposits using bivalve shell taphonomy. *Geology*, 36, 3, 199–202.

Donnelly, J.P., (2005) Evidence of Past Intense Tropical Cyclones from Backbarrier Salt Pond Sediments: A Case Study from Isla de Culebrita, Puerto Rico, USA. *Journal of Coastal Research*, SI 42, 201-210.

Donnelly, J.P., Butler, J., Roll, S., Wengren, M., Webb III, T., (2004) A backbarrier overwash record of intense storms from Brigantine, New Jersey. *Marine Geology*, 210, 123-134.

Donnelly, J.P., Roll, S., Wengren, M., Butler, J., Lederer, R., Webb III, T., (2001) Sedimentary evidence of intense hurricane strikes from New Jersey. *Geology*, 29, 615-618.

Donnelly, J.P., Woodruff, J.D., (2007) Intense hurricane activity over the past 5,000 years controlled by El Nino and the West African monsoon. *Nature*, 447, 465-468.

Duarte, J.C., Terrinha, P., Rosas, F.M., Valadares, V., Pinheiro, L.M., L.Matias, Magalhães, V., Roque, C., (2010) Crescent-shaped morphotectonic features in the Gulf of Cadiz (offshore SW Iberia). *Marine Geology*, 271, 236-249.

Eakins, J.D., Morrison, R.T., (1978) A new procedure for the determination of lead ^{210} in lake and marine sediments. *Int. J. Appl. Radiation*, Isotopes 29, 531-536.

Eijkelkamp, (2008) Operating instructions:08.53 calcimeter (Ed. by Eijkelkamp), pp. 6, The Netherlands.

Einsele, G., Chough, S.K., Shiki, T., (1996) Depositional events and their records - an introduction. *Sedimentary Geology*, 104(1-4), 1-9.

Engineers, U.A.C.o., (1984) Shore Protection Manual. In: W.E.S. Dept. of the Army, Corps of Engineers, Coastal Engineering Research Center (Ed.), *II* (Ed. by W.E.S. Dept. of the Army, Corps of Engineers, Coastal Engineering Research Center), pp. 106, Vicksburg, Miss., U.S.

Engineers, U.S.A.C.o., (2003) Coastal Engineering Manual - Appendix A - Glossary, pp. 95. Crear.

Esaguy, A., (1984) Ria de Faro - Barra da Armona - Evolução 1873-1983, pp. 5. Direcção Geral de Portos Lisbon.

Etienne, S., Paris, R., (2010) Boulder accumulations related to storms on the south coast of the Reykjanes Peninsula (Iceland). *Geomorphology*, 114(1-2), 55-70.

Fagherazzi, S., Du, X., (2008) Tsunamigenic incisions produced by the December 2004 earthquake along the coasts of Thailand, Indonesia and Sri Lanka. *Geomorphology*, 99(1-4), 120-129.

Felton, E.A., (2002) Sedimentology of rocky shorelines: 1. A review of the problem, with analytical methods, and insights gained from the Hulopoe Gravel and the modern rocky shoreline of Lanai, Hawaii. *Sedimentary Geology*, 152(3-4), 221-245.

Fettes, D.J., Mendum, J.R., Smith, D.I., Watson, J.V., (1992) Geology of the Outer Hebrides. Memoir of the British Geological Survey, 1:100 000 Sheets, Lewis and Harris, Uist and Barra (Scotland). In: HMSO (Ed.) (Ed. by HMSO), pp. 197, London.

Fichaut, B., Suanez, S., (2010) Quarrying, transport and deposition of cliff-top storm deposits during extreme events: Banneg Island, Brittany. *Marine Geology*, 283(1-4), 36-55.

Flinn, D., (1977) The erosion history of Shetland: a review. *Proc. Geol. Ass.*, 88(3), 129-146.

Folk, R.L., Ward, W.C., (1957) Brazos river bar: a study of significant of grain size parameters. *Journal of Sedimentary Petrology*, 27, 3-26.

Font, E., Nascimento, C., Omira, R., Baptista, M.A., Silva, P.F., (2010) Identification of tsunami-induced deposits using numerical modeling and rock magnetism techniques: A study case of the 1755 Lisbon tsunami in Algarve, Portugal. *Physics of the Earth and Planetary Interiors*, 182(3-4), 187-198.

Fortnum, B.C.H., (1981) Waves recorded off South Uist in the Hebrides. Data from March 1976 to February 1978 at position 57,18'N, 07,38'W. Summary analysis and interpretation report. In: *Institute of Oceanographic Sciences Report,(115)*, pp. 6. Institute of Oceanographic Sciences, Wormley, UK.

Friedman, G.M., (1961) Distinction between dune, beach and river sands from their textural characteristics. *J. Sediment. Petrology*, 31(4), 514-529.

Friedman, G.M., (1967) Dynamic processes and statistical parameters compared for size frequency distribution of beach river sands. *Journal of Sedimentary Petrology*, 37(2), 327-354.

Fujino, S., Naruse, H., Matsumoto, D., Jarupongsakul, T., Sphawajruksakul, A., Sakakura, N., (2009) Stratigraphic evidence for pre-2004 tsunamis in southwestern Thailand. *Marine Geology*, 262(1-4), 25-28.

Fujiwara, O., Kamataki, T., (2007) Identification of tsunami deposits considering the tsunami waveform: An example of subaqueous tsunami deposits in Holocene shallow bay on southern Boso Peninsula, Central Japan. *Sedimentary Geology*, 200(3-4), 295-313.

Fujiwara, O., Masuda, F., Sakai, T., Irizuki, T., Fuse, K., (2000) Tsunami deposits in Holocene bay mud in southern Kanto region, Pacific coast of central Japan. *Sedimentary Geology*, 135(1-4), 219-230.

Gelfenbaum, G., Jaffe, B., (2003) Erosion and Sedimentation from the 17 July, 1998, Papua New Guinea Tsunami. *Pure and Applied Geophysics*, 160, 1969–1999.

Gelfenbaum, G., Jaffe, B., Morton, R.A., Richmond, B.M., (2002) Distinguishing tsunami and hurricane overwash deposits. In: *AGU* (Ed. by W.P.G. Meeting), Wellington.

Gelfenbaum, G., Vatvani, D., Jaffe, B., Dekker, F., (2007) Tsunami inundation and sediment transport in the vicinity of coastal mangrove forest. In: *Sixth International Symposium on Coastal Engineering and Science of Coastal Sediment Processes ISBN: 978-0-7844-0926-8*, pp. http://dx.doi.org/10.1061/40926(239)86. ASCE.

GITEC-2, (1995) Project proposal to the EC in the Field of Research and Technological Development, pp. 61. Genesis and Impact of Tsunamis on the European Coasts: Tsunami Warning and Observations.

Godwin, H., (1962) Half life of radiocarbon. *Nature*, 195, 944.

Goff, J., Chagué-Goff, C., Nichol, S., (2001) Palaeotsunami deposits: a New Zealand perspective. *Sedimentary Geology*, 143(1-2), 1-6.

Goff, J., Dominey-Howes, D., (2009) Australasian palaeotsunamis -- Do Australia and New Zealand have a shared trans-Tasman prehistory? *Earth-Science Reviews*, 97(1-4), 147-154.

Goff, J., Dudley, W.C., deMaintenon, M.J., Cain, G., Coney, J.P., (2006) The largest local tsunami in 20th century Hawaii. *Marine Geology*, 226, 65–79.

Goff, J., McFadgen, B., Wells, A., Hicks, M., (2008) Seismic signals in coastal dune systems. *Earth-Science Reviews*, 89(1-2), 73-77.

Goff, J., McFadgen, B.G., Chagué-Goff, C., (2004) Sedimentary differences between the 2002 Easter storm and the 15th-century Okoropunga tsunami, southeastern North Island, New Zealand. *Marine Geology*, 204(1-2), 235-250.

Goff, J., Pearce, S., Nichol, S.L., Chagué-Goff, C., Horrocks, M., Strotz, L., (2010a) Multi-proxy records of regionally-sourced tsunamis, New Zealand. *Geomorphology*, 118(3-4), 369-382.

Goff, J., Weiss, R., Courtney, C., Dominey-Howes, D., (2010b) Testing the hypothesis for tsunami boulder deposition from suspension. *Marine Geology*, 277(1-4), 73-77.

Goff, J.R., Chagué-Goff, C., (1999) A late Holocene record of environmental changes from coastal wetlands: Abel Tasman National Park, New Zealand. *Quaternary International*, 56, 39-51.

Goff, J.R., Crozier, M., Sutherland, V., Cochran, U., Shane, P., (1998) Possible tsunami deposits from the 1855 earthquake, North Island, New Zealand. *Geological Society of London*, Special Publication 146, 353-376.

Goff, J.R., Rouse, H.L., Jones, S.L., Hayward, B.W., Cochran, U., McLea, W., Dickinson, W.W., Morley, M.S., (2000) Evidence for an earthquake and tsunami about 3100-3400 yr ago, and other catastrophic saltwater inundations recorded in a coastal lagoon, New Zealand. *Marine Geology*, 170(1-2), 231-249.

Goto, K., Chavanich, S.A., Imamura, F., Kunthasap, P., Matsui, T., Minoura, K., Sugawara, D., Yanagisawa, H., (2007) Distribution, origin and transport process of boulders deposited by the 2004 Indian Ocean tsunami at Pakarang Cape, Thailand. *Sedimentary Geology*, 202, 821–837.

Goto, K., Kawana, T., Imamura, F., (2010a) Historical and geological evidence of boulders deposited by tsunamis, southern Ryukyu Islands, Japan. *Earth-Science Reviews*, 102(1-2), 77-99.

Goto, K., Miyagi, K., Kawana, T., Takahashi, J., Imamura, F., (2011) Emplacement and movement of boulders by known storm waves -Field evidence from the Okinawa Islands, Japan. *Marine Geology*, 283, 66-78.

Goto, K., Okada, K., Imamura, F., (2010b) Numerical analysis of boulder transport by the 2004 Indian Ocean tsunami at Pakarang Cape, Thailand. *Marine Geology*, 268(1-4), 97-105.

Goverment, T.S., (2006) Contaminated Land: Implementation of Part IIA of the Environmental Protection Act (Ed. by A.B. 06/06), pp. 199. Scottich Executive, Edimburgh.

Gràcia, E., Vizcaino, A., Escutia, C., Asioli, A., Rodés, A., Pallàs, R., Garcia-Orellana, J., Lebreiro, S., Goldfinger, C., (2010) Holocene earthquake record offshore Portugal (SW Iberia): testing turbidite paleoseismology in a slow-convergence margin. *Quaternary Science Reviews*, 29, 1156-1172.

Grauert, M., Bjork, S., Bondevik, S., (2001) Storegga tsunami deposits in a coastal lake on Suduroy, the Faroe Islands. *Boreas*, 30, 263-271.

Guerra, S.S., Pires, H.O., Taborda, R.P., (2000) Mean Sea Level, North Atlantic Oscillation and climate variability in Portugal. *3rd Symposium on the Iberian Atlantic margin*, 351-352.

Guilbault, J.-P., Clague, J.J., Lapointe, M., (1996) Foraminiferal evidence for the amount of coseismic subsidence during a late holocene earthquake on Vancouver Island, West Coast of Canada. *Quaternary Science Reviews*, 15(8-9), 913-937.

Gutscher, M.-A., Baptista, M.A., Miranda, J.M., (2006) The Gibraltar Arc seismogenic zone (part 2): constraints on a shallow east dipping fault plane source for the 1755 Lisbon earthquake provided by tsunami modelling and seismic intensity. *Tectonophysics*, 426, 153-166.

Hails, J.R., (1967) Significance of statistical parameters for distinguishing sedimentary environments in New South Wales, Australia. *Journal of Sedimentary Petrology*, 37(4), 1059-1070.

Hall, A.M., Hansom, J.D., Williams, D.M., Jarvis, J., (2006) Distribution, geomorphology and lithofacies of cliff-top storm deposits: Examples from the high-energy coasts of Scotland and Ireland. *Marine Geology*, 232, 131–155.

Hall, R., (2002) Cenozoic geological and plate tectonic evolution of SE Asia and the SW Pacific: computer-based reconstructions, model and animations. *Journal of Asian Earth Sciences*, 20, 353-431.

Hall, R., (2009) Hydrocarbon basins in SE Asia: understanding why they are there. *Petroleum Geoscience*, 15, 131-146.

Hanes, D.M., (1986) Grain Flows and Bed-Load Sediment Transport: Review and Extension. *Acta Mechanica*, 63, 131-142.

Hansom, J.D., Angus, S., (2001) Tir a'Mhachair (Land of the Machair): sediment supply and climate change scenarios for the future of the Outer Hebrides machair. In: J.E. Gordon, K.F., Lees (Eds.), *Natural Heritage of Scotland Series, Earth Science and the Natural Heritage: Interactions and Integrated management*, *9* (Ed. by J.E. Gordon, K.F., Lees), pp. 68-81. The Stationery Office, Edinburgh.

Hansom, J.D., Barltrop, N.D.P., Hall, A.M., (2008) Modelling the processes of cliff-top erosion and deposition under extreme storm waves. *Marine Geology*, 253(1-2), 36-50.

Hataori, T., (1979) Relation between tsunami magnitude and wave energy. *Bulletin Earthquakes*, 54, 541.

Hawkes, A.D., Bird, M., Cowie, S., Grundy-Warr, C., Horton, B.P., Shau Hwai, A.T., Law, L., Macgregor, C., Nott, J., Ong, J.E., Rigg, J., Robinson, R., Tan-Mullins, M., Sa, T.T., Yasin, Z., Aik, L.W., (2007) Sediments deposited by the 2004 Indian Ocean Tsunami along the Malaysia-Thailand Peninsula. *Marine Geology*, 242(1-3), 169-190.

Hayne, M., Chappell, J., (2001) Cyclone frequency during the last 5,000 years from Curacoa Island, Queensland. *Palaeogeogr. Palaeoclimat. Palaeoecol.*, 168, 201-219.

Hemphill-Haley, E., (1996) Diatoms as an aid in identifying late-Holocene tsunami deposits. *The Holocene*, 6(4), 439-448.

Higman, B., Bourgeois, J., (2008) Deposits of the 1992 Nicaragua tsunami. In: T. Shiki, Y. Tsuji, T. Yamazaki, K. Minoura (Eds.), *Tsunamiites - Features and implications* (Ed. by T. Shiki, Y. Tsuji, T. Yamazaki, K. Minoura), pp. 81-103. Elsevier, Amsterdam.

Higman, B., Jaffe, B., (2005) A comparison of grading in deposits from five tsunamis: Does tsunami wave duration affect grading patterns? *Eos (Transactions, American Geophysical Union)*, 86(52), Abstract T11A-0362.

Hindson, R.A., Andrade, C., (1999) Sedimentation and hydrodynamic processes associated with the tsunami generated by the 1755 Lisbon earthquake. *Quaternary International*, 56(1), 27-38.

Hindson, R.A., Andrade, C., Dawson, A.G., (1996) Sedimentary processes associated with the tsunami generated by the 1755 Lisbon earthquake on the Algarve coast, Portugal. *Physics and Chemistry of The Earth*, 21(1-2), 57-63.

Hori, K., Kuzumoto, R., Hirouchi, D., Umitsu, M., Janjirawuttikul, N., Patanakanog, B., (2007) Horizontal and vertical variation of 2004 Indian tsunami deposits: An example of two transects along the western coast of Thailand. *Marine Geology*, 239, 163-172.

Horton, B.P., Innes, J.B., Shennan, I., Gehrels, W.R., Lloyd, J.M., McArthur, J.J., Rutherford, M.M., (1999) The Quaternary of North-East England. Field Guide. In: D.R. Bridgland, B.P. Horton, J.P. Innes (Eds.) (Ed. by D.R. Bridgland, B.P. Horton, J.P. Innes), pp. 146-165. Quaternary Research Association.

Horton, B.P., Rossi, V., Hawkes, A.D., (2009) The sedimentary record of the 2005 hurricane season from the Mississippi and Alabama coastlines. *Quaternary International*, 195, 15-30.

Horton, B.P., Zong, Y., Hillier, C., Engelhart, S., (2007) Diatoms from Indonesian mangroves and their suitability as sea-level indicators for tropical environments. *Marine Micropaleontology*, 63(3-4), 155-168.

Hsu, K.J., (2004) Physics of Sedimentology, pp. 240. Springer.

Huntington, K., Bourgeois, J., Gelfenbaum, G., Lynett, P., Jaffe, B., Yeh, H., Weiss, R., (2007) Sandy signs of a tsunami's onshore depth and speed. *Eos (Transactions, American Geophysical Union)*, 88(52), 577-578.

Huntley, D.J., Clague, J.J., (1996) Optical dating of tsunami-laid sands. *Quaternary Research*, 46(2), 127-140.

Hurrell, J.W., (2003) Climate Variability: North Atlantic and Arctic Oscillation. In: J.P. In J. Holton, and J. Curry (Ed.), *Encyclopedia of Atmospheric Sciences* (Ed. by J.P. In J. Holton, and J. Curry), pp. 439-445. Academic Press, Amsterdam.

Iida, K., (1963) Magnitude, energy and generation mechanisms of tsunamis and a catalogue of earthquakes associated with tsunasmis. *International Union of Geodesy and Geophysics Monograph*, 24, 7-17.

Iida, K., Cox, D.C., Pararas-Carayannis, G., (1967) Preliminary catalog of tsunamis occurring in the Pacific Ocean. In: H.I. of, Geophysics (Eds.), *67-10* (Ed. by H.I. of, Geophysics), pp. 131. University of Hawaii, Honolulu.

Imamura, F., Goto, K., Ohkubo, S., (2008) A numerical model for the transport of a boulder by tsunami. *Journal of Geophysical Research*, 113, C01008, doi:10.1029/2007JC004170.

Imamura, F., Lee, H.J., Takahashi, T., Shuto, N., (1997) The highest run-up of the 1993 Hokkaido Nansei-Oki earthquake tsunami. In: *IAMAS - IAPSO Joint Assemblies*, Melbourne, Australia.

Iverson, H.W., (1951) Studies of wave transformation in shoaling water, including breaking. *Gravity Waves*, Nat. Bureau of Standards(Circular 521).

Jaffe, B., Buckley, M., Richmond, B., Strotz, L., Etienne, S., Clark, K., Watt, S., Gelfenbaum, G., Goff, J., (2011) Flow speed estimated by inverse modeling of sandy sediment deposited by the 29 September 2009 tsunami near Satitoa, east Upolu, Samoa. *Earth-Science Reviews*, 107(1-2), 23-37.

Jaffe, B.E., Gelfenbuam, G., (2007) A simple model for calculating tsunami flow speed from tsunami deposits. *Sedimentary Geology*, 200, 347–361.

Jagodzinski, R., Sternal, B., Szczucinski, W., Lorenc, S., (2009) Heavy minerals in 2004 tsunami deposits on Kho Khao Island, Thailand. *Pol. J. Environ. Studies* 18, 103-110.

Jelgersma, S., Stive, M.J.F., van der Valk, L., (1995) Holocene storm surge signatures in the coastal dunes of the western Netherlands. *Marine Geology*, 125, 95-110.

Jonhnson, H., Richards, P.C., Long, D., Graham, C.C., (1993) United Kingdom offshore regional report: the geology of the North Sea. In: B.G. Survey (Ed.) (Ed. by B.G. Survey). NERC, London.

Kaabouben, F., Brahim, A.I., Toto, E.A., Baptista, M.A., Miranda, J.M., Soares, P., Luis, J.F., (2008) On the focal mechanism of the 26.05.1975 North Atlantic event contribution from tsunami modeling. *J. Seismology*, 12(4), 575-583.

Kaas, E., von Storch, H., Lozano, I., (2000) Wind driven sea level variations in the past and future. *In: Smith, D., Raper, S., Zerbini, S., Sanchez-Arcilla, A. (Eds.), Sea Level Change and Coastal Processes. Implications for Europe. Research Results and Recommendations. Energy, Environment and Sustainable Development, European Commission, Brussels*, 110- 123.

Kelletat, D., (2008) Comments to Dawson, A.G. and Stewart, I. (2007), Tsunami deposits in the geological record. -- Sedimentary Geology 200, 166-183. *Sedimentary Geology*, 211(3-4), 87-91.

Kench, P.S., Brander, R.W., Parnell, K.E., O'Callaghan, J.M., (2009) Seasonal variations in wave characteristics around a coral reef island, South Maalhosmadulu atoll, Maldives. *Marine Geology*, 262(1-4), 116-129.

Kienle, J., Kowalik, Z., Murty, T., (1987) Tsunami generated by eruption from Mt. St. Augustine volcano, Alaska. *Science*, 236, 1442-1447.

Kirov, B., Georgieva, K., (2002) Long-term variations and interrelations of ENSO, NAO and solar activity. *Phys. Chem. of the Earth*, A/B/C, 27((6-8)), 441-448.

Komar, P.D., Wang, C., (1984) Processes of selective grain transport and the formation of placers on beaches. *Journal of Geology*, 92, 637-655.

Kortekaas, S., Dawson, A.G., (2007) Distinguishing tsunami and storm deposits: An example from Martinhal, SW Portugal. *Sedimentary Geology*, 200, 3-4, 208-221.

Koster, B., Reicherter, K., Vött, A., Grützner, C., (2011) The evidence of tsunamigenic deposits in the gulf of Corinth (Greece) with geophysical methods for spatial distribution. In: *2nd INQUA-IGCP-567 International Workshop on Active Tectonics, Earthquake Geology, Archaeology and Engineering, Corinth, Greece*, pp. 107-110.

Krastel, S., Schmincke, H.U., Jacobs, C.L., Richm, R., Le Bas, T.P., Alibe's, B., (2001) Submarine landslides around the Canary Islands. *Journal of Geophysical Research*, 106(B3), 3977-3997.

Krinsley, D., Margolis, S., (1969) A study of quartz sand grain surface textures with the scanning electron microscope. *Trans. N.Y. Acad. Sci.*, 31, 457.

Krinsley, D.H., Donahue, J., (1968) Environmental Interpretation of Sand Grain Surface Textures by Electron Microscopy. *Geological Society of America Bulletin*, 79(6), 743-748.

Krumbein, W.C., (1941) Measurement and geological significance of shape and roundness of sedimentary particles. *Journal of Sedimentary Petrology*, 11, 64-77.

Krumbein, W.C., Sloss, L.L., (1963) Stratigraphy and Sedimentation. Freeman, San Francisco, United States.

Kruskal, W.H., Wallis, W.A., (1952) Use of ranks in one-criterion variance analysis. *Journal of the American Statistical Association*, 47(260), 583-621.

Kudrass, H.R., (1987) Improvement of deep-sea dredging operations through the use of a depth meter. *J. Sediment. Petrology*, 54, 39-43.

Lakshmi, C.S.V., Srinivasan, P., Murthy, S.G.N., Trivedi, D., Nair, R.R., (2010) Granularity and textural analysis as a proxy for extreme wave events in southeast coast of India. *J. Earth Syst. Sci.*, 119(3), 297-305.

Lambert, W.J., Aharon, P., Rodriguez, A.V., (2003) An assessment of the late Holocene record of severe storm impact from Lake Shelby, Alabama. *Gulf Coast Association of Geological Societies Transactions*, 53, 443-452.

Lambert, W.J., Aharon, P., Rodriguez, A.V., (2008) Catastrophic hurricane activity revealed by organic geochemical proxies in coastal lake sediments: a case study of Lake Shelby, Alabama (USA). *Journal of Paleolimnology*, 39, 117-131.

Lane, P., Donnelly, J.P., Woodruff, J.D., Hawkes, A.D., (2011) A decadally-resolved paleohurricane record archived in the late Holocene sediments of a Florida sinkhole. *Marine Geology*, 287, 14-30.

Langenberg, H., Pfizenmayer, A., von Storch, H., Suendermann, J., (1999) Storm related sea level variations along the North Sea coast: natural variability and anthropogenic change. *Continental Shelf Research*, 19, 821- 842.

Lapidus, D.F., (1990) Collins Dictionary of Geology, pp. 565. Harper Collins, London.

Lario, J., Zazo, C., Goy, J.L., Silva, P.G., Bardaji, T., Cabero, A., Dabrio, C.J., (2011) Holocene palaeotsunami catalogue of SW Iberia. *Quaternary International*, 242(1), 196-200.

Lavigne, F., Paris, R., Grancher, D., Wassmer, P., Brunstein, D., Vautier, F., Leone, F., Flohic, F., De Coster, B., Gunawan, T., Gomez, C., Setiawan, A., Cahyadi, R., Fachrizal, (2009) Reconstruction of tsunami inland propagation on December 26, 2004 in Banda Aceh, Indonesia, through field investigations. *Pure and Applied Geophysics*, 166, 259-281.

Le Roux, J.P., Vargas, G., (2005) Hydraulic behavior of tsunami backflows: insights from their modern and ancient deposits. *Environ Geol*, 49, 65-75.

Leatherman, S.P., Williams, A.T., (1983) Vertical sedimentation units in a barrier island washover fan. *Earth Surface Processes and Landforms*, 8, 141-150.

Leroy, S., Kazancl, N., Ileri, Ö., Kibar, M., Emre, O., McGee, E., Griffiths, H.I., (2002) Abrupt environmental changes within a late Holocene lacustrine sequence south of the Marmara Sea (Lake Manyas, N-W Turkey): possible links with seismic events. *Marine Geology*, 190(1-2), 531-552.

Li, L.L., Huang, Z.H., (2011) Modelling the change of the beach profile under tsunami waves: a comparison of selected sediment transport models. In: *Sixth International Conference on Asian and Pacific Coasts*, pp. 183-190, Hong Kong, China.

Libby, W.F., (1955) Radiocarbon dating, pp. 175. University of Chicago Press, Chicago, United States.

Lindé, K., Mycielska-Dowgiallo, E., (1980) Some experimentally produced microtextures on grain surfaces of quartz sand. *Geografiska Annaler, Series A, Physical Geography*, 62(3/4), 171-184.

Lisá, L., (2004) Exoscopy of Moravian eolian sediments. *Bulletin of Geosciences*, 79(3), 177-182.

Liu, K.-b., Fearn, M.L., (1993) Lake-sediment record of late Holocene hurricane activities from coastal Alabama. *Geology*, 21, 793-796.

Liu, K.-b., Fearn, M.L., (2000) Reconstruction of prehistoric landfall frequencies of catastrophic hurricanes in northwestern Florida from lake sediment record. *Quaternary Research*, 54, 238-245.

Liu, K.-b., Lu, H., Shen, C., (2008) A 1200-year proxy record of hurricanes and fires from the Gulf of Mexico coast: testing the hypothesis of hurricane-fire interactions. *Quaternary Research*, 69, 29-41.

LNEC, (1987) Agitação Marítima Portuguesa. Dados de base. Temporais. In: C. Pita, M. Carvalho, J. Santos, E. Veloso, A. Damião, L. Botelho (Eds.), *Agitação marítima na costa portuguesa. Dados de base. Temporais* (Ed. by C. Pita, M. Carvalho, J. Santos, E. Veloso, A. Damião, L. Botelho), pp. 17. DGP/LNEC (unpublished report).

Long, D., Smith, D.E., Dawson, A.G., (1989) A Holocene tsunami deposit in eastern Scotland. *Journal of Quaternary Science* 4, 61-66.

Lorang, M., (2000) Predicting the threshold entrainment mass for a boulder. *Journal of Coastal Research*, 16(2), 432-445.

Lorang, M., (2010) A wave-competence approach to distinguish between boulder and megaclast deposits due to storm waves versus tsunamis. *Marine Geology*, 283(1-4), 90-97.
Lowe, D.J., de Lange, W.P., (2000) Volcano-meteorological tsunamis, the c. AD 200 Taupo eruption (New Zealand) and the possibility of a global tsunami. *The Holocene*, 10(401-407).
Lu, H.-Y., Liu, K.-b., (2005) Phytolith assemblages as indicators of coastal environmental changes and hurricane overwash deposition. *The Holocene*, 15, 965-972.
Luque, L., Lario, J., Zazo, C., Goy, J.L., Dabrio, C.J., Silva, P.G., (2001) Tsunami deposits as paleoseismic indicators: examples from Spanish coast. *Acta Geologica Hispanica*, 36, 197-211.
Madeira, J., Mata, J., Moreira, M., Hoffmann, D.L., (2011) Deposits of a major Pleistocene tsunami in the Island of Maio (Cape Verde). *Geophysical Research Abstracts*, 13(EGU2011-1995), 1.
Madhavaraju, J., García y Barragán, J.C., Hussain, S.M., Mohan, S.P., (2009) Microtextures on quartz grains in the beach sediments of Puerto Peñasco and Bahia Kino, Gulf of California, Sonora, Mexico. *Revista Mexicana de Ciencias Geológicas*, 26(2), 367-379.
Mahaney, W.C., (2002) Atlas of sand grain surface textures and applications, pp. 237. Oxford University Press, Oxford, United Kingdom.
Mahaney, W.C., Dohm, J.M., (2011) The 2011 Japanese 9.0 magnitude earthquake: Test of a kinetic energy wave model using coastal configuration and offshore gradient of Earth and beyond. *Sedimentary Geology*, 239(1-2), 80-86.
Mahaney, W.C., Dohm, J.M., Costa, P., Krinsley, D.H., (2010) Tsunamis on Mars: Earth analogues of projected Martian sediment. *Planetary and Space Science*, 58(14-15), 1823-1831.
Mahaney, W.C., Stewart, A., Kalm, V., (2001) Quantification of SEM microtextures useful in environment discrimination. *Boreas*, 30, 165-171.
Mamo, B., Strotz, L., Dominey-Howes, D., (2009) Tsunami sediments and their foraminiferal assemblages. *Earth-Science Reviews*, 96(4), 263-278.
Mange, M.A., Wright, D.T., (2007) Heavy Minerals in Use. In: M.A. Mange, D.T. Wright (Eds.), *Developments in Sedimentology* (Ed. by M.A. Mange, D.T. Wright), pp. 1283. Elsevier, Amsterdam, The Netherlands.
Manickam, S., Barbaroux, L., (1987) Variations in the surface texture of suspended quartz grains in the Loire river: an SEM study. *Sedimentology*, 34, 495-510.
Manupella, G., (1992) Carta Geológica da Região do Algarve (1: 100 000) - Folha Ocidental. *Instituto Geológico e Mineiro*, Lisboa.
Martin, M.E., Bourgeois, J., (2012) Vented sediments and tsunami deposits in the Puget Lowland, Washington – differentiating sedimentary processes. *Sedimentology*, 59(2), 419-444.
Mason, C.L., Folk, R.L., (1958) Differentiation of beach, dune and aeolian flat environments by size analysis, Mustang Island, Texas. *Sedimentary Geology*, 56, 167-192.
Masson, D.G., Le Bas, T.P., Grevemeyer, I., Weinrebe, W., (2008) Flank collapse and largescale landsliding in the Cape Verde Islands, off West Africa. *Geochemistry, Geophysics, Geosystems*, 9(7), Q07015.
Masson, D.G., Watts, A.B., Gee, M.R.J., Urgeles, R., Mitchell, N.C., Le Bas, T.P., Canals, M., (2002) Slope failures on the flanks of the western Canary Islands. *Earth Science Reviews*, 57, 1-35.
Matias, A., Ferreira, Ó., Vila-Concejo, A., Garcia, T., Dias, J.A., (2008) Classification of washover dynamics in barrier islands. *Geomorphology*, 97(3-4), 655-674.
Matsumoto, D., Naruse, H., Fujino, S., Surphawajruksakul, A., Jarupongsakul, T., Sakakura, N., Murayama, M., (2008) Truncated flame structures within a deposit of the Indian Ocean Tsunami: evidence of synsedimentary deformation. *Sedimentology*, 55, 1559-1570.
McCloskey, T.A., Keller, G., (2009) 5000 year sedimentary record of hurricane strikes on the central coastal of Belize. *Quaternary International*, 195, 53-68.
McKee, E.D., (1959) Storm sediments on a Pacific atoll. *Journal of Sedimentary Petrology*, 29, 354-364.
McLaren, P., Bowles, D., (1985) The effects of sediment transport on grain-size distribution. *Journal Sedimentary Petrology* 55, 457-470.
Mclaren, P.A., (1981) Interpretation of trends in grain-size measurements. *Journal of Sedimentary Petrology*, 51, 611-624.
McMurtry, G.M., Watts, P., Fryer, G., Smith, J.R., Imamura, F., (2004) Giant landslides, mega-tsunamis, and paleo-sea level in the Hawaiian Islands. *Marine Geology*, 203, 219-233.
McSaveney, M., Goff, J., Darby, D., Goldsmith, P., Barnett, A., Elliott, S., Nongkas, M., (2000) The 17th July 1998 Tsunami, Sissano Lagoon, Papua New Guinea-evidence and initial interpretation. *Marine Geology*, 170, 81-92.
Meilianda, E., Dohmen-Janssen, C.M., Maathuis, B.H.P., Hulscher, S.J.M.H., Mulder, J.P.M., (2007) Beach morphology at Banda Aceh, Indonesia in response to the tsunami on 26 December 2004. In: *Coastal Sediments*, pp. 14, New Orleans, United States.

Meilianda, E., Dohmen-Janssen, C.M., Maathuis, B.H.P., Hulscher, S.J.M.H., Mulder, J.P.M., (2010) Short-term morphological responses and developments of Banda Aceh coast, Sumatra Island, Indonesia after the tsunami on 26 December 2004. *Marine Geology*, 275, 96-109.

Middleton, G.V., Hampton, M.A., (1973) Sediment gravity flows: mechanics of flow and deposition. In: G.V.M.a.A.H. Bouma (Ed.), *Turbidites and Deep Water Sedimentation* (Ed. by G.V.M.a.A.H. Bouma), pp. 38. SEPM. Short Course Notes, Anaheim, California.

Minoura, K., Imamura, F., Kuran, U., Nakamura, T., Papadopoulos, G.A., Takahashi, T., Yalciner, A.C., (2000) Discovery of Minoan tsunami deposits. *Geology*, 28(1), 59-62.

Minoura, K., Imamura, F., Takahashi, T., Shuto, N., (1997) Sequence of sedimentation processes caused by the 1992 Flores tsunami: Evidences from Babi Island. *Geology*, 25, 523-526.

Minoura, K., Nakaya, S., (1991) Traces of tsunami preserved in inter-tidal lacustrine and marsh deposits: some examples from northeast Japan. *Journal of Geology*, 99, 265-287.

Minoura, K., Nakaya, S., Uchida, M., (1994) Tsunami deposits in a lacustrine sequence of the Sanriku coast, northeast Japan. *Sedimentary Geology*, 89(1-2), 25-31.

Mischke, S., Schudack, U., Bertrand, S., Leroy, S.A.G., (2010) Ostracods from a Marmara Sea lagoon (Turkey) as tsunami indicators. *Quaternary International*, DOI:10.1016/j.quaint.2010.11.013.

Monecke, K., Finger, W., Klarer, D., Kongko, W., McAdoo, B.G., Moore, A.L., Sudrajat, S.U., (2008) A 1,000-year sediment record of tsunami recurrence in northern Sumatra. *Nature*, 455, 1232-1234.

Moore, A., Nishimura, Y., Gelfenbaum, G., Kamataki, T., Triyono, R., (2006) Sedimentary deposits of the 26 December 2004 tsunami on the northwest coast of Aceh, Indonesia. *Earth Planets Space*, 58, 253-258.

Moore, A.L., McAdoo, B.G., Ruffman, A., (2007) Landward fining from multiple sources in a sand sheet deposited by the 1929 Grand Banks tsunami, Newfoundland. *Sedimentary Geology*, 200(3-4), 336-346.

Moore, G.W., Moore, J.G., (1984) Deposits from a giant wave on the island of Lanai, Hawaii. *Science*, 226, 1312-1315.

Moore, G.W., Moore, J.G., (1988) Large scale bedforms in bolder gravel produced by giant waves in Hawaii. *Geological Society of America*, 229, 101-109.

Moore, J.G., Clague, D.A., Holcomb, R.T., Lipman, P.W., Normark, W.R., Torresan, M.E., (1989) Prodigious submarine landslides on the Hawaiian Ridge. *Journal of Geophysical Research*, 94, 17465-17484.

Moore, J.G., Moore, G.W., (1986) Large-scale bedforms in boulder gravel produced by giant waves in Hawaii. *Geological Society of America Special*, 229, 101-110.

Moore, J.G., Normark, W.R., Holcomb, R.T., (1994) Giant Hawaiian landslides. *Annual Reviews in Earth and Planetary Sciences*, 22, 119-144.

Morales, J.A., Borrego, J., San Miguel, E.G., López-González, N., Carro, B., (2008) Sedimentary record of recent tsunamis in the Huelva Estuary (south-western Spain). *Quaternary Science Reviews*, 27, 734-746.

Morton, R.A., (1978) Large-scale rhomboid bed forms and sedimentary structures associated with hurricane washover. *Sedimentology*, 25, 183-204.

Morton, R.A., Gelfenbaum, G., Jaffe, B.E., (2007) Physical criteria for distinguishing sandy tsunami and storm deposits using modern examples. *Sedimentary Geology*, 200, 184-207.

Morton, R.A., Richmond, B.M., Jaffe, B.E., Gelfenbaum, G., (2008) Coarse-clast ridge complexes of the Caribbean: a preliminary basis for distinguishing tsunami and storm-wave origins. *Journal of Sedimentary Research*, 78, 624-637.

Moura, D., Veiga-Pires, C., Albardeiro, L., Boski, T., Rodrigues, A.L., Tareco, H., (2007) Holocene sea level fluctuations and coastal evolution in the central Algarve (southern Portugal). *Marine Geology*, 237, 127-142.

Mulder, T., Alexander, J., (2001) The physical character of subaqueous sedimentary density flows and their deposits. *Sedimentology*, 48, 269-299.

Murphy, C.P., (1986) Thin section preparation of soils and sediments, pp. 149. AB Academic Publishers, Berkhamsted, Herts, United Kingdom.

Nanayama, F., Furukawa, R., Shigeno, K., Makino, A., Soeda, Y., Igarashi, Y., (2007) Nine unusually large tsunami deposits from the past 4000 years at Kiritappu marsh along the southern Kuril Trench. *Sedimentary Geology*, 200(3-4), 275-294.

Nanayama, F., Shigeno, K., (2006) Inflow and outflow facies from the 1993 tsunami in southwest Hokkaido. *Sedimentary Geology*, 187(3-4), 139-158.

Nanayama, F., Shigeno, K., Satake, K., Shimokawa, K., Koitabashi, S., Miyasaka, S., Ishii, M., (2000) Sedimentary differences between the 1993 Hokkaido-nansei-oki tsunami and the 1959 Miyakojima typhoon at Taisei, southwestern Hokkaido, northern Japan. *Sedimentary Geology*, 135(1-4), 255-264.

Nandasena, N.A.K., Paris, R., Tanaka, N., (2011a) Numerical assessment of boulder transport by the 2004 Indian ocean tsunami in Lhok Nga, West Banda Aceh (Sumatra, Indonesia). *Computers and Geosciences*, 37(9), 1391-1399.

Nandasena, N.A.K., Paris, R., Tanaka, N., (2011b) Reassessment of hydrodynamic equations: Minimum flow velocity to initiate boulder transport by high energy events (storms, tsunamis). *Marine Geology*, 281(1-4), 70-84.

Narayana, A.C., Tatavarti, R., Shinu, N., Subeer, A., (2007) Tsunami of December 26, 2004 on the southwest coast of India: post-tsunami geomorphic and sediment characteristics. *Marine Geology*, 242, 155-168.

Nelson, A.R., Jennings, A.E., Kashima, K., (1996) An earthquake history derived from stratigraphic and microfossil evidence of relative sea-level change at Coos Bay, southern coast of Oregon. *Geological Society of America Bulletin*, 108(2), 141-154.

Newson, M.D., (1979) Hydrology: Measurement and Application. Macmillan, Basingstoke, United kingdom.

Nichol, S.L., Kench, P.S., (2008) Sedimentology and preservation potential of carbonate sand sheets deposited by the December 2004 Indian Ocean tsunami: South Baa Atoll, Maldives. *Sedimentology*, 55, 1173-1187.

Noda, A., Katayama, H., Sagayama, T., Suga, K., Uchida, Y., Satake, K., Abe, K., Okamura, Y., (2007) Evaluation of tsunami impacts on shallow marine sediments: An example from the tsunami caused by the 2003 Tokachi-oki earthquake, northern Japan. *Sedimentary Geology*, 200(3-4), 314-327.

Noormets, R., Crook, K.A.W., Felton, E.A., (2004) Sedimentology of rocky shorelines: 3.: Hydrodynamics of megaclast emplacement and transport on a shore platform, Oahu, Hawaii. *Sedimentary Geology*, 172(1-2), 41-65.

Noormets, R., Felton, E.A., Crook, K.A.W., (2002) Sedimentology of rocky shorelines: 2: Shoreline megaclasts on the north shore of Oahu, Hawaii--origins and history. *Sedimentary Geology*, 150(1-2), 31-45.

Normark, W.R., Moore, J.G., Torresan, M.E., (1993) Giant volcano-related landslides and the development of the Hawaiian Islands. In: W.C. Schwab, H.J. Lee, D.C. Twichell (Eds.) (Ed. by W.C. Schwab, H.J. Lee, D.C. Twichell), pp. 184-196. US Geology Survey Bulletin.

Nott, J., (1997) Extremely high-energy wave deposits inside the Great Barrier Reef, Australia: determining the cause--tsunami or tropical cyclone. *Marine Geology*, 141(1-4), 193-207.

Nott, J., (2003) Waves, coastal boulder deposits and the importance of the pre-transport setting. *Earth and Planetary Science Letters*, 210(1-2), 269-276.

Nott, J., Hayne, M., (2001) High frequency of 'super-cyclones' along the Great Barrier Reef over the past 5,000 years. *Nature*, 413, 508- 512.

Nott, J., Smithers, S., Walsh, K.R., E., (2009) Sand beach ridges record 6000 year history of extreme tropical cyclone activity in northeastern Australia. *Quaternary Science Reviews*, 28, 1511-1520.

Oehler, J.-F., Labazuy, P., Lénat, J.F., (2004) Recurrence of major flank landslides during the last 2 Ma-history of Réunion Island. *Bulletin of Volcanology*, 66, 585-598.

Okal, E.A., Synolakis, C.E., (2004) Source discriminants for nearfield tsunamis. *Geophysical Journal International*, 158, 899-912.

Okal, E.O., Synolakis, C.E., (2003) A Theoretical Comparison of Tsunamis from Dislocations and Landslides. *Pure and Applied Geophysics*, 160(10/11), 2177-2188.

Oliveira, C.S., (2005) Descrição do Terramoto de 1755, sua extensão, causas e efeitos. O sismo. O tsunami. O incêndio. In: F.a. Público (Ed.), *O Grande Terramoto de Lisboa*, *1* (Ed. by F.a. Público), pp. 23-86, Lisbon.

Oliveira, M.A., Andrade, C., Freitas, M.C., Costa, P., (2008) Using the historical record and geomorphological setting to identify tsunami deposits in the southwestern coast of Algarve (Portugal). In: *2nd International Tsunami Field Symposium, IGCP Project 495*, *Abstract Book*, pp. 85-88.

Oliveira, M.A., Andrade, C., Freitas, M.C., Costa, P., Taborda, R., Janardo, C., Neves, R., (2011) Transport of large boulders quarried from shore platforms of the Portuguese west coast. *Journal of Coastal Research*(SI 64), 1871 - 1875.

Oliveira, M.A., Andrade, C., Freitas, M.C., Costa, P.J., (2009) Modeling Volume Transfer between Beach-Foredune and the Backshore by the 1755 Lisbon Tsunami at Boca Do Rio Lowland, Algarve (Portugal). *Journal of Coastal Research*, 1547-1551.

Oliveira, M.A. (2011) Advanced Training Course - PhD program. *Unpublished report (Departamento de Geologia, University of Lisbon)*.

Ollerhead, J., Huntley, D.J., Nelson, A.R., Kelsey, H.M., (2001) Optical dating of tsunami-laid sand from an Oregon coastal lake. *Quaternary Science Reviews*, 20(18), 1915-1926.

Olsson, I., (1986) Handbook of Holocene Palaeoecology and Palaeohydrology. In: B.E. Berglund (Ed.), *Radiometric dating* (Ed. by B.E. Berglund), pp. 273-312. Wiley, Chicherster.

Orford, J., Wheeler, A., McCloskey, J., Dardis, O., Doherty, J., Gallaher, K., (1996) Variations in Climate Forcing of Coastal Processes and the Coastal Response along the European Shoreline. *Final Report, EU Environmental Programme EV5V-CT94-0455, Climate Change and Coastal Evolution in Europe, XII Directorate-General, Commission of the European Communities.*

Ota, Y., Pirazzoli, P.A., Kawana, T., Moriwaki, H., (1985) Late Holocene coastal morphology and sea-level records on three small islands, the South Ryukyus, Japan. *Geographical Review of Japan*, B 58(2), 185-194.

Otvos, E.G., Carter, G.A., (2008) Hurricane degradation-barrier development cycles, northeastern Gulf of Mexico. Landform evolution and island chain history. *Journal of Coastal Research*, 24, 463-478.

Papadopoulos, G.A., Imamura, F., (2001) Proposal for a new tsunami intensity scale. In: *International Tsunami Conference*, pp. 569 - 577, Seattle.

Paris, R., Cachao, M., Fournier, J.V., O., (2010a) Nannoliths abundance and distribution in tsunami deposits: example from the December 26, 2004 tsunami Lhok Nga (northwest Sumatra, Indonesia). *Géomorphologie: Relief, Processus, Environnement 1*.

Paris, R., Fournier, J., Poizot, E., Etienne, S., Morin, J., Lavigne, F., Wassmer, P., (2010b) Boulder and fine sediment transport and deposition by the 2004 tsunami in Lhok Nga (western Banda Aceh, Sumatra, Indonesia): A coupled offshore-onshore model. *Marine Geology*, 268(1-4), 43-54.

Paris, R., Giachetti, T., Chevalier, J., Guillou, H., Frank, N., (2011a) Tsunami deposits in Santiago Island (Cape Verde archipelago) as possible evidence of a massive flank failure of Fogos volcano. *Sedimentary Geology*, 239(3-4), 129-145.

Paris, R., Lavigne, F., Wassmer, P., Sartohadi, J., (2007) Coastal sedimentation associated with the December 26, 2004 tsunami in Lhok Nga, west Banda Aceh (Sumatra, Indonesia). *Marine Geology*, 238(1-4), 93-106.

Paris, R., Naylor, L.A., Stephenson, W.J., (2011b) Boulders as a signature of storms on rock coasts. *Marine Geology*, 283, 1-11.

Paris, R., Pérez Torrado, F.J., Carracedo, J.C., (2005) Massive flank failures and tsunamis in the Canary Islands: past, present, future. *Zeitschrift für Geomorphologie*, 140, 37-54.

Paris, R., Wassmer, P., Sartohadi, J., Lavigne, F., Barthomeuf, B., Desgages, É., Grancher, D.B., Ph., Vautier, F., Brunstein, D., Gomez, C., (2009) Tsunamis as geomorphic crisis: lessons from the December 26, 2004 tsunami in Lhok Nga, west Banda Aceh (Sumatra, Indonesia). *Geomorphology*, 104, 59-72.

Paskoff, R., (1991) Likely occurance of a mega-tsunami in the Middle Pleistocene, near Coquimbo, Chile. *Revista Geologica de Chile*, 18(1), 87-91.

Patterson, R.T., Fowler, A.D., (1996) Evidence of self organization in planktic foraminiferal evolution: implications for interconnectedness of paleoecosystems. *Geology*, 24(3), 215-218.

Pereira, A.R., Trindade, J., M., N., Borges, B., (2007) Indicadores geomorfológicos de tsunamino Parque Natural do SW Alentejano e Costa Vicentina (Malhão). In: *VI Congresso da Assoc. Portuguesa de Geomorfólogos*, pp. 51-56, Braga.

Pereira de Sousa, F.L., (1919) O terremoto do 1 de Novembro de 1755 em Portugal: um estudo demográfico, *I, II, III and IV*. Serviços Geológicos, Lisbon.

Pessanha, L., Pires, H.O., (1981) Elementos sobre o clima de agitação marítima na costa sul do Algarve, *unpublished report*, pp. 67. Instituto Nacional de Meteorologia e Geofísica, Lisbon.

Peters, R., Jaffe, B., Gelfenbaum, G., (2007) Distribution and sedimentary characteristics of tsunami deposits along the Cascadia margin of western North America. *Sedimentary Geology*, doi: 10.1016/j.sedgeo.2007.01.015, 42.

Phantuwongraj, S., Choowong, M., (2011) Tsunamis versus storm deposits from Thailand. *Natural Hazards*, 63(1), 31-50.

Pinto, C., Teixeira, S.B., (2002) Morphodynamics of the sandy barrier of Salgados coastal lagoon, Armação de Pêra Bay (Algarve - Portugal). In: *Eurocoast Littoral 2002, The Changing Coast* (Ed. by E. Portugal), pp. 403-409. Eurocoast/EUCC, Porto.

Powers, M.C., (1953) A new roundness scale for sedimentary particles. *Journal of Sedimentary Research*, 23(2), 117-119.

Pratt, B.R., (2001) Oceanography, bathymetry and syndepositional tectonics of a Precambrian intracratonic basin: integrating sediments, storms, earthquakes and tsunamis in the Belt Supergroup (Helena Formation, ca. 1.45 Ga), western North America. *Sedimentary Geology*, 141-142, 371-394.

Pratt, B.R., (2002) Tepees in peritidal carbonates: origin via earthquake-induced deformation, with example from the Middle Cambrian of western Canada. *Sedimentary Geology*, 153(3-4), 57-64.

Pritchard, D., Dickinson, L., (2008) Modelling the sedimentary signature of long waves on coasts: implications for tsunami reconstruction. *Sedimentary Geology*, 206, 42-57.

Pyökäri, M., (1997) The provenance of beach sediments on Rhodes, southeastern Greece, indicated by sediment texture, composition and roundness. *Geomorphology*, 18(3-4), 315-332.

Regnauld, H., Nichol, S.L., J.R., G., Fontugne, M., (2004) Maoris, middens and dune front accretion rate on the NE coast of New Zealand: resilience of a sedimentary system after a tsunami. *Géomorphologie : relief, processus, environnement*, 1, 45-54.

Regnauld, H., Planchon, O., Goff, J., (2008) Relative roles of structure, climate, and of a tsunami event on coastal evolution of the Falkland Archipelago. *Géomorphologie: relief, processus, environnement*, 1, 15-26.

Reicherter, K., Vonberg, D., Koster, B., Fernández-Steeger, T., Grützner, C., Mathes-Schmidt, M., (2010) The sedimentary inventory of tsunamis along the southern Gulf of Cádiz (southwestern Spain). *Zeitschrift für Geomorphologie*, SI 54(3), 147-173.

Reinhart, M.A., (1991) Sedimentological analysis of postulated tsunami-generated deposits from Cascadia great-subduction earthquakes along southern coastal Washington: Seattle, *MSc*, pp. 77. University of Washington.

Richards, L.A.R., Phipps, P.J., (2007) Managing the impact of climate change on vulnerable areas: a case study of the Western Isles, UK, pp. 9. Mott MacDonald, Croydon, UK.

Richmond, B.M., Watt, S., Buckley, M., Jaffe, B.E., Gelfenbaum, G., Morton, R.A., (2011) Recent storm and tsunami coarse-clast deposit characteristics, southeast Hawai`i. *Marine Geology*, 283, 79-89.

Ritchie, W., (1971) The Beaches of Barra and the Uists: a Survey of the Beach, Dune and Machair Areas of Barra, South Uist, Benbecula, North Uist and Berneray. In: *Department of Geography*, pp. 83. University of Aberdeen,, Aberdeen.

Ritchie, W., (1979) Machair chronology and development in the Uists and adjacent islands. *Proceedings of the Royal Society of Edinburgh*, 77, 107-122.

Ritchie, W., (1985) Inter-tidal and sub-tidal organic deposits and sea level changes in the Uists, Outer Hebrides. *Scottish Journal of Geology*, 21, 161- 176.

Ritchie, W., Whittington, G., (1994) Non-synchronous aeolian sand movements in the Uists: the evidence of the intertidal organic and sand deposits at Cladach Mor, North Uist. *Scottish Geographical Magazine* 110, 40- 46.

Rodriguez-Vidal, J., Ruiz, F., Caceres, L.M., Abad, M., Gonzalez-Regalado, M.L., Pozo, M., Carretero, M.I., Monge Soares, A.M., Toscano, F.G., (2011) Geomarkers of the 218-209 BC Atlantic tsunami in the Roman Lacus Ligustinus (SW Spain): A palaeogeographical approach. *Quaternary International*, 242(1), 201-212.

Rossetti, D.F., (1997) Internal architecture of mixed tide and storm-influenced deposits: an example from the Alcântara Formation, northern Brazil. *Sedimentary Geology*, 114, 163-188.

Ruiz, F., Abad, M., Cáceres, L.M., Rodríguez Vidal, J., Carretero, M.I., Pozo, M., González-Regalado, M.L., (2010) Ostracods as tsunami tracers in Holocene sequences. *Quaternary Research*, 73(1), 130-135.

Ruiz, F., Borrego, J., López-González, N., Abad, M., González-Regalado, M.L., Carro, B., Pendón, J.G., Rodríguez-Vidal, J., Cáceres, L.M., Prudêncio, M.I., Dias, M.I., (2007) The geological record of a mid-Holocene marine storm in southwestern Spain. *Geobios*, 40(5), 689-699.

Ruiz, F., Rodríguez-Ramírez, A., Cáceres, L.M., Vidal, J.R., Carretero, M.I., Abad, M., Olías, M., Pozo, M., (2005) Evidence of high-energy events in the geological record: Mid-holocene evolution of the southwestern Doñana National Park (SW Spain). *Palaeogeography, Palaeoclimatology, Palaeoecology*, 229, 212-229.

Samsuddin, M., (1986) Textural differentiation of foreshore and breaker zone sediments on the northern Kerala coast, India. *Sedimentary Geology*, 45, 135-145.

Santos, F.D., Forbes, K., Moita, R., (2002) Climate Change in Portugal. Scenarios, Impacts and Adaptation Measures - SIAM Project. Gradiva, Lisbon.

Santos, F.D., Miranda, P., (2006) Alterações Climáticas em Portugal. Cenários, Impactos e Medidas de Adaptação - Projecto SIAM II. Gradiva, Lisbon.

Satake, K., Tanioka, Y., (2003) The July 1998 Papua New Guinea Earthquake: Mechanism and Quantification of Unusual Tsunami Generation. *Pure Applied Geophys.*, 160, 2087-2118.

Sato, H., Shimamoto, T., Tsutsumi, A., Kawamoto, E., (1995) Onshore Tsunami Deposits Caused by the 1993 Southwest Hokkaido and 1983 Japan Sea Earthquakes. *Pure and Applied Geophysics*, 144, 693-717.

Sawai, Y., (2002) Evidence for 17th century tsunamis generated on the Kuril-Kamchatka subduction zone, Lake Tokotan, Hokkaido, Japan. *Journal of Asian Earth Sciences*, 20, 903-911.

Sawai, Y., Jankaew, K., Martin, M.E., Prendergast, A., Choowong, M., Charoentitirat, T., (2009) Diatom assemblages in tsunami deposits associated with the 2004 Indian Ocean tsunami at Phra Thong Island, Thailand. *Marine Micropaleontology*, 73, 70-79.

Scheffers, A., (2004) Tsunami imprints on the Leeward Netherlands Antilles (Aruba, Curaçao, Bonaire) and their relation to other coastal problems. *Quaternary International*, 120(1), 163-172.

Scheffers, A., (2008) Tsunami Boulder Deposits. In: T. Shiki, Y. Tsuji, T. Yamazaki, K. Minoura (Eds.), *Tsunamiites - Features and implications* (Ed. by T. Shiki, Y. Tsuji, T. Yamazaki, K. Minoura), pp. 299-317. Elsevier, Amsterdam.

Scheffers, A., Kelletat, D., (2003) Sedimentologic and geomorphologic tsunami imprints worldwide--a review. *Earth-Science Reviews*, 63(1-2), 83-92.

Scheffers, A., Kelletat, D., (2005) Tsunami relics on the coastal landscape west of Lisbon, Portugal. *Science of Tsunami Hazards*, 23, 1, 3-16.

Scheffers, A., Kelletat, D., Vött, A., May, S.M., Scheffers, S., (2008) Late Holocene tsunami traces on the western and southern coastlines of the Peloponnesus (Greece). *Earth and Planetary Science Letters*, 269(1-2), 271-279.

Scheffers, A., Scheffers, S., (2007) Tsunami deposits on the coastline of west Crete (Greece). *Earth and Planetary Science Letters*, doi: 10.1016/j.epsl.2007.05.041, 32.

Schneider, H., Höfer, D.T., C., Busch, S., Schneider, M., Baade, J., Daut, G., Mäusbacher, R., (2009) Holocene estuary development in the Algarve Region (Southern Portugal) - A reconstruction of sedimentological and ecological evolution. *Quaternary International*, 221(1-2), 141-158.

Schnyder, J., Baudin, F., Deconinck, J.-F., (2005) A possible tsunami deposit around the Jurassic-Cretaceous boundary in the Boulonnais area (northern France). *Sedimentary Geology*, 177(3-4), 209-227.

Schwartz, R.K., (1975) Nature and genesis of some storm washover deposits. *U.S. Army Corps of Engineers, Coastal Engineering Research Center* Technical Memorandum No. 61.

Scicchitano, G., Monaco, C., Tortorici, L., (2007) Large boulder deposits by tsunami waves along the Ionian coast of south-eastern Sicily (Italy). *Marine Geology*, 238, 75–91.

Scotland, T.G.o., (2003) N H Trewin. Geological Society of London, London.

Sedgwick, P.E., Davis, R.A., . . 2000, . (2003) Stratigraphy ofwashover deposits in Florida: implications for recognition in the stratigraphic record. *Marine Geology*, 2000, 31-48.

Shennan, I., Horton, B., Innes, J., Gehrels, R., Lloyd, J., McArthur, J.J., Rutherford, M.M., (2000) Late Quaternary sea-level changes, crustal movements and coastal evolution in Northumberland, UK. *Journal of Quaternary Science*, 15(3), 215-237.

Shennan, I., Rutherford, M.M., Innes, J.B., Walker, K.J., (1996) Late glacial sea level and ocean margin environmental changes interpreted from biostratigraphic and lithostratigraphic studies of isolation basins in northwest Scotland. *Geological Society of London*, 111, 229-244.

Shepard, F.P., Young, R., (1961) Distinguishing between beach and dune sands. *Journal of Sedimentary Petrology*, 31, 196-214.

Shetland, G.S.M.o., (2012) Shetland Landscapes. Geoparks Shetland.

Shi, S., (1995) Observational and Theoretical Aspects of Tsunami Sedimentation, *PhD*, pp. 333. Coventry University, Coventry, United Kingdom.

Shi, S., Dawson, A.G., Smith, D.E., (1995) Coastal sedimentation associated with the December 12th, 1992 Tsunami in Flores, Indonesia. *Pure and Applied Geophysics*, 144, 525-536.

Shi, S., Smith, D.E., (2003) Coastal tsunami geomorphological impacts and sedimentation processes:case studies of modern and prehistorical events. In: *International Conference on Estuaries and Coasts*, Hangzhou, China.

Shiki, T., Tachibana, T., Fujiwara, O., Goto, K., Nanayama, F., Yamazaki, T., (2008) Characteristic features of tsunamiites. In: T. Shiki, Y. Tsuji, T. Yamazaki, K. Minoura (Eds.), *Tsunamiites - Features and Implications* (Ed. by T. Shiki, Y. Tsuji, T. Yamazaki, K. Minoura), pp. 319-340. Elsevier, Amsterdam.

Silva Lopes, J.B.L., (1841) Corografia ou Memória Económica, Estatística e Topográfica do Reino do Algarve, pp. 528, Lisboa.

Smit, J., Montanari, A., Swinburne, N.H.M., Alvarez, W., Hilderbrand, R., Margolis, S.V., Claeys, P., Lowrie, W., Asaro, F., (1992) Tektite-bearing deep-water clastic unit at the Cretaceous-Tertiary boundary in north-eastern Mexico. *Geology*, 20, 99-103.

Smith, D.E., Shi, S., Cullingford, R.A., Dawson, A.G., Dawson, S., Firth, C.R., Foster, I.D.L., Fretwell, P.T., Haggart, B.A., Holloway, L.K., Long, D., (2004) The Holocene Storegga Slide tsunami in the United Kingdom. *Quaternary Science Reviews*, 23, 2291-2321.

Soloviev, S.L., (1970) Recurrence of tsunamis in the Pacific. In: *Tsunamis in the Pacific Ocean* (Ed. by W.M. Adams), pp. 149-164, Honolulu.

Spiske, M., Böröcz, Z., Bahlburg, H., (2008) The role of porosity in discriminating between tsunami and hurricane emplacement of boulders — A case study from the Lesser Antilles, southern Caribbean. *Earth and Planetary Science Letters*, 268, 384-396.

Spiske, M., Weiss, R., Bahlburg, H., Roskosch, J., Amijaya, H., (2010) The TsuSedMod inversion model applied to the deposits of the 2004 Sumatra and 2006 Java tsunami and implications for estimating flow parameters of palaeo-tsunami. *Sedimentary Geology*, 224(1-4), 29-37.

Srinivasalu, S., Thangadurai, N., Switzer, A.D., Ram Mohan, V., Ayyamperumal, T., (2007) Erosion and sedimentation in Kalpakkam (N Tamil Nadu, India) from the 26th December 2004 tsunami. *Marine Geology*, 240, 65-75.

St-Onge, G., Chapron, E., Salas, M., Viel, M., Mulsow, S., Debret, M., Foucher, A., Mulder, T., Desmet, M., Costa, P., Ghaleb, B., Jaouen, A., Locat, J., (2012) Comparison of earthquake-triggered turbidites from the Saguenay (Eastern Canada) and Reloncavi (Chilean margin) Fjords: implications for paleoseismicity and sedimentology. *Sedimentary Geology*, 243–244, 89-107.

Stuiver, M., Reimer, P.J., (1993) Extended ^{14}C database and revised CALIB radiocarbon program. *Radiocarbon*, 35, 215-230.

Stuiver, M., Reimer, P.J., Bard, E., Beck, J.W., Burr, G.S., Hughen, K.A., Kromer, B., McCormac, G., van der Plicht, J., Spurk, M., (1998) IntCal98 radiocarbon age calibration, 24,000-0 cal BP. *Radiocarbon*, 40(3), 1041-83.

Sugawara, D., Minoura, K., Imamura, F., (2008) Tsunamiites Features and Implications - Chapter 3 - Tsunamis and Tsunami Sedimentology, pp. 9-49. Elsevier.

Switzer, A.D., (2008) 20 years of palaeotsunami studies on coastal sandsheets: a review. In: *2nd International Tsunami Fiedl Symposium*, Italy.

Switzer, A.D., Bristow, C.S., Jones, B.G., (2006) Investigation of large-scale washover of a small barrier system on the southeast Australian coast using ground penetrating radar. *Sedimentary Geology*, 183, 145-156.

Switzer, A.D., Burston, J.M., (2010) Competing mechanisms for boulder deposition on the southeast Australian coast. *Geomorphology*, 114, 42-54.

Switzer, A.D., Jones, B.G., (2008) Large-scale washover sedimentation in a freshwater lagoon from the southeast Australian coast: tsunami or exceptionally large storm? *The Holocene*, 18, 787-803.

Switzer, A.D., Pucillo, K., Haredy, R.A., Jones, B.G., Bryant, E.A., (2005) Sea-level, storms or tsunami; enigmatic sand sheet deposits in sheltered coastal embayment from southeastern New South Wales Australia. *Journal of Coastal Research*, 21, 655-663.

Synolakis, C.E., Imamura, F., Tsuji, Y., Matsutomi, H., Tinti, S., Cook, B., Chandra, Y.P., Usman, M., (1995) Damage conditions of East Java tsunami of 1994 analyzed. *Eos, Trans. AGU*, 76, 257 and 261-262.

Szczucinski, W., (2011) The post-depositional changes of the onshore 2004 tsunami deposits on the Andaman Sea coast of Thailand. *Natural Hazards*, DOI: 10.1007/s11069-011-9956-8.

Szczucinski, W., Chaimanee, N., Niedzielski, P., Rachlewicz, G., Saisuttichai, D., Tepsuwan, T., Lorenc, S., Siepak, J., (2006) Environmental and Geological Impacts of the 26 December 2004 Tsunami in Coastal Zone of Thailand – Overview of Short and Long-Term Effects. *Polish J. of Environ. Stud.*, 15, 5, 793-810.

Szczucinski, W., Niedzielski, P., Kozak, L., Frankowski, M., Zioła, A., Lorenc, S., (2007) Effects of rainy season on mobilization of contaminants from tsunami deposits left in a coastal zone of Thailand by the 26 December 2004 tsunami. *Environ Geol*, DOI 10.1007/s00254-007-0639-4, 12.

Szczucinski, W., Niedzielski, P., Rachlewicz, G., Sobczynski, T., Zioła, A., Kowalski, A., Lorenc, S., Siepak, J., (2005) Contamination of tsunami sediments in a coastal zone inundated by the 26 December 2004 tsunami in Thailand. *Environ Geol*, 49, 321–331.

Taborda, R., Dias, J.A., (1992) Análise da Sobreelevação do Mar de Origem Meteorológica durante os Temporais de Fevereiro/Março de 1978 e Dezembro de 1981. *Geonovas*, A Geologia e o Ambiente(1), 89-97.

Tappin, D.R., (2007) Sedimentary features of tsunami deposits -- Their origin, recognition and discrimination: An introduction. *Sedimentary Geology*, 200(3-4), 151-154.

Tappin, D.R., Watts, P., McMurtry, G.M., Lafoy, Y., Matsumoto, T., (2001) The Sissano, Papua New Guinea tsunami of July 1998 -- offshore evidence on the source mechanism. *Marine Geology*, 175, 1-23.

Terrinha, P., Pinheiro, L.M., Henriet, J.P., Matias, L., Ivanov, M.K., Monteiro, J.H., Akhmetzhanov, A., Volkonskaya, A., Cunha, T., Shaskin, P., Rovere, M., (2003) Tsunamigenic-seismogenic structures, neotectonics, sedimentary processes and slope instability on the southwest Portuguese Margin. *Marine Geology*, 195(1-4), 55-73.

Tinti, S., (1990) Tsunami research in Europe. *Terra Nova*, 2, 19-22.

Tooley, M.J., Smith, D.E., (2005) Relative sea-level change and evidence for the Holocene Storegga Slide tsunami at a site in Fife, Scotland, United Kingdom. *Quaternary International*, 113-114, 107-119.

Trigo, R.M., Pozo-Vásquez, D., Osborne, T., Castro-Díez, Y., Gámin-Fortis, S., Esteban-Parra, M.J., (2004) North Atlantic Oscillation influence on precipitation, river flow and water resources in the Iberian peninsula. *International Journal of Climatology*, 24, 925-944.

Tuttle, M.P., Ruffman, A., Anderson, T., Hewitt, J., (2004) Distinguishing tsunami from storm deposits in eastern North America. The 1929 Grand Banks tsunami versus the 1991 Halloween storm. *Seismological Research Letters*, 75, 117-131.

Uchida, J., Abe, K., Hasegawa, S., Fujiwara, O., (2007) Studies on the source of run-up tsunami deposits based on foraminiferal tests and their hydrodynamic verification. *Quaternary Research*, 46(6), 533-540.

van den Bergh, G.D., Boer, W., de Haas, H., van Weering, T.C.E., van Wijhe, R., (2003) Shallow marine tsunami deposits in Teluk Banten (NW Java, Indonesia), generated by the 1883 Krakatau eruption. *Marine Geology*, 197(1-4), 13-34.

Visher, G.S., (1969) Grain size distributions and depositional processes. *Journal of Sedimentary Petrology*, 39, 1074-1106.

Wagner, B., Bennike, O., Klug, M., Cremer, H., (2007) First indication of Storegga tsunami deposits from East Greenland. *Journal of Quaternary Science*, 22, 321-325.

Wallace, D.J., Anderson, J.B., (2010) Evidence of similar probability of intense hurricane strikes for the Gulf of Mexico over the late Holocene. *Geology*, 38, 511-514.

Wassmer, P., Schneider, J.-L., Fonfrage, A.-V., Lavigne, F., Paris, R., Gomez, C., (2010) Use of anisotropy of magnetic susceptibility (AMS) in the study of tsunami deposits: Application to the 2004 deposits on the eastern coast of Banda Aceh, North Sumatra, Indonesia. *Marine Geology*, 275(1-4), 255-272.

Weidong, D., Baoguo, Y., Xiaogen, W., (1997) Studies of storm deposits in China - A review. *Continental Shelf Research*, 17, 1645-1658.

Weiss, R., (2008) Sediment grains moved by passing tsunami waves: Tsunami deposits in deep water. *Marine Geology*, MARGO-04157, 7.

Weiss, R., Bahlburg, H., (2006) A note on the preservation of offshore tsunami deposits. *Journal of Sedimentary Research*, 76, 1267-1273.

Weiss, R., Wünnemann, K., Bahlburg, H., (2006) Numerical modeling of generation, propagation and run-up of tsunamis caused by oceanic impacts. *Geophys. J. Int.*, 167(77-88).

Wentworth, C.K., (1922) A scale of grade and class terms for clastic sediments. *Journal of Geology*, 30, 377-392.

Whalley, W.B., (1990) Geomorphological Techniques. In: A.S. Goudie (Ed.), *Part 3: material properties* (Ed. by A.S. Goudie), pp. 109-192. Unwin Hyman, London and Boston.

Whelan, F., Kelletat, D., (2005) Boulder deposits on the Southern Spanish Atlantic Coast: Possible evidence for the 1775 AD Lisbon Tsunami. *Science of Tsunami Hazards*, 23, 25-38.

Williams, D.M., Hall, A.M., (2004) Cliff-top megaclast deposits of Ireland, a record of extreme waves in the North Atlantic--storms or tsunamis? *Marine Geology*, 206(1-4), 101-117.

Williams, H.F.L., Hutchinson, I., (2000) Stratigraphic and microfossil evidence for late Holocene tsunamis at Swantown Marsh, Whidbey Island, Washington. *Quaternary Research*, 54, 218-227.

Wintle, A.G., Lancaster, N., Edwards, S.R., (1994) Infrared stimulated luminescence (IRSL) dating of late-Holocene aeolian sands in the Mojave desert, California, USA. *The Holocene*, 4, 74-78.

Woodruff, J.D., Donnelly, J.P., Okusu, A., (2009) Exploring typhoon variability over the mid-to-late Holocene: evidence of extreme coastal flooding from Kamikoshiki. *Quaternary Science Reviews*, 28, 1774-1785.

Yawsangratt, S., Szczucinski, W., Chaimanee, N., Chatprasert, S., Majewski, W., Lorenc, S., (2011) Evidence of probable paleotsunami deposits on Kho Khao Island, Phang Nga Province, Thailand. *Nat Hazards*, DOI: 10.1007/s11069-011-9729-4.

Young, R., Bryant, E., Price, D., (1996) Catastrophic wave (tsunami?) transport of boulders in southern New South Wales, Australia. *Geomorphology*, 40(2), 191-207.

Zitellini, N., Mendes, L.A., Cordoba, D., Danobeitia, J., Nicolich, R., Pellis, G., Ribeiro, A., Sartori, R., Torelli, L., Bartolome, R., Bortoluzzi, G., Calafato, A., Carrilho, F., Casoni, L., Chierici, F., Corela, C., Correggiari, A., Della Vedova, B., Gracia, E., Jornet, P., Landuzzi, M., Ligi, M., Magagnoli, A., Marozzi, G., Matias, L., Penitenti, D., Rodriguez, P., Rovere, M., Terrinha, P., Vigliotti, L., Ruiz, A.Z., (2001) Source of 1755 Lisbon earthquake and tsunami investigated. *Eos (Transactions, American Geophysical Union)*, 26(285), 290-291.

Zong, Y.Q., Tooley, M.J., (1999) Evidence of mid-Holocene storm surge deposits from Morecambe Bay, northwest England: a biostratigraphical approach. *Quaternary International*, 55, 43-50.

Annex 1 – Geological legend lithostratigraphy of the windward sector of the Algarve

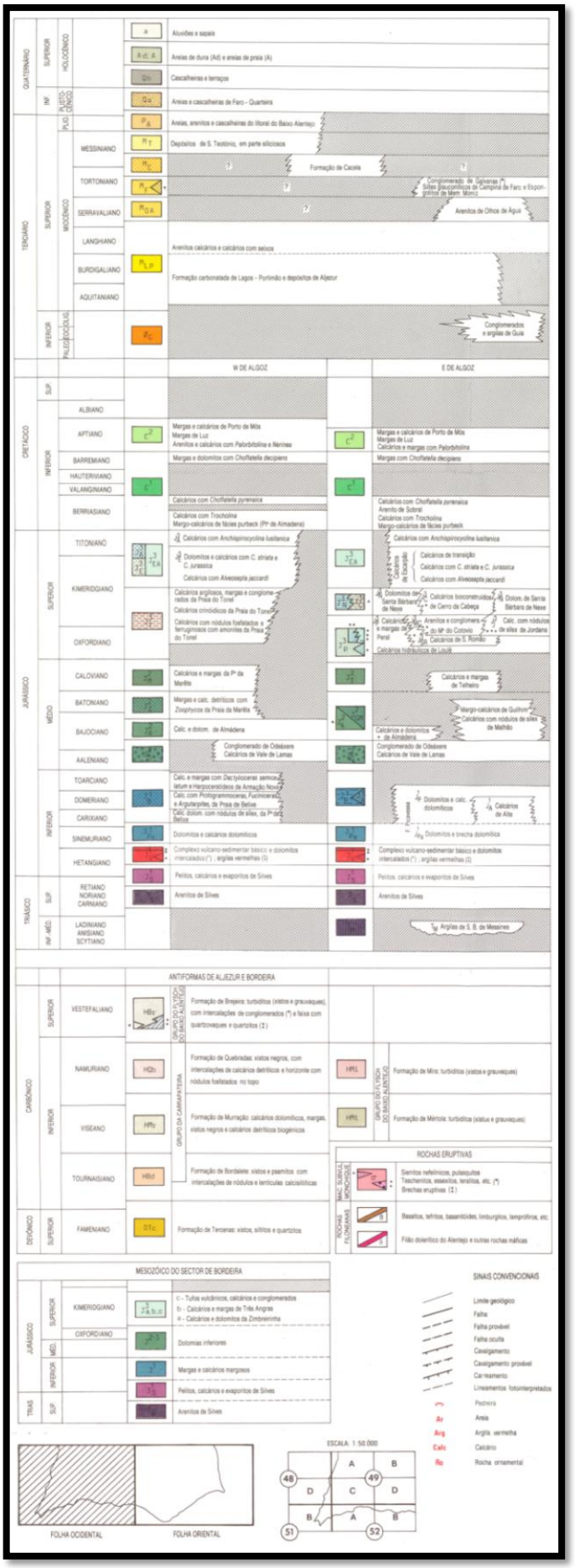
W DE ALGOZ
E DE ALGOZ
ANTIFORMAS DE ALJEZUR E BORDEIRA
ROCHAS ERUPTIVAS
MESOZÓICO DO SECTOR DE BORDEIRA
SINAIS CONVENCIONAIS
FOLHA OCIDENTAL
FOLHA ORIENTAL
ESCALA: 1:50 000

Annex 2 – Atlas of quartz grains

With the samples collected, and after laboratory treatment, a group of SEM photos of the quartz grains was gathered (Table A2.1). A group of microtextures visible in the surface of the quartz grains was identified and an atlas was compiled to facilitate the identification of microtextures. The grains were analysed and the microtextures were classified according with the area of the surface of the grain that they occupied.

Table A2.1 –Samples used to compose the SEM Atlas of quartz grains.

Location	Sample	Sedimentary Environment
Boca do Rio	BDR Alv Dir	Alluvial
Boca do Rio	BDR Duna Trep	Dune
Boca do Rio	BDR Face de Praia	Beach face
Boca do Rio	BDR Lagoa Budens	Fluvial\lagoonal
Boca do Rio	BDR SS3	Tsunami
Martinhal	Mart 3	Tsunami
Martinhal	Mart 4	Tsunami
Martinhal	Mart 5	Tsunami
Martinhal	Mart 6	Tsunami
Salgados	SG 14 (0.20-0.28)	SG_X_storm?
Salgados	SG 14 (0.40-0.82)	Tsunami
Salgados	SG Berma	Beach berm
Salgados	SG Duna	Dune
Salgados	SG Praia	Beach
Praia do Barranco	PB AM4 Duna	Dune
Praia do Barranco	PB Face de Praia	Beach face
Praia do Barranco	PB Berma	Beach berm
Praia do Barranco	PB Duna F	Dune
Praia do Barranco	PB Duna R	Dune
Praia do Barranco	PB Duna T	Dune
Praia do Barranco	PB Duna Trp Margem	Dune
Praia do Barranco	PB Duna Trp Rib	Dune

Microtextures:

a) **Roundness** – classified using Powers scale. The grains were classified from 1 to 6 (Very rounded to very angular).

- Very angular *(Classification: 6)*

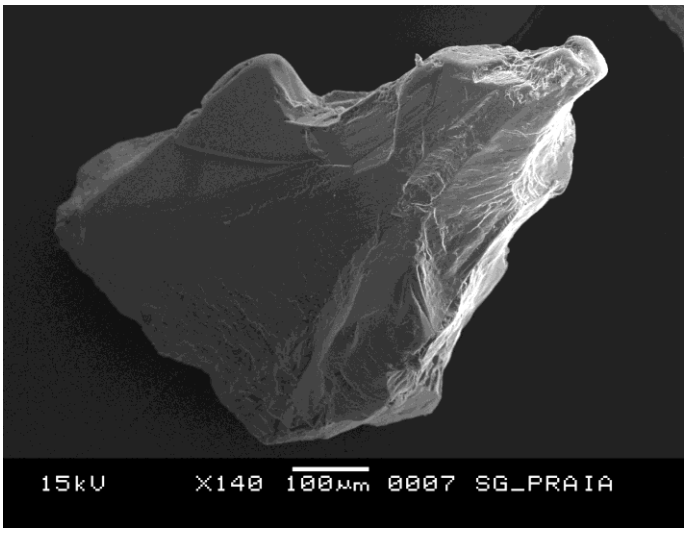

Figure A2.1 – SEM photo of very angular grain. Sample SG_Praia_2_1

- Angular *(Classification: 5)*

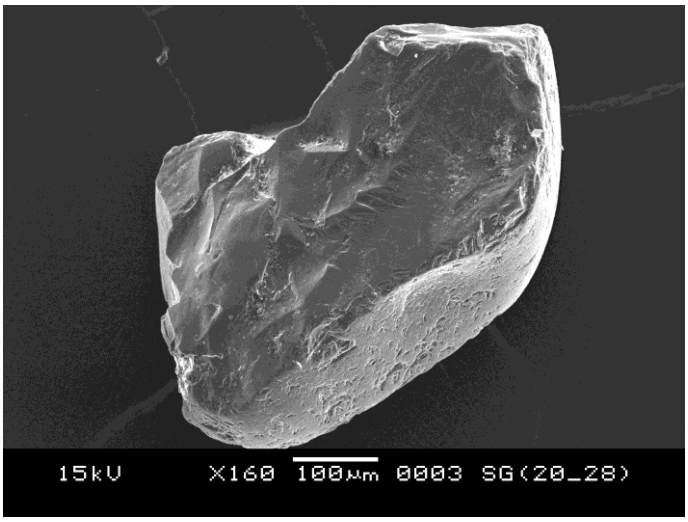

Figure A2.2 – SEM photo of angular grain. Sample SG_20_28_3_1

- Sub-angular *(Classification: 4)*

Figure A2.3 – SEM photo of sub-angular grain. Sample BDR_SS3_8_1

- Sub-rounded *(Classification: 3)*

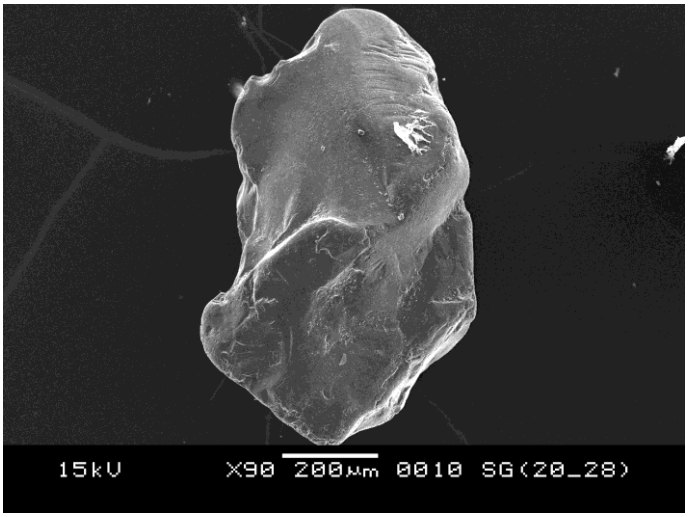

Figure A2.4 – SEM photo of sub-rounded grain. Sample SG_20_28_10_1

- Rounded *(Classification: 2)*

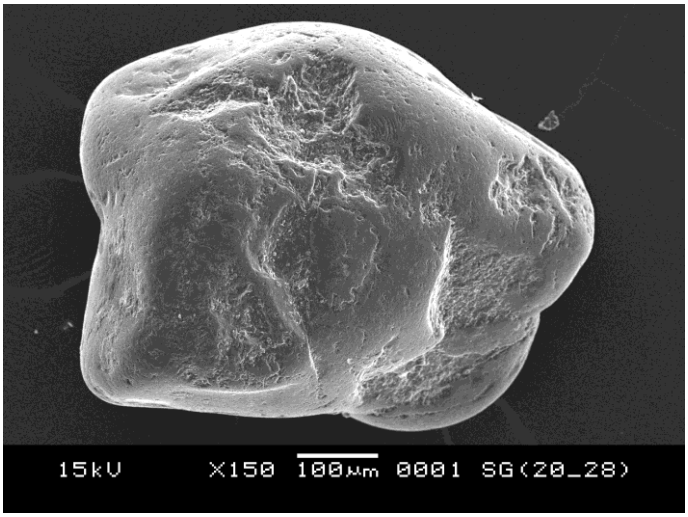

Figure A2.5 – SEM photo of rounded grain. Sample SG_20_28_1_1

- Well rounded *(Classification: 1)*

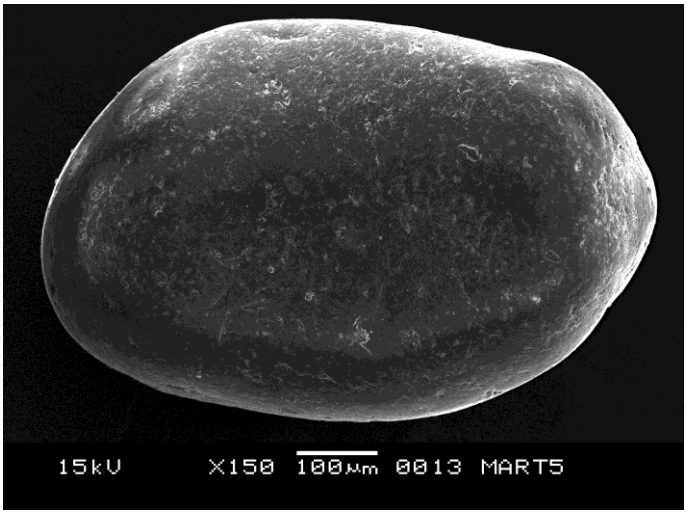

Figure A2.6 – SEM photo of well rounded grain. Sample MART_5_13_1

b) Relief – analysed based on the topographic differences in the surface of the grain and, therefore, is classified as Low, Medium and High (values from 1 to 3, respectively).

- High *(Classification: 3)*

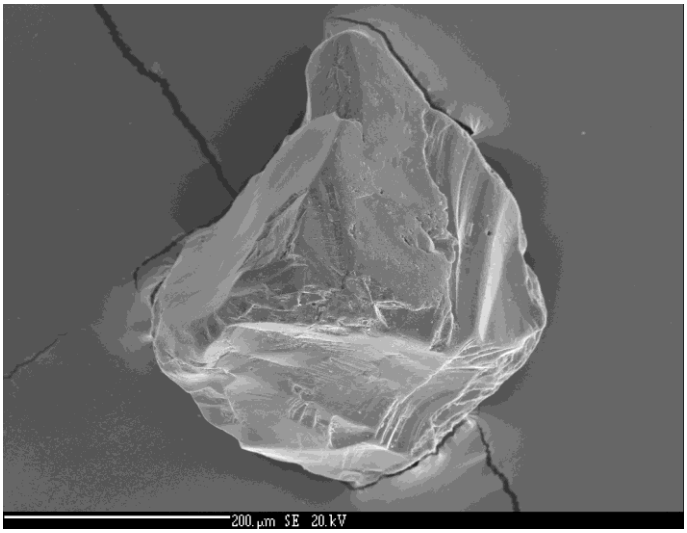

Figure A2.7 – SEM photo of grain with high relief. Sample PB_Duna_Trep_Mrg_8

- Medium *(Classification: 2)*

Figure A2.8 – SEM photo of grain with medium relief. Sample MART_4_6_1

- Low *(Classification: 1)*

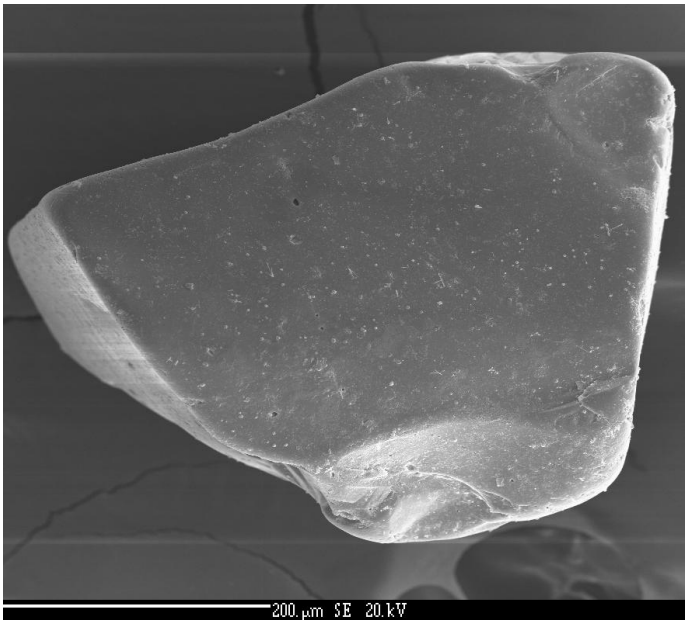

Figure A2.9 – SEM photo of grain with low relief. Sample PB_Berma_08

c) **Dissolution –** microtexture of chemical nature indicating the degree of dissolution on the surface of the grain. The effects of dissolution are noticed by the destruction of fresh surfaces and sharp edges on the surface of the grain and by the formation of grooves. Classified as Low, Medium and High (values from 1 to 3, respectively).

- High *(Classification: 3)*

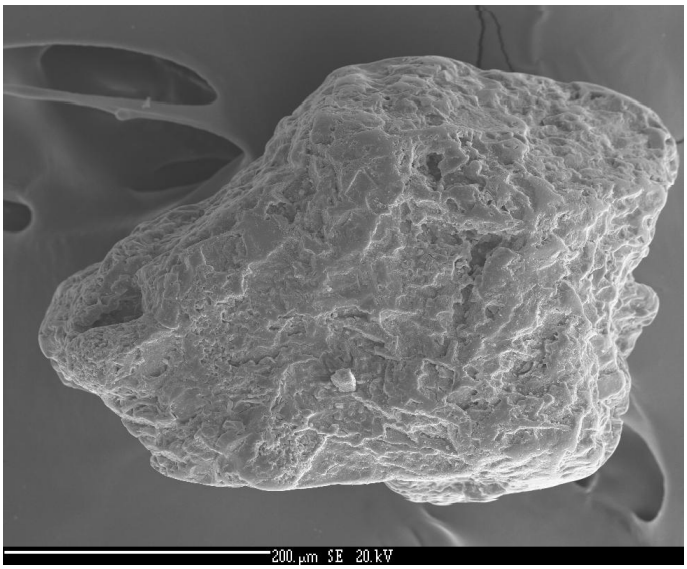

Figure A2.10 – SEM photo of grain with high dissolution. Sample MART_4_8_1

- Medium *(Classification: 2)*

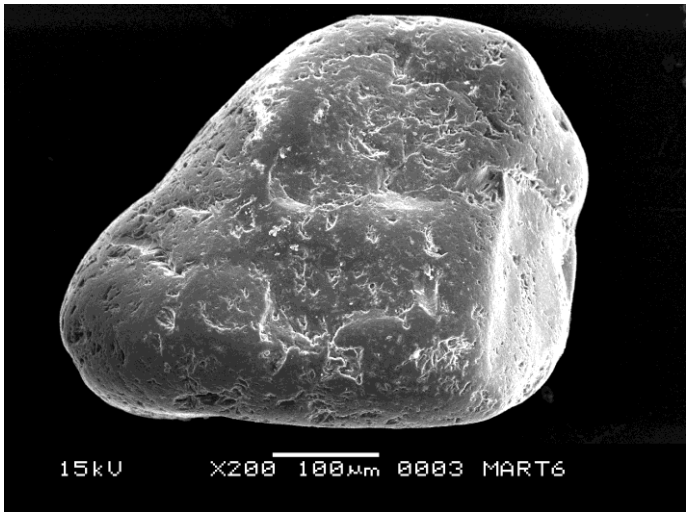

Figure A2.11 – SEM photo of grain with medium dissolution. Sample MART_6_3_1

- Low *(Classification: 1)*

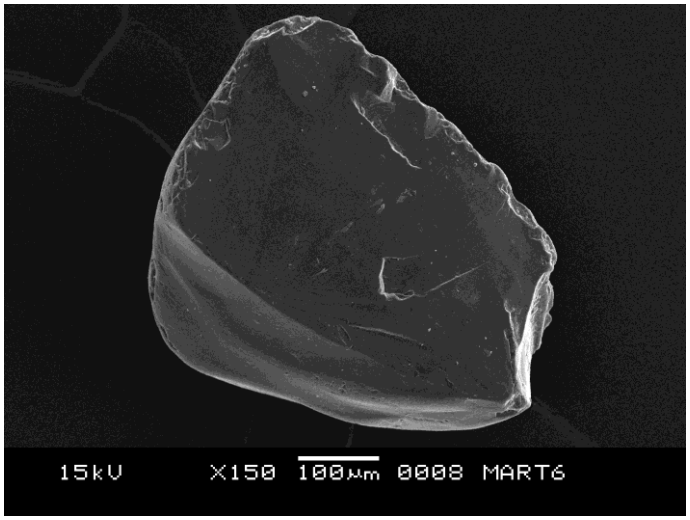

Figure A2.12 – SEM photo of grain with low dissolution. Sample MART_6_8_1

d) **Precipitation** - This microtexture indicates the degree of chemical precipitation on the surface of the quartz grain. It is noticed by the high number of microparticles in the surface of the grain. Classified as Low, Medium and High (values from 1 to 3, respectively).

- High *(Classification: 3)*

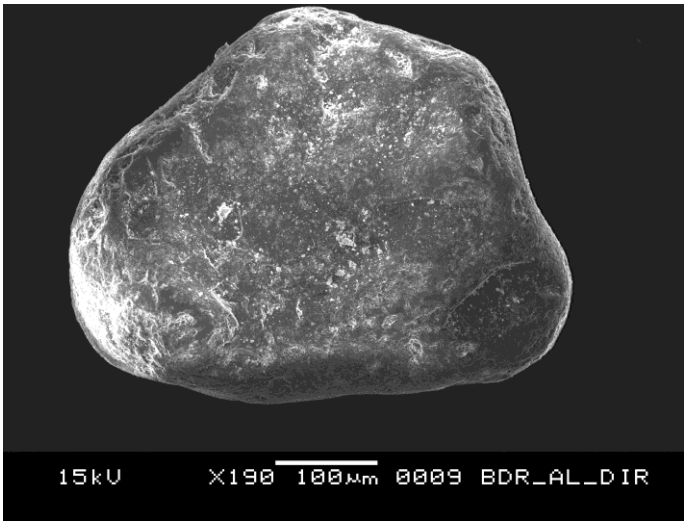

Figure A2.13 – SEM photo of grain with high precipitation. Sample BDR_ALV_DIR_8_1

- Medium *(Classification: 2)*

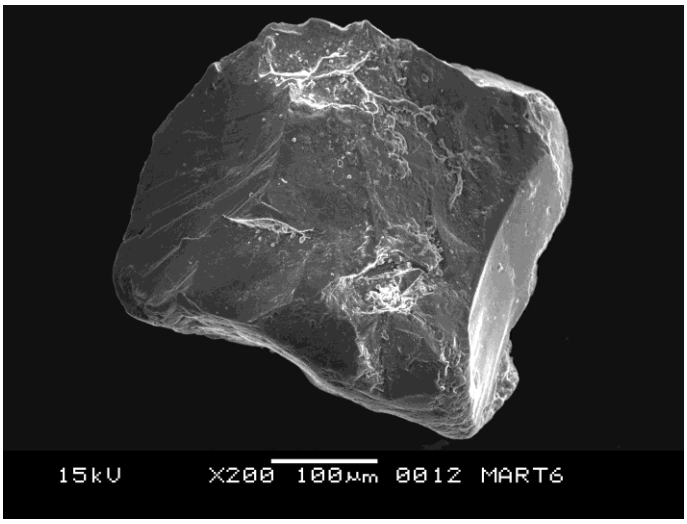

Figure A2.14 – SEM photo of grain with médium precipitation. Sample MART_6_12_1

- Low *(Classification: 1)*

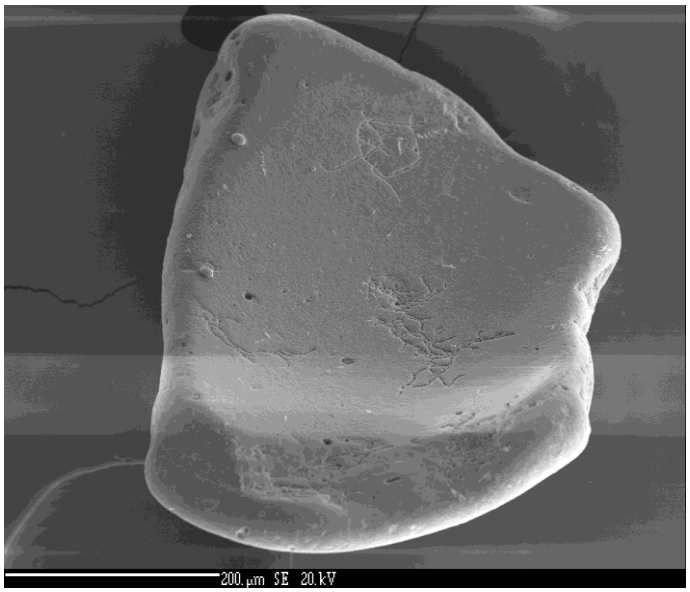

Figure A2.15 – SEM photo of grain with low precipitation. Sample PB_Berma_9

All the remaining microtextures were classified having in consideration the area of the surface of the quartz grain that they occupy. They have been classified has:

0- If absent of the surface of the grain.

1- If they ocuppy between 1 and 10% of the surface of the grain.

2- If they ocuppy between 10 and 25% of the surface of the grain.

3- If they ocuppy between 25 and 50% of the surface of the grain.

4- If they ocuppy between 50 and 75% of the surface of the grain.

5- If they ocuppy more than 75% of the surface of the grain.

e) **Fresh surfaces** – It is characterized by the absence of chemical dissolution or precipitation and, in many cases, by the presence of mechanical marks (*e.g.* fractures, abrasion marks) that are responsible for their recent exposure.

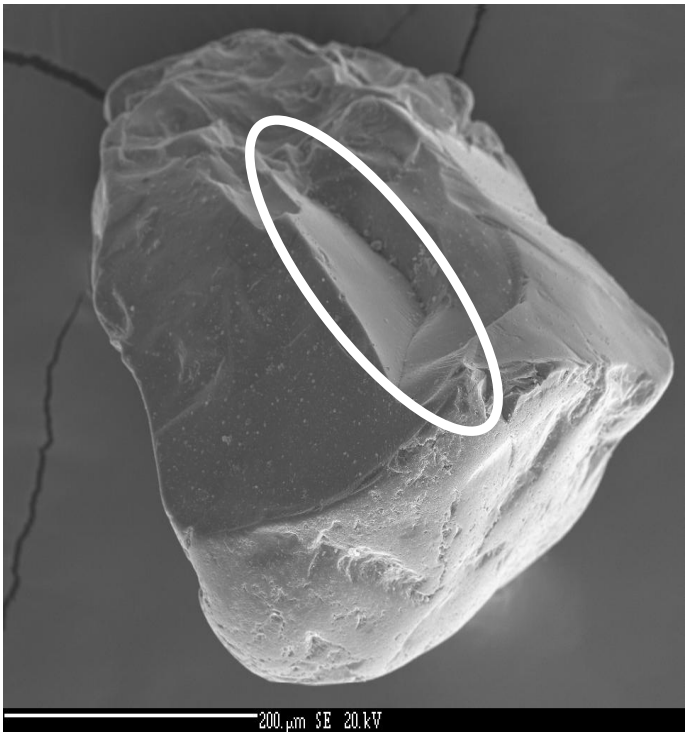

Figure A2.16 – SEM photo of grain with fresh surfaces (white ellipse). Sample SG_Praia_2_1

Adhearing particles – It is characterized by the presence of microparticles in the surface of the quartz grain. Normally, these microparticles are within grooves and they are attached to the surface of the grain.

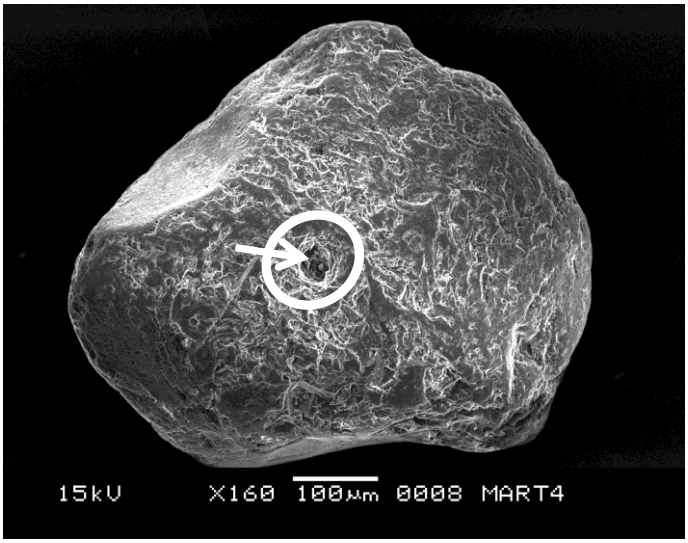

Figure A2.17 – SEM photo of grain with adhearing particles (white circle and arrow). Sample MART_4_8_1

f) **Linear and conchoidal fractures** – It is detectable by the presence of linear, planar or conchoidal structures in the surface of the grain. It is the result of mechanical action.

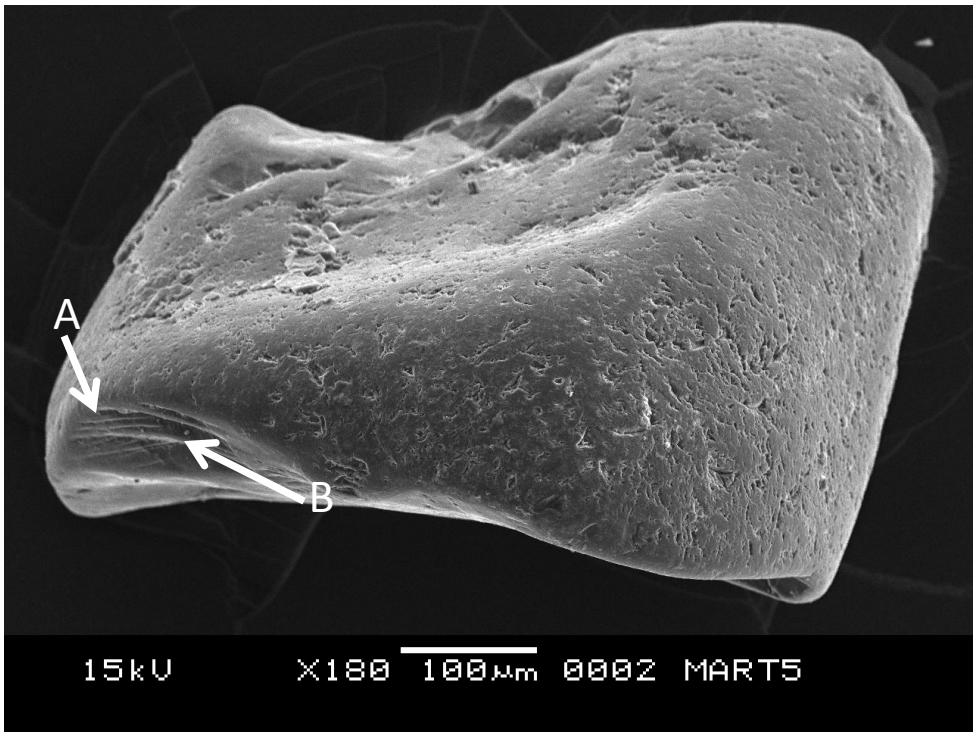

Figure A2.18 – SEM photo of grain with linear fractures (A) and conchoidal fractures (B). Sample MART_5_2_1

g) **Parallel fractures** – Noticed by the presence of parallel linear or planar structures in the surface of the grain. This microtexture is the result of mechanical action.

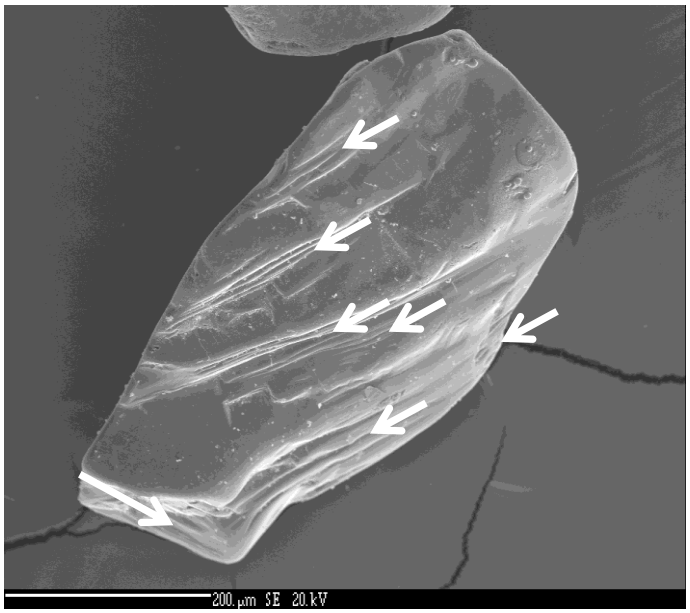

Figure A2.19 – SEM photo of grain with parallel fractures (white arrows). Sample BDR_SS3_5_1

h) **Steps** – detectable by the presence of linear or conchoidal structures that cause a considerable gap between the different levels of the surface of the grain.

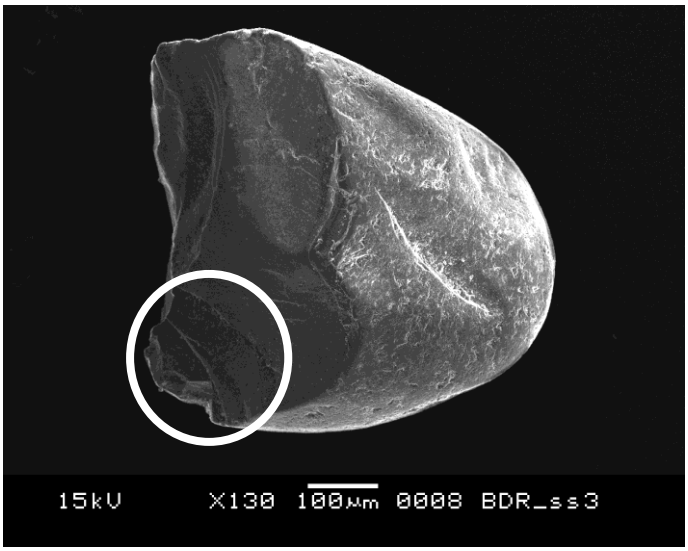

Figure A2.20 – SEM photo of grain with steps (white circle). Sample BDR_SS3_8_1

i) **Sharp edges** – Produced by mechanical action.

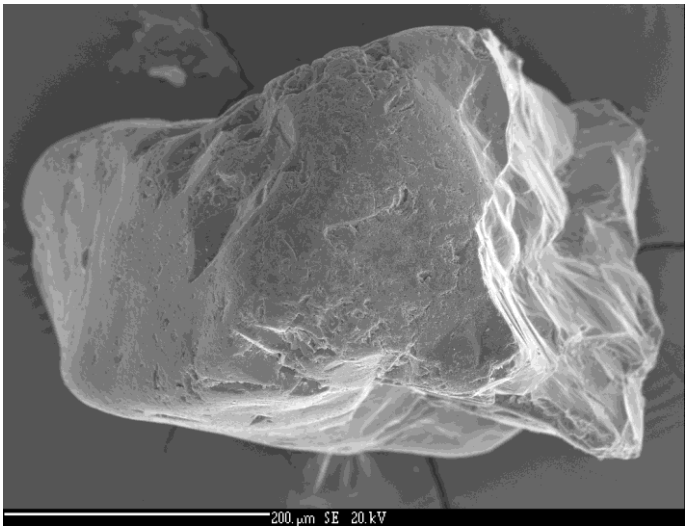

Figure A2.21 – SEM photo of grain with sharp edges (right sector of the grain). Sample PB_Duna_F_03

j) **Cracked grains** – Grains that are broken in several fractions. They are the result of the colision between grains.

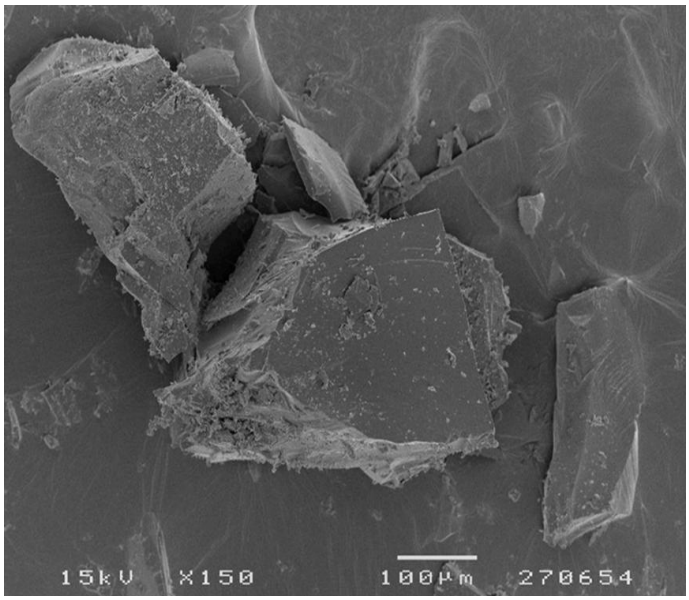

Figure A2.22 – SEM photo of cracked grain. Sample GALS3_3_12

k) **Upturned plates –** Impacted surfaces with small to large plates partially torn loose from the mineral surface.

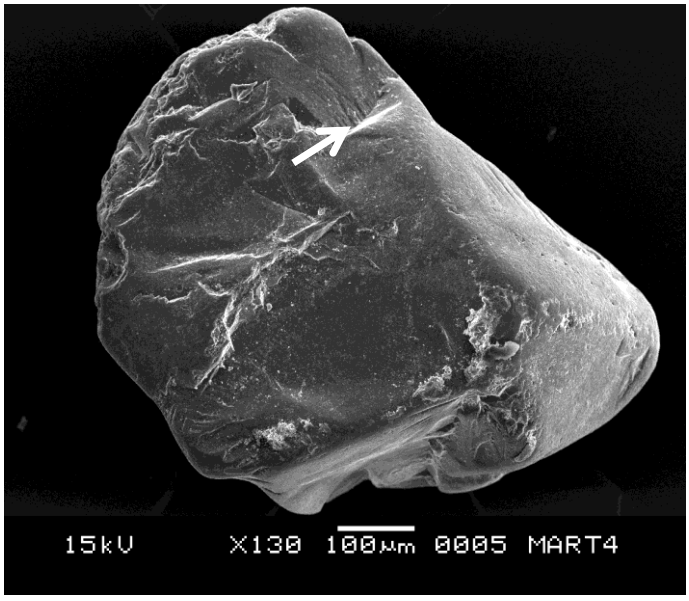

Figure A2.23 – SEM photo of grain with upturned plate (white arrow). Sample Mart_4_5_1

l) **V-marks** – This microtexture is characterised by the presence of V shaped depressions, normally the result of the collision between grains.

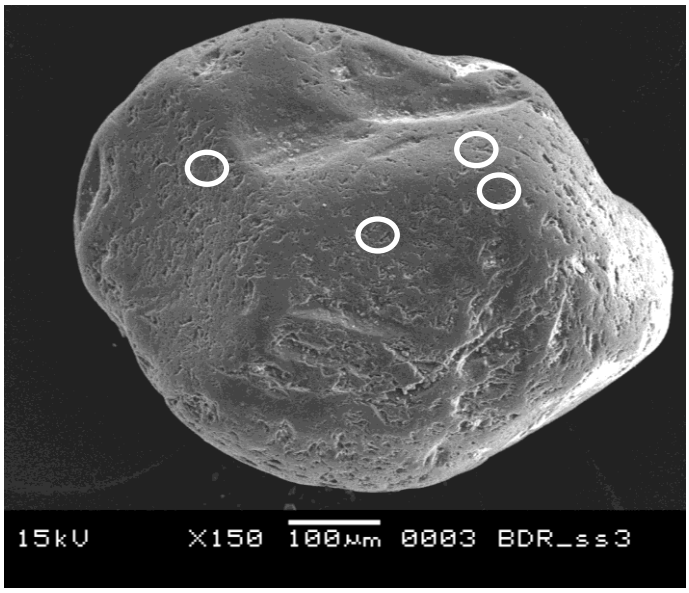

Figure A2.24 – SEM photo of grain with V-mark (white circles). Sample BDR_SS3_3_1

m) **Crescent marks** - This microtexture is characterised by the presence of crescent-shaped depressions, normally the result of the collision between grains.

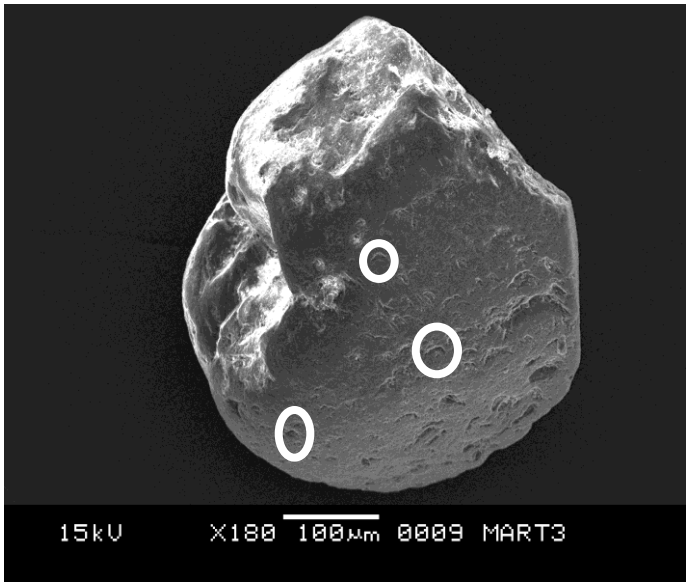

Figure A2.25 – SEM photo of grain with crescent marks (white circles). Sample BDR_SS3_9_1

n) **Abrasion marks** – Microtexture characterized by cracked, dislocated and broken surface caused by the collision between grains.

Figure A2.26 – SEM photo of grain with abrasion marks (white circle). Sample PB_Duna_T_9

o) **Craters** – Depression of all shapes and sizes caused by impact.

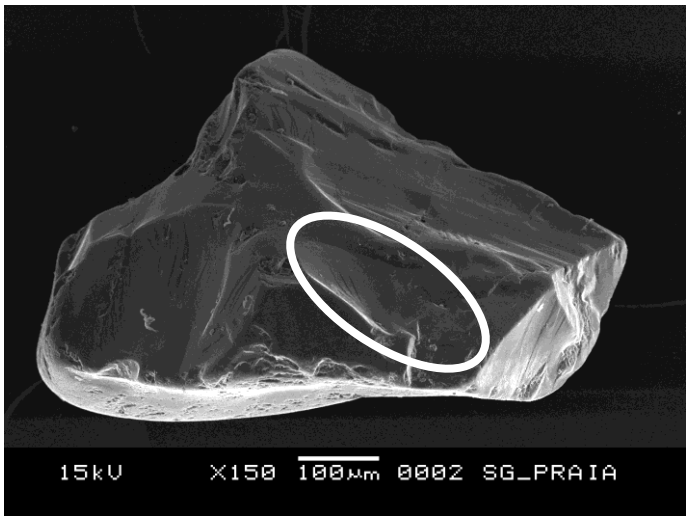

Figure A2.27 – SEM photo of grain with craters (white circle). Sample SG_Praia_2_1

p) **Linear grooves** – Linear depressions on the grain surface, caused by chemical action.

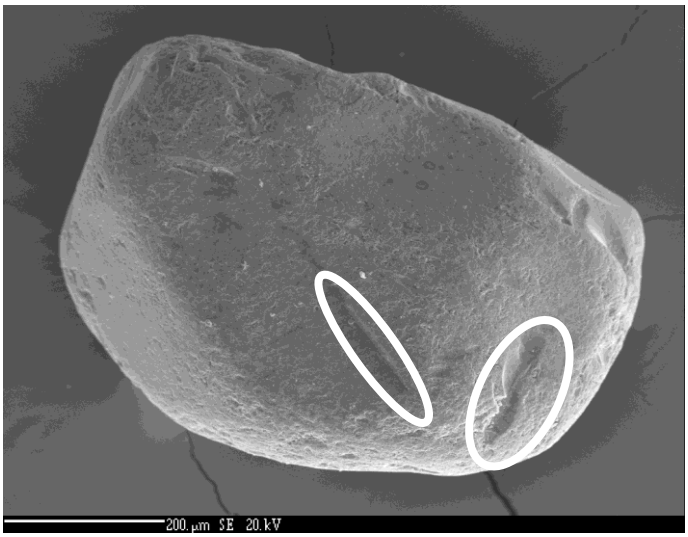

Figure A2.28 – SEM photo of grain with linear grooves (white circles). Sample PB_Berma_12

q) **Deep grooves** - Deep depressions on the grain surface, caused by chemical action.

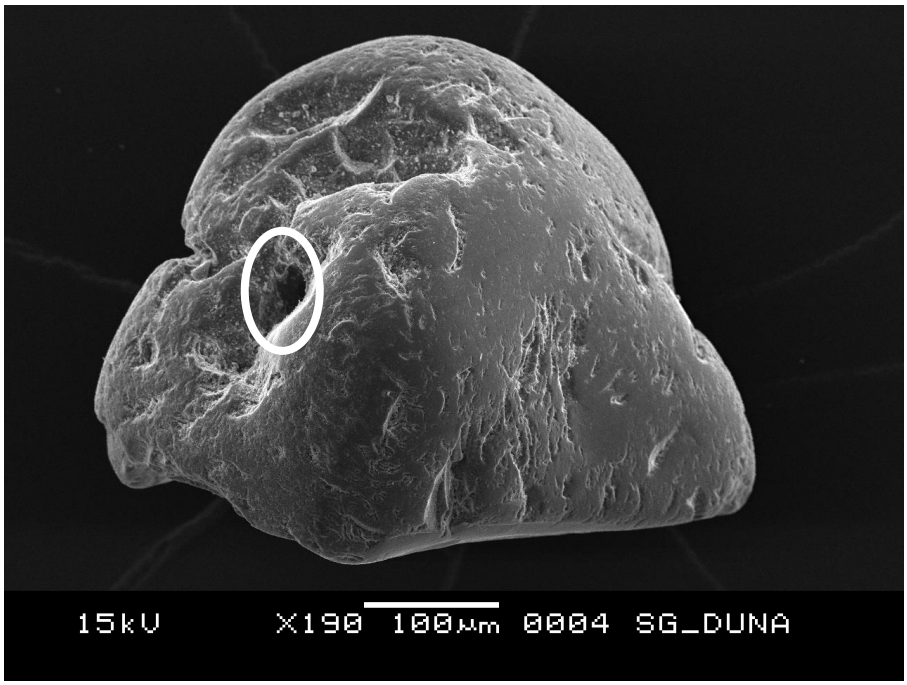

Figure A2.29 – SEM photo of grain with deep groove (white circle). Sample SG_Duna_5_1

r) **Circular grooves** – Circular depressions on the grain surface, caused by chemical action. In contrast with craters this microtextures presents strong dissolution.

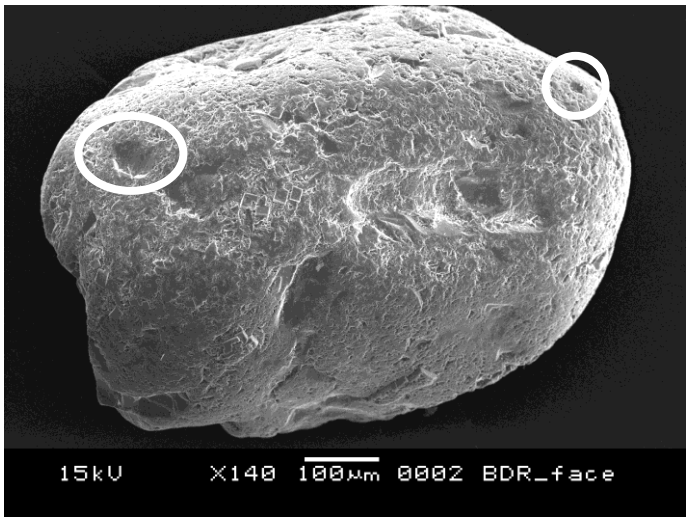

Figure A2.30 – SEM photo of grain with circular grooves (white circles). Sample BDR_Face_2_1

The microtextural analysis and classification was conducted for each grain.

Average and median values for each variable characterizing each set of grains were calculated after normalization by the largest value.